TECH LIBRARY KAFB, NM
0099744

NASA CONTRACTOR REPORT

NASA CR-100

NASA CR
COPY RETURN TO
(WLIL-2)
KIRTLAND AFB, N MEX

EVALUATION OF INFRARED SPECTROPHOTOMETRY FOR COMPOSITIONAL ANALYSIS OF LUNAR AND PLANETARY SOILS

Part II: Rough and Powdered Surfaces

by R. J. P. Lyon

Prepared under Contract No. NASr-49(04) *by*
STANFORD RESEARCH INSTITUTE
Menlo Park, Calif.
for

NATIONAL AERONAUTICS AND SPACE ADMINISTRATION • WASHINGTON, D. C. • NOVEMBER 1964

NASA CR-100

TECH LIBRARY KAFB, NM

0099744

EVALUATION OF INFRARED SPECTROPHOTOMETRY FOR COMPOSITIONAL ANALYSIS OF LUNAR AND PLANETARY SOILS

Part II: Rough and Powdered Surfaces

By R. J. P. Lyon

Distribution of this report is provided in the interest of information exchange. Responsibility for the contents resides in the author or organization that prepared it.

Prepared under Contract No. NASr-49(04) by
STANFORD RESEARCH INSTITUTE
Menlo Park, California

for

NATIONAL AERONAUTICS AND SPACE ADMINISTRATION

For sale by the Office of Technical Services, Department of Commerce,
Washington, D.C. 20230 -- Price $4.00

ABSTRACT

Lunar rock compositions are still unknown. However, terrestrial rock compositions can be defined by the shift in wavelength of the fundamental Si-O vibration, between 9 and 11 μ. Absorption spectra (in KBr pellets) make it possible to estimate, semi-quantitatively, the content of individual minerals in a rock. If a sample can be polished, either normal reflectance or normal emittance spectra will permit definition of the individual minerals, and the rock composition can be determined with fair precision.

Compositions of rock with roughened surfaces or mineral aggregates with particle sizes above 1 mm are readily determined by normal spectral emittance or hemispherical spectral reflectance techniques. Both show lower precision than absorption techniques.

With all three techniques, high-silica glasses (tektites) and low-silica, stony meteorites (chondrites) show a 2.0 μ displacement in wavelength of their spectral peaks. Roughness or particle size does not shift the position of such peaks but only decreases the depth (or contrast) of their spectra.

Definition of rock composition, by either reflectance or emittance techniques, diminishes with decreasing particle sizes below 1 mm until, near 50 μ size, only materials with marked spectral contrast (dunite, quartz) can be distinguished. Carefully sized material—specifically without finer powder—can be analyzed down to 10 μ size, although this analysis too is composition-dependent.

Initial experiments with frustrated multiple internal reflectance (FMIR) techniques indicate that compositional analysis of silicate powders (1 to 40 μ in size) is feasible, and that the finer particle sizes may increase rather than diminish the spectral contrasts obtained.

Emittance and reflectance processes are determined to a large extent by the "surface skin" on each grain—equal-sized clear grains, frosted grains, and grains dusted with a finer powder (of the same material) should show spectra of successively diminishing contrast, each spectrum is a modification of that of the original solid material.

Low-density surfaces (powder in fairy castle structure) do not further decrease the spectral contrast, at 9 to 11 μ, beyond that already controlled by the fineness of the particles themselves. Conversely, pelletizing the same fine powder does not markedly increase the spectral contrast.

The report includes more than 330 normal emittance, reflectance and transmittance spectra of roughened and powdered rock and mineral surfaces from 8 to 25 μ wavelengths.

This research leads to the conclusion that additional laboratory studies are needed to assess the scattering properties of powders under simulated lunar conditions. Subsequent field operation of flight-weight spectrometers would be invaluable for calibration purposes before an attempt is made to determine the composition of the lunar surface.

CONTENTS

ABSTRACT iii

LIST OF ILLUSTRATIONS ix

LIST OF TABLES xix

SYMBOLS, ABBREVIATIONS, AND GLOSSARY xxi

I INTRODUCTION 1

II SUMMARY AND CONCLUSIONS 3

A. Summary 3

B. Conclusions 4

III RECOMMENDATIONS 9

A. Sample Parameters 9

B. Instrument Parameters on Flight-Weight Equipment 10

C. Electronic Parameters and Telemetry Effects on Data 10

D. Operational Modes 10

IV SAMPLE ACQUISITION 13

V COMPUTER REDUCTION OF DATA 15

VI ABSORPTION ANALYSIS 21

A. Previous Studies 21

B. Present Studies 21

1. Sample Preparation 24
2. Experimental Technique 24
3. Computation of Absorption Data 25
4. Error Analyses 27

VII REFLECTION ANALYSIS 29

A. Previous Studies 29

B. Present Study 31

1. Solid Specimens 31

CONTENTS (Continued)

a. Sample Preparation 31
b. Experimental Technique 31
c. Computation of Reflection Data 35
d. Error Analysis 35

2. Powdered Specimens 38

a. Sample Preparation 38
b. Experimental Techniques. 39
c. Computation of the Reflection Data 42
d. Error Analysis 42

VIII EMISSION ANALYSIS 45

A. Blackbody Radiation 45

B. Normal Spectral Emittance 49

1. Previous Studies 49
2. Present Study 51

a. Sample Preparation 52
b. Experimental Techniques. 54
c. Reproducibility of the Spectra 58
d. Results 63
e. Error Analysis 68

3. Effects of Compositional Differences between Samples 71

a. Acid Rock Types 73
b. Intermediate Compositions 79
c. Basic Rock Types 79

4. Effects of Surficial Differences between Samples 82

a. Roughness 82
b. Particle Size 86
c. Theoretical Treatment of Scattering Effects on the Emittance of Material 104
d. Experiments Designed for an Understanding of the Scattering Process 121

5. Functional Groups (Anions) Other than Silicates . 135

6. Longer Wavelength (15 to 25 μ) Studies 144

IX COMBINED TECHNIQUES 149

A. Results of Studies on Stony Meteorites (Chondrites). . 149

B. Studies on Rock Samples 156

C. Studies on the Rock Suite Supplied by the U.S. National Museum (Appendix A) 159

CONTENTS (Continued)

X ATMOSPHERIC ATTENUATION OF INFRARED RADIATION 161

ACKNOWLEDGMENTS 168

PRESENTATION OF PROFESSIONAL PAPERS 169

REFERENCES 170

APPENDIX A A-1

APPENDIX B B-1

APPENDIX C C-1

LIST OF ILLUSTRATIONS

Fig. 1 Normal Emission Curves for Quartz and Quartz Powder Sifted into Fairy Castle Structures 16

Fig. 2 Normal Spectral Emittance Curves for Quartz as a Function of Roughness and Particle Size 18

Fig. 3 Normal Spectral Emittance Curves of Quartz as a Function of Particle Size, Using a Lagrangian Interpolation Between Data Points 19

Fig. 4 Absorption Spectra of Plagioclase and Pyroxene from the Stillwater Gabbro, Before and After a 350-kilobar Shock Loading 23

Fig. 5 Absorption Spectra of the Principal Inorganic Anions 26

Fig. 6 Reflectance Spectra of Tektites and Chondritic Meteoritic Materials, Compared with Typical Rock Specimens 30

Fig. 7 Variation of Near-Normal Spectral Reflection with Orientation of a Quartz Oscillator Plate 32

Fig. 8 Comparison of Absorption and Reflection Spectra for Various Silica Modifications 33

Fig. 9 Reflectance Measurements on a Polished Dunite Sample Replotted as Normal Spectral Emittance Curve 36

Fig. 10 Optical Configuration of the STL Paraboloid Reflectometer 40

Fig. 11 Spectral Emittance Curves of Granite and Dunite Samples, Both Polished and Powdered 41

Fig. 12 Spectral Emittance Curves for Alumina in Various Surface Aggregations, Calculated from Reflectance Data by STL 41

Fig. 13 Spectral Emittance Curves for Quartz, Calculated from Reflectance Data by STL, Shown for Samples in Various Surface Aggregations 42

Fig. 14 Hemispherical Spectral Emittance from a Blackbody Calculated from the Planck Radiation Formula, for a Series of Temperatures ($T^{o}K$) from 200 through 500° . . . 47

LIST OF ILLUSTRATIONS (Continued)

Fig. 15 Spectral Emittance Curves of a Blackbody at 640°K as Recorded on the Single-Beam PE112 Spectrometer 48

Fig. 16 Hemispherical Emittance Spectra of Quartz and a Blackbody as a Function of Wavelength and Temperature, Calculated from Reflectance Spectra Obtained at Ambient Temperatures 50

Fig. 17 Hemispherical Emittance Spectra of a Blackbody at 350°K Compared with Four Greybody Emission Curves of Rocks at the Same Temperature 51

Fig. 18 Photomicrograph of the Surface of the Quartz Monzonite Porphyry, from the Nevada Test Site, Used for Direct Emittance Measurements 53

Fig. 19 Photomicrograph of the Surface as Used of the Augite Diorite 53

Fig. 20 Photomicrograph of the Surface as Used of the Nepheline Basalt for Direct Emittance Measurements . . . 53

Fig. 21 Water-Cooled Furnace Used for the Emittance Measurements, Showing the Method of Installation Adjacent to the Spectrometer 55

Fig. 22 Direct Tracings of the Recorder Response from the Spectrometer as a Function of Wavelength for a Series of Materials (Approximating Blackbodies) at 643°K (370°C) 57

Fig. 23 Close-Up View of the Razor-Blade Blackbody 58

Fig. 24 Normal Spectral Emittance Curves of Repeated Measurements on 0.02 μ Alumina Powder, Showing its Very High Average Emittance, Despite its White Color in Visible Light. 59

Fig. 25 Electron Micrograph of the 0.02 μ Alumina Powder 60

Fig. 26 Normal Spectral Emittance Curves for Repeated Measurements on Quartz Basalt Sample Studied on Each of Two Sawed Faces, Showing the Variance in Measurements 61

Fig. 27 Normal Spectral Emittance Curves for Repeated Measurements on Sample of Granite Gneiss, Showing the Variance in Measurements 62

Fig. 28 Normal Spectral Emittance Curves for Samples of Quartz Monzonite Porphyry, Syenite, and Peridotite 69

Fig. 29 Radiant Flux Plots for the Same Three Samples as in Fig. 28 72

LIST OF ILLUSTRATIONS (Continued)

Fig. 30 Normal Spectral Emittance Curves for Tektite Sample and the Glassy Equivalent of Granite, Obsidian . . . 74

Fig. 31 Normal Spectral Emittance Curves for a Frothy Pumice Specimen Compared with that of a Welded Tuff 75

Fig. 32 Normal Spectral Emittance Curves for a Roughened Quartz Plate and a Cleavage Fragment of K-feldspar, Compared with that of a Graphic Granite Sample Which Contains Quartz and Feldspar as its Measured Constituents 77

Fig. 33 Normal Spectral Emittance Curves of Granite Compared with That of an Aplite Vein from the SHOAL Test Site, Nevada 78

Fig. 34 Normal Spectral Emittance Curves for Quartz Diorite Compared with the Calculated Emittance Curve Obtained from Reflectance Data from the Polished Surface of the Same Sample 80

Fig. 35 Normal Spectral Emittance Curve of the Acidic Rock Sample, Tektite, Showing that its Minimum at 9.30 μ Contrasts Markedly with that of the Haven Meteoritic Chondrite, Obtained from Reflectance Data 81

Fig. 36 Transmission Spectrum of Finely Powdered Quartz in a KBr Pellet, with the Normal Spectral Emittance Curve for a Z-Cut Quartz Oscillator Plate 83

Fig. 37 Normal Spectral Emittance of Dunite Samples as a Function of Surface Roughness and Particle Size 85

Fig. 38 Normal Spectral Emittance Curves for Polished Quartz and for Roughened Quartz, Compared with the Spectra from a Quartz Sand and a Fine-Grained Chert 88

Fig. 39 Normal Spectral Emittance Curves for the Chert Sample and the Quartz Powder, Sized to Contain 1 to 10 μ Particles 89

Fig. 40 Normal Spectral Emittance Curves for Dunite with a Polished Surface and in a Roughened Condition, Compared With the Calculated Emittance Spectrum Obtained from the Reflectance Data from the Polished Surface 91

Fig. 41 Photomicrograph of the 25 to 45 μ Quartz Powders Used in the Emittance Experiments 92

Fig. 42 Photomicrograph of the Particle Sizes in the 10 to 25 μ Quartz Powders 93

Fig. 43 Photomicrograph Showing the Particle Size in the 1 to 10 μ Quartz Powders Used in the Emittance Experiments 94

LIST OF ILLUSTRATIONS (Continued)

Fig. 44 Emission Spectra Showing the Effect of Decreasing Void Space in the Curves for Quartz Powders 95

Fig. 45 Stereo-Pair of Fairy Castle Structures in the 1 to 10 μ Quartz Powder 96

Fig. 46 Stereo-Pair of Fairy Castle Structures With Dunite Powder of a Particle Size Less than 10 μ 97

Fig. 47 Stereo-Pair of Fairy Castle Structures in 17 μ Silicon Carbide Powder 98

Fig. 48 Normal Spectral Emittance Curves for Dunite in Various Degrees of Surface Roughness and Particle Sizes 100

Fig. 49 Normal Spectral Emittance Curves for Silicon Carbide (Carborundum) of Varying Particle Size 102

Fig. 50 Normal Spectral Emittance Curves for Alumina in Various Degrees of Crystallinity 103

Fig. 51 Emittance from Grooves and Cavities as a Function of the Geometry of the Surface 106

Fig. 52 Effect of Void Spaces in a Surface 108

Fig. 53 Effect of Surface Roughness on the Emittance of a Surface 110

Fig. 54 Diffuse Emittance as a Function of the Ratio of Scattering to Absorption 112

Fig. 55 Normal Spectral Emittance of Quartz with Various Surface Roughnesses 113

Fig. 56 Photomicrograph of the Rough Surface of the X-Cut Quartz Plate 115

Fig. 57 Section Through the X-Cut Quartz Plate as Roughened, Showing a View Across a Central Break 115

Fig. 58 Enlarged Plan View of the Roughened X-Cut Quartz Plate. . 116

Fig. 59 Highly Enlarged Plan View of the X-Cut Roughened Quartz Plate 116

Fig. 60 Spectral Emittance Curve for Polished Quartz and for Dunite, Compared with the Curve for a Composite Sample. . 123

Fig. 61 Spectral Curves Showing the Effect of Multiple Reflection of 640°K Quartz Emission After a Single- and Double-Reflection from Additional Quartz Plates, at Ambient Temperatures 124

Fig. 62 Variation in Reflectance with Temperature for a Z-Cut Quartz Plate 127

LIST OF ILLUSTRATIONS (Continued)

Fig. 63 Normal Spectral Emittance Curves, Calculated from Reflectance Data, for Quartz Z-Cut Plate Shown in Fig. 62 128

Fig. 64 Normal Spectral Emittance Curves Calculated from Reflectance Data of Fig. 63 129

Fig. 65 Normal Spectral Emittance Curve of Z-Cut Quartz at 640°K with Multiple Reflections from a Further Z-Cut Quartz Plate at 80°K 131

Fig. 66 Normal Spectral Emittance Curves for Z-Cut Quartz at 640°K, with Multiple Reflections from a Further Z-Cut Quartz Plate at 623°K 132

Fig. 67 Normal Spectral Emittance Curve of a Z-Cut Quartz Plate at 640°K with Multiple Reflections from a Further Z-Cut Quartz Plate at 873°K 133

Fig. 68 Direct Tracing of the Spectrum Obtained with a Single-Beam Spectrometer for a Cleavage Plate of Calcite with a Highly "Polished" Surface 136

Fig. 69 Normal Spectral Emittance Curve Calculated from Ratios Observed in Fig. 68, for Calcite as a Cleavage Plate . . . 138

Fig. 70 Normal Spectral Emittance Curve for Aragonite, Calculated in the Manner of Data from Fig. 68 139

Fig. 71 Normal Spectral Emittance Curve for Dolomite 140

Fig. 72 Normal Spectral Emittance Obtained for Sand-Size Samples of Anhydrite and Quartz Sands 141

Fig. 73 Radiant Emittance from Anhydrite and Quartz Sands Plotted as a Function of Wavelength 142

Fig. 74 Emittance Spectra Obtained for Gypsum and Silica Sand . . 143

Fig. 75 Normal Spectral Emittance for X-Cut and Z-Cut Quartz Plates in the Longer Wavelength Region from 14.0 to 24.0 μ 145

Fig. 76 Normal Spectral Emittance Curves for Fused Quartz and Roughened X-Cut Quartz in the Longer Wavelength Region from 14.0 to 24.0 μ 146

Fig. 77 Normal Spectral Emittance for a Sapphire Sheet, in the Longer Wavelength Region from 14.0 to 24.0 μ 148

Fig. 78 Normal Spectral Emittance Curves for Meteoritic Materials 152

Fig. 79 Calculated Normal Spectral Emittance Curve of Reflectance Data from Haven Chondrite with an Emittance Minimum at 10.75 μ, Compared with the Absorption Spectrum for Bruderheim Chondrite 153

Fig. 80 Normal Spectral Emittance Curve of Farmington Chondrite Sample (Side 2) with an Emittance Minimum at 11.30 μ, Compared with the Emittance Curve Calculated from Reflectance Data for Farmington-B Sample, at 11.24 μ 154

Fig. 81 Normal Spectral Emittance Curve for Farmington Chondrite (Side 1) with an Emittance Minimum at 11.20 μ, Compared with Farmington-A Sample with an Emittance Minimum Calculated from Reflectance at 10.87 μ 155

Fig. 82 Normal Spectral Emittance for a Sample of HARD HAT Quartz Monzonite Porphyry with an Emittance Minimum at 8.92 μ 157

Fig. 83 Normal Spectral Emittance Curves for Dunite 158

Fig. 84 Atmospheric Transmission Over a Sea-Level Path as a Function of Wavelength, from 7 to 14 μ 162

Fig. 85 Atmospheric Transmission on a Sea-Level Path as a Function of Wavelength, from 6 to 24 μ 163

Fig. 86 Transmission Spectra as a Function of Wavelength for an Infinite Length Slant-Path at a Zenith Angle of 60°, from a 100,000-Foot Altitude 166

Fig. 87 Hemispherical Emittance Curves for a 400°K Blackbody and the Same Blackbody When Seen Through the Total Atmospheric Ozone 167

Fig. A-1 Opal: Normal Spectral Emittance, with Absorption Data A-3

Fig. A-2 Dacite: Normal Spectral Emittance, with Absorption Data A-5

Fig. A-3 Granite: Normal Spectral Emittance, with Absorption Data A-7

Fig. A-4 Graphic Granite: Normal Spectral Emittance, with Absorption Data A-9

Fig. A-5 Pyroxene Aplite: Normal Spectral Emittance, with Absorption Data A-11

Fig. A-6 Rhyolite Pumice: Normal Spectral Emittance, with Absorption Data A-13

Fig. A-7 Granite Gneiss: Normal Spectral Emittance, with Absorption Data A-15

Fig. A-8 Trachyte: Normal Spectral Emittance, with Absorption Data A-17

Fig. A-9 Quartz Syenite: Normal Spectral Emittance, with Absorption Data A-19

LIST OF ILLUSTRATIONS (Continued)

Fig. A-10 Andesite (Monzonite Porphyry): Normal Spectral Emittance, with Absorption Data A-21

Fig. A-11 Nepheline Syenite: Normal Spectral Emittance, with Absorption Data A-23

Fig. A-12 Quartz Basalt: Normal Spectral Emittance, with Absorption Data A-25

Fig. A-13 Hypersthene Andesite: Normal Spectral Emittance, with Absorption Data A-27

Fig. A-14 Hypersthene Andesite Vitrophyre: Normal Spectral Emittance, with Absorption Data A-29

Fig. A-15 Quartz Diorite: Normal Spectral Emittance, with Absorption Data A-31

Fig. A-16 Augite Diorite: Normal Spectral Emittance, with Absorption Data A-33

Fig. A-17 Garnetiferous Gabbro: Normal Spectral Emittance, with Absorption Data A-35

Fig. A-18 Augite Diorite (Gabbro): Normal Spectral Emittance, with Absorption Data A-37

Fig. A-19 Schist (Muscovite Quartz): Normal Spectral Emittance, with Absorption Data A-39

Fig. A-20 Diabase: Normal Spectral Emittance, with Absorption Data A-41

Fig. A-21 Basalt: Normal Spectral Emittance, with Absorption Data A-43

Fig. A-22 Plagioclase Basalt: Normal Spectral Emittance, with Absorption Data A-45

Fig. A-23 Monchiquite: Normal Spectral Emittance, with Absorption Data A-47

Fig. A-24 Hornblende Gabbro Gneiss: Normal Spectral Emittance, with Absorption Data A-49

Fig. A-25 Peridotite: Normal Spectral Emittance, with Absorption Data A-51

Fig. A-26 Olivine Gabbro: Normal Spectral Emittance, with Absorption Data A-53

Fig. A-27 Nepheline Basalt: Normal Spectral Emittance, with Absorption Data A-55

Fig. A-28 Serpentine: Normal Spectral Emittance, with Absorption Data A-57

Fig. A-29 Limburgite: Normal Spectral Emittance, with Absorption Data A-59

LIST OF ILLUSTRATIONS (Continued)

Fig. B-1 Dacite: Normal Spectral Emittance, Radiant Flux B-2

Fig. B-2 Granite: Normal Spectral Emittance, Radiant Flux B-3

Fig. B-3 Graphic Granite: Normal Spectral Emittance, Radiant Flux B-4

Fig. B-4 Rhyolite Pumice: Normal Spectral Emittance, Radiant Flux B-5

Fig. B-5 Andesite (Monzonite Porphyry): Normal Spectral Emittance, Radiant Flux B-6

Fig. B-6 Nepheline Syenite: Normal Spectral Emittance, Radiant Flux B-7

Fig. B-7 Hypersthene Andesite: Normal Spectral Emittance, Radiant Flux B-8

Fig. B-8 Hypersthene Andesite Vitrophyre: Normal Spectral Emittance, Radiant Flux B-9

Fig. B-9 Quartz Diorite: Normal Spectral Emittance, Radiant Flux B-10

Fig. B-10 Schist (Muscovite Quartz): Normal Spectral Emittance, Radiant Flux B-11

Fig. B-11 Basalt: Normal Spectral Emittance, Radiant Flux B-12

Fig. B-12 Serpentine: Normal Spectral Emittance, Radiant Flux B-13

Fig. B-13 Obsidian: Normal Spectral Emittance, Radiant Flux . . . B-14

Fig. B-14 Obsidian: Normal Spectral Emittance, Radiant Flux . . . B-15

Fig. B-15 Tektite: Normal Spectral Emittance, Radiant Flux . . . B-16

Fig. C-1 Carbon Black: Normal Spectral Emittance, Radiant Flux C-2

Fig. C-2 Dunite, Polished: Normal Spectral Emittance, Radiant Flux C-3

Fig. C-3 Dunite, Rough: Normal Spectral Emittance, Radiant Flux C-4

Fig. C-4 Dunite, Rough Plus Sand: Normal Spectral Emittance, Radiant Flux C-5

Fig. C-5 Dunite, Rough Plus Dust: Normal Spectral Emittance, Radiant Flux C-6

LIST OF ILLUSTRATIONS (Continued)

Fig. C-6 X-Cut Quartz, Polished: Normal Spectral Emittance, Radiant Flux C-7

Fig. C-7 Quartz, Fused: Normal Spectral Emittance, Radiant Flux C-8

Fig. C-8 X-Cut Quartz, Rough: Normal Spectral Emittance, Radiant Flux C-9

Fig. C-9 Quartz Powder, 25 to 45 μ Size: Normal Spectral Emittance, Radiant Flux C-10

Fig. C-10 Quartz Powder, 10 to 25 μ Size: Normal Spectral Emittance, Radiant Flux C-11

Fig. C-11 Quartz Powder, 1 to 10 μ Size: Normal Spectral Emittance, Radiant Flux C-12

Fig. C-12 Alumina, Sapphire Sheet: Normal Spectral Emittance, Radiant Flux C-13

Fig. C-13 Alumina, Sapphire Rod: Normal Spectral Emittance, Radiant Flux C-14

Fig. C-14 Alumina, Alundum Platelets: Normal Spectral Emittance, Radiant Flux C-15

Fig. C-15 Alumina, Alundum Tubing: Normal Spectral Emittance, Radiant Flux C-16

Fig. C-16 Alumina, Powder: Normal Spectral Emittance, Radiant Flux C-17

LIST OF TABLES

I	Summary of Experimental Data Computed	20
II	Spectral Minima for a Series of Rock Surfaces: Emittance Measurements	64
III	Emittance Values for Various Surfaces on a Dunite Specimen	84
IV	Emittance Values for Dunite Sand (150 to 300 μ) at Various Temperatures	86
V	Emittance Values Calculated from Reflectance Data of Polished Surface	87
VI	Absorption Coefficients for Quartz (X-cut) Plates	119
VII	Reflection Percentages for Quartz Plates	125
VIII	Quartz Emittance Levels Following N-Reflections from Similar Plates (X-cut)	135
IX	Characteristics of Chondrites Used for Analysis	149
X	Bruderheim Modal Analysis	150
XI	Electron Probe Analysis of Chondritic Minerals	150

SYMBOLS, ABBREVIATIONS, AND GLOSSARY

Symbols as used in this report are:

λ	wavelength (microns)
ν	frequency
$\bar{\nu}$	wavenumber
τ	transmittance
α	absorbance (also used for atmospheric attenuation as α_λ)
ϵ	emittance
ρ	reflectance
μ	microns
σ	Stefan-Boltzmann's constant (5.6686×10^{-12} watts cm^{-2} deg^{-4})
λ_m	wavelength of maximum of blackbody radiation curve
a	blackbody constant (2897.9 micron degrees) $= \frac{C_2}{4.965}$
c	velocity of light (3×10^{14} micron sec^{-1})
C_1	$2\pi c^2 h = 3.7413 \times 10^{-4}$ watt-microns
C_2	$hc/k = 1.4388 \times 10^4$ micron degree
h	Planck's constant (6.6252×10^{-34} watt sec^2)
k	Boltzmann's constant (1.38042×10^{-23} watt sec $degree^{-1}$)
$1/\pi$	total radiant flux per unit solid angle (central steradian)
T	absolute temperature (degrees Kelvin)
W	total radiant flux emitted per unit area (watts cm^{-2})
W_λ	radiant flux per unit area per increment of wavelength--watts cm^{-2} (micron $d\lambda)^{-1}$

Definitions as used in this report are:

Absorbance, (α). Logarithm to the base 10 of the reciprocal of the transmittance, thus $A = \log_{10} (1/\tau)$. Equivalent to absorptance.

Absorptance is a property of a sample; it is the ratio of the rate of absorption of radiant energy to its rate of incidence.

Absorption coefficient is a fundamental property of a material. It is a quantitative expression for the rate of decrease in radiant flux density in the direction of propagation of radiant energy through a material. Expressed mathematically,

$$W = W_o e^{-ax} \tag{1}$$

in which: W = flux density after passing through thickness x of the nonscattering material, W_o is the flux density at zero thickness just after penetrating the surface (thus not including the reflected portion of the incident radiation), a is the absorption coefficient, and e is the base of natural logarithms.

Absorption Length is thickness to opacity.

Absorptivity, a. Absorbance divided by the product of the concentration (c) of the substance (in gm/ℓ) and the sample path length (b, in cms),

$$a = \frac{\alpha}{bc}$$

Absorptivity, Molar. Product of the absorptivity and the molecular weight of the substance.

Attenuation length: distance in a material before energy declines to 1/e, i.e., to 0.368 of its original value.

Emissive power is the rate of thermal emission expressed as radiant flux per unit surface area.

Emissivity is a special case of emittance; it is a fundamental property of a material and is measured as the emittance of a specimen of the material that has an optically smooth surface and is sufficiently thick to be opaque.

Emittance is a property of a specimen; it is the ratio of its emissive power to that of a blackbody radiator at the same temperature and under the same conditions.

Extinction coefficient is a fundamental property of a material. It is a quantitative expression for the rate of decrease of radiant flux density in the direction of propagation of radiant energy through a material, due to both absorption and scattering. It is expressed mathematically by Eq. (1), in which case a represents the extinction coefficient.

Frequency, (ν): number of cycles per unit time.

Infrared: the region of the electromagnetic spectrum extending from approximately 0.78 to 300 μ.

Micron: unit of length equal to 10^{-6} meter.

Normal spectral emittance, (ϵ_λ) is the emittance ratio, taken at a specific wavelength (λ) between the sample emissive power and the blackbody power observed normal to the radiating surface. The energy ($\epsilon_\lambda \cdot W_\lambda$) expressed as the ordinate in the radiant energy calculation (and plots--see figures in Appendix B and C) was obtained by multiplying the energy found by the Planck formula (W_λ) by the emittance ratio (ϵ_λ) found in the experimental studies. These data were observed normal to the sample surface and hence have been considered as normal spectral emittance ratios. Ordinate numerical values should be decreased by $1/\pi$ for the total radiant flux per unit solid angle ("normal spectral emittance ").

Radiant flux is the rate of flow of radiant energy. It is analogous to current as applied to electricity.

Reflectance is a property of a specimen and is the ratio of the rate of reflection of radiant energy to its rate of incidence.

Reflectivity is a special case of reflectance; it is a fundamental property of a material and is measured as the reflectance of a specimen of the material that has an optically smooth surface and is sufficiently thick to be completely opaque.

Scattering coefficient is a fundamental property of a material. It is a quantitative expression for the rate of decrease in radiant flux density in the direction of propagation of radiant energy through a material, due to scattering. It is expressed mathematically by Eq. (1), in which case a represents the scattering coefficient.

Spectral: having a stated wavelength, or at a stated wavelength.

Spectral Contrast: A spectrum which has one or more peaks that diverge markedly from the average level of the remainder of the curve is said to have spectral contrast. (This may be seen by subtracting the last two columns in Table II).

Spectral emittance is the emittance ratio, taken at a specific wavelength.

Spectrograph: Instrument with an entrance slit and dispersing device that uses photography to obtain a record of spectral range. The radiant power passing through the optical system is integrated over time, and the quantity recorded is a function of radiant energy.

Spectrometer, Optical: Instrument with an entrance slit, a dispersing device, and with one or more exit slits, with which measurements are made at selected wavelengths within spectral range, or by scanning over the range. The quantity detected is a function of radiant power.

Spectrophotometer: Spectrometer with associated equipment, so that it furnishes the ratio, or a function of the ratio, of the radiant power of two beams as a function of spectral wavelength. These two beams may be separated in time, space, or both.

Thermal emission is the act or process by which radiant energy is emitted by a body as a consequence of its temperature only. This term is frequently shortened to "emission."

Transmittance, (τ) is a property of a specimen; it is the ratio of the rate of transmission of radiant energy to its rate of incidence.

Wavelength, (λ). The distance, measured along the line of propagation, between two points that are in phase on adjacent waves. The usual units are Å, mμ, and μ.

Wavenumber, ($\bar{\nu}$). Number of waves per unit length. The usual unit of wavenumber is the reciprocal centimeter, cm^{-1}. In terms of this unit, the wavenumber is the reciprocal of the wavelength when the latter is in centimeters in vacuo.

Frequency (sec^{-1})	Wavenumber (cm^{-1})	Wavelength (μ)
3×10^{14}	10^4	1
3×10^{13}	10^3	10
3×10^{12}	10^2	10^2

Although the dimensions of wavenumber ($\bar{\nu}$) and frequency (ν) differ from one another, it is conventional to express the frequency by the wavenumber unit. For example, a phrase such as "a frequency shift of 25 cm^{-1}" is often employed.

I INTRODUCTION

For many years the infrared spectrophotometer has been used chiefly for the structural analysis of organic materials. Recently it has been applied in the inorganic and mineralogical[1-4] fields, although its value as a quantitative tool[5] has been little utilized in compositional analysis of rocks.

The analysis of reflected infrared radiation from polished surfaces of minerals and rocks is an almost unexplored field, except for the works of Coblentz,[6,7] and Pfund,[8] and classic studies of Simon and McMahon,[9,10] and Gardon[11] on the radiative cooling properties of glass slabs.

The spectral analysis of emitted infrared radiation has been given prominence of late, with the studies of nose-cone reentry and the attendant problems of heat dissipation from refractory coatings. Again, however, the wavelength range of this interest is in the near-infrared, 1 to 5 μ(in wavenumbers, from 10,000 to 2,000 cm^{-1}),* and little investigation has been made in the region of diagnostic analysis for rock and mineral composition, i.e., the region of 10 to 25 μ (1000 to 400 cm^{-1}) and beyond.

With an eye to the ultimate application of infrared instrumentation in a system for remote compositional mapping of surfaces like that of the moon, a need was felt for more complete understanding of the fundamentals of infrared spectra, obtained by either absorption, reflection, or emission methods. Complicating effects due to the frequent compositional changes within mineral species in a rock needed to be evaluated at the same time that the mineral content was determined. Following the earlier work it was clear that studies should be directed toward:

(a) The feasibility of spectral <u>emission</u> analysis to determine lunar or planetary compositions, and

(b) The application of emission and reflection analysis using <u>powdered</u> samples.

---

* Wavelengths (in microns) may be readily converted to wavenumber notation (in cm^{-1}) by multiplying their reciprocals by 10^4.

In January, 1962, Stanford Research Institute (SRI) undertook a program of research for the National Aeronautics and Space Administration (NASA) under Contract No. NASr-49(04). A Final Report (I) was issued in September 1962.[12]

This contract was further extended; under this extension, SRI has had the following research objectives:

1. To define the characteristic infrared spectral peaks of minerals in mixtures such as are found in typical rocks.
2. To evaluate the effect of volcanic glass of varying composition upon the ability to determine these mixtures.
3. To evaluate the effect of particle size of the minerals upon their infrared spectra.
4. To show by infrared methods the possible modes of inclusion of water in minerals--bonded hydroxyl, free hydroxyl, zeolitic water, adsorbed water--and to establish means of determining the presence of water in lunar rock minerals.
5. To study the infrared emissivity of the major rock-forming minerals as a function of temperature.

These objectives were written in April 1962; by the time this research began, in February 1963, there had been a partial reorientation toward evaluation of methods more applicable to analysis of the lunar surface. Accordingly maximum effort was devoted to objectives 1, 3, and 5, emphasizing the effects of surface roughness and powdering on the emittance spectra of rock and rock-forming minerals.

This is the Final Report (II) on the work performed from February 1, 1963, to February 29, 1964.

II SUMMARY AND CONCLUSIONS

A. Summary

Three hundred thirty four spectra--256 emittance, 38 reflectance, and 40 absorption spectra--of selected rock and mineral samples were prepared in the wavelength region 2.5 to 25.0 μ (4000 to 400 cm^{-1}). Considerable emphasis has been placed upon direct emittance measurements of roughened rocks and powdered materials. From these spectra, 98 emittance, 37 reflectance, and 34 absorption spectra have been digitized at 0.1 μ (or equivalent wavenumber) intervals within the wavelength range from 5 to 25 μ.

The emission (W_{BB}) of the blackbody and the sample emission (W_S) have been compared by use of the computer, and an emittance ratio (ϵ_λ) has been calculated for each wavelength interval (λ). Computer programs have been developed which derive this emittance ratio ϵ_λ (from either emittance or reflectance data) and calculate the energy ($\epsilon_\lambda . W_\lambda$) from the sample for that interval, over 10 temperatures (from 150°K through 500°K). Absorption spectra are also recomputed and plotted.

The effect of a typical atmospheric attenuation was studied. There are few published data available and one must choose from a few sea-level paths. In this study, attenuations were computed by multiplying the sample emittance curve by the attenuation (α_λ) recorded by Taylor and Yates on March 30, 1956[13] for the atmosphere in a sea-level path length of 3.4 miles. This ($\epsilon_\lambda . W_\lambda . \alpha_\lambda$) curve then represents that portion of the radiant energy of the sample at 375°K which would be seen by an instrument 3.4 miles away, under the conditions of Taylor's and Yates' original experiment.

Average emittance over the wavelength interval 7.8 to 13 μ is in the vicinity of 0.87; emission minima for any given 0.1 μ interval average approximately 0.76. In other words, although the average emittance is 0.87, individual segments of the spectral emission

consistently average around 0.76, a considerable departure from blackbody (called "spectral contrast" in this report). Literature references are greatly confused on this point and often quote emissivities as $\epsilon = 1.0$ (blackbody) or as some arbitrary value, such as $\epsilon = 0.4$.

The identification and cataloging of the characteristic spectral peaks from infrared analyses of typical rocks are treated in Appendix A. The spectra included, for a suite of 29 rocks from the U.S. National Museum, were obtained by absorption, reflection, and emission techniques. All three sets of data for a single rock are plotted on the same figure so that a comparison may be made of the methods.

The effect of volcanic glasses (that is, noncrystalline material) on the absorption spectra of rock was treated in Final Report I. The effect of volcanic glass on the emittance spectra is discussed in the text of the present report (Section VIII) and in Appendix A, where spectra of several glassy and crystalline rocks, of equivalent chemical composition, are shown.

Particle size problems and the effect of fine grain size (and surface roughness) on reflectance and emittance of rock-forming minerals formed the bulk of this study. Section VIII is devoted primarily to these phenomena.

The possible modes of inclusion of water in minerals, and means of determining the presence of water, were discussed in detail in Final Report I (pp. 29-35). Several attempts were made during 1963 to obtain reflectance spectra of water-bearing minerals and rocks, in the region near 2.9 μ (3450 cm^{-1}), but these were not successful. Samples with surface moisture showed reflection maxima in these regions but the curves were not suitable for inclusion in this report.

B. Conclusions

1. Rock and mineral types can be determined from the wavelength position of the minima of absorption and emission, or the maxima of reflection, in their infrared spectra. Detailed study of the shape, intensity, and position of individual secondary minima (or maxima)

can reveal specific differences within mineral groups and between mineral assemblages in rocks. In essence, if a well-resolved infrared spectrum can be obtained, then the mineralogical composition of the sample can be defined, regardless of the technique used to obtain the spectrum.

2. Rock types can be defined if contrast appears on the spectrum. The converse is also true--if a contrast is present then the source must be definable. If the signal is seen through an atmosphere, the attenuation effect of the atmosphere itself must be considered in evaluating the source contrast.

3. Surface roughness, particle size, and physical discontinuities occurring within a surface (to a depth of a few attenuation lengths) have very significant effects on the contrast of the infrared spectrum of the material.

These effects are capable of severely limiting the usefulness of the emission method. A typical example of increased roughness is that shown by a quartz plate, 6 mm thick, one side of which was roughened by sandblasting. The normal spectral emittance (ϵ_λ) at 9.0 μ (the location of the fundamental vibration of the Si-O bond) increased from 0.28 on the polished side to 0.62 on the roughened side. The flat "shoulder" of the spectra at 10.0 μ also rose upon roughening, but only from a ϵ_λ value of 0.82 to 0.86, while at 11.0 μ roughening had no effect. A loose, fluffy powder of 25 to 45 μ particle size had a value of ϵ_λ at 9.0 μ of 0.91-- a much diminished spectral contrast.

Sample Type or Particle Size	Quartz Emittance (ϵ_λ)		Spectral Contrast
	Peak (9 μ)	Shoulder (11 μ)	(Shoulder - Peak)
Polished	0.28	0.89	0.61
Rough	.62	.89	.27
25 to 45 μ	.81	.90	.09
10 to 20 μ	.85	.91	.06
1 to 10 μ	.91	.89	--

Particle size causes problems only when it is below about 50 to 100 μ. These effects can modify the spectral contrast but in no case do they cause a wavelength shift great enough to confuse the composition of the source. With these grain sizes the distribution and percentage of finest sizes is far more significant than the average size in a powder.

4. All surfaces examined by emittance methods appeared as grey-bodies; that is, the envelope of their spectral radiance was not equal to that of the reference blackbody, but mostly had an average emittance (ϵ) of 0.75 or 0.80 over the wavelength range 7 to 13 μ. Samples were either grey and resembled a blackbody by possessing no spectral contrast, or were grey over most of their spectrum but departed markedly from the blackbody reference in localized regions of spectral contrast. In either case equivalent average emittance (ϵ) values could be obtained.

5. If the roughness of a surface of an optically thick body with no subsurface discontinuities can be adequately measured, the emittance of that particular surface should be mathematically predictable by factors relating it to the known emittance of a perfectly smooth surface of that composition.

6. The effects of subsurface discontinuities are much more serious, but the scattering caused by them is imperfectly understood. As a consequence it is impossible to predict the reduction in spectral contrast this mechanism can produce.

7. Absorption spectra have the highest spectral contrast and are the most definitive with which to work.

8. If reflection methods are used, flat polished surfaces must be prepared on the solid samples or hemispherical collection (or irradiation) techniques must be employed to avoid loss of energy by scattering. Powdered samples may be analyzed by the latter technique.

9. Of the three techniques, emission analysis is the most simple to perform, yet the most complex to interpret. Radiation from heated samples is collected by an optical system and reflected into the spectrometer for analysis. But the problems of surface porosity and

particle size in rough and powdery materials so affect the scattering coefficients that under most nonideal conditions it is only with difficulty that rock compositions can be differentiated by emission analysis. If the rocks are moderately smooth or if the grain size is relatively large ($\approx$ 1 mm), analysis of the emitted radiation is relatively simple.

10. Emission analysis is the method most attractive for lunar operations--in fact it is the only practical method if orbiting platforms are employed--but analysis by reflection of infrared radiation from a lunar roving vehicle still offers the greatest attraction, regardless of the degree of powdering of the surface to be analyzed.

III RECOMMENDATIONS

The scientific research itemized below is urgently required for the implementation of a compositional mapping program. The scientific basis for compositional analysis must be further evaluated as outlined. Detailed consideration can then be given to the most suitable mode of transportation of the experiment. In view of the over-all potential of this mapping technique, it is recommended that the several operational modes mentioned be considered.

Because of the lead times usually required to effect a completed spacecraft experiment, it is recommended that this work be initiated as early as possible. Portions of Part A (Sample Parametric Studies) have been performed already under NASA Contract NASr-49(04) with Stanford Research Institute.

The relative sequence of these studies should be as follows.

A. Sample Parameters

The effect of the following sample parameters should be determined by the use of both emission and reflection techniques on the same sample surface, using first standard spectrometers and then flight-weight units:

1. Solid rock, of possible lunar materials (dunite, chondritic meteorite, pumice, basalt, etc.)
2. Solid rock, with varying thicknesses of dusts:
   a. Of the same composition
   b. Of different compositions
3. Rock powders of varying:
   a. Particle size
   b. Porosity and void percentages (fairy castle structures, etc.)
   c. Grain angularities, frosting and internal impurity phases
   d. Surface stainings (either solid or liquid)
4. Vacuum sedimentation—effects on powders of single minerals or rocks, for varying:
   a. Packing densities
   b. Surface films (gases, etc.)

5. Dependence of emittance of powders with viewing angle for a selection of macrostructures

6. Absorption length (thickness to opacity) as a function of the viewing wavelength

B. Instrument Parameters on Flight-Weight Equipment

An SG-4 spectrophotometer unit, such as that built by the Perkin-Elmer (P.E.) Corporation under a NASA contract in 1961, should be used on this program to evaluate real responses from a prototype spacecraft instrument. The grating in this instrument should be replaced by one with a 7 to 14 μ range, used with cooled detectors of the Cd-, Cu-, or Hg-doped germanium or the Hg-, Cd- telluride types.

Samples would be those used in Part A. Source temperatures would be as low as possible (around 350°K). This unit can produce spectral scans with periods from 1 to as long as 20 seconds. This rate determines that portion of the areal coverage which is contributed by the motion of the spacecraft—the shorter the scan time the better the areal resolution.

Other units (for example, the PE "subminiature grating spectrometer" or units of comparable design) should then be reevaluated on the basis of the actual data from the SG-4 prototype.

C. Electronic Parameters and Telemetry Effects on Data

Spectral sampling rates, noise levels, and the necessary telemetry rates for maximum and minimum levels of data transmission should be established from the SG-4 prototype. Degradation of the signal by the spacecraft telemetry should be investigated.

D. Operational Modes

The following modes can be considered for emittance observations:

1. Balloon platforms at altitudes high enough to minimize the ozone absorption effects
2. Lunar orbiter
3. Lunar roving vehicle

Hemispherical reflectance should also be considered for a lunar-roving vehicle, if the lunar surface is not very rough with respect to the diameter of the hemisphere. Such a unit would use an active emission source and utilize a hemispherical collector for the returning (and scattered) radiation.

Multiple internal reflection techniques (FMIR) using Si- or Ge-probes with powdered samples should be carefully evaluated. This method, developed by J. Harrick of Philips Laboratories, appears not to suffer from particle size effects we have found with finely divided powders. It has already been demonstrated by Harrick that high-contrast absorption-type spectra can be obtained from powdered quartz, even when these powders are below 50 μ in particle size. Such probes, mounted on surface-roving vehicles, would be inserted into (or laid onto) the powdered materials and infrared spectra could be obtained, regardless of particle size.

A study of these factors would occupy about two to three man-years effort.

IV SAMPLE ACQUISITION

In this study many of the samples previously studied by absorption analysis were restudied by emission and reflection analysis. Where possible, purified rocks and mineral samples were used for these studies. Many of these samples came from the author's private collection which has been built up over the past eight years by requesting materials described in detail in the mineralogical literature. Thus each sample has a "pedigree" of known information.

A suite of 29 standard rock samples was received from the U.S. National Museum collection, following a request by Dr. William Fischer, Theoretical Geophysics Branch, U. S. Geological Survey, Washington, D.C. for their emission analysis. Detailed chemical and petrological analyses were available for most of the suite. Infrared absorption and reflection analyses have now been secured for them.

Samples used for absorption analyses were ground to below 5 μ in size and were embedded at 0.15% in potassium bromide (KBr) pellets for examination.

For reflection from a solid sample, a surface was prepared with a high polish by standard metallographic techniques, but with some of the more friable or vesicular volcanic materials it was exceedingly difficult to secure an adequate polish. These samples were analyzed by the emittance and transmittance techniques. Powdered samples were tamped into small containers so that they could be examined in the vertical sample positions of the hemispherical reflectance unit.

Samples used for emission analyses were analyzed in the condition in which they were received. If a surface was fresh and rough, it was placed uppermost in the heating chamber and allowed to radiate into the spectrometer. Some samples were sawed on one side and rough on the other, or sawed and polished, so that the emission from various types of surfaces on the same rock could be examined. With the quartz, silicon carbide (carborundum), and dunite samples, particle size separations

were made by elutriation in a water column. Sample ranges were obtained for particle sizes from 10 to 40, 40 to 80, 80 to 150 μ, etc.

Several samples of chondritic meteorites were obtained from Dr. Carleton B. Moore, Director of the Nininger Meteorite Collection at Arizona State University. These were samples of the Leedey, Farmington, Bruderheim, Haven, and Ladder Creek chondrites (or stony meteorites). Some were obtained in both powdered and solid condition, but whenever possible, one or more surfaces on the harder materials were polished to obtain reflection analyses.

V COMPUTER REDUCTION OF DATA

During the course of this study, approximately 40 curves were prepared by absorption analyses,38 curves by reflection analyses, and 256 curves by infrared emission analyses. These were analog curves drawn on standard x-y instrument recorders of conventional types.

Each infrared spectrometer has a different form of presentation of the data. Some presentations are linear with wavelength (in microns) or wavenumber (cm^{-1}). Instruments are either single beam or double beam and thus do not always have equal pen deflection for the same energy. It is necessary therefore, to normalize the data to a standard format. One can then directly compare absorption, reflection, and emission data of the same sample, on the same plate or drawing. In this study we have manually digitized the analog curves, processed the ensuing data through a digital computer, and replotted the digital output on a corrected, normalized format. Most of the figures used in the report have been prepared in this manner.

This normally results in a graph which has a sawtooth appearance if there are widely spaced data points. It is possible, however, to interpolate a smooth curve to pass through most of these points, but programming for this step became available only toward the conclusion of the project. Nevertheless, several figures have been included to show the possibilities of this type of interpolation (see Figs. 3, 84, 85).

Normal spectral emission curves for quartz in various particle sizes are shown in Fig. 1. This is a direct tracing of the analog curves obtained for five samples and a blackbody run consecutively on a single-beam Perkin-Elmer Model 112 infrared spectrometer. The energy represented by the blackbody curve (dotted) declines as a function of wavelength shown from 8.0 to 13.0 μ. The energy obtained by the spectrometer as a function of wavelength, for a source which is a polished X-cut quartz plate, is represented by the solid curve in the figure. The normal

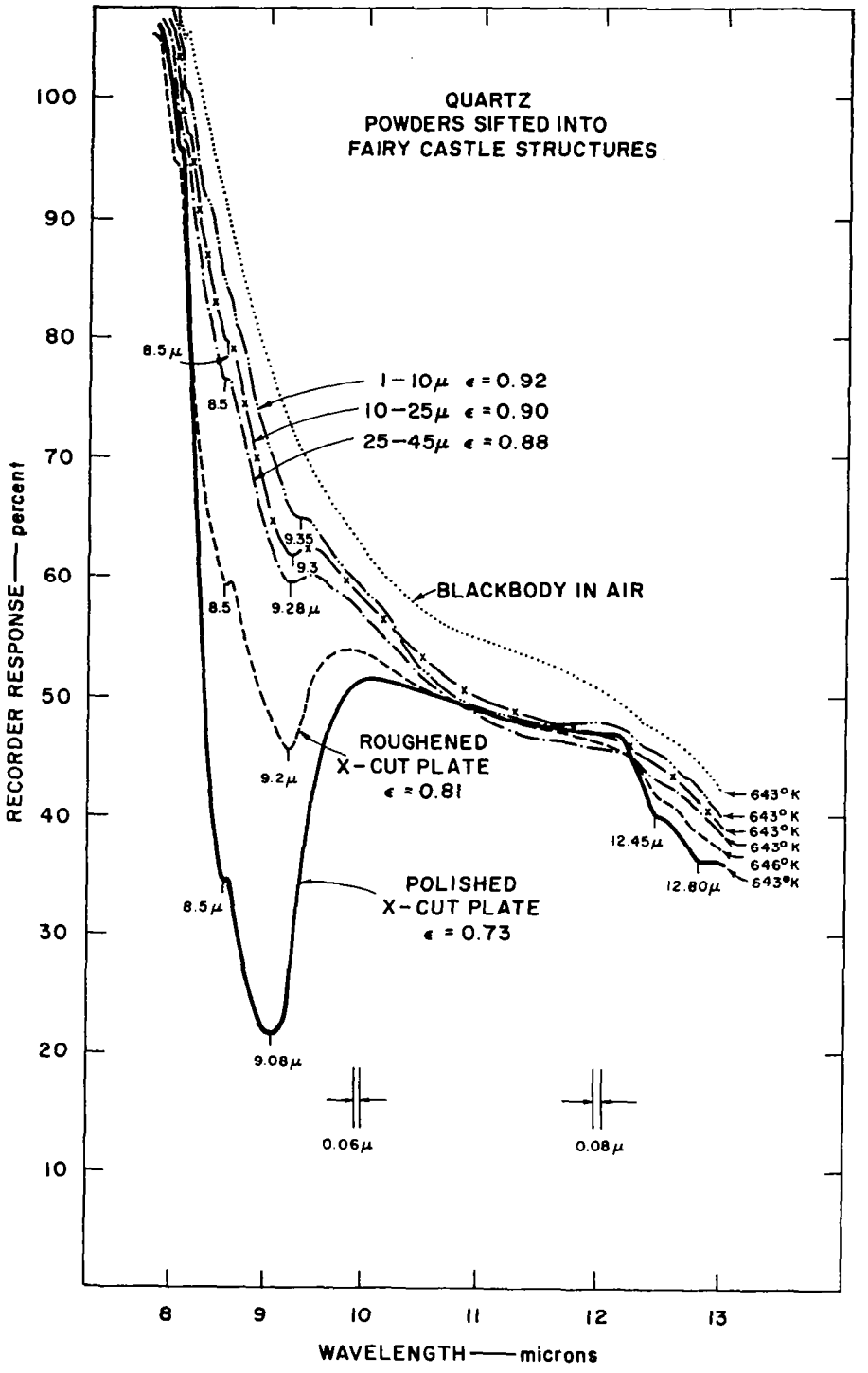

FIG. 1 NORMAL EMISSION CURVES FOR QUARTZ AND QUARTZ POWDER SIFTED INTO FAIRY CASTLE STRUCTURES.

spectral emittance (ϵ_λ) is defined as the ratio of the blackbody radiation to that of the sample radiation at any specific wavelength. This is obtained by scaling off both curves at the requisite wavelength interval (λ) on Fig. 1.

The normalized printout of the same data, after computer processing, is shown on the digital plot of Fig. 2. In Fig. 3 the data for the polished X-cut quartz plate and a standard absorption spectrum for powdered quartz have been processed by the Lagrangian interpolation and a smooth curve has been fitted through the two sets of data points. Thus, Figs. 1 through 3 represent the complete stages in the evolution of our computer processing and plotting programs.

The computer program was designed to process measurements made at 0.1 μ (or at 10 cm^{-1} intervals, depending upon whether the original measurements were recorded in wavelength or wavenumber format). Inputs for the absorption computations were values of absorbance ($\log_{10} 1/\tau$) taken at 10 cm^{-1} intervals, where "τ" is the transmission through the sample. Reflection measurements were also taken at 10 cm^{-1} intervals of the reflection (R_{100}) of a highly reflecting mirror (considered as 100% reflection) and the sample (R_s) reflection.

Calculations were made of the following parameters. For the <u>absorption</u> data a calculation of transmittance (τ), expressed in the form (0.XX τ), was made. For the <u>reflection</u> data the ratio (ρ) of the R_s/R_{100} was made and the calculation ($1-\rho$) was given as calculated emittance (ϵ). Calculations for <u>emission</u> data enabled the derivation of emittance (ϵ) from the ratio W_s/W_{BB}, where W_s and W_{BB} were the energy levels of the sample and blackbody curves, respectively.

Output statements were printed in the following forms:

1. Tabulation of ϵ_λ for each interval of wavelength (λ), where ϵ_λ is the normal spectral emittance ratio computed either from emission measurements or ($1-\rho$) reflectance measurements. In the case of the absorption measurements the value τ was tabulated. This was called an "unnormalized" value of the transmission (a more correct value would need a correction for baseline absorption effects).

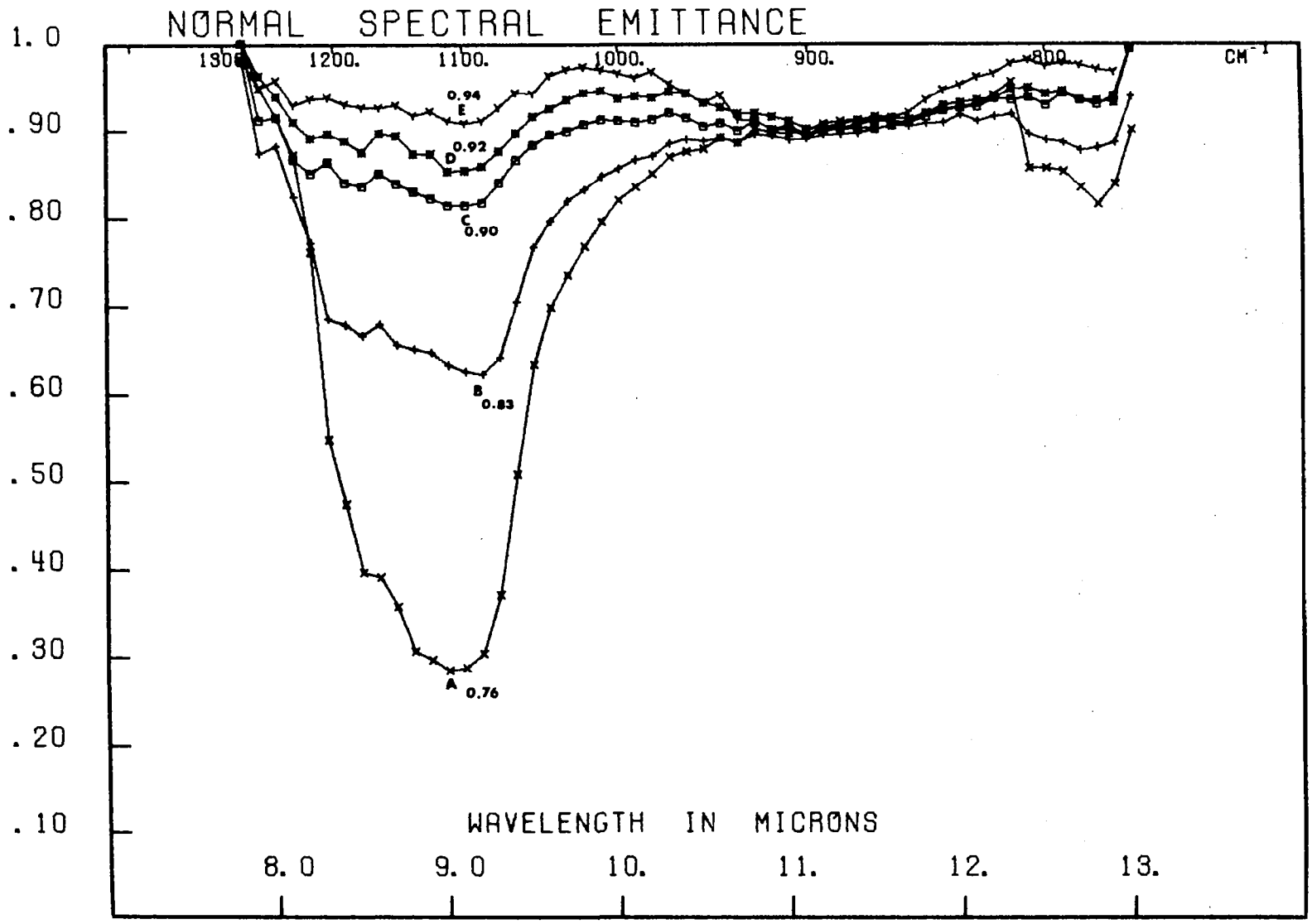

FIG. 2 NORMAL SPECTRAL EMITTANCE CURVES FOR QUARTZ AS A FUNCTION OF ROUGHNESS AND PARTICLE SIZE. Curve A, polished X-cut; Curve B, roughened X-cut; Curve C, 25 to 45 μ powder; Curve D, 10 to 25 μ powder; Curve E, 1 to 10 μ powder.

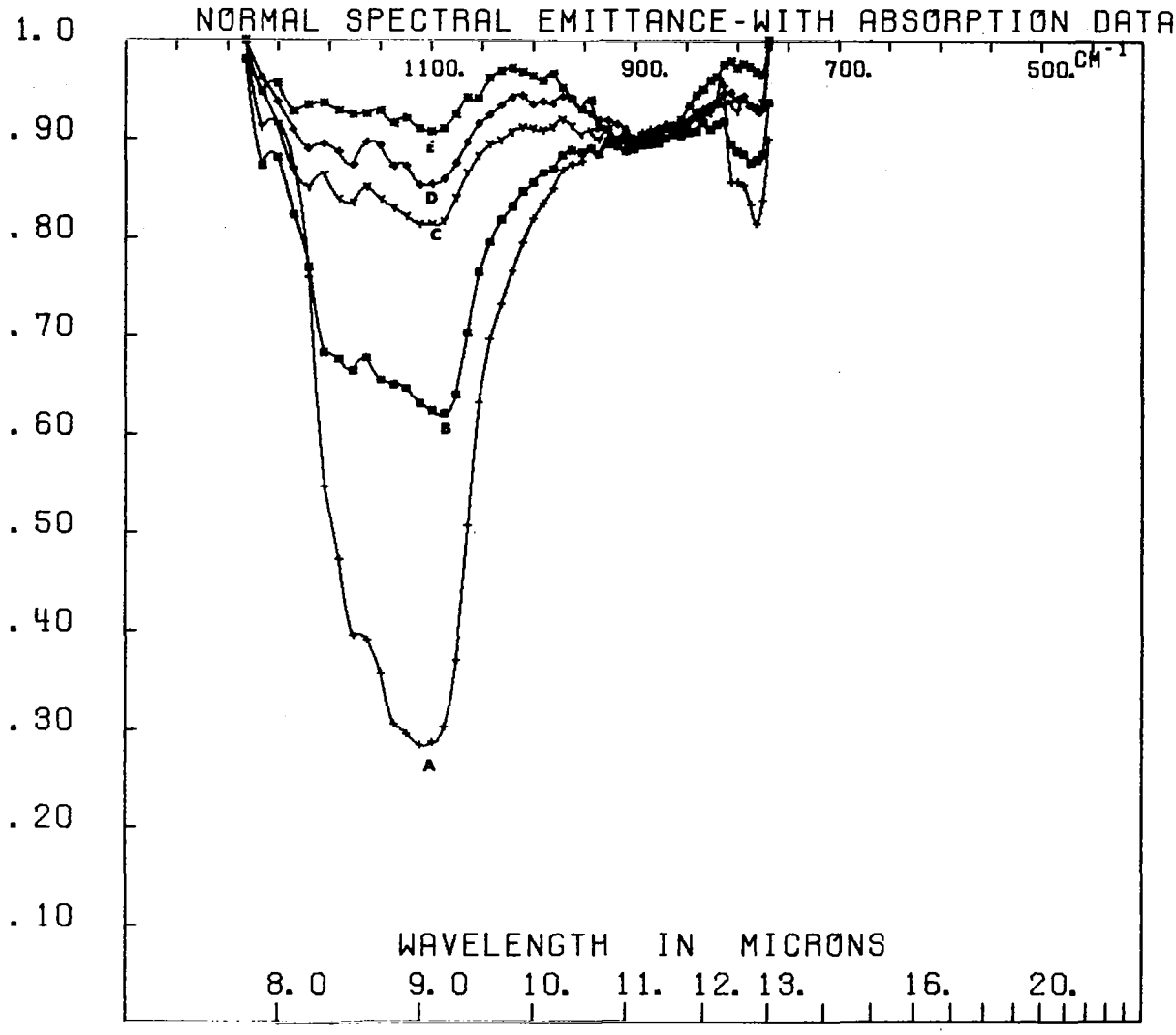

FIG. 3 NORMAL SPECTRAL EMITTANCE CURVES OF QUARTZ AS A FUNCTION OF PARTICLE SIZE, USING A LAGRANGIAN INTERPOLATION BETWEEN DATA POINTS.

2. Tabulation of the product $\epsilon_\lambda \cdot W_\lambda$ for a series of temperatures, at those intervals where W_λ is the hemispherical radiant flux per unit area, per unit increment of wavelength for a series of given temperatures--150, 200, 250, 300, 325, 350, 375, 400, 450, and 500°K. This was called "normal spectral emittance - radiant flux in watts/sq. cm - $\mu \times 10{,}000\ \pi$."

3. The calculated value at 375°K of $\epsilon_\lambda \cdot W_\lambda \cdot \alpha_\lambda$, (where α_λ is a typical 3.4 miles sea-level path, with atmospheric attenuation, as obtained from Taylor and Yates, 1956.[13]

Table I summarizes the computations of the experimental data.

Table I

SUMMARY OF EXPERIMENTAL DATA COMPUTED

Type of Analysis	No. of Spectra Run	No. of Spectra Digitized
Emittance Spectra	256[a]	98
Reflectance Spectra	38	37
Absorption Spectra	40	34
	334	169

Spectra normalized and replotted by digital plotter	
Shown in report text	53
Shown in appendices	116
Total	169

[a] Includes exploratory calibration, and repeat runs.

VI ABSORPTION ANALYSES

A. Previous Studies

Final Report I contained the results of extensive studies on the absorption analysis of many different types of rock-forming minerals. Absorption studies were made at that time of 370 rock and mineral samples and spectral information was collected in the range 2.5 to 25 μ (4000 to 400 cm^{-1}).

These early studies indicated that the methods of mineral analysis were not dependent upon the crystallinity of the sample, and that the composition of volcanic glasses, lavas, or crystalline rocks could be determined. The presence or absence of "water" could be determined and its form, whether as bounded hydroxyl $(OH)^{1-}$, or as loosely attached water molecules could be defined. It was considered feasible for a manned lunar laboratory to use the absorption analytical technique for rock analysis, although it was not deemed suitable to apply the potassium bromide sampling process to an unmanned operation. There is nothing intrinsically different between the operation of the infrared equipment on the lunar surface and its operation on earth. In fact the lack of lunar atmosphere would be a decided advantage, removing many of the absorptions from gases and obviating the necessity of using double-beam instruments. The sun could be used as a source of intensive infrared radiation for absorption measurements by being kept in view by sun-seeking mirrors during the two-week period of sunlight.

B. Present Studies

During 1963, 40 more curves were prepared of samples studied by absorption analysis. Minerals which were analyzed include synthetic stishovite (a high-density form of silica, SiO_2), low-temperature potassium feldspar, a suite of garnets, and several pyroxenes (the latter being a most complex type of mineral found in the basic igneous rocks).

Studies were made of the role of water in minerals. Attention was directed to the analyses of minerals such as buddingtonite (a new ammonium-bearing feldspar), hydrozircon (zircon containing several percent water), hydrogarnet, and several specimens of beryl and phenakite. Most of the 30 rocks studied by absorption analysis belong to the suite of rocks obtained from the U.S. National Museum. The resultant data after computer processing appear plotted in Appendix A. A suite of five chondrite (stony) meteorites obtained from the Nininger Collection was also studied by absorption analysis methods. The spectra are plotted on the same format and appear in Section IX of this report.

Shock-loading experiments on minerals, rocks, and meteoritic material also formed the basis for several absorption analyses. In addition to the results shown in Fig. 9 of Final Report I, dealing with quartz and albite feldspar samples after shock loading, the plagioclase and pyroxene extracted from samples of the Stillwater gabbro, after being submitted to a 350-kilobar shock, were studied. In Fig. 4 the infrared spectra of these mineral specimens (taken before and after the shock) have been displayed. The spectra have been displaced vertically for comparison purposes and are presented linearly in wavenumber along the abscissa.

As a result of this shock, the plagioclase spectrum has lost all its detail and now closely resembles that of a silicate glass. The post-shock pyroxene spectrum has a similar form, but still retains some of its characteristics, indicating the retention of some of the crystalline structure after the passage of the shock wave.

Other spectra of the Shergotty stony meteorite were prepared but have not been figured. These show that the plagioclase "glass" has a structure very similar to that shown by the shock-loaded plagioclase of Fig. 4. The pyroxene spectra also enforce this indication that the Shergotty meteorite underwent a considerable shock-loading during its passage through the atmosphere. Thus the study of the infrared absorption spectra of mineral and rock samples can yield considerable information about their structural history.

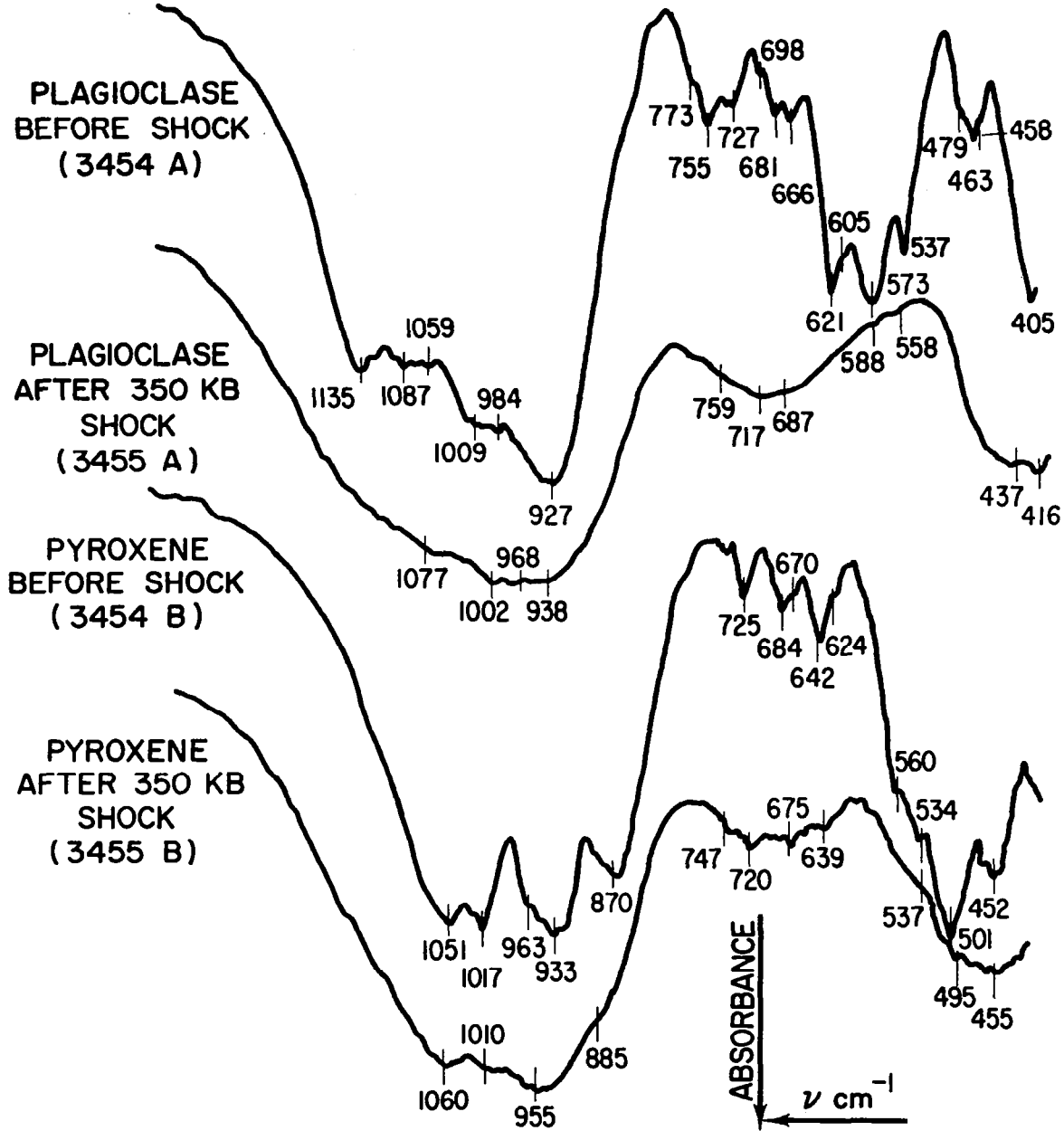

FIG. 4 ABSORPTION SPECTRA OF PLAGIOCLASE AND PYROXENE FROM THE STILLWATER GABBRO, BEFORE AND AFTER A 350 KILOBAR SHOCK LOADING. Wavenumbers quoted may be converted to microns by multiplying their reciprocals by 10^4.

1. Sample Preparations

A full description of the method for sample preparation using potassium bromide (KBr) pellets was contained in Final Report I (page 10). As a general method, the following technique of sample preparation has been developed.

Excellent infrared absorption spectra of minerals and rocks can be obtained with discs containing about 0.15% of the sample. A well-used technique involves hand-grinding 10 mg of the sample with 10 drops of absolute alcohol in a 60-mm mullite mortar, until the alcohol evaporates. This grinding reduces the grain size to below 5 μ (about 50% -2 μ) and this minimizes the scattering effects due to particle size. One and one-half milligrams of this preground sample are added to 1.00 gm of infrared quality KBr and blended in a dentist's amalgamator (Wig-L-Bug). Care must be taken to use a steel capsule with a small (4 mm) hard-glass bead during this step, or spurious peaks from the containers will result. About 350 mg of the blend are weighed out and then pressed into a vacuum die. About 65 tons per square inch pressure is adequate to obtain permanently clear discs which can be stored and reused years later.

It has been found extremely useful to dry the prepared KBr pellet overnight in a vacuum oven before analysis. If the oven is set at 110°C and a vacuum is drawn approximating one-third of an atmosphere, most of the water physically absorbed on the KBr pellet will be removed overnight. Such a preanalysis treatment results in a perfectly flat spectrum around 2.95 μ (3390 cm^{-1}), the region of strong absorption due to water. If the sample itself contains water, this is retained within the KBr pellet, although this too can be removed after prolonged drying at elevated temperatures. The structural position of the water, in samples with as little as 0.5% H_2O, can be clearly established by this method.

2. Experimental Technique

The KBr pellet is placed in the sample beam of a two-beam spectrophotometer and the spectrum is run in the standard manner. It has been found quite useful to continue the wavelength of study beyond that of

the NaCl prism (2.5 to 15 μ, 4000 to 667 cm^{-1}) into the longer wavelength region, that of the KBr prism (10 to 25 μ, 1000 to 400 cm^{-1}). Should additional instrumental facilities be available, it is strongly recommended that absorption analysis be carried still farther out into the longer wavelength regions towards 35 or even 40 μ.

The experimental techniques used in the absorption analyses of rock or mineral samples differ in no way from the standard analytical procedures used in the analysis of KBr pellets for organic or inorganic materials. Our spectra are run from 2.5 to 25 μ (4000 to 400 cm^{-1}) over the wavelength ranges of the NaCl and KBr prisms. If the rock samples contain water-bearing minerals, absorptions due to the OH stretching frequency will be observed in the vicinity of 2.7 to 2.85 μ (3700 to 3510 cm^{-1}).

If the sample contains carbonate, sulphate, phosphate, or any other simple anionic functional group, marked absorptions will occur in the vicinity of 7.0 to 9.5 μ (1400 to 1050 cm^{-1}) as in Fig. 5 (redrawn from Miller and Wilkins, 1952).[14] If the samples are silicates, as are most rock-forming minerals, then the strongest absorptions will be in the vicinity of 9.0 to 10.0 μ (1100 to 1000 cm^{-1}). Considerable detail will also be observed in absorption analyses of rocks and rock-forming minerals from the vicinity of 13.3 μ out to 25 μ (750 to 400 cm^{-1}). This spectral detail often continues well beyond 25 μ.

3. Computation of Absorption Data

The absorption data were digitized at 10 cm^{-1} wavenumber intervals from spectral curves run linear in wavenumber (cm^{-1}). The absorbance values were determined and from these a value of transmittance (τ) was obtained. This value of transmittance has been plotted on the curves in the report, but is expressed as an "unnormalized" value. By this term is meant that, for a true expression of the sample absorbance as distinct from sample plus pellet absorbance, correction should be made for the "baseline" absorbance of the pellet. This correction has not been made. The curves, therefore, lie at lower transmittance values than they should if only the effects due to the sample were considered.

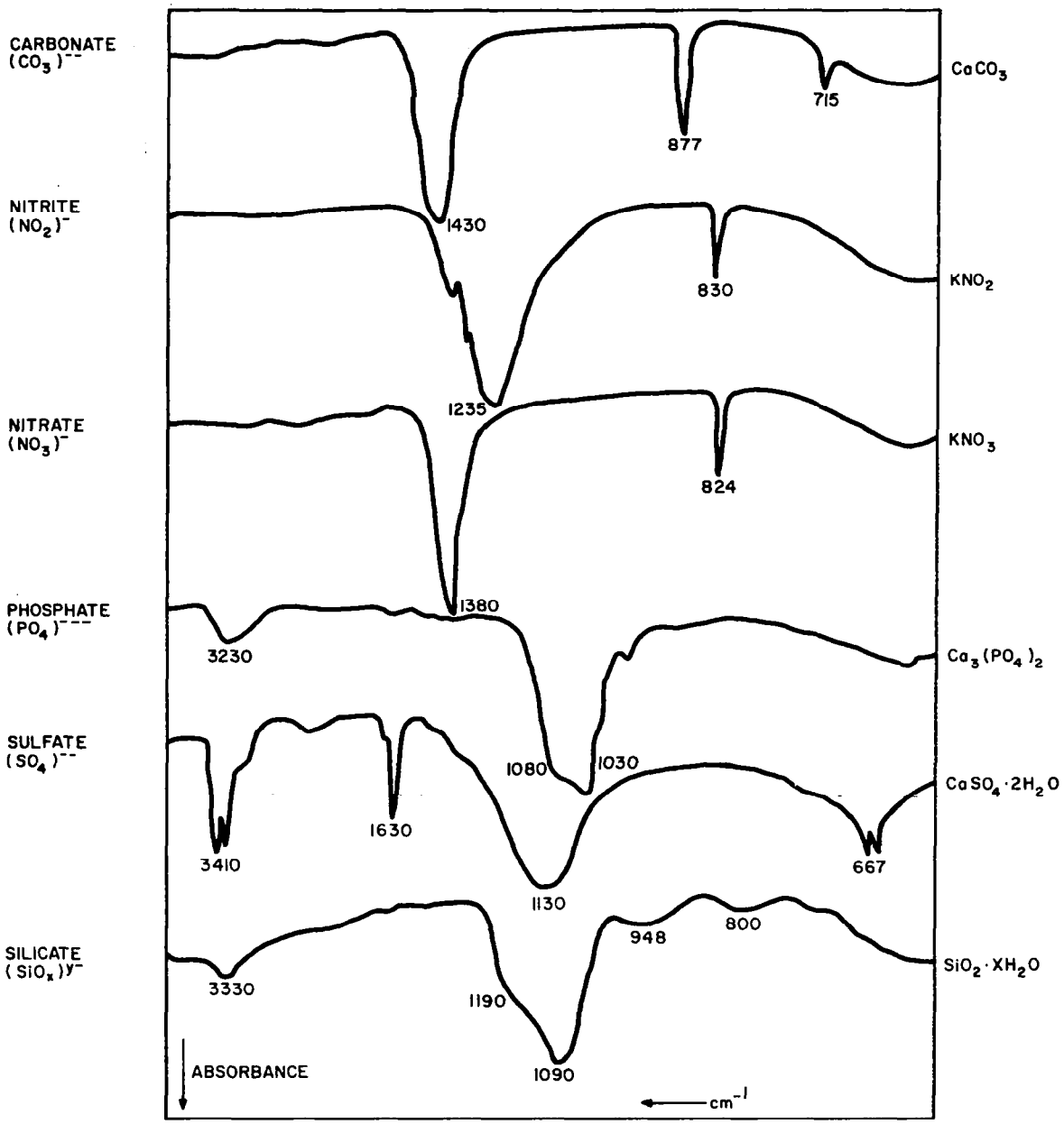

FIG. 5 ABSORPTION SPECTRA OF THE PRINCIPAL INORGANIC ANIONS.
This figure is redrawn from one in Ref. 14.

A further computational step should be performed and a baseline value should be selected for each frequency interval to complete the normalization of the absorbance data. Despite this omitted correction, radiant flux computations were obtained on the basis that the transmittance values were correct. Areas under the curve were also computed. Average transmittance values (indicated as τ) appear, together with the values for emittance and reflectance, in the descriptive material facing the curves in Appendix A.

4. Error Analyses

Spectrophotometer settings for absorption analyses were contained in Final Report I, Table II, page 13, for the Perkin-Elmer PE221 prism-grating machine. As an adjunct to such settings calibration points were placed on each sheet before each analysis was made. Absorption peaks for water vapor (2.676 μ, 3737 cm^{-1}; and 23.87 μ, 419 cm^{-1}), for carbon dioxide (14.99 μ, 667 cm^{-1}), for ammonia vapor (10.07 μ, 993 cm^{-1} and 11.01 μ, 908 cm^{-1}) and for a polystyrene film (6.25 μ, 1600 cm^{-1}) were used for this purpose. Each point on the absorption curve could be corrected to an absolute value based on the known wavelength or frequency values for these calibration points. In most curves it was not necessary to correct each peak more than ± 3 cm^{-1}.

These corrections, however, were not applied to the 100 points sampled between 1400 and 400 cm^{-1} for the computational program, as the corrections invariably were within the sampling interval (10 cm^{-1}). This is not to say that such corrections should not have been made, but this particular aspect was not written into the computational program.

Reproducibility of the method was assessed in Final Report I (Figs. 13 and 14). In almost every case ± 2 cm^{-1} errors could be expected between replicate discs prepared from the original sample. This is the variance of the total sampling process.

VII REFLECTION ANALYSIS

A. Previous Studies

The technique of analysis by reflection of infrared radiation was discussed at length in Final Report I, commencing on page 87. In the present report several of these figures have been reintroduced, showing the variation of reflection with the specific orientation of a quartz oscillator plate (Fig. 7), the changing reflectance with temperature in a Z-cut quartz plate (Fig. 62), and the relationship between absorption and reflection spectra (Fig. 8).

Most of the reflection studies performed during the first study were of polished surfaces of rocks. It was established that the positions of the spectral peaks were dependent upon the bulk composition of the rock. Thus an "acid" rock composition would show a spectral reflectance peak near 9.26 μ (1080 cm^{-1}), and a "basic" rock composition would show a peak in its reflectance spectrum near 10.87 μ (920 cm^{-1})--a "peak shift" of 1.6 μ (about 160 cm^{-1} at this point). Figure 6 shows reflectance spectra for a series of rocks ranging in composition from acid to basic showing a serial peak shift with changing composition.

These peaks also did not change in wavenumber with increasing grain size (Fig. 6). If a rock had a given chemical composition and was in the physical form of glass, felsite, fine-grained volcanic flow, or medium-grained or coarse-grained plutonic rock, its spectral maximum in reflection remained fixed in wavelength (or frequency). As the crystals formed in the earliest stages of crystallization from glass, smaller peaks appeared as modifications superimposed on the main spectral maxima. These modifications increased in size as the crystals grew and the rock lost its content of disordered silicate glass. Spectra may be considered to change from a simple bimodal curve to that multipeaked spectral curve which is typical of crystalline rock.

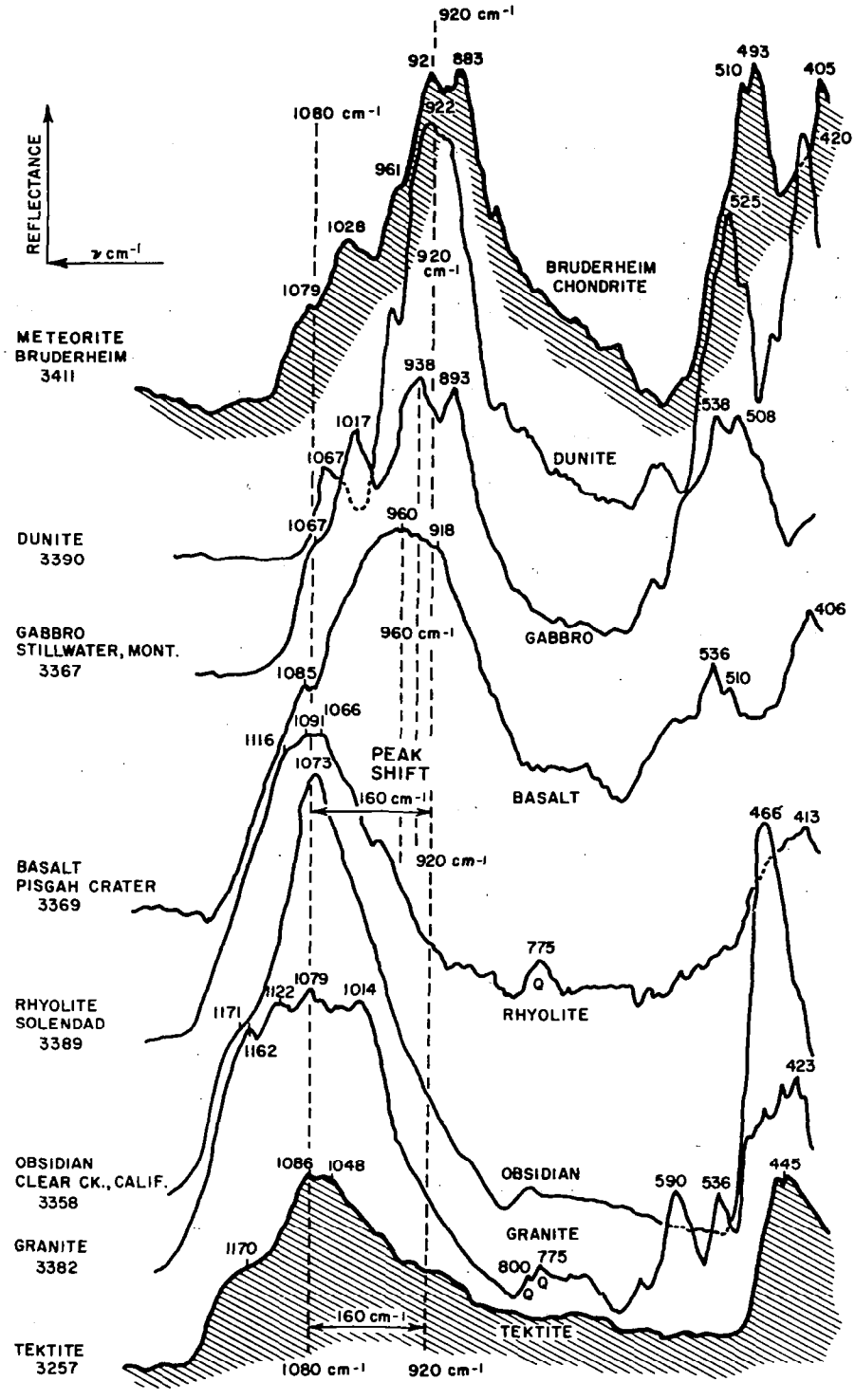

FIG. 6 REFLECTANCE SPECTRA OF TEKTITES AND CHONDRITIC METEORITIC MATERIALS (shaded), COMPARED WITH TYPICAL ROCK SPECIMENS. All samples were highly polished before measurement, curves have been displaced vertically for display, and reference beam was attenuated approximately 40% during the measurements.

Using these criteria, the acid rocks (granite) can be differentiated from the basic (diabase and peridotite) rocks by infrared reflection analyses, and the degree of crystallization from a glass can be assessed.

B. Present Study

During the present study, a total of 38 spectral reflectance curves has been prepared, but this does not include 10 curves prepared by TRW--Space Technology Laboratories (STL) using integrated reflectance methods of powdered samples.*

1. Solid Specimens

a. Sample Preparation

A surface of high polish is prepared over a flat surface about 2 cm × 2 cm square. If the sample is a single crystal, the orientation of that polished face is recorded since it will clearly influence the spectrum obtained. Figure 7 shows the differences between reflectance spectra of X-cut, Y-cut and Z-cut (basal section) of quartz oscillator plates, including the effect of a 45° rotation of the X-cut plate. Figure 8 compares absorption and reflection spectra for various forms of silica, redrawn from Sevchenko and Florinskaya (1956).[15]

b. Experimental Techniques

For infrared spectral reflection analysis it is necessary to attach a small, front-surfaced, prism-mirror system to one beam of the spectrometer. This prism deflects the beam sideways onto the polished surface at an incident angle of 30° to the normal. The radiation, when specularly reflected by the polished surface, is caught on a second mirror and passed along the original optical path into the instrument. The setting of the mirrors, the angle of attachment of the polished surface, and the attenuation of the reference beam are all parameters which must be kept optimum.

---

* These 10 curves were prepared by Drs. Eugene A. Burns and J. T. Bevans of STL, Redondo Beach, California.

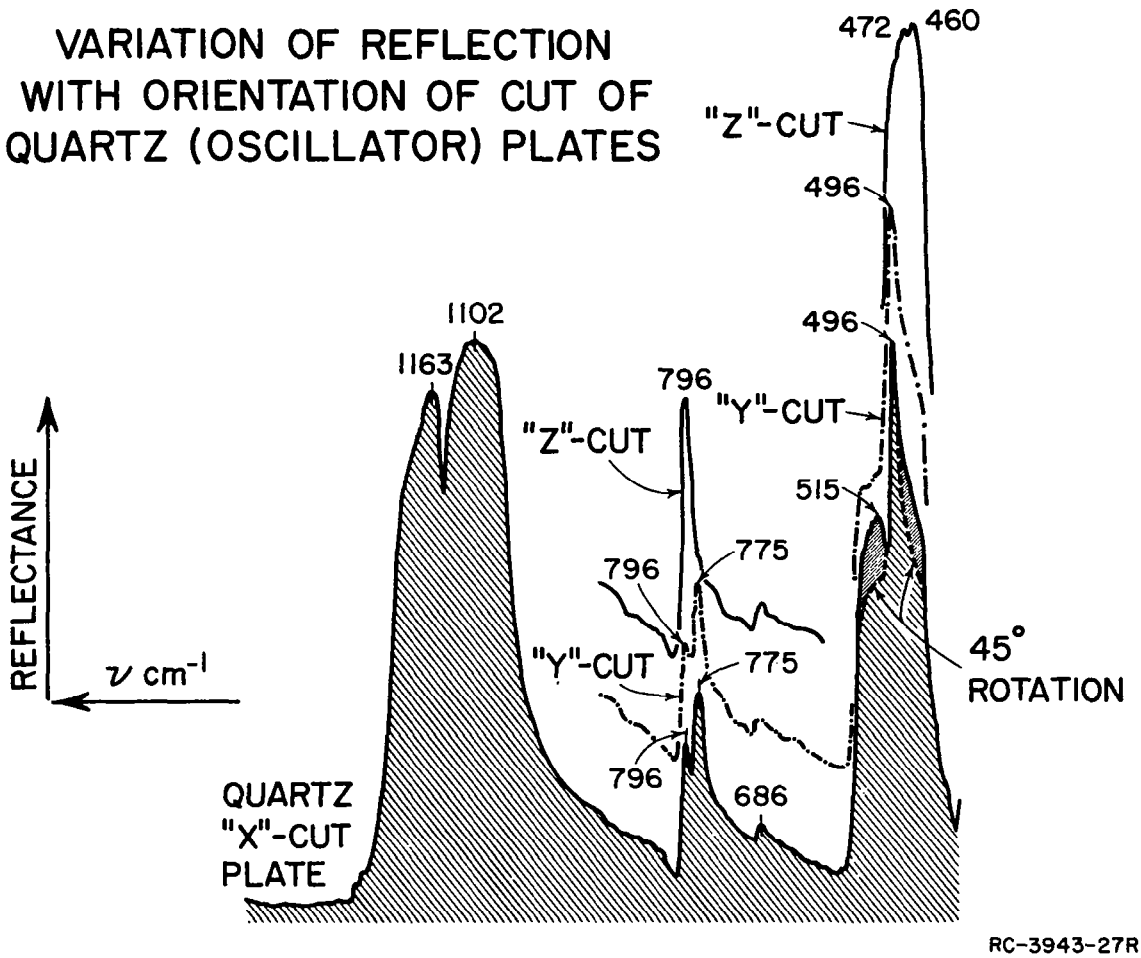

FIG. 7 VARIATION OF NEAR-NORMAL SPECTRAL REFLECTION WITH ORIENTATION OF A QUARTZ OSCILLATOR PLATE.
The curves are displaced vertically.

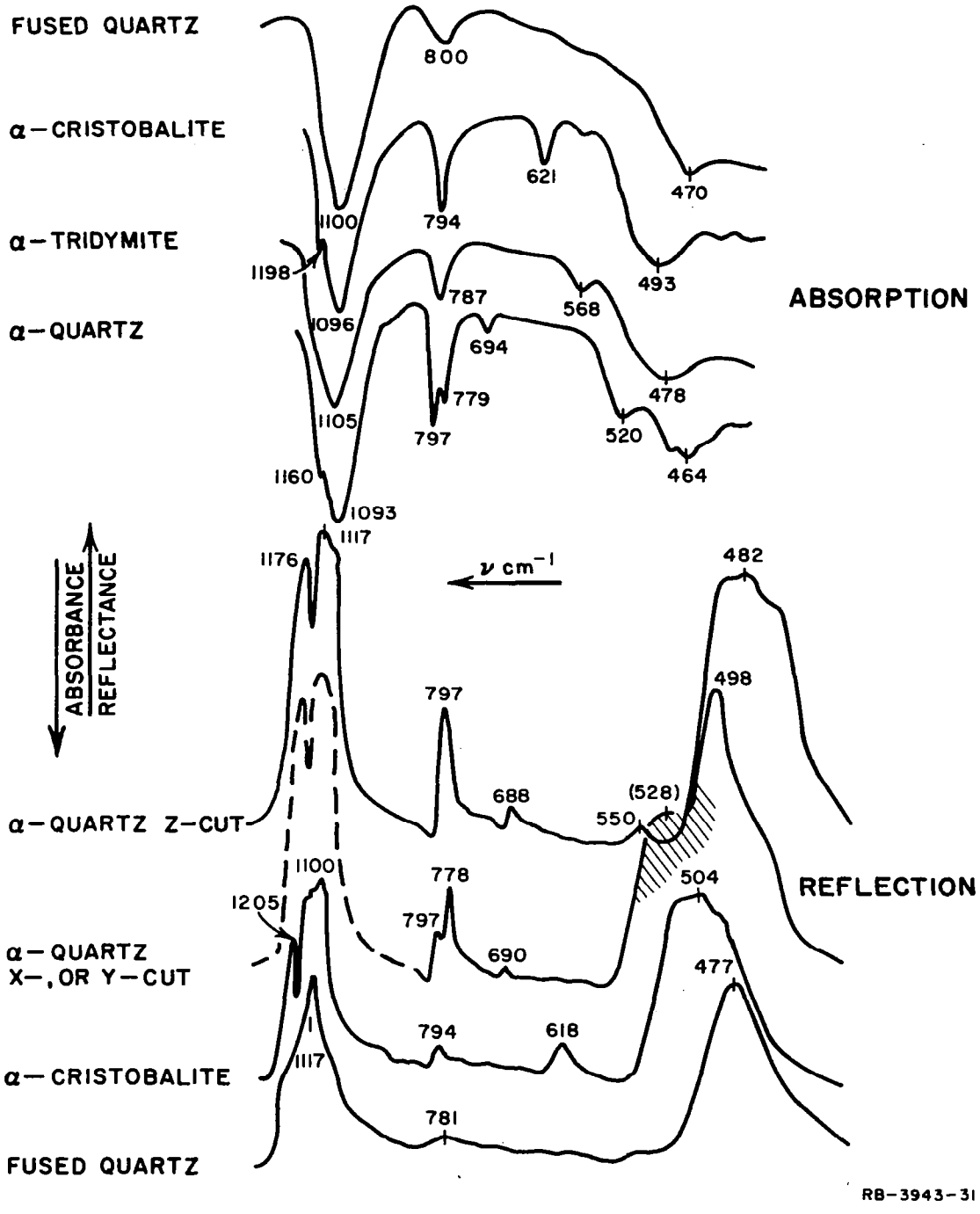

FIG. 8 COMPARISON OF ABSORPTION AND REFLECTION SPECTRA FOR VARIOUS SILICA MODIFICATIONS. The curves are displaced vertically. The figure is redrawn from Figs. 1 and 2 of Ref. 15.

The amount of reflected radiation which can pass from the polished surface into the entrance slits of the instrument is strongly conditional upon the quality of the polish. We have termed the reflectance measurements "normal spectral reflectance" although they were obviously obtained at a moderate angle (30°) away from the normal. All spectra discussed in this report were obtained in the same manner and the results are directly comparable.

No attempt was made to collect the scattered radiation hemispherically with the solid samples, although this method was used with the powdered samples. It would be most beneficial to have such a collecting mechanism, as more of the energy incident upon the surface could be refocused into the optics of the spectrometer. It is considered that such scattering will be constant as a function of wavelength within the relatively small intervals under discussion (7.14 to 25 μ, 1400 to 400 cm^{-1}) although it is clear that at the shorter wavelengths this could be an appreciable problem.

Experimental technique is relatively simple.

(1) A "100% baseline" curve is run by fixing a highly reflecting mirror to the sample position of the reflectance attachment when mounted in the sample beam. The spectrum of this mirror (R_{100},λ) is scanned over the wavelength range of interest.

(2) The mirror is then replaced by the polished surface and the sample spectrum (R_s,λ) is prepared in the same manner. The reference beam was also attenuated to 40% of its original level and the polished surface is scanned again to produce an "attenuated spectrum." This optical exaggeration of the original curve form the basis for the tracings used in Final Report I. The spectra used in the calculations in the present report were those of the unattenuated sample in all cases.

(3) Calibration points were again impressed in the same manner as with the absorption analysis. All spectra were run on the Perkin-Elmer PE221 prism-grating instrument over the wavelength range 2.5 to 25 μ (4000 to 400 cm^{-1}), from which the section 7.14 to 25 μ (1400 to 400 cm^{-1}) was used in the reflectance calculations. Data were read at 10 cm^{-1} intervals from spectral curves linear in wavenumber (cm^{-1}).

c. Computation of Reflection Data

The ratio between the two reflectance measurements, R_s and R_{100}, at any wavelength (λ) was calculated as the parameter (ρ_λ). Kirchhoff's Law states that, for a polished surface at thermal equilibrium conditions, $\alpha = \epsilon$ and $\alpha = \epsilon = 1.0 - \rho$, where α = absorptivity, ρ = reflectivity, and ϵ = emissivity. With such a polished surface (where scatter is almost zero), the spectral emittance can be computed from reflectance measurements.

Such a calculation was performed on reflectance measurements of the polished dunite sample and has been plotted as ($1 - \rho$) in Fig. 9, over the interval between 7.14 and 25 μ (1400 to 400 cm^{-1}). Between 9 and 12.5 μ (1110 and 800 cm^{-1}) a strong reflection maximum appears, represented in the re-plotted data by a strong minimum (of emittance) centered at 10.80 μ (925 cm^{-1}). Additional reflection maxima (and thus emission minima) occur at 19 μ (525 cm^{-1}) and at 23 μ (435 cm^{-1}). The 10.80 μ peak and the 23.0 μ peak are both Si-O stretching fundamentals. The 19.00 μ peak is probably related to the Mg-O stretching frequency of the magnesium silicate minerals in the dunite.

d. Error Analysis

The level of error in wavenumber (cm^{-1}) is again dependent upon the calibration points impressed on the chart paper before the sample curve is run. Approximately ± 2 cm^{-1} was found to be the usual error between replicate runs standardized by this calibration procedure.

Errors in the ordinate (reflectance) measurement are much more serious, and are dependent primarily upon the degree of polish and the orientation of the sample on the mirror mounting. If, in consecutive runs,

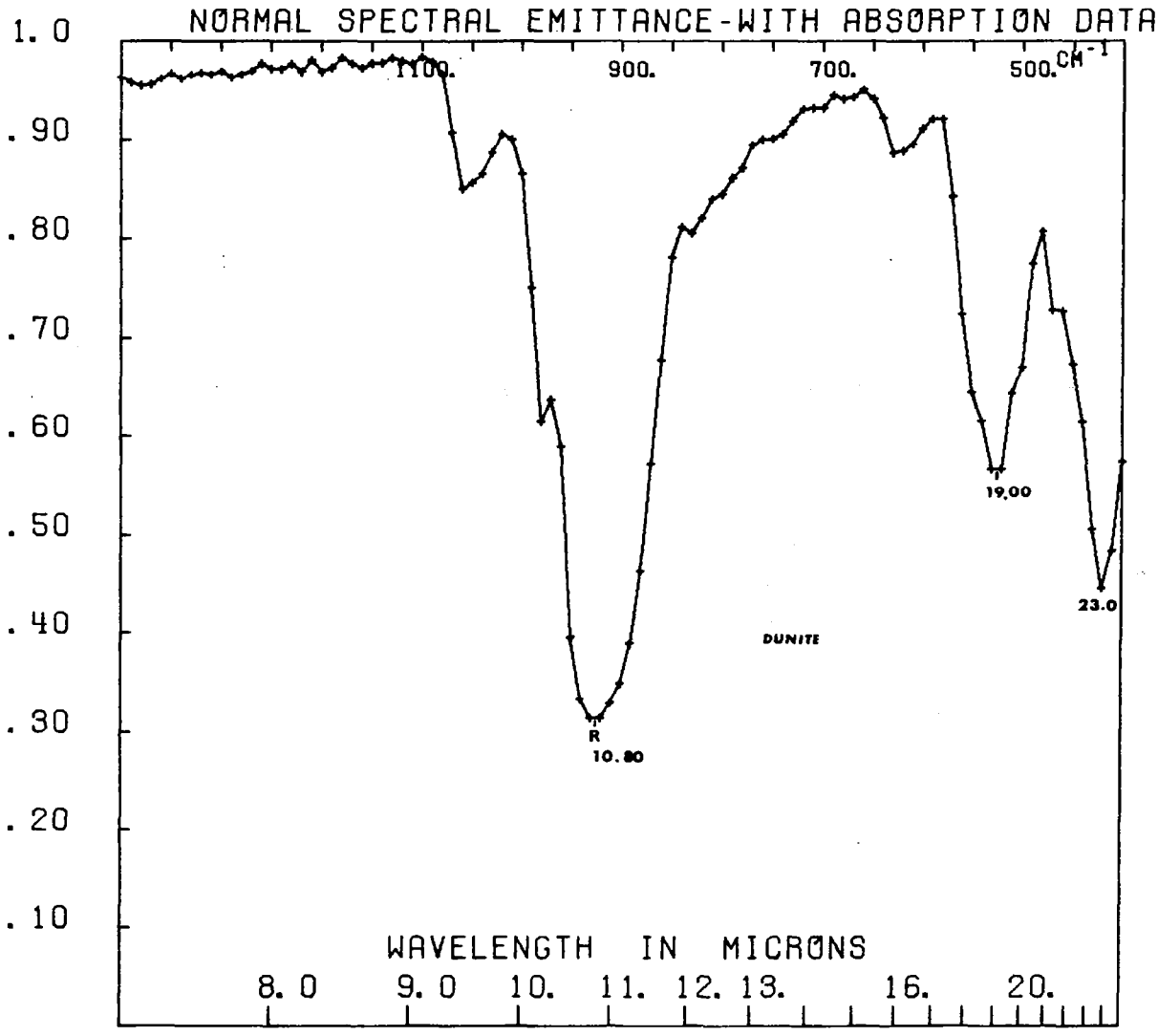

FIG. 9 REFLECTANCE MEASUREMENTS ON A POLISHED DUNITE SAMPLE, REPLOTTED, (1 - ρ), AS NORMAL SPECTRAL EMITTANCE CURVE. Three reflectance maxima now appear as emittance minima at 10.80, 19.00, and 23.0 μ.

a sample remains unchanged in its orientation, the spectrophotometer pen will trace almost precisely the same curve as before. Should the sample be changed in its orientation (for example, rotated 180°), the type of polish on the surface will have an effect upon the percentage of the incident beam which is reflected through the constricted geometry of the reflectance attachment. One might imagine, for example, a sawtooth, fine-scaled grid on the sample, which could give a markedly different orientation depending on which side of the sawtooth the rays were incident. It has been our experience, however, that replicate runs are within 5 to 10% of the energy level of the original run. In almost all cases, however, the samples were not rotated and, if run, were run consecutively in their original orientation. In this case, less than 5% error was experienced in the energy levels of these consecutive runs.

Another problem appears in the rotation of specimens which differ in their crystallographic orientation or mineral content with direction. The graphic granite specimen (USNM 377) and the granite samples (USNM 158) shown on Figs. A3 and A4 (Appendix A) indicate the difference with rotation of the specimen. In each case there was a strong fabric or mineralogical orientation and different minerals thus were sampled by the spectrophotometer in the consecutive spectra. This is an additional complicating factor to that of a changed surface characteristic or angle of orientation during a rotation of the specimen. In Fig. 7, a solid quartz plate (X-cut) shows a rotation effect.

Attenuation of the reference beam results in an optical magnification of the subsequent curve on the chart paper. If one knew precisely, wavenumber by wavenumber, the attenuation factor (which is approximately 45%, that is, 2-1/2 × magnification), it would be possible to digitize the expanded curve (which shows greater detail than its original), and then mathematically correct the optical exaggeration by the known attenuation factors. We have used only the original sample spectrum in this report and have made no attempt as yet to work with the more detailed attenuated spectrum. The attenuated spectra which were traced onto the figures of Final Report I were thereby enhanced by this optical exaggeration, but this exaggeration remained a constant function of a specific wavenumber for consecutive samples.

Computation of the data to yield emittance values is therefore conditional upon the same type of error to which the reflectance measurements were subjected, that is, consecutive runs (with an unchanged orientation) yield closely comparable calculated emittance curves. Samples which were rotated between consecutive runs often show a discrepancy between their two calculated emittance spectra.

2. Powdered Specimens

In Final Report I there was a short discussion (page 14) of reflectance spectra obtained from powdered samples which were bricketted and polished by standard metallographic techniques. There is less material to reflect with a powdered sample than with a solid sample, and the reference beam had to be attenuated 40% in all cases to obtain adequate response from the spectrophotometer.

Reflectance analysis offers an extremely diversified and significant approach to the problems of rock analysis, particularly under lunar conditions. It has been found that when adequate account is taken of the scattered radiation (by the use of hemispherical collection mirrors or by the use of multiple internal reflection) the spectra of powdered samples of rock-forming minerals can be readily obtained with a high degree of spectral contrast. By measurement of the reflectance integrated over a hemispherical mirror, thereby including scattered components, it is possible to determine ϵ_λ by calculation from the reflectance (ρ_λ) for powdery substances. Harrick* was able to obtain high contrast spectra of powdered quartz samples (1 to 45 μ size) by using multiple internal reflection at a silicon slab-powder interface.

a. Sample Preparation

Samples of rock and mineral powders were elutriated in water columns to secure particle sizes with ranges within certain required limits. Care was taken to remove the finer powders adhering to the samples so that the emission and reflectance could be obtained from the material at that particular particle size without additional scattering

* Personal communication to the author.

effects from finer material. Although it is preferable to perform reflectance measurements with samples in a light, fluffed-up condition (such as in the Hapke fairy castle structures), the experimental conditions imposed by Bevans' equipment (at STL) were such that samples were required to be packed into the sample-holder; thus pore space was reduced to a minimum.

Point by point plots were made at every wavelength interval by rotating the sample-holder, obtaining first a reflectance from a polished gold plate on the back of the holder, then, by rotation, the reflectance of the sample. The ratio of these two measurements gave the hemispherical spectral reflectance. By subtraction from unity this then gave the (calculated) hemispherical spectral emittance.

b. Experimental Techniques

The experimental unit which was employed was developed by J. T. Bevans at STL. With the cooperation of Dr. Eugene A. Burns, the reflectance spectra of powdered rock and mineral samples, previously used in other aspects of this study, can be shown, prepared from the integrated reflectance measurements made on Bevans' apparatus.

The apparatus incorporates a blackbody source (with a temperature range of 500 to 1400°K), two 7-1/2° off-axis, paraboloid, front-surfaced mirrors, temperature-controlled sample-holder, and a Perkin-Elmer model PE13C infrared monochrometer and detector (see Fig. 10). For this work the powders were compacted into a sample cup since the examination was carried out at a vertical sample-surface inclination. The mirrors and sample-holders were maintained by ambient temperature throughout the measurements by conduction with circulating, cooled water.

The spectral emittance curves (calculated from reflectance measurements) using this apparatus are shown in Figs. 11, 12, and 13. As the original reflectance measurements yielded absolute values of spectral reflectance, the emittance values ($\epsilon_\lambda = 1 - \rho_\lambda$) were of a similar caliber.

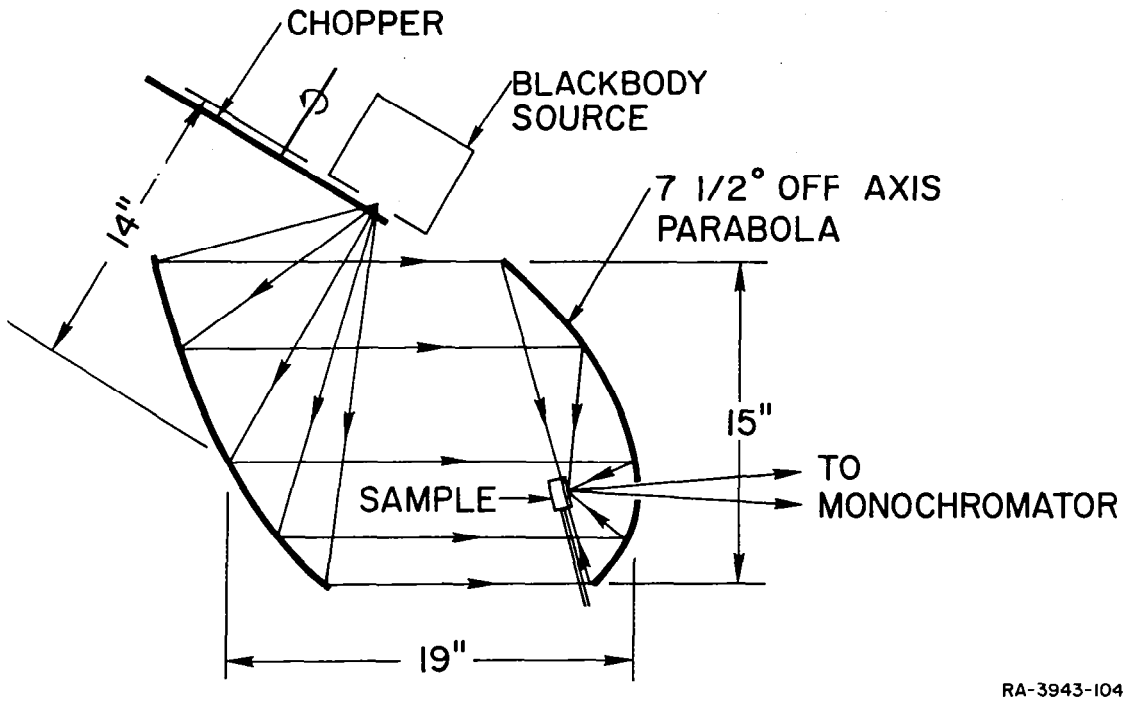

FIG. 10 OPTICAL CONFIGURATION OF THE STL PARABOLOID REFLECTOMETER. *Sample holder rotates in the plane of the figure so that alternately the sample surface and a polished gold plate may be viewed at any selected wavelength.*

These curves clearly indicate that acid and basic rocks (granite and dunite) may be differentiated even down to the particle size range of 100 μ. As might be expected, some of the finer structure which is seen with polished specimens is obliterated, or is less definite, in the spectra of powdered samples; however, the diagnostic use of the spectral emittance curves is clearly demonstrated.

The effect of particle size on the calculated emittance curves for alumina is shown in Fig. 12 and that for quartz in Fig. 13. As the particle size of alumina is lowered from that of a single-crystal sapphire to those of polycrystalline platelets, to coarse-grained material, and finally to a 0.02 μ powder, the calculated emittance curves approach a blackbody radiation curve. In fact the 0.02 μ alumina is an almost perfect blackbody in the wavelength range 8.0 to 25.0 μ (1250 to 400 cm^{-1}). Similar studies of quartz, shown in Fig. 13, reveal the same

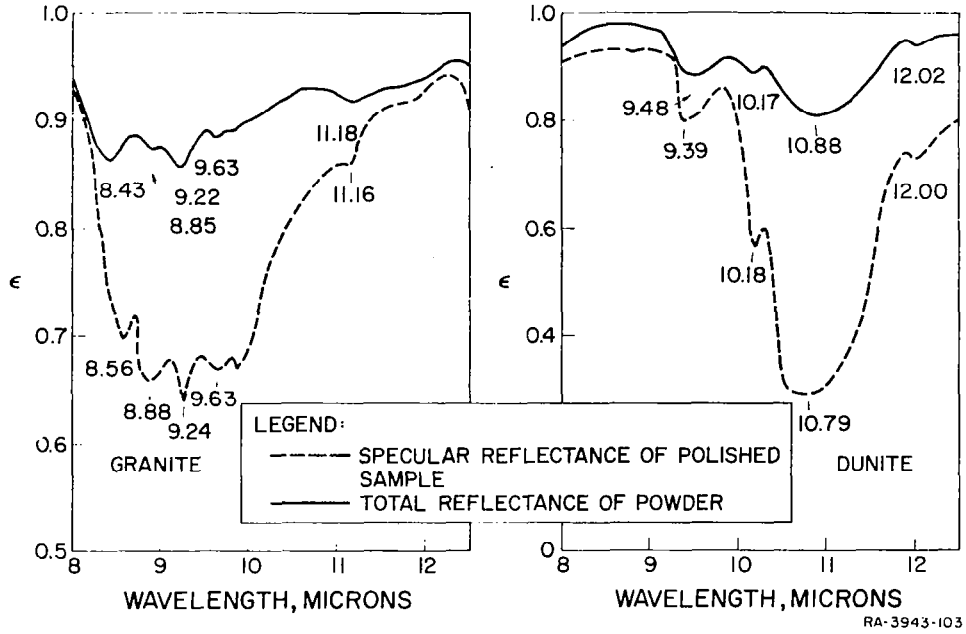

FIG. 11 SPECTRAL EMITTANCE CURVES OF GRANITE (left) AND DUNITE (right) SAMPLES, BOTH POLISHED (dashed) AND POWDERED (solid curve). Powder is approximately 100 μ in size. Data from STL.

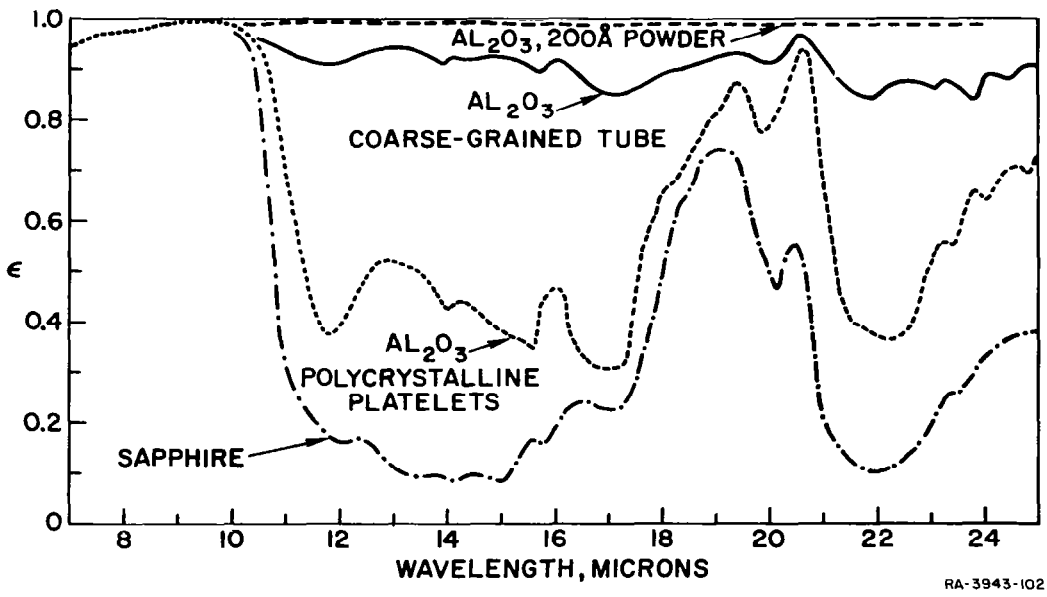

FIG. 12 SPECTRAL EMITTANCE CURVES FOR ALUMINA (Al_2O_3) IN VARIOUS SURFACE AGGREGATIONS, CALCULATED FROM REFLECTANCE DATA BY STL. Curves for 0.02 μ (200 A) powder appear almost as a blackbody. Curves for a coarse-grained tube (solid curves) and for polycrystalline platelets (dashed curves) are contrasted with that of a sapphire single crystal plate (dash-dot curves) in the figure.

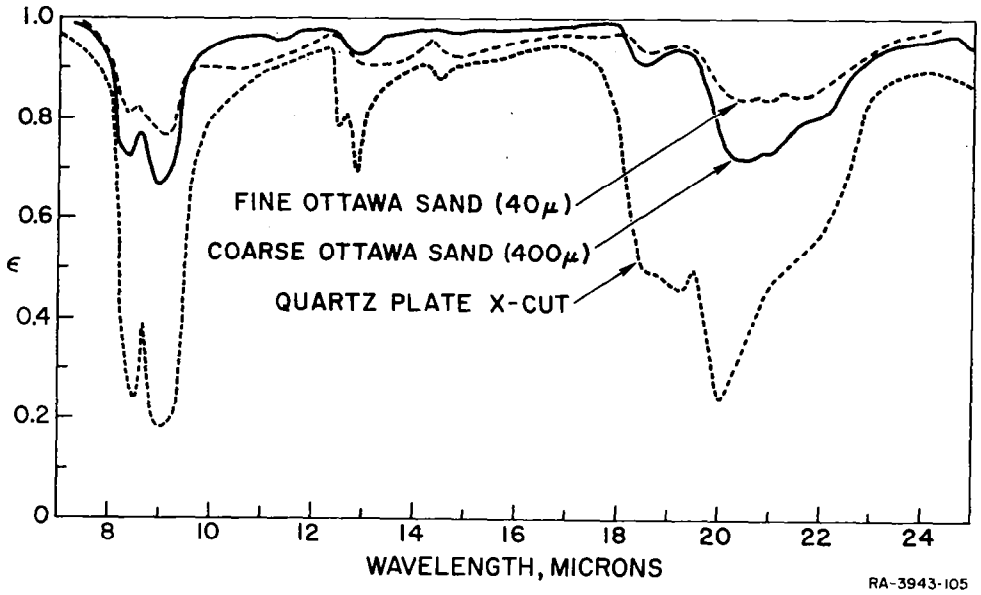

FIG. 13 SPECTRAL EMITTANCE CURVES FOR QUARTZ, CALCULATED FROM REFLECTANCE DATA BY STL, SHOWN FOR SAMPLES IN VARIOUS SURFACE AGGREGATIONS. Spectra for fine Ottawa sand (40 μ) are dashed and for coarse Ottawa sand (400 μ) are as solid curves. An X-cut quartz plate is shown as the lower (dashed) curve in the figure.

generalities; detail of the quartz emittance minimum is evident at a 44 μ particle size; however, some of the fine structure evident for a polished quartz X-cut plate and 400 μ silica sand is missing.

c. Computation of the Reflection Data

Computation and plotting of the reflectance data to yield emittance values were performed at STL. Data values were not requested from STL for inclusion in the computational programs, although the same samples were used by the author in the direct emittance measurements at SRI. Both sets of normalized curves can be compared in the text.

d. Error Analysis

Wavelength values are correct to ±0.01 μ, but the values of the reflectance, and hence the calculated emittance, are quite dependent upon the surface characteristics of the powdered sample. In the case of these materials, it is clear that the degree of packing can cause

considerable variation in the amplitude of the spectral peaks, although it is also quite apparent that the positions of the peaks do not change with surface characteristics.

Bevans* indicates that the reflectance reproducibility (on the same sample surface) is approximately 1% absolute.

---

* Personal communication to the author.

VIII EMISSION ANALYSIS

A. Blackbody Radiation

There are certain surfaces which radiate in such a manner that their characteristics are completely specified if their absolute temperatures are defined. These surfaces, which are continuous spectrum sources, are known as ideal thermoradiators or blackbodies.[16]

The radiant energy is proportional to the fourth power of the absolute temperature (T), according to the relationship

$$W_{BB} = \sigma T^4 \tag{1}$$

where W_{BB} is the power per unit area radiated into a hemisphere by a blackbody, and σ is the Stefan-Boltzmann constant.

Equation (1) provides a means for readily determining the radiance of a blackbody source for which the temperature can be determined. The emittance (ϵ) of any other surface is defined as the ratio W_s/W_{BB}.

Using the radiation formula of Planck, the spectral radiance may be calculated,

$$W_\lambda = C_1\lambda^{-5} (\exp [C_2/\lambda T] - 1)^{-1} \tag{2}$$

where W_λ is the radiant flux per unit area per unit increment of wavelength and has units of watts per square centimeter per micron $d\lambda$. C_1 and C_2 are constants, where $C_1 = \pi c^2 h = 3.7413 \times 10^{-4}$ watt-microns, $C_2 = hc/k = 1.4388 \times 10^4$ micron degrees, and λ is the wavelength in microns.

The Wien displacement law states that the maximum of the radiation curve (λ_m) is related to the absolute temperature by the relationship

$$\lambda_m = \frac{a}{T} \tag{3}$$

where a is a constant, for a blackbody, of 2897 micron degrees.

The combination of these laws enables one to compute for any given absolute temperature, T, the spectral distribution of radiation emitted from a blackbody. This is shown in Fig. 14, on which the radiant flux in 10^{-4} watts/cm^2-microns is plotted as the ordinate and the abscissa is wavelength (in microns). The temperature of lunar noon is approximately 375°K, whereas earth ambient temperature is approximately 300°K. The relative change in radiant energy from a square centimeter source can be read from the graph for any given wavelength interval. The value for the earth ambient peak is approximately 3100 microwatts/cm^2-micron, whereas the value for the lunar temperature peak is approximately 9000 microwatts/cm^2-micron.

The hemispherical spectral emittance curve of a blackbody at 640°K recorded on the single-beam PE112 unit is shown by a heavy dashed line in Fig. 15. The true peak of the curve occurs off-scale at 4.5 μ and the limits of the curve may be seen from the figures.

With a single-beam instrument the radiation is transmitted through the atmosphere. There are serious absorptions superimposed on the spectra of any blackbody source, due to the pathlength of approximately 100 cm through which the radiation must pass in order to reach the detector. The actual observed tracing of the spectrometer is shown as the solid black line on the drawing. Due to the strong absorptions between 2 and 3 μ the resultant curve rises sharply to peak at about 4.3 μ, decreasing again around 6.5 to 7 μ in a series of H_2O and CO_2 absorptions.

It is possible to program slit change as a function of wavelength, so that some correction may be made for this rapidly decreasing energy level. The solid curve (within the area closely stippled) indicates the trace of the spectrum with the slit change program in operation. The area normally used for spectral emission experiments is clearly indicated in the portion of the figure. In order to calibrate the absorption peaks,

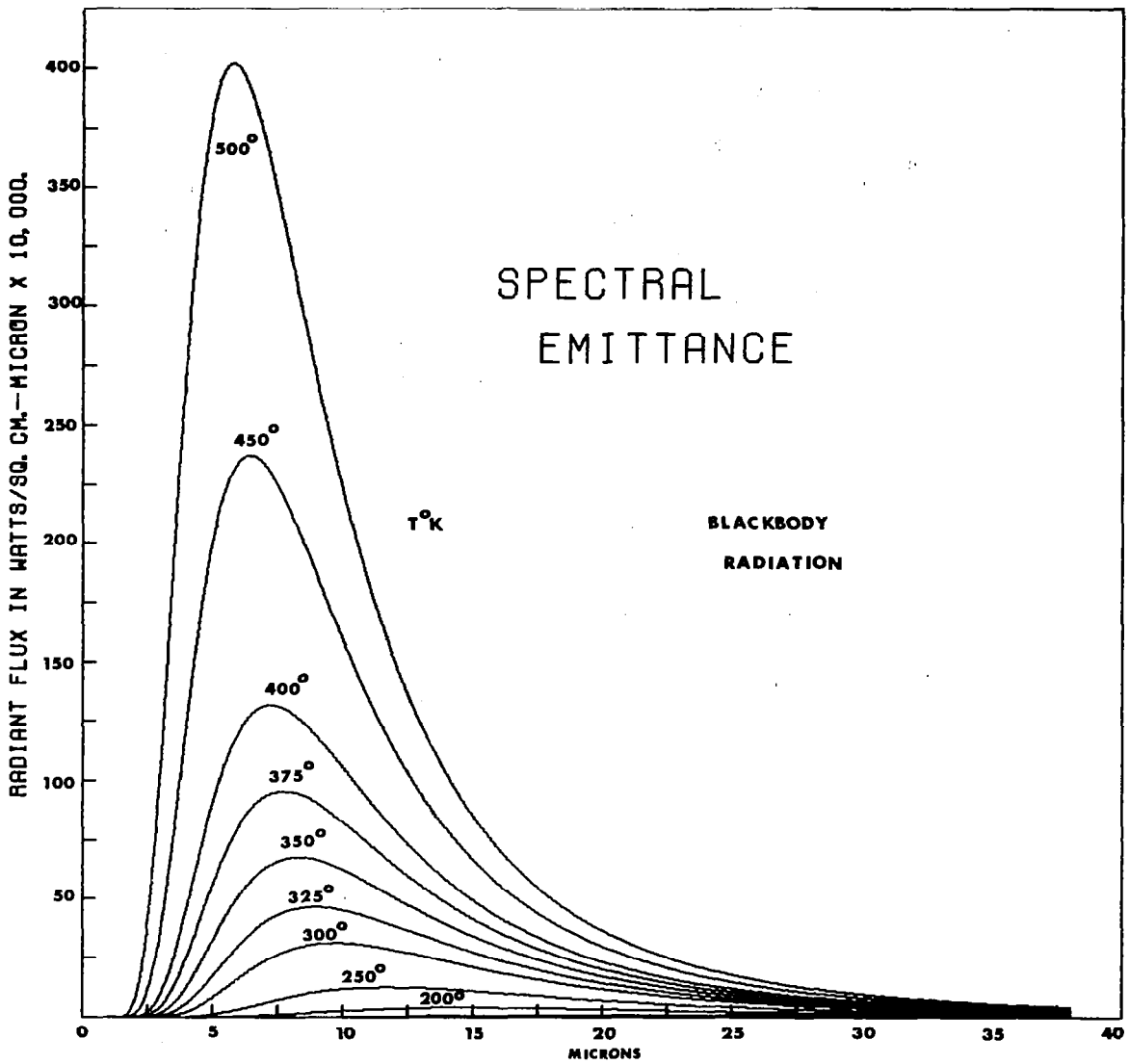

FIG. 14 HEMISPHERICAL SPECTRAL EMITTANCE FROM A BLACKBODY CALCULATED FROM THE PLANCK RADIATION FORMULA, FOR A SERIES OF TEMPERATURES (T °K) FROM 200 THROUGH 500 °. These values of the radiant flux (W_λ) were multiplied by the normal spectral emittance determinations (ϵ_λ) for the radiant energy calculations prepared in this study.

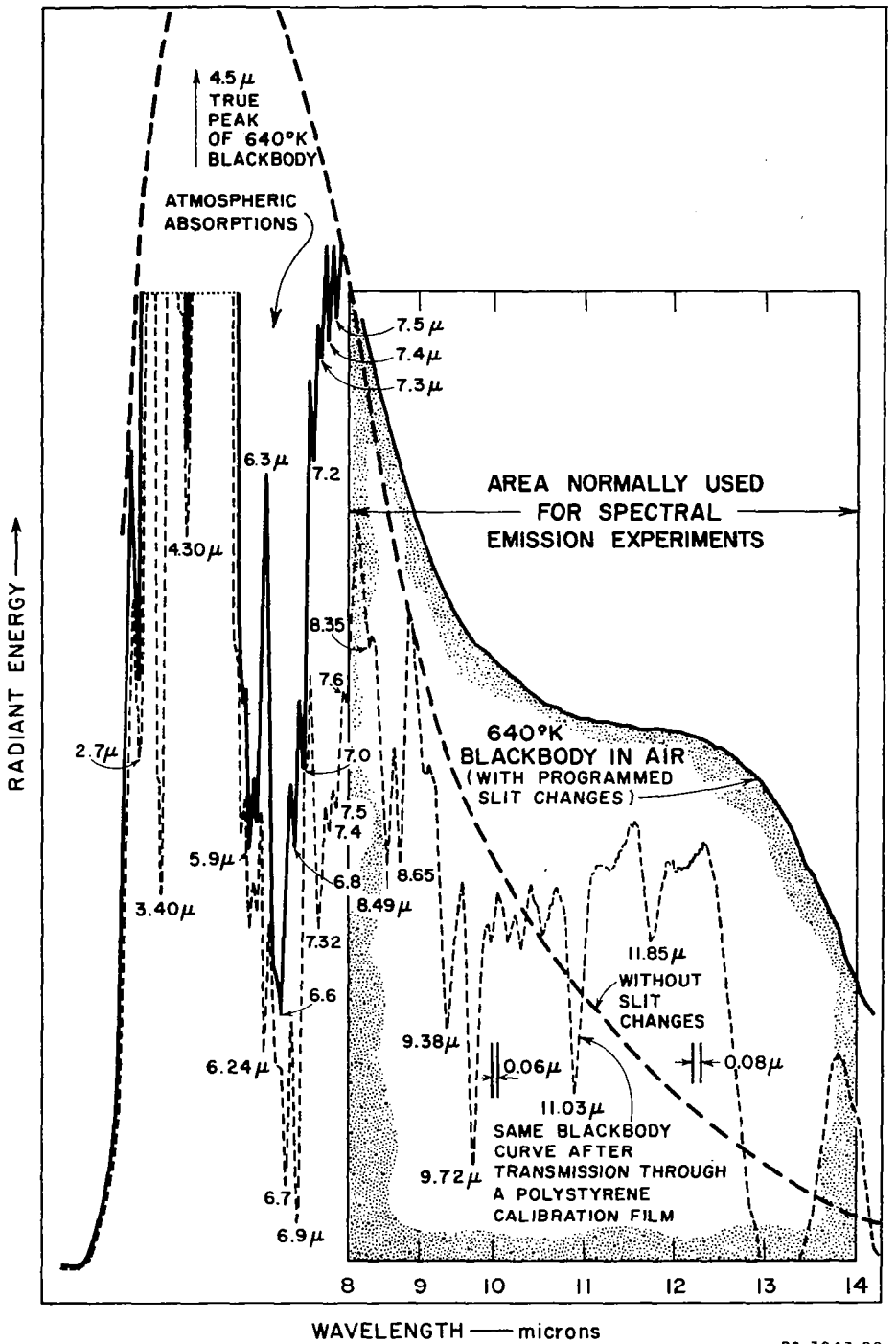

FIG. 15 SPECTRAL EMITTANCE CURVES OF A BLACKBODY AT 640°K AS RECORDED ON THE SINGLE-BEAM PE-112 SPECTROMETER AND SHOWN BY THE HEAVY DASHED LINE. The true peak of the curve occurs off scale at 4.5 μ. The observed tracing of the spectrometer (including atmospheric attenuations) is shown as the solid black line, with the area normally used for emission experiments stippled.

the blackbody radiation was passed through a polystyrene film. The curve with the short, dashed lines shows the marked absorption by the polystyrene film. There are now two sets of absorptions superimposed on this energy curve--that of the atmosphere, which cannot be removed without purging the equipment, and that of the polystyrene, which has been added as a calibration.

B. Normal Spectral Emittance

1. Previous Studies

The basis of any emittance study is the quality of the blackbody which is used as the standard. The emittance of a surface is defined as the ratio of its emissive power to that of a blackbody radiating at the same temperature and under the same conditions.

In double-beam spectrometry it is usual to pass the energy from the blackbody along one beam, while the energy from the sample passes along the other beam through the unit. The ratio between the two beams at any point is the emittance of the sample, unless the geometry or pathlength of the unit has been disturbed.

In Final Report I it was indicated that compositional analysis techniques used for the reflection and absorption spectra could be used for emission spectra, although the spectral data now appear as minima superimposed on the Planck radiative curve. Spectral position again can be used to determine minerals; spectral shape and complexity can be used to determine the mineral content of the rock.

During 1962 we conducted only theoretical studies of thermally emitted infrared radiation. The spectra shown in Fig. 16 were obtained at that time by mathematically computing the spectral emittance curves, the relationship ($\epsilon_\lambda = 1-\rho_\lambda$), using the reflectance data (ρ_λ) obtained at ambient temperatures. The data of Fig. 16 indicate the shape of the spectral emittance curve (stippled) obtained in this manner for radiating surfaces at 250°, 300°, 350°, 400°, 450°, and 500°K.

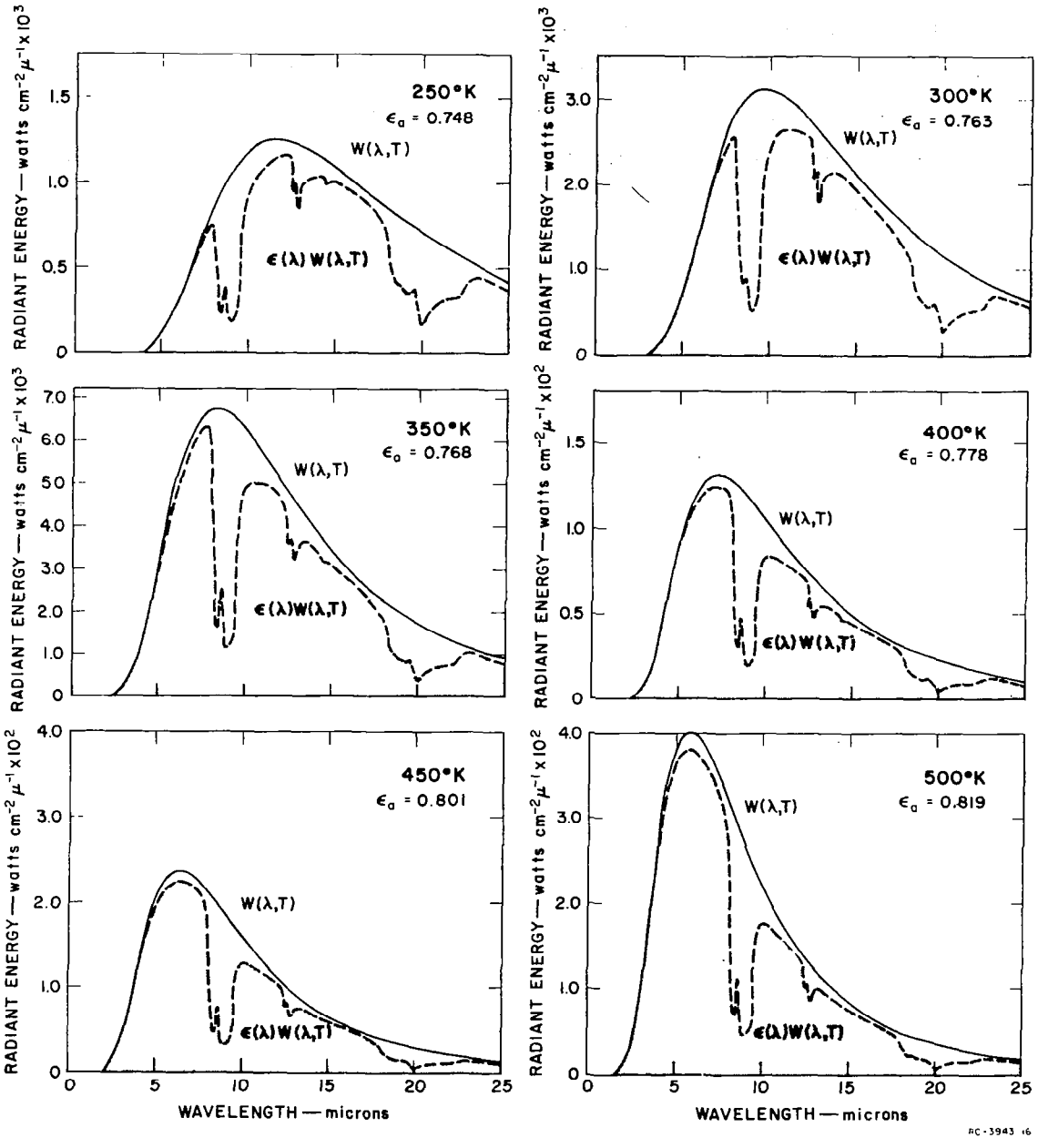

FIG. 16 HEMISPHERICAL EMITTANCE SPECTRA OF QUARTZ AND A BLACKBODY AS A FUNCTION OF WAVELENGTH AND TEMPERATURE, CALCULATED FROM REFLECTANCE SPECTRA OBTAINED AT AMBIENT TEMPERATURES.

In a comparable manner spectral emittance curves were derived (Fig. 17) for granite, dunite, obsidian, and the Haven meteoritic chondrite; in each case the source was presumed to be at 350°K. The average emissivity (ϵ) was computed by integrating the area under the curve and was expressed as a fraction of the total energy from the blackbody curve at that temperature (the solid line).

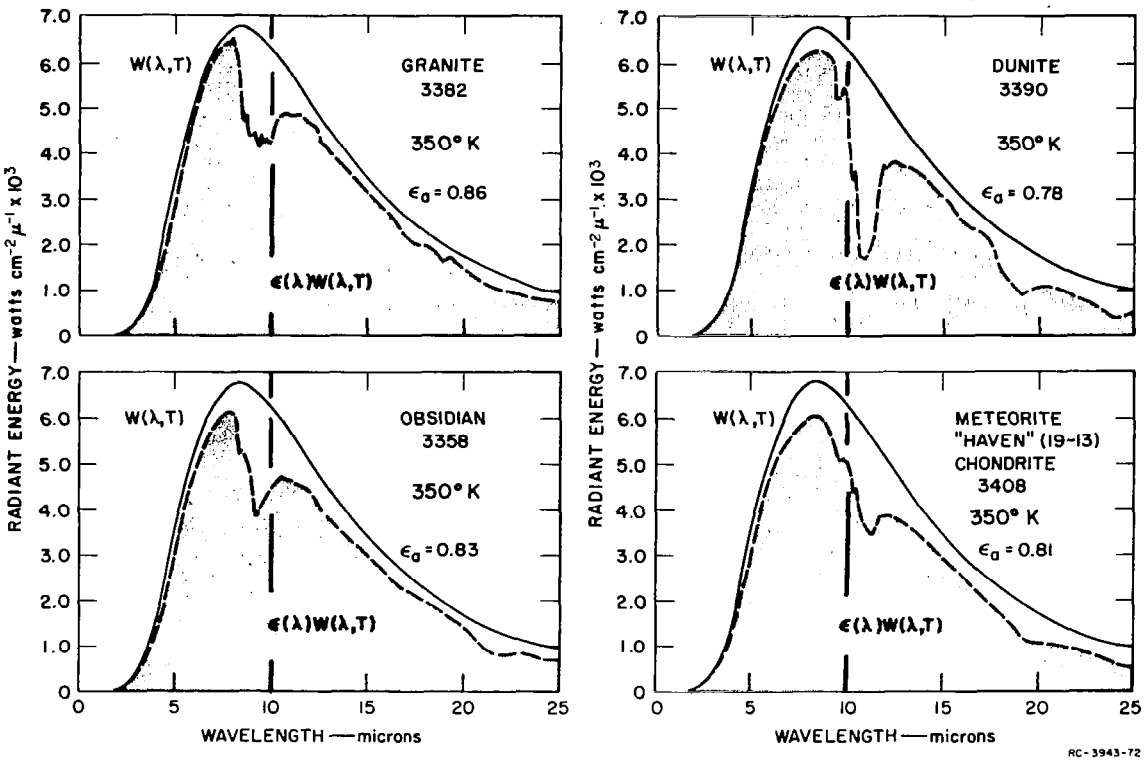

FIG. 17 HEMISPHERICAL EMITTANCE SPECTRA OF A BLACKBODY AT 350°K COMPARED WITH FOUR GREYBODY EMISSION CURVES OF ROCKS AT THE SAME TEMPERATURE. Samples are granite (3382) and its glassy equivalent obsidian (3358), compared with the more basic dunite (3390) and a chondritic meteorite (Haven, 19-13). The emittance minima for the granite and the obsidian occur at a wavelength shorter than 10 μ, whereas those for the basic dunite and meteoritic chondrite occur at a wavelength longer than 10 μ.

2. Present Study

During 1963 extensive studies were conducted of the normal spectral emittance of solid and powdered rocks and rock-forming minerals. A total of 256 samples has been run by this method; of these, 98 have been digitized and converted to a normalized format for plotting.

a. Sample Preparation

In order to exactly duplicate the possible operational conditions, samples were heated so that a rough, unbroken surface was uppermost and allowed to radiate into the optics of the spectrometer. The surfaces shown in Figs. 18, 19, and 20 are typical of those used in the emittance studies, and the surface roughness can be seen by the shadow projected onto the scale marker.

B. Hapke and H. Van Horn of Cornell University have studied the manner in which fine dust, from about 1 to 25 μ in size, stack up into highly porous structures (fairy castles).[17] They find that these structures exactly reproduce the backscattering properties of the lunar surface, and postulate that they constitute the structure of the outermost layer of the moon. As this outermost layer is the one that determines the albedo (for both the visible and the infrared radiations), we have considered that the study of the effect of such porous structures on the emissive properties of rock and minerals is very important. Accordingly all powders below 25 μ size were sifted in the fairy castle macrostructure before emission analysis. This fluffy structure, however, did not impose any marked additional changes on the spectra, beyond those already introduced by the scattering phenomena common to fine particle radiation. It may greatly modify the thermal diffusivity of the surface, but we have found little evidence for related marked spectral changes.

It is most important that the infrared emission and reflection be obtained on the same sample surface, whether this be a solid or a powder. It is further necessary that some manner of comparison be developed between a powdered surface prepared by operator A in California and one prepared by operator B in New York. The best parameter for this is a measurement of the angular photometric response, probably of visible light. One must also express the particle sizes and their distribution range if possible, but the manner of packing of a powder is almost impossible to describe adequately. Once a surface of a sample is prepared for infrared examination, then the emission, reflection, and the photometric angular response should all be measured so that comparable surfaces can be developed for study elsewhere.

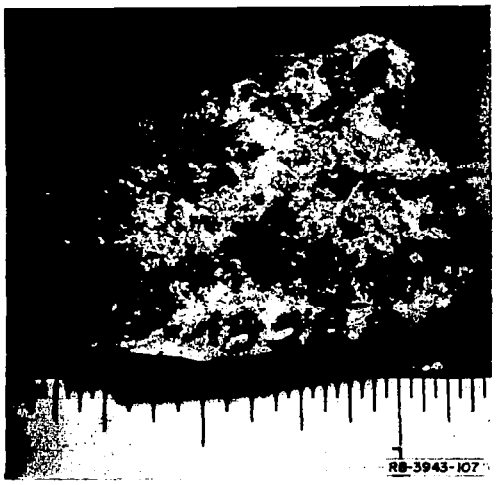

FIG. 18 PHOTOMICROGRAPH OF THE SURFACE OF THE QUARTZ MONZONITE PORPHYRY, FROM THE NEVADA TEST SITE, USED FOR DIRECT EMITTANCE MEASUREMENTS. Scale is in inches, and a profile of the surface is shown by the shadow.

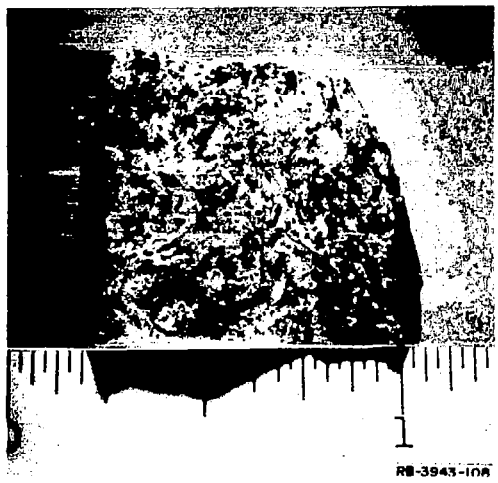

FIG. 19 PHOTOMICROGRAPH OF THE SURFACE AS USED OF THE AUGITE DIORITE (USNM 5 to 9). Scale is in inches, and a profile of the surface is shown by the shadow.

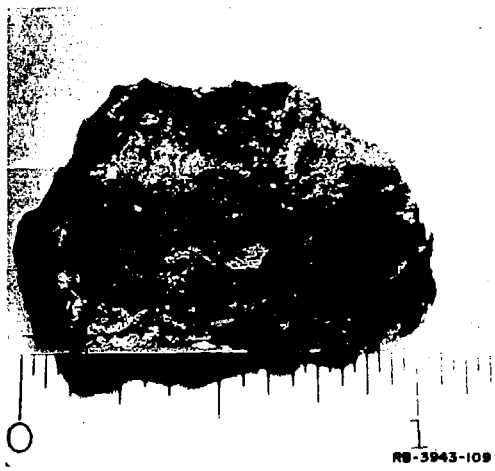

FIG. 20 PHOTOMICROGRAPH OF THE SURFACE AS USED OF THE NEPHELINE BASALT (USNM 1065) FOR DIRECT EMITTANCE MEASUREMENTS. Scale is in inches, and a profile of the surface is shown by the shadow.

b. Experimental Techniques

All of the spectra shown in this report were derived from the output of a single-beam Perkin-Elmer PE112 instrument, modified for direct emission measurements. To study the emitted radiation from heated rock and mineral samples the Globar infrared source was removed and replaced by a small, water-cooled furnace with an internal sample heater. A comparable sample-to-slit distance was achieved by using a front-surfaced water-cooled mirror inclined at 45° to the horizontal, directly over the original source position. The image of the sample on the spectrometer entrance slit was then refocused by adjustment of the concave mirror. All the other (front-surfaced) mirrors and optical adjustments were left untouched. The furnace which was developed for this work (Fig. 21) holds the solid or powdered sample on a horizontal tray covered with bright aluminum foil (ρ is very high, therefore, $\epsilon = 1 - \rho$ is very low). The mirrors and aperture are also water-cooled so that the self-emission of the equipment--one of the major troubles in emission studies at low temperatures--can be kept to a minimum. The furnace temperature is controlled through a Variac resistance unit.

A chromel-alumel thermocouple is placed on the emitting surface, and by adjusting the Variac the emitting surface can be heated to a prearranged temperature. This outermost surface reaches a significantly different level of temperature than the body of the material if the sample is a lightly-sifted powder in the fairy castle structure. It is difficult to obtain the true temperature of such a surface. It is also necessary to avoid thermal sensors with a high thermal capacity, which may themselves further modify the temperature while they are sensing it, a factor very noticeable with fluffy powders.

The furnace design produces a thermal gradient in the sample, since it is heated from below and allowed to radiate under the spectrometer only from its upper surface. The temperature of solid samples is relatively easy to record and a metal sample would give the best possible temperature measurement. The thermocouple is mounted on a micrometer

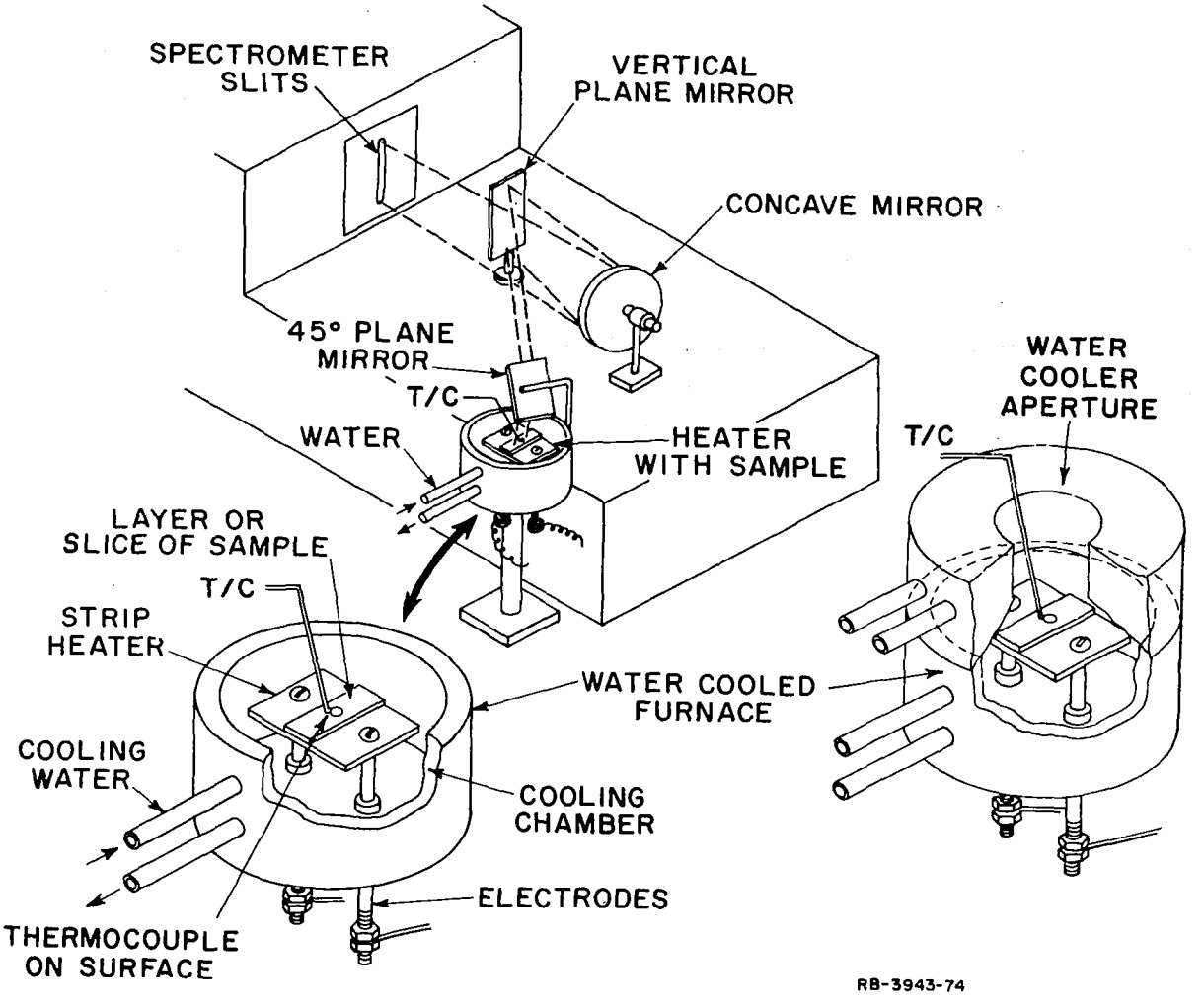

FIG. 21 WATER-COOLED FURNACE USED FOR THE EMITTANCE MEASUREMENTS, SHOWING THE METHOD OF INSTALLATION ADJACENT TO THE SPECTROMETER.

screw by which it can be exactly positioned on the surface. For a dust surface we allow the flattened thermocouple bead to just dent the surface of the powder, but not to become embedded in the powder or covered over by it.

The aperture of the furnace is covered by a 3mm-thick flat plate of optical grade NaCl (optical blanks cleaved into three pieces), to reduce the thermal convection and eddying of the air contained in the furnace.

The temperature is controlled to at least $\pm 2^{\circ}C$ (and probably to $\pm 1^{\circ}C$). The output of the thermocouple is continually monitored on a strip-chart recorder and usually shows a smooth trace, free from any cycling or

excursions. When the NaCl coverplate was not used, rapid excursions were noted, and although these had a time constant far shorter than that of the spectrometer, it was considered better to avoid the effect.

Absolute temperature accuracy is not essential, particularly for emittance ratio calculations, as long as one can reproduce the temperature for the sample and the blackbody standard. The furnace used in this study was designed so that either the sample or blackbody would fit inside the furnace chamber, with the temperature of the upper emitting controlled through a servo-loop with the thermocouple on its surface.

The first "blackbody" used was a small quantity of carbon black (Norit A), whose spectral emission curve is shown in Fig. 22 and in Appendix C, Fig. C-1. Later experimental work showed that a particularly fine-grained sample of Al_2O_3, with a particle size of 0.02 μ had a markedly high emission at almost all wavelengths to about 10 μ, where it dropped slightly and then maintained this level to the end of the record at 13.0 μ. The hemispherical reflectance spectrum of this powdered sample is shown in Fig. 12.

C. B. Neel and G. C. Robinson at NASA (Ames) prepared a small, light-weight blackbody source of very high emittance by bolting together single-edged razor blades, which they used in the S-16 Orbiting Solar Observatory as a standard for absorbtivity/emissivity experiments in space.[18] We decided this would be a good blackbody source for our requirements. Accordingly, 30 blades (Schick Injector, single-edged) were bolted together to form a metal block 4 × 1.5 × 0.75 cm thick (see Fig. 23). Being metal, the block came to equilibrium temperature quickly and held this temperature (within $\pm 2^{\circ}$) over a several-hour period when measured by the thermocouple placed in contact with the upper* grooved emitting surface.

---

* In all probability there was a slight temperature increase towards the bottom of each groove, but it was not considered practical to measure the temperature gradient down the depth of the groove at these low temperatures. (In Fig. 22 the divergence between the Al_2O_3 sample and the blackbody curves at 11.0 μ only represents a "temperature" difference of $10^{\circ}C$; that is, the "brightness temperature" of the Al_2O_3 is only $10^{\circ}C$ different from that of the razor-blade blackbody.)

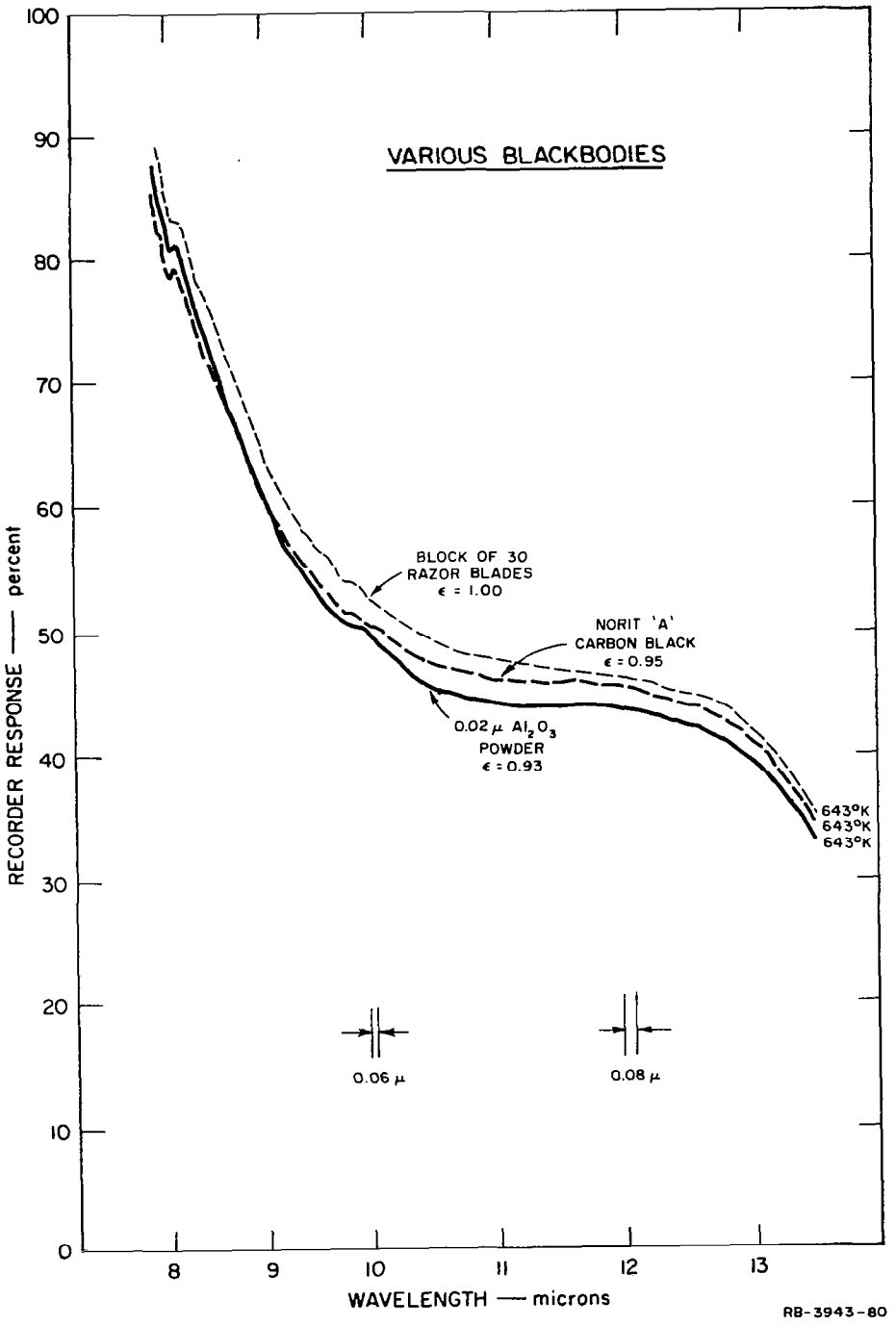

FIG. 22 DIRECT TRACINGS OF THE RECORDER RESPONSE FROM THE SPECTROMETER AS A FUNCTION OF WAVELENGTH FOR A SERIES OF MATERIALS (approximating blackbodies) AT 643°K (370°C). The block of razor blades (light dashed curve) is considered to be a blackbody with an emittance of 1.00. Carbon black (heavy dashed curve) had an emittance of 0.95, and the 0.02 μ alumina had an emittance of 0.93.

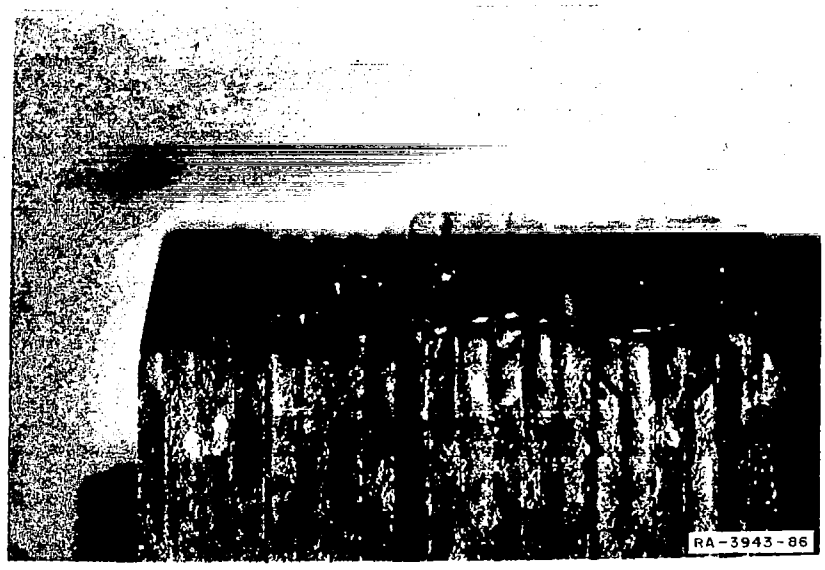

FIG. 23 CLOSE-UP VIEW OF THE RAZOR-BLADE BLACKBODY. Oxide coatings are now present on the metal. Emitting surface is the deeply grooved, uppermost one in this view. About X15.

The normalized plot of the spectral emittance of this 0.02 μ Al_2O_3 powder compared with the razor-blade blackbody appears in Fig. 24 on the rectangular format from the digital plotter. The near-blackbody characteristics of this white, fine-grained sample proved so unusual that it was decided to check the grain size by electron microscope. Figure 25 shows an electron micrograph of this sample with the scale of a 1 μ bar on the figure. The even, fine-grained size was very surprising and no doubt contributes to its unusual radiative properties.

c. Reproducibility of Spectra

Figures 26 and 27 indicate the experimental reproducibility of the sampling method. The quartz basalt sample was studied on each of two sawed faces; the resultant data were computed, normalized, and replotted as Fig. 26. Calculated emittances for the two runs were 0.73 and 0.72, respectively.

A slightly larger discrepancy in the emittance occurs in the granite gneiss sample (Fig. 27). The upper curve was run on a rough, broken surface while the lower curve was run on a smooth surface. The

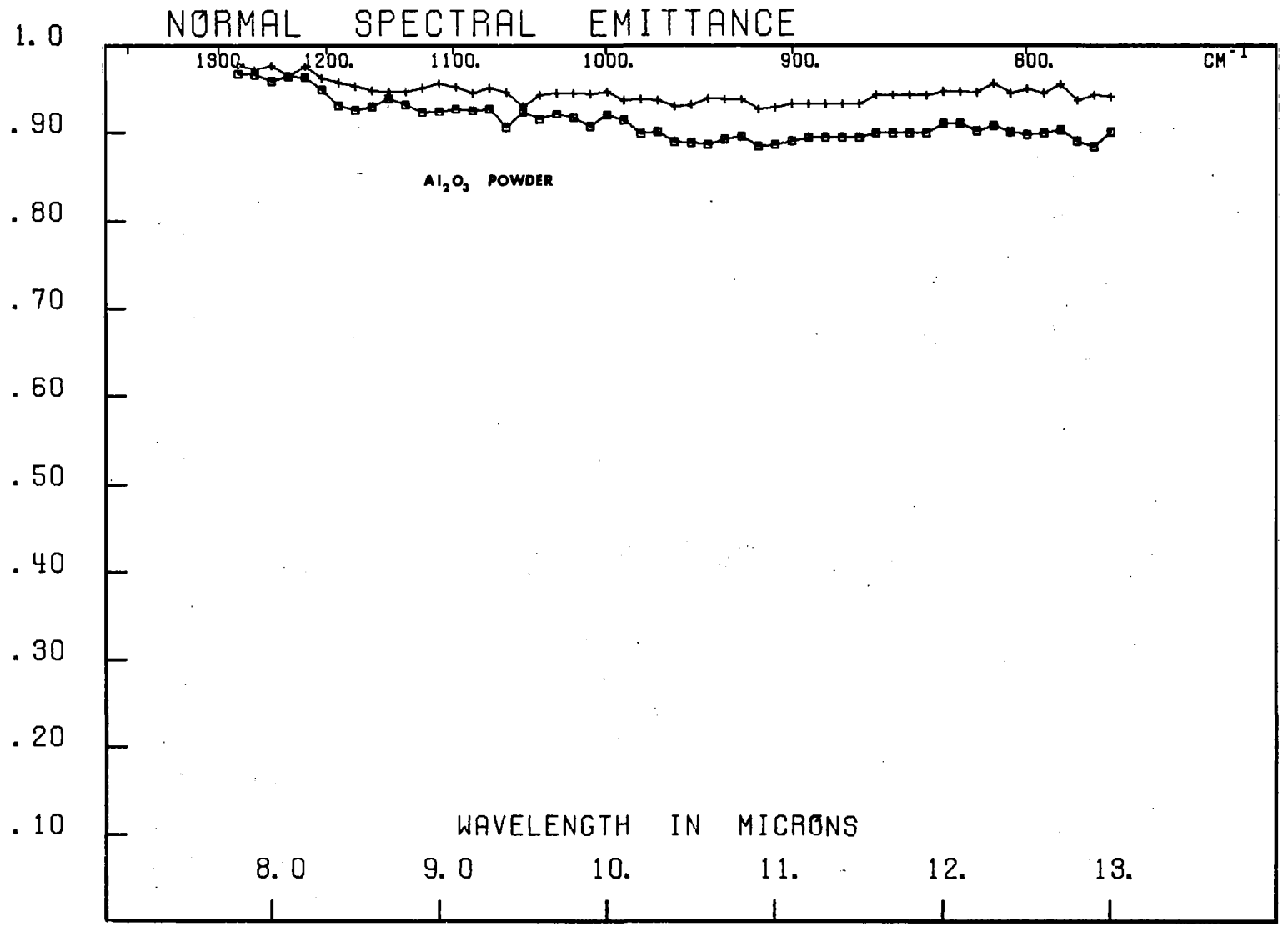

FIG. 24 NORMAL SPECTRAL EMITTANCE CURVES OF REPEATED MEASUREMENTS ON 0.02 μ ALUMINA (Al_2O_3) POWDER, SHOWING ITS VERY HIGH AVERAGE EMITTANCE, DESPITE ITS WHITE COLOR IN VISIBLE LIGHT.

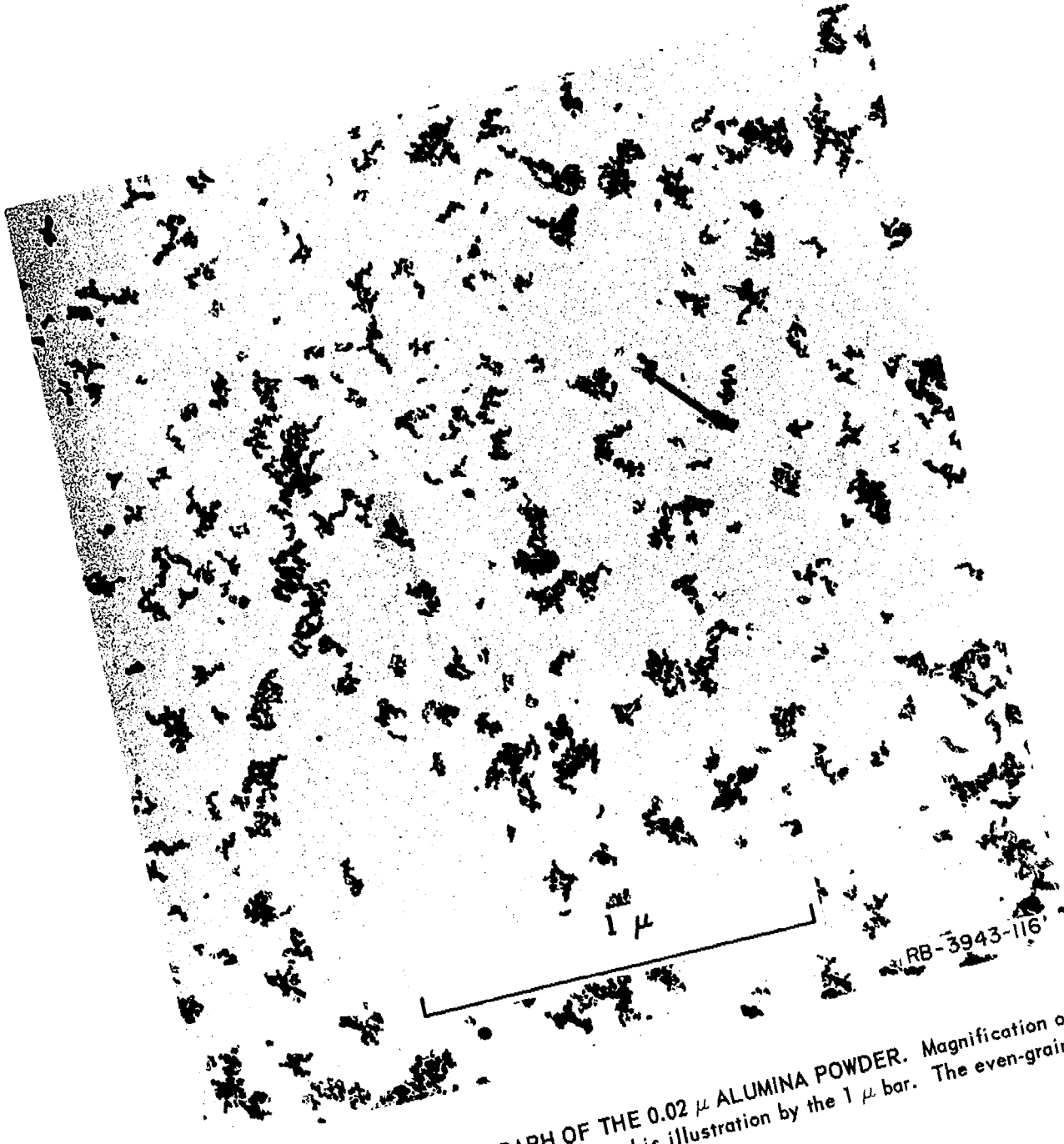

FIG. 25 ELECTRON MICROGRAPH OF THE 0.02 μ ALUMINA POWDER. Magnification on the original X80,000. Scale given for this illustration by the 1 μ bar. The even-grained size of the particles is most striking.

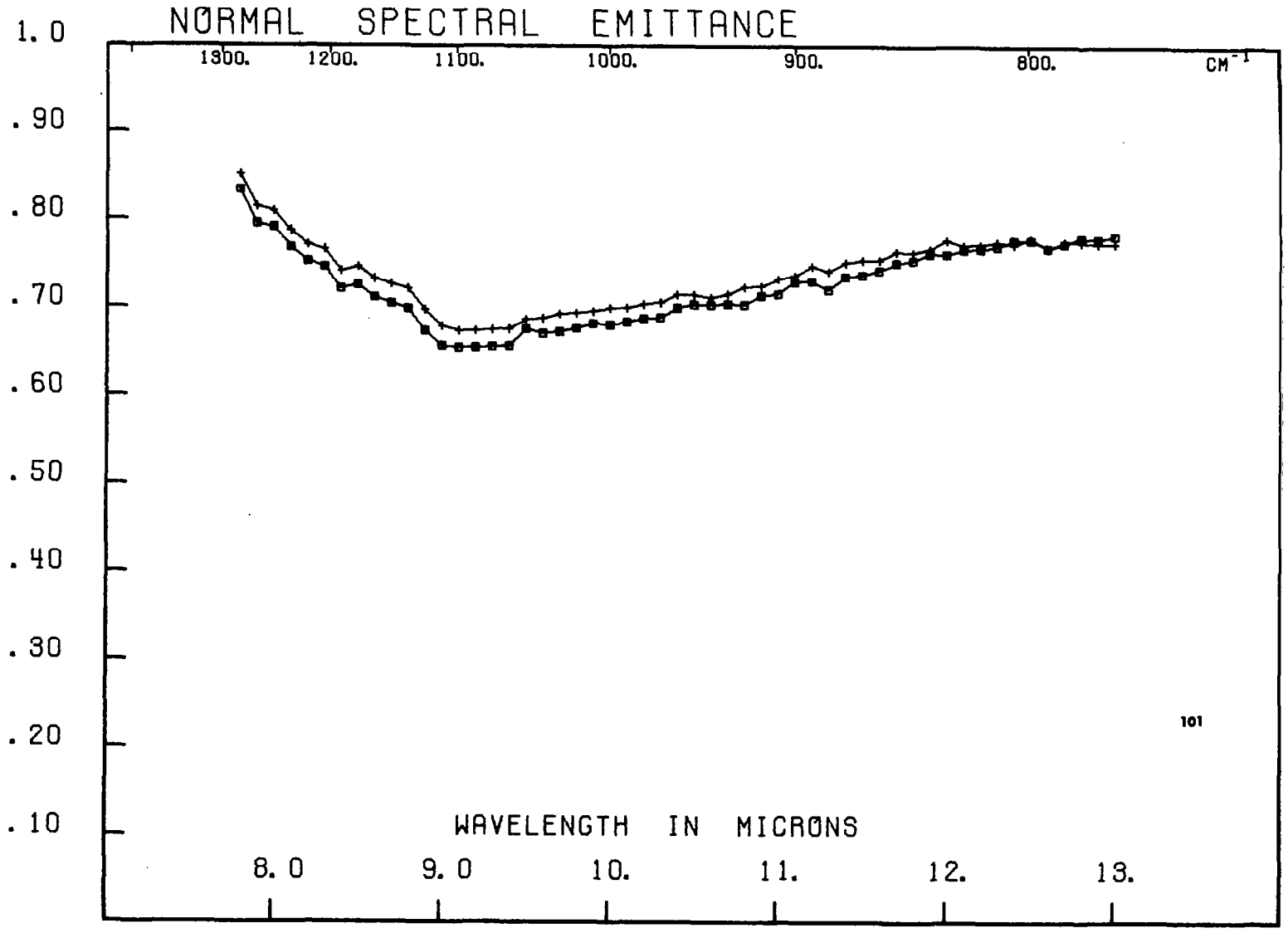

FIG. 26 NORMAL SPECTRAL EMITTANCE CURVES FOR REPEATED MEASUREMENTS ON QUARTZ BASALT SAMPLE (USNM 101) STUDIED ON EACH OF TWO SAWED FACES, SHOWING THE VARIANCE IN MEASUREMENTS.

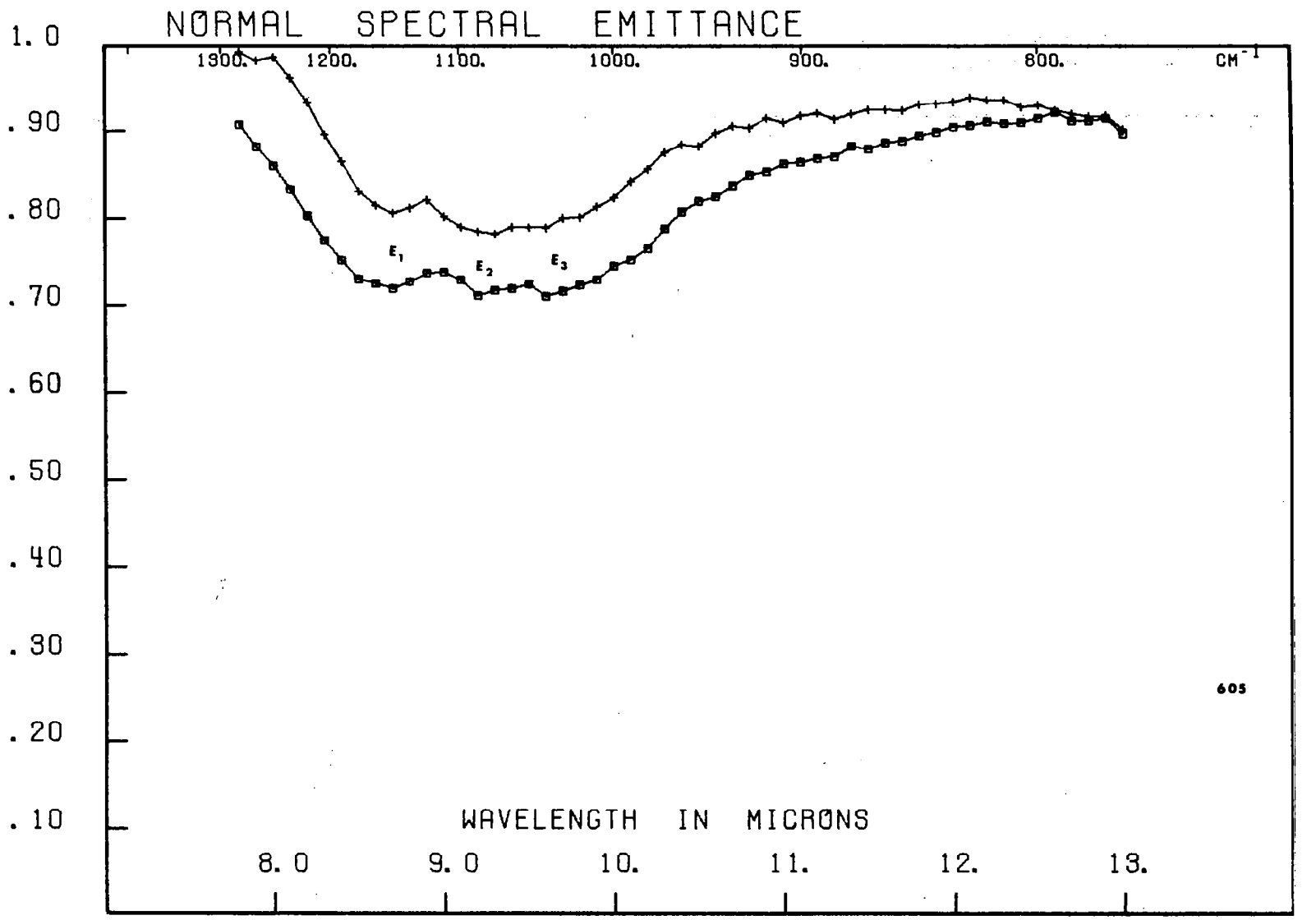

FIG. 27 NORMAL SPECTRAL EMITTANCE CURVES FOR REPEATED MEASUREMENTS ON SAMPLE OF GRANITE GNEISS (USNM 605) SHOWING THE VARIANCE IN MEASUREMENTS. Despite the discrepancy in the absolute levels of the two curves, the peaks E_1, E_2, E_3 appear on both spectra.

calculated emittances were 0.88 and 0.82, respectively. Despite this apparent discrepancy in the level of the emittance as calculated, it is important that the three spectral peaks (E_1, E_2, E_3) appear on both of the diagrams.

d. Results

The spectra from the series of rocks received from the U. S. National Museum collection have been represented in Appendix A. Their absorption, reflection, and emission spectra have been computed, normalized, and digitally plotted to form the figures in the appendix. By comparing the areas under the spectral curves for the samples and a blackbody, for the wavelength interval under consideration, the emittance of each of the samples can be derived. The emittance ratios determined by direct measurement in the interval 8.0 to 13.0 μ lie between 0.72 and 0.95; that is, the integrated energy over those wavelengths is only 0.72 times that of a blackbody at the same temperature (see Table II).

This is an important consideration, if one is measuring the energy radiated from a surface and thereby deducing the temperature (T) of that surface from the relationship of Stefan-Boltzmann's equation

$$T = \left[\frac{W}{\sigma \epsilon_\lambda}\right]^{\frac{1}{4}} \qquad (4)$$

where T is the temperature in degrees Kelvin, ϵ_λ is the emittance of that surface, at wavelength λ (or over the wavelength range $\lambda_1 - \lambda_2$), σ is Stefan-Boltzmann's constant, and W is the radiant energy recorded.

The effect of the emittance upon the radiant energy spectrum is important for interpreting temperatures from the radiometer data in such satellites as the TIROS and NIMBUS series. The question has been debated in several recent papers. Kern[19], and Buettner and Kern[20], using data from our earlier studies[21] have critically reexamined the TIROS III data for the 8 to 12 μ window, from passes of TIROS over the Mediterranean Sea and Libyan Desert. They conclude that an emittance of $\epsilon = 0.8$ would be necessary to explain the drop in energy received by TIROS on passing from the sea to over the desert.

Table II

SPECTRAL MINIMA FOR A SERIES OF ROCK SURFACES: EMITTANCE MEASUREMENTS

A. ACID (HIGH SILICA, 65%+) ROCKS

Sample (and USNM No.)	SiO_2 (%, or surface texture)	Spectral Minima[a] (stronger underlined)	Emittance		Roughness
			ε_λ min	ε average (7.8 to 13.0 μ)	
Quartz					
Polished Z-cut	100	9.0	0.20	0.72	- -
Polished X-cut		8.6 9.0 12.4	.28	.76	- -
Rough X-cut		8.5 9.2 12.7	.62	.83	- -
Fused, plate		8.3 9.0	.45	.75	Polished
Powder					
25 to 45 μ	Fairy castle	9.0	.81	.90	- -
10 to 25 μ	f.c.	9.0	.85	.92	- -
1 to 10 μ	f.c.	9.10 11.1	.91	.94	- -
Sand	Loose	9.10	.67	.80	- -
Opal	96.7	9.09 (reflectance,R)	.62 (R)	.92 (R)	- -
Chert (SRI 3560)	-	9.2	.59	.84	Uneven, smooth
Obsidian (SRI 3424)	-	8.7 9.4	.64	.72	Smooth
(SRI 3365)	-	9.2 11.6	.72	.80	Smooth
Rhyolite pumice (SRI 3570)	-	9.2	.79	.88	Rough, pitted
Welded tuff (SRI 3622)	-	8.90	.69	.76	Very rough
Tektite (SRI 3535)	-	9.3	.64	.74	Uneven, smooth
Quartz monzonite porphyry) (SRI 3582)	-	8.9	.70	.81	Rough, broken
Dacite (82)	68.7	8.8/9.0	.83/.85	.92/.95	Sawed
Granite (158)	-	8.8/8.9 9.1	.73/.76	.88/.90	Rough, broken
Graphic granite (377)	-	9.30	.70/.71	.87/.88	Rough, broken
Granite aplite (SRI 3624)	-	8.8	.60	.77	Rough, broken
Pyroxene aplite (1924)	68.0	8.8	.76	.85	Rough, broken
Rhyolite pumice (59)	67.4	9.30	.80	.86	Sawed, porous
Granite gneiss (605)	66.9	9.30/9.60	.78/.71	.88/.82	Rough, broken
Trachyte (70)	66.03	8.70 9.60	.75/.79	.84/.86	Sawed

[a] Slash (/) = repeat run

Table II (Continued)

B. INTERMEDIATE ROCKS (53 to 65% SiO_2)

Sample (and USNM No.)	SiO_2 (%, or surface texture)	Spectral Minima[a] (stronger underlined)	Emittance		Roughness
			ε_λ min	ε average (7.8 to 13.0 μ)	
Quartz syenite (631)	63.2	9.6	0.71	0.86	Rough
Andesite (monzonite porphyry) (1331)	62.3	9.6 10.1	.70	.77	Rough, broken
Nepheline syenite (77)	60.4	9.6/9.7 <u>9.9</u>	.74/.76,.77	.88/.91	Rough, broken
Quartz basalt (101)	57.2	9.2/9.15	.67/.65	.73/.72	Sawed
Hypersthene andesite (86)	56.2	9.2/9.2	.72/.73	.78/.78	Sawed
Hypersthene andesite vitrophyre (371)	ca 56.2	9.2	.74	.83	Rough, broken
Quartz diorite (758)	54.6	10.0/10.1	.81/.82	.91/.92	Rough, broken
Augite diorite (529)	53.8	9.6	.75	.85	Sawed

[a] Slash (/) = repeat run

Table II (Continued)

C. BASIC (AND ULTRABASIC) ROCKS (below 53% SiO_2)

Sample (and USNM No.)	SiO_2 (%, or surface texture)	Spectral Minima[a] (stronger underlined)	Emittance		Roughness
			ε_λ min	ε average (7.8 to 13.0 μ)	
Garnet gabbro (109)	52.3	9.1 10.2	0.77	0.81	Sawed
Augite diorite gabbro (199)	52.0	9.8	.78	.84	Sawed
Schist (1585)	51.9	9.6/9.6	.70/.74	.84/.86	Rough, broken
Diabase (106)	51.8	9.0 (See Appendix A-20)	.78	.83	Sawed
Basalt (102)	51.4	10.4 10.1	.65	.69	Rough, broken
Plagioclase basalt (535)	49.7	9.1 9.4/9.7	.79/.81	.86/.89	Sawed
Monchiquite (1499)	47.8	9.2	.77	.84	Rough, broken
Hornblende gabbro gneiss (143)	46.8	10.0/10.1	.72/.69	.82/.79	Sawed
Peridotite (111)	41.0	10.4	.79	.88	Sawed
Olivine gabbro (1734)	40.4	10.3	.78	.83	Sawed
Nepheline basalt (1065)	40.3	9.7	.84	.90	Rough, broken
Serpentine (145)	39.1	10.1 10.4	.76	.87	Rough, broken
Limburgite (296)	36.8	10.5	.72	.82	Rough, broken
Dunite					Rough, sawed
Polished		9.5 10.7	.44	.71	
Rough		9.6 10.7	.66	.80	
Above 850 μ (grit)	Loose	9.6 10.7	.73	.78	
150-30 μ (sand)	Sifted	10.6	.74	.79	
40-80 μ (dust)	Fairy castle	10.7	.79	.86	
10-25 μ (powder)	Fairy castle	10.7	.86	.89	
Rough + sand	Loose	9.6 10.6	.69	.76	
Rough + dust	Fairy castle	9.6 10.6 11.1	.82	.84	

[a] Slash (/) = repeat run

Table II (Concluded)

D. METEORITIC CHONDRITES

Sample (and USNM No.)	SiO_2 (%, or surface texture)	Spectral Minima (stronger underlined)	Emittance	
			ϵ_λ min	ε average (7.8 to 13.0 μ)
Haven (SRI 3408)	-	10.75 (reflectance)	0.68 (R)	0.81 (R)
Leedey (489.15)				
(SRI 3604-1)	Sawed	10.7	.70	.77
(SRI 3604-2)	Sawed	10.8	.73	.79
Ladder Creek (SRI 3456)	-	10.8 11.1	.72	.76
Farmington (No. 48.5)	-			
(SRI 3605-1)	Sawed	11.2	.76	.87
(SRI 3605-2)	Sawed	11.3	.76	.88

E. MISCELLANEOUS MATERIALS

Sample (and USNM No.)	SiO_2 (%, or surface texture)	Spectral Minima (stronger underlined)	Emittance	
			ϵ_λ min	ε average (7.8 to 13.0 μ)
K-feldspar	Rough	9.60	0.61	0.81
Silicon carbide (SiC)				
12 μ powder	Fairy castle	12.5	.80	.93
17 μ powder	Fairy castle	12.5	.83	.93
75 to 150 μ	Rough	12.3	.56	.81
Crystals	Smooth	12.2	.27	.54
Alumina (Al_2O_3)				
0.02 μ powder	Fairy castle	10.9	.88/.90	.91/.96
Fine-grained tubing	Smooth	11.8 (broad)	.58	.71
Alundum platelets	Smooth	11.8	.36	.54
Sapphire rods	Frosted	11.85	.61	.77
Sapphire sheet	Frosted	11.5	.53	.68
Aluminum foil (sample base)	Polished	13.0	.08	.09
Sulfate ($CaSO_4$)				
Anhydrite sand	Loose	8.3 8.6	.76	.84
Carbonate				
Calcite ($CaCO_3$)	Smooth	6.7 11.3	.32	.76
Dolomite ($(Ca,Mg)CO_3$	Rough	6.45 11.2	.72	.90
Aragonite ($CaCO_3$)	Rough	6.7 11.5	.47	.76

The emittance values tabulated in Table II and in Appendix A are for the rock samples obtained from the U.S. National Museum collection. Other values are marked on the emittance curves; for example, in Fig. 2, for quartz in various size fractions, the numbers resembling 0.85 represent the emittance values over the wavelength range of the measurements (7.8 to 13.0 μ).

These values do not indicate the spectral differences or "contrasts" which are often marked between the sample surface and the blackbody. They only give the integrated departure from the standard. This spectral aspect of an emission curve has been underestimated by previous workers, since most of the experimentation has been performed using integrating radiometers rather than spectrometers. Much more diagnostic use can be made of the spectral contrast* in the curves, for example, in Fig. 28, in differentiating the sample of the quartz monzonite porphyry (A) from that of the syenite (B) and from the peridotite (C), although all three samples have approximately the same average emittance (0.81, 0.86, and 0.88, respectively).

A series of spectral peaks is tabulated in Table II. The data were processed by the computer, normalized, and replotted on rectangular coordinates, before extracting the minimal values. The table lists sample name and composition (where known), spectral minimal position and emittance value, and the average emittance over the 7.8 to 13.0 μ region.

e. Error Analysis

Analysis of the possible errors in this measurement should be divided into the following three categories:

---

* Spectral contrast may be readily obtained by subtracting the last two columns in Table II. This represents the variation of the strongest peak away from the average level of the spectrum.

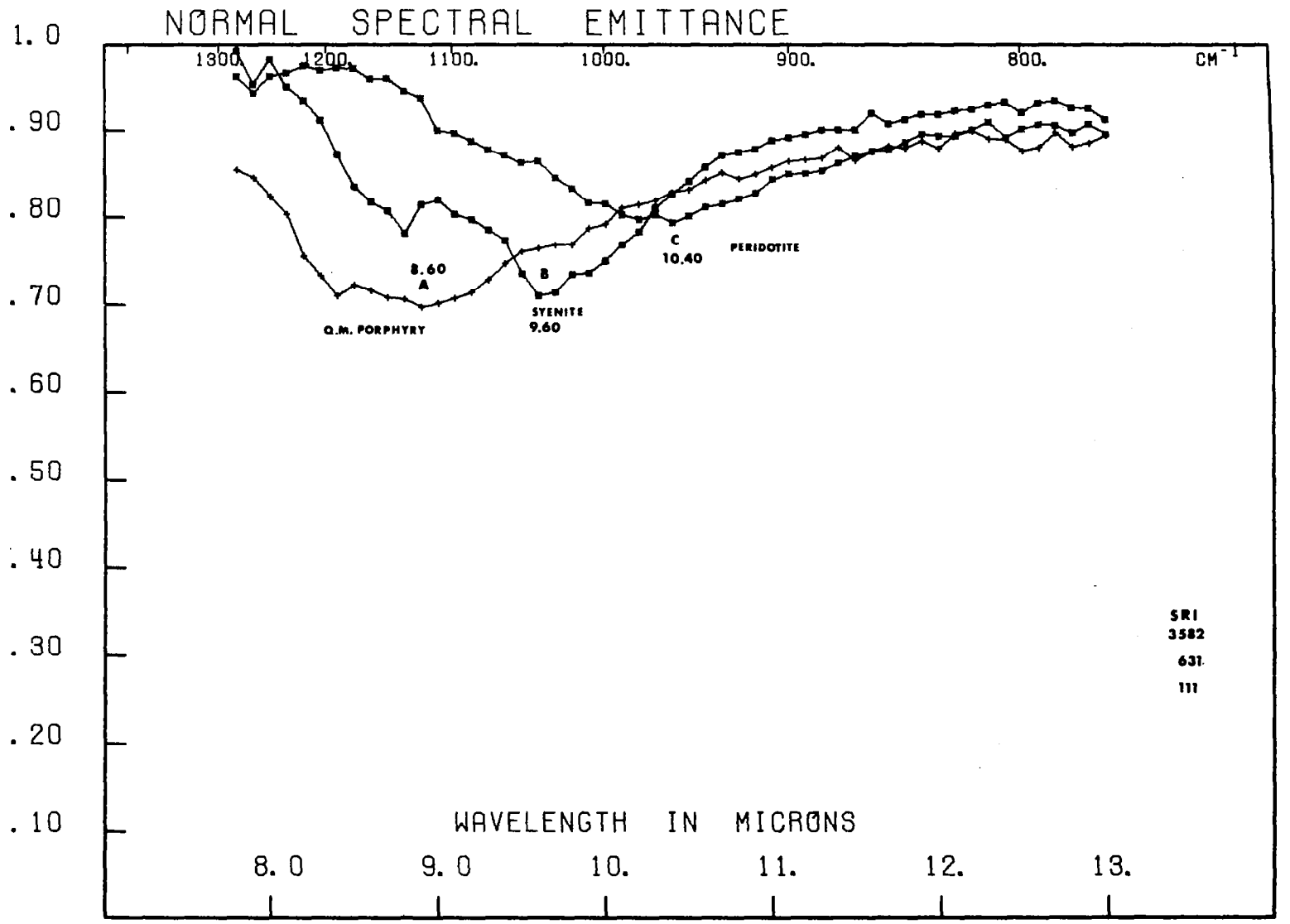

FIG. 28 NORMAL SPECTRAL EMITTANCE CURVES FOR SAMPLES OF QUARTZ MONZONITE PORPHYRY (SRI 3582), SYENITE (USNM 631), AND PERIDOTITE (USNM 111). Despite the fact that the three samples have almost the same average emittance, the spectral minima are displaced markedly among these three compositions.

1. Wavelength inaccuracies
2. Lack of spectral resolution
3. Temperature differences between blackbody and the sample

The drum of the PE112 spectrometer may be recalibrated in either wavelength (microns) or wavenumber (cm^{-1}) on the basis of observed peak values with known absorption maxima. Such calibration can be made on water vapor peaks, on polystyrene, carbon dioxide, or ammonia placed in the sample beam (Fig. 15). By varying the chart speed with respect to the drum speed (expanding the scale), individual peaks can be located on the chart of a spectrum to ± 1 cm^{-1}.

Spectral resolution denotes the extent to which closely adjacent spectral bands can be split or separated and is determined by the spectral interval incident on the detector and hence by the optics and mechanical slit widths. It is possible to calculate the spectral resolution at any desired wavelength.

Such calculations for the direct emittance experiments have yielded the spectral resolution* ($d\lambda$) of 0.06 μ at 10 μ and 0.08 μ at 12 μ (6 cm^{-1} at 1000 cm^{-1} and 5.5 cm^{-1} at 833 cm^{-1}). This should be quite suitable to resolve the broad spectral bands found in the rock studies.

Inaccuracies in reading the temperature of either the sample or the blackbody are hard to correct and are the direct cause of error in the average emittance calculations. The continuous recording of the thermocouple output indicates that the temperature remained constant during both the sample and the blackbody spectra, but it does not indicate that the temperature all over the sample or blackbody was equal to that being recorded at the point of contact with the thermocouple bead. With the metal blackbody this difference was probably small, but with the rock sample

---

* Shown by the small symbols in the lower half of Figs. 1 and 22.

(and specifically in the case of the powdered surface), there could be considerable lateral differences in temperature across the sample surface. If the sample was too low in temperature relative to that of the blackbody, its spectral curve indicates a lower emittance; if the temperature of the surface was high relative to that of the blackbody, then the spectral data indicate a high emittance. Thus the values of average emittance which represent the integrated area under the blackbody at the same temperature should be used with care. Consecutive runs (including runs with both sides of a sample being examined) did not show great changes in these emittance values (Figs. 26 and 27).

The purpose of this investigation was not to derive absolute emittance values but to indicate that the spectral differences between rock surfaces can be used to indicate their composition. It was likewise not intended that the integrated area under the curve would yield an absolute value for the temperature at which the experiment was conducted. It is significant, though, that the three rock curves plotted in Fig. 28, all having a roughly equivalent average emittance (0.81 to 0.88), show their spectral minima displaced from 8.90 μ for the quartz-monzonite porphyry to 9.60 μ for the syenite to 10.40 μ for the peridotite, a total shift of 2.50 μ.

Figure 29 shows plots with the radiant energy format (of Appendices B and C) of these three samples, and the fraction of the energy remaining after a 3.4-mile sea-level transmission of a comparable set of spectra. In a similar manner it is still possible to see both their spectral contrast and the shift in the peaks between the three rock compositions, although their average emittances (as indicated) are quite similar.

3. Effects of Compositional Differences between Samples

The shift in wavelength of the major spectral peak for each sample with the increase in SiO_2 content of the rock is most important. Quartz crystal (9.0 μ) and fused quartz (9.0 μ) are at the shortest wavelengths of any peaks noted for common silicate rock materials. Obsidian (9.2 to 9.4 μ) and tektite (9.3 μ) occupy the "acid" end of the rock

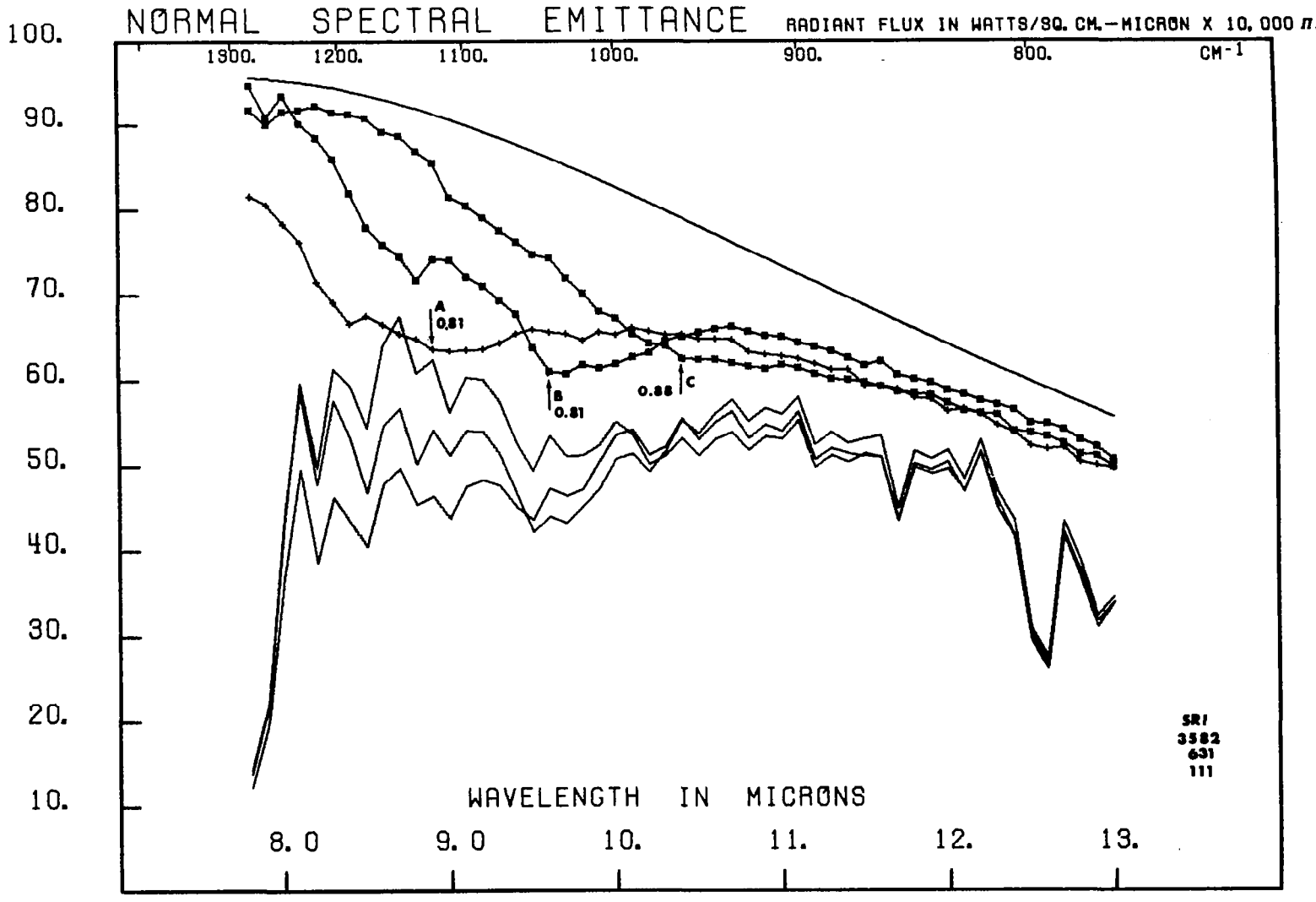

FIG. 29 RADIANT FLUX PLOTS FOR THE SAME THREE SAMPLES AS IN FIG. 28, (QUARTZ MONZONITE PORPHYRY (A), SYENITE (B), PERIDOTITE (C). Central numbers refer to the emittance averaged over the wavelength interval 7.8 to 13 μ. The jagged curves in the lower half of the drawing are the same radiant flux spectra after passage through the 3.4 miles of atmosphere, with attenuation factors as given in the text. Differentiation of the composition of the source materials is thus markedly complicated by the effects of atmospheric attenuation. Note that values on the ordinate have been multiplied by $10^4 \cdot \pi$.

compositional studies, but there is a gap before reaching andesite (9.6 μ), basalt (10.4 μ), and serpentine (10.1 μ).

The most "basic" end of the rock suites, dunite (10.7 μ) and the stony meteorite or chondrite (10.8 μ), shows the greatest departure toward the longer wavelength. This shift in wavelength with compositional change has been previously noted. In Final Report I, attention was drawn to this phenomenon as a means of determining the bulk composition of the rock sample. This also formed the basis of two of the technical papers. The spread of about 2.1 μ in wavelength of the peak of the emittance spectra from obsidian to the meteoritic composition (9.2 to 11.3 μ) almost represents the 2.2 μ spread found by infrared absorption analysis (9.35 to 11.5 μ), and the 2.0 μ spread found by infrared reflection analysis (9.2 to 11.2 μ) for similar samples.

a. Acid Rock Types

In discussing the infrared spectra of the acidic rock types, reference will be made to several of the figures. Figure 30 shows two emittance curves (E_1 and E_2) from 7.8 to 13.0 μ from an obsidian and a tektite sample. These curves represent direct emission measurements on these two materials and should be contrasted with the reflection curve (R) extending from 7 to 25 μ (1400 to 400 cm^{-1}). The similarity in the curve shapes between obsidian and tektite makes for an interesting comparison with their similarities in chemical composition. The obsidian sample (E_2) has a minimum at 9.20 μ (1087 cm^{-1}) and the tektite sample has a minimum at 9.30 μ (1075 cm^{-1}). These are in close agreement with the obsidian sample whose reflection data, replotted on the emittance format, yield a minimum at 9.17 μ (1090 cm^{-1}). These three similar materials have yielded similar infrared emission and reflectance spectra. (The peak at 21.9 μ or 460 cm^{-1} is another fundamental of the silicon-oxygen stretching vibration.

Figure 31 shows two emittance spectra, one for a frothy pumice specimen (E_1) from the Mono Lake, California, locality and one for a welded tuff specimen (E_2) from the top of Rainier Mesa, Nevada Test Site.

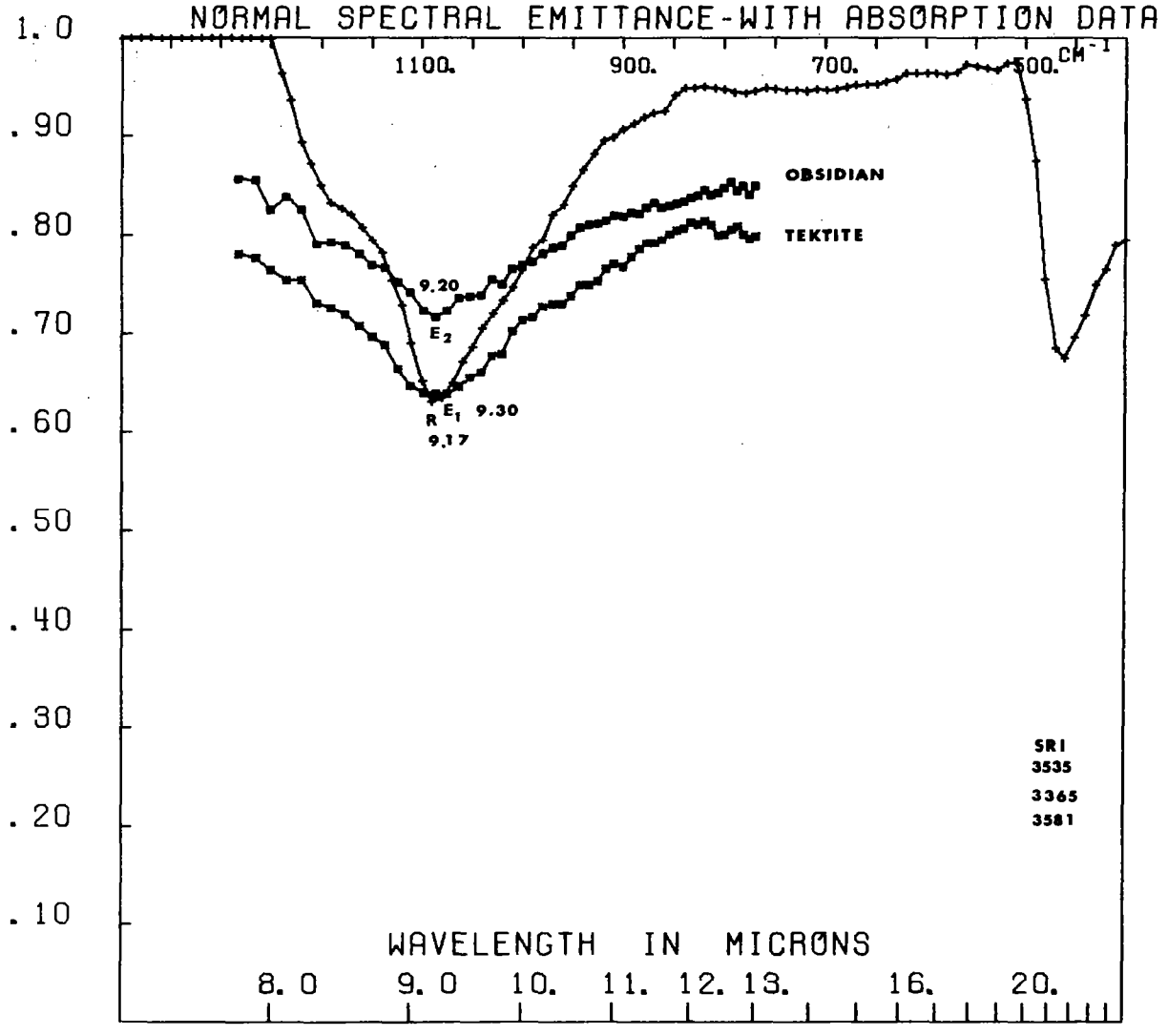

FIG. 30 NORMAL SPECTRAL EMITTANCE CURVES FOR A TEKTITE SAMPLE (E_1) AND THE GLASSY EQUIVALENT OF GRANITE, OBSIDIAN (CURVE E_2). The calculated emittance spectra obtained from reflection data for the Snowflake obsidian sample (R) are included for comparison.

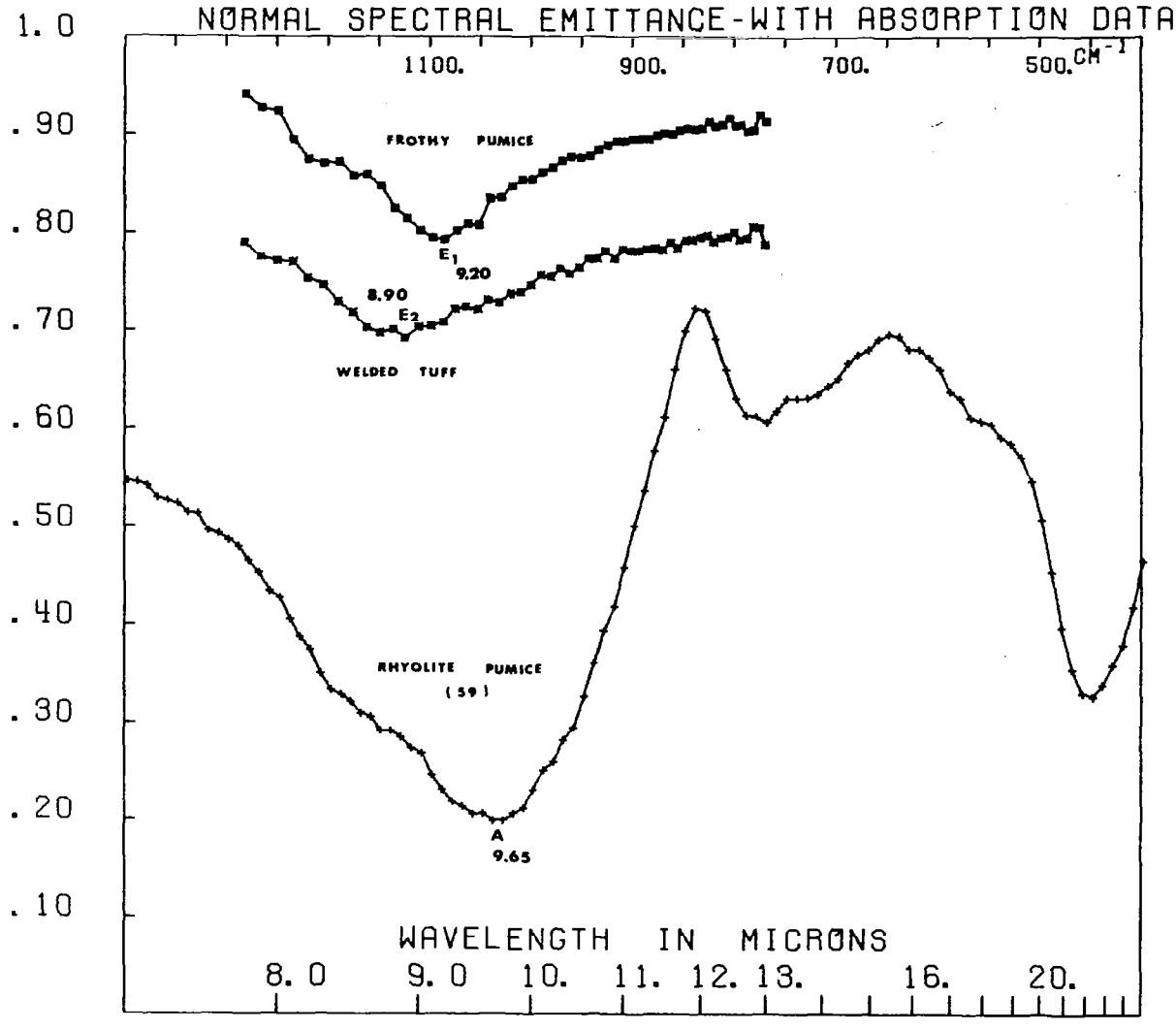

FIG. 31 NORMAL SPECTRAL EMITTANCE CURVES FOR A FROTHY PUMICE SPECIMEN (E_1) COMPARED WITH THAT OF A WELDED TUFF (E_2). The absorption spectrum of the rhyolite pumice (USNM 59) has been included (A) for comparison of the methods of analysis.

These two emittance spectra are compared on the figure with an absorption spectrum of a rhyolite pumice specimen (USNM 59), described in detail in Appendix A. Analyses are not available for the (E_1) and (E_2) samples but it is known that they represent a fairly high SiO_2 content (above 65% SiO_2). Their emission minima at 9.2 μ (1085 cm^{-1}) for the frothy pumice (E_1) and at 8.9 μ (1125 cm^{-1}) for the welded tuff (E_2) agree with the emission minima of the preceding figure. The minimum of the absorption curve for the rhyolite pumice occurs at 9.65 μ (1035 cm^{-1}), at a much longer wavelength. This long-wavelength shift, characteristic of the absorption spectra, will be discussed in Section IX.

Three emission spectra appear in Fig. 32. The spectrum of a graphic granite (USNM 377) appears in the figure as curve C. Its two main constituents--quartz and potassium feldspar (K-feldspar)--are themselves represented by emission spectra, curves A and B respectively. The quartz spectrum is that of a roughened, X-cut quartz plate, comparable to the pattern which might be expected from fractured, discrete grains of quartz in a rock matrix (see Fig. 38 for other similar spectra). The feldspar curve (B) was obtained from a rough cleavage flake, also comparable to that expected in a rock. The combination of the two curves could have yielded the curve (C), showing that mixtures of two materials could result in a composite curve (i.e., a rock spectrum) comparable to that of the graphic granite. (See also dunite and quartz in Fig. 60.) Another granite specimen (USNM 158) was used to produce the emission curve in Fig. 33 (upper curve), with the lower curve derived from a rough specimen of aplite (occurring as a vein in a granite mass at the SHOAL Test Site, Fallon, Nevada). The similarity between the two curves is quite striking, and their emission minimum occurs at the same point in each curve. This is perhaps to be expected as the composition of aplite is often equivalent to that of granite, except that it is finer grained. Unfortunately no chemical or mineralogical analysis is available for the aplite specimen but it macroscopically resembles the granite.

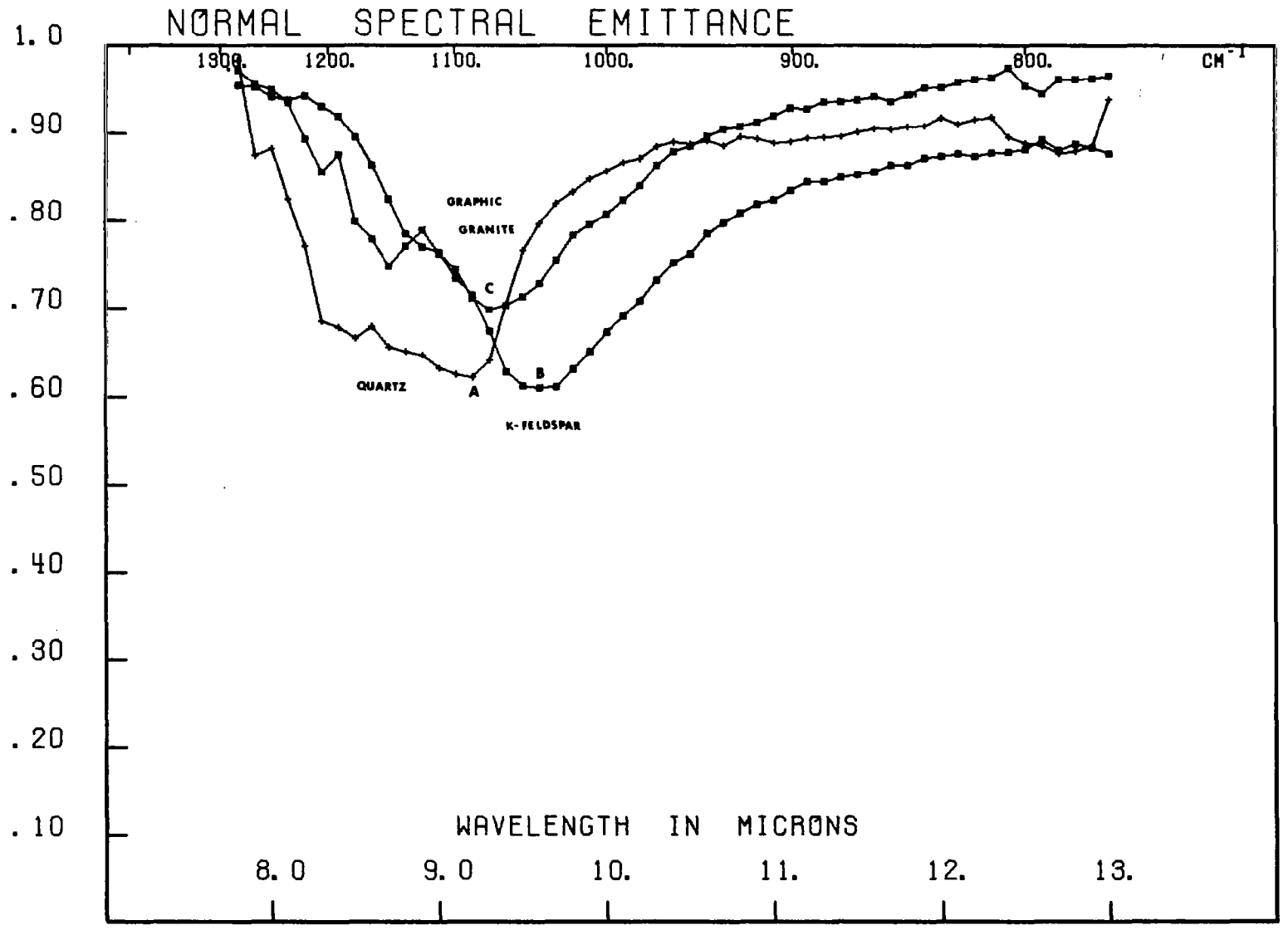

FIG. 32 NORMAL SPECTRAL EMITTANCE CURVES FOR A ROUGHENED QUARTZ PLATE (X-CUT) AND A CLEAVAGE FRAGMENT OF K-FELDSPAR, COMPARED WITH THAT OF A GRAPHIC GRANITE (USNM 377) SAMPLE WHICH CONTAINS QUARTZ AND FELDSPAR AS ITS MEASURED CONSTITUENTS.

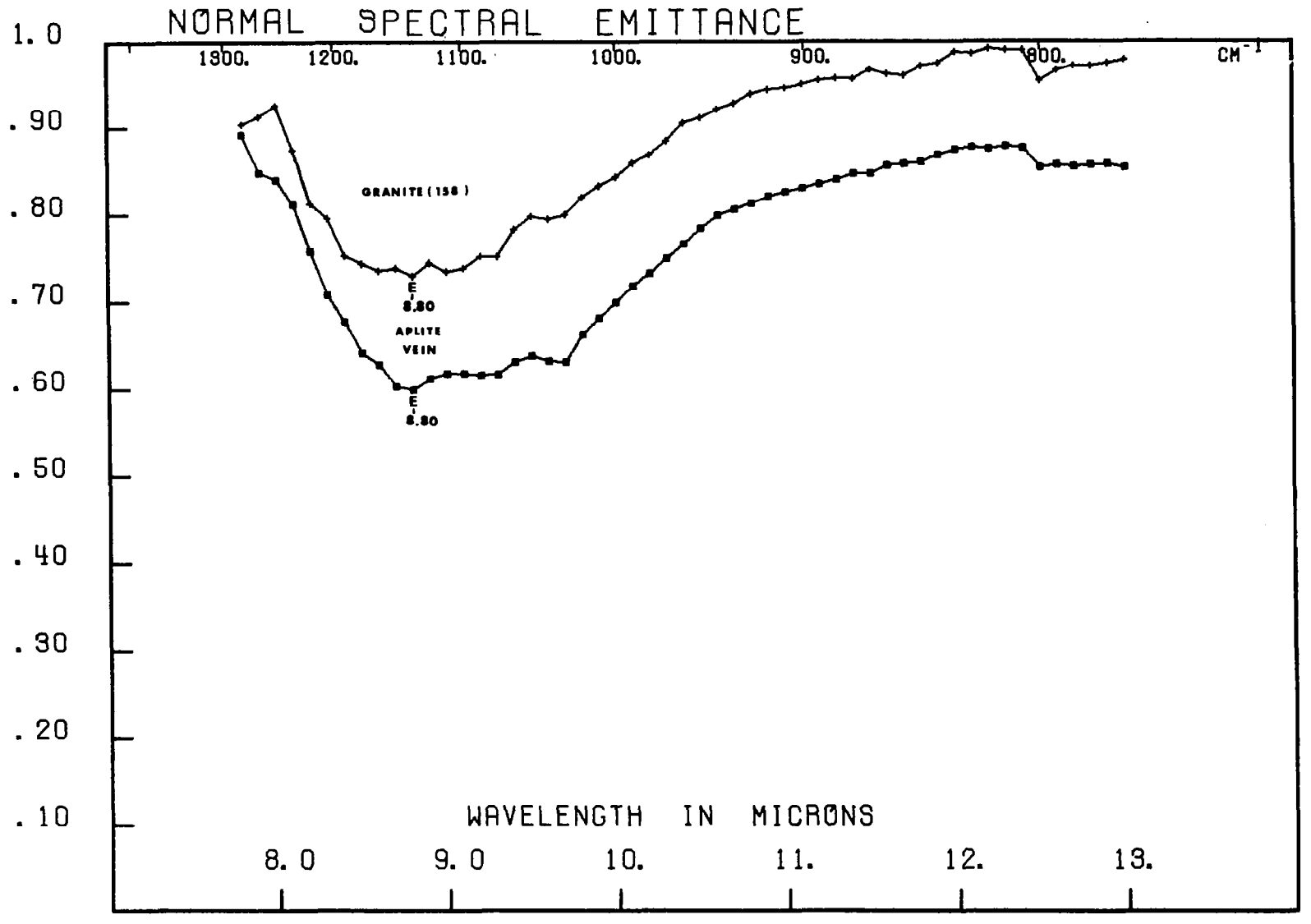

FIG. 33 NORMAL SPECTRAL EMITTANCE CURVES OF GRANITE (USNM 158) COMPARED WITH THAT OF AN APLITE VEIN (A FINE-GRAINED GRANITIC VEINLET) FROM THE SHOAL TEST SITE, NEVADA.

b. Intermediate Composition

Quartz diorite (USNM 758) was analyzed and its absorption, reflection, and emission curves were digitized, computed, and replotted in Fig. 34 as an example of a rock of an intermediate composition (54.6% SiO_2; see Appendix A-15). The three spectra show differences only in their minima as defined by the different methods. The emission curve (E) has a minimum at 10.00 μ (100 cm^{-1}) and the reflection curve (R) has a similar minimum, while the absorption spectrum (A) shows its trough to be at 10.10 μ (990 cm^{-1}). The fundamental peak at 21.74 μ (460 cm^{-1}) appears in both the reflection and the absorption spectra, but the peak at 13.0 μ (770 cm^{-1}) does not occur in the reflection spectrum. The emission spectrum was not carried past 13.0 μ so the presence of this particular band cannot be adequately established in that spectrum.

c. Basic Rock Types

The Haven chondritic meteorite and the dunite specimens represent two of the most basic rocks available for study. This is shown by their reflection (R) and absorption (A) spectra in Fig. 35, which show minima at 10.75 μ (930 cm^{-1}) and 11.23 μ (8.90 cm^{-1}), respectively. These peaks are in sharp contrast with the tektite specimen whose emission minimum (E) occurs at 9.30 μ (1075 cm^{-1}).

The emission spectrum of the tektite only contains data from 7.8 to 13 μ, but it is obvious that the material is quite different in its infrared emittance characteristics from the dunite or meteorite samples.

Figure 35 is of significance to the lunar problem, for represented on this diagram are the infrared spectra of three possible lunar surface rock materials. It is believed that the tektite represents material ejected from the lunar surface following meteoritic impact. It is possible, although by no means proven, that the lunar material may be composed of dunite, as its density (3.3 grams per cc) is very close to that computed for the average density of the moon. To show that these three rock types can be differentiated by means of their infrared spectra is an important step in the utilization of this technique for lunar surface analysis.

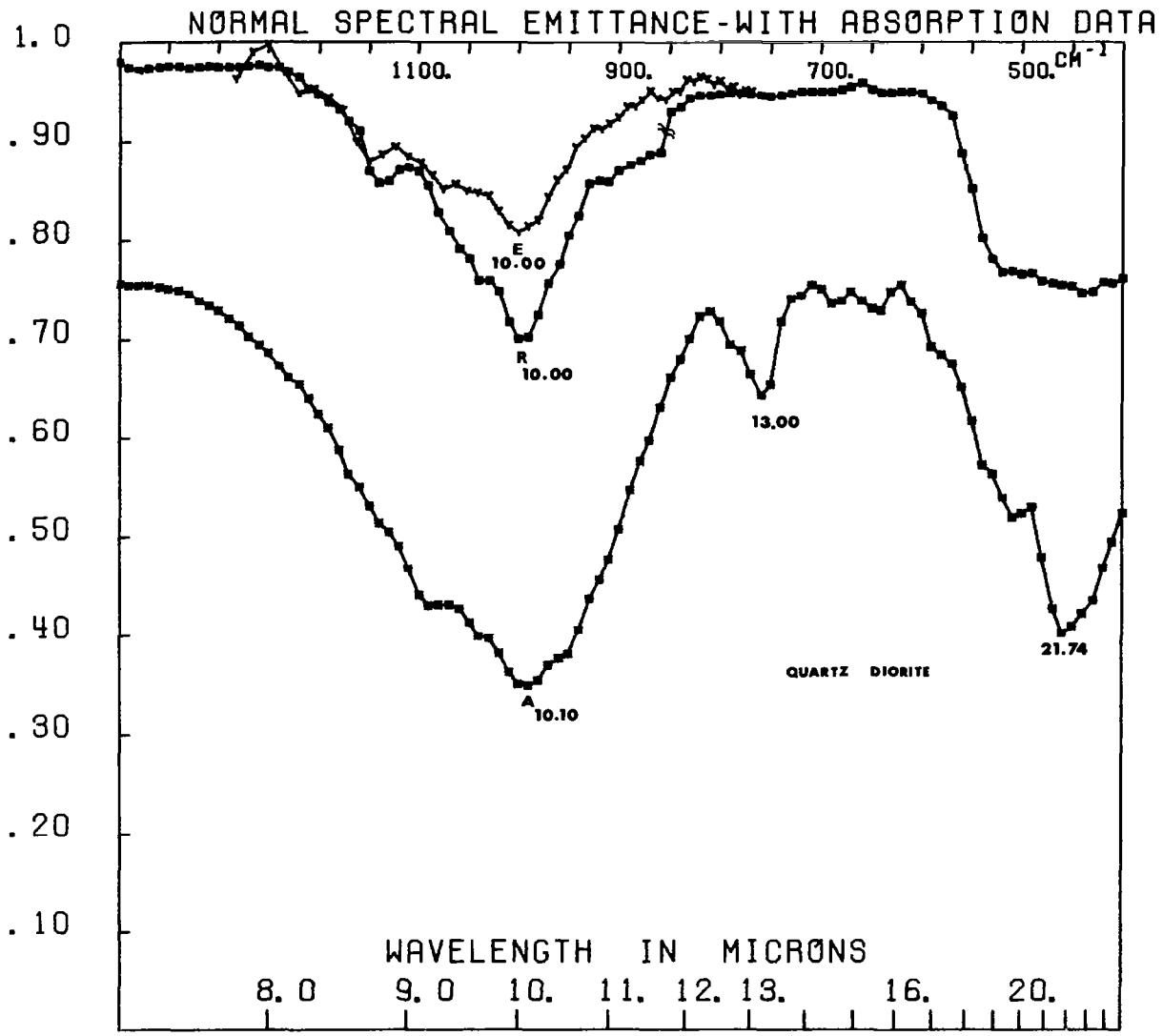

FIG. 34 NORMAL SPECTRAL EMITTANCE CURVES FOR QUARTZ DIORITE (USNM 758) COMPARED WITH THE CALCULATED EMITTANCE CURVE (R) OBTAINED FROM REFLECTANCE DATA FROM THE POLISHED SURFACE OF THE SAME SAMPLE. The lower curve (A) represents the absorption spectrum of the same material.

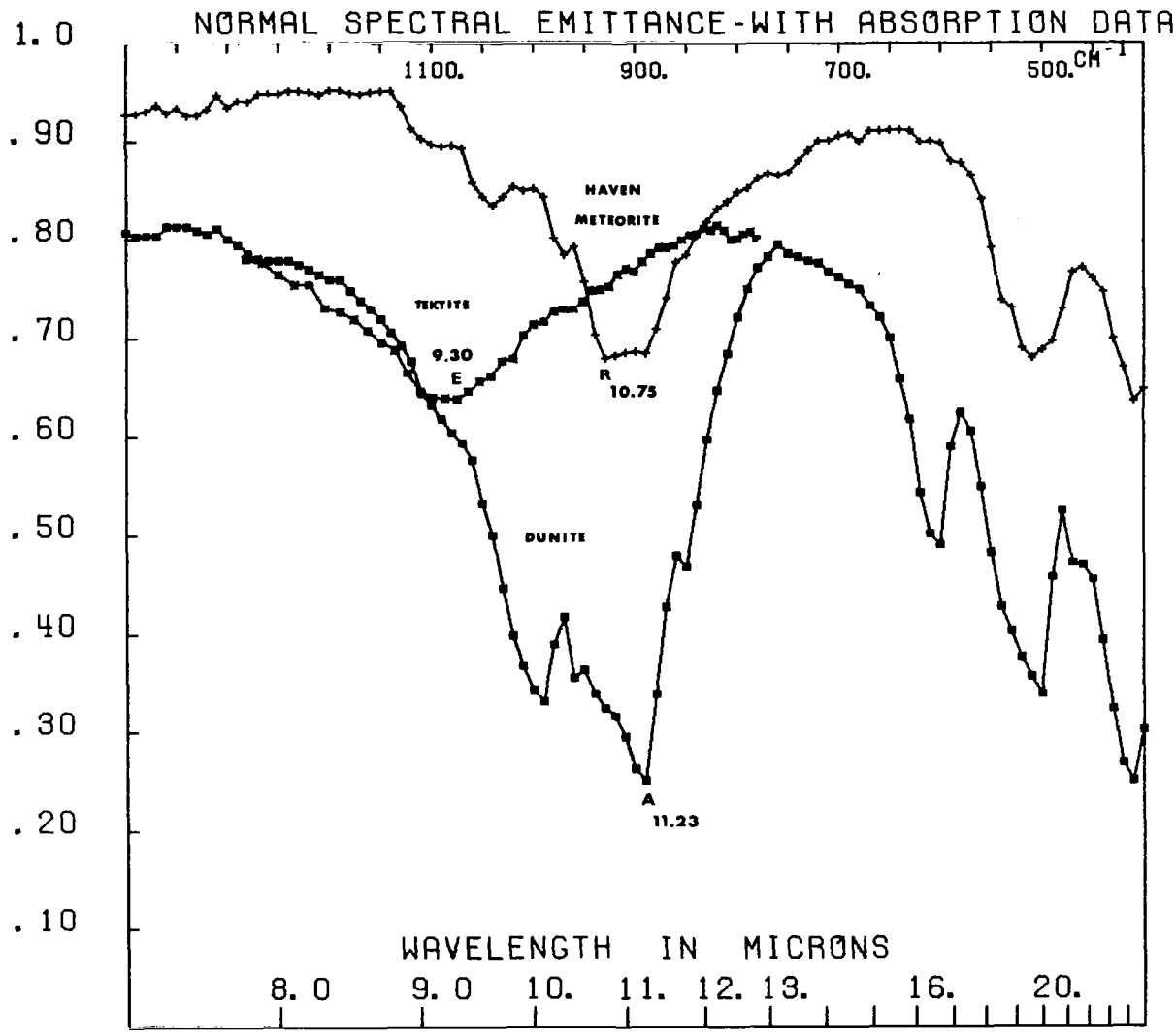

FIG. 35 NORMAL SPECTRAL EMITTANCE CURVE OF THE ACIDIC ROCK SAMPLE, TEKTITE (E), SHOWING THAT ITS MINIMUM AT 9.30 μ CONTRASTS MARKEDLY WITH THAT OF THE HAVEN METEORITC CHONDRITE (R), OBTAINED FROM REFLECTANCE DATA. The absorption curve (A) for dunite, a similar basic rock type, is included for comparison.

4. Effects of Surficial Differences between Samples

Recent studies by B. Hapke of Cornell University[22] (presented at the Lunar Surface Materials Conference in May 1963) have shown that powders of 10 μ diameter sifted on to a flat surface will form into a highly porous, fluffy formation. These "fairy castle" structures almost exactly reproduce the photometric backscattering properties of the lunar surface. This is a most important photometric observation. There is a similarity in the size of the powders used by Hapke and the wavelength of infrared radiation used in our compositional studies (8 to 25 μ, 1250 to 400 cm^{-1}), and we are therefore extremely interested in both theoretical and experimental studies of the scattering effects from such roughened and powdered surfaces.

a. Roughness

In Fig. 36 curve A represents the normal emittance spectrum obtained from a polished Z-cut quartz oscillator plate, compared with the absorption spectrum of quartz in a KBr pellet.

In Figs. 1-3 the normal emittance spectrum of a polished X-cut plate is shown, contrasted with rough and powdered quartz. The Z-cut orientation shows more spectral detail than the X-cut (Fig. 2), as seen also in Fig. 7. Like reflection spectra*, emission spectra are dependent upon the orientation of the particular crystal surface under study.

Curves C, D, and E (shown originally in Fig. 2) are the emittance spectra from quartz powders of 25 to 45 μ, 10 to 25 μ, and 1 to 10 μ particle sizes, respectively. The values given underneath the curves are the emittance ratios for the wavelength 7.8 to 13.0 μ, representing the fact that the average emittance rises markedly as the surface is roughened.

---

* The strong reflecting power of metals, and that of quartz for wavelengths near 9 μ, is due to an absorption so intense that it occurs within a fraction of one wavelength of the surface. Under these conditions true absorption no longer occurs. The process becomes indistinguishable from elastic scattering--namely, reflection.

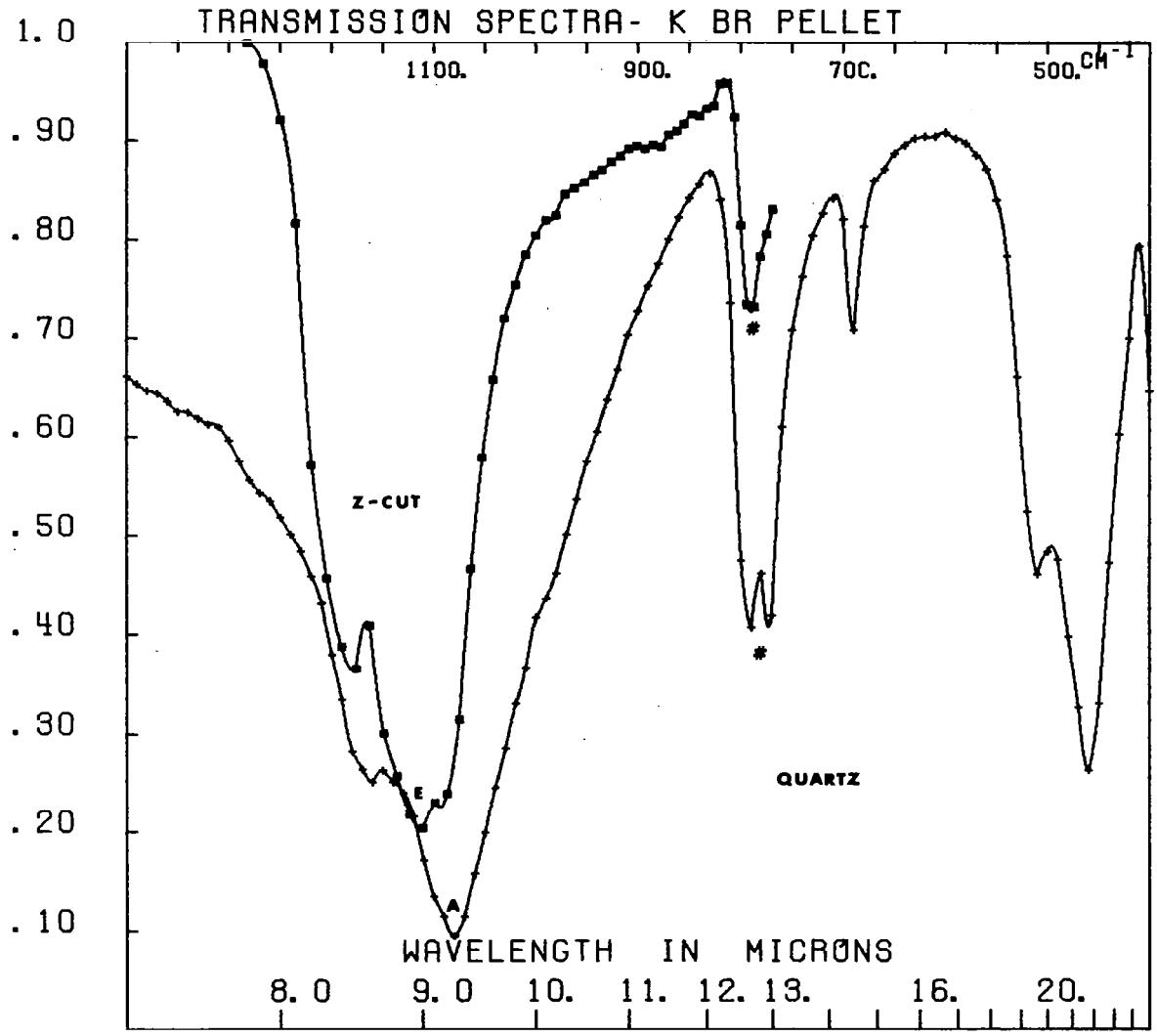

FIG. 36 TRANSMISSION SPECTRUM OF FINELY POWDERED QUARTZ IN A KBr PELLET IS SHOWN AS THE LOWER SPECTRUM (A) IN THE FIGURE, WITH THE NORMAL SPECTRAL EMITTANCE CURVE (E) FOR A Z-CUT QUARTZ OSCILLATOR PLATE. The smooth curves have been obtained by passing a second-order curve (by a Lagrangian interpolation) through the existing data points.

All the powders were sifted into the fairy castle structures to produce a high degree of voids in the emitting surface. These voids apparently increase in wavenumber as the particle size decreases and emit as small blackbody cavities contributing to the masking of the spectral "contrast" on the curve (see Table II). Part of the problem with the fine powders is due to the presence of a greatly increased number of voids. Part is also due to a scattering effect, which may be seen from the sandblasted and polished surfaces of the same piece of pure crystal quartz in Fig. 2 in which the introduction of surface cavities and subsurface fractures has markedly changed the scattering characteristics.

Returning to dunite, a typical (basic) rock sample, spectral data appear in Fig. 37 for a variety of textures and particle sizes. A decrease in spectral "contrast" with roughness is seen, identical to that seen in quartz. Average emittance values are shown in Table III.

Table III

EMITTANCE VALUES FOR VARIOUS SURFACES ON A DUNITE SPECIMEN

Surface	Emittance Minimum	Average Emittance (ϵ)[a] (8 to 13.5 μ)	"Spectral Contrast"
Polished	0.44	0.77	0.33
Rough (other side)	.66	.80	.14
Grit (above 850 μ)	.73	.78	.05
Sand (150 to 300 μ)	.74	.79	.05
Dust (40 to 80 μ)	.79	.86	.07
Powder (40 to 25 μ)	.86	.89	.03
Rough + sand[b]	.69	.76	.07
Rough + dust[b]	.82	.84	.02

[a] At 370° C (643°K)

[b] Layers about 2 mm thick

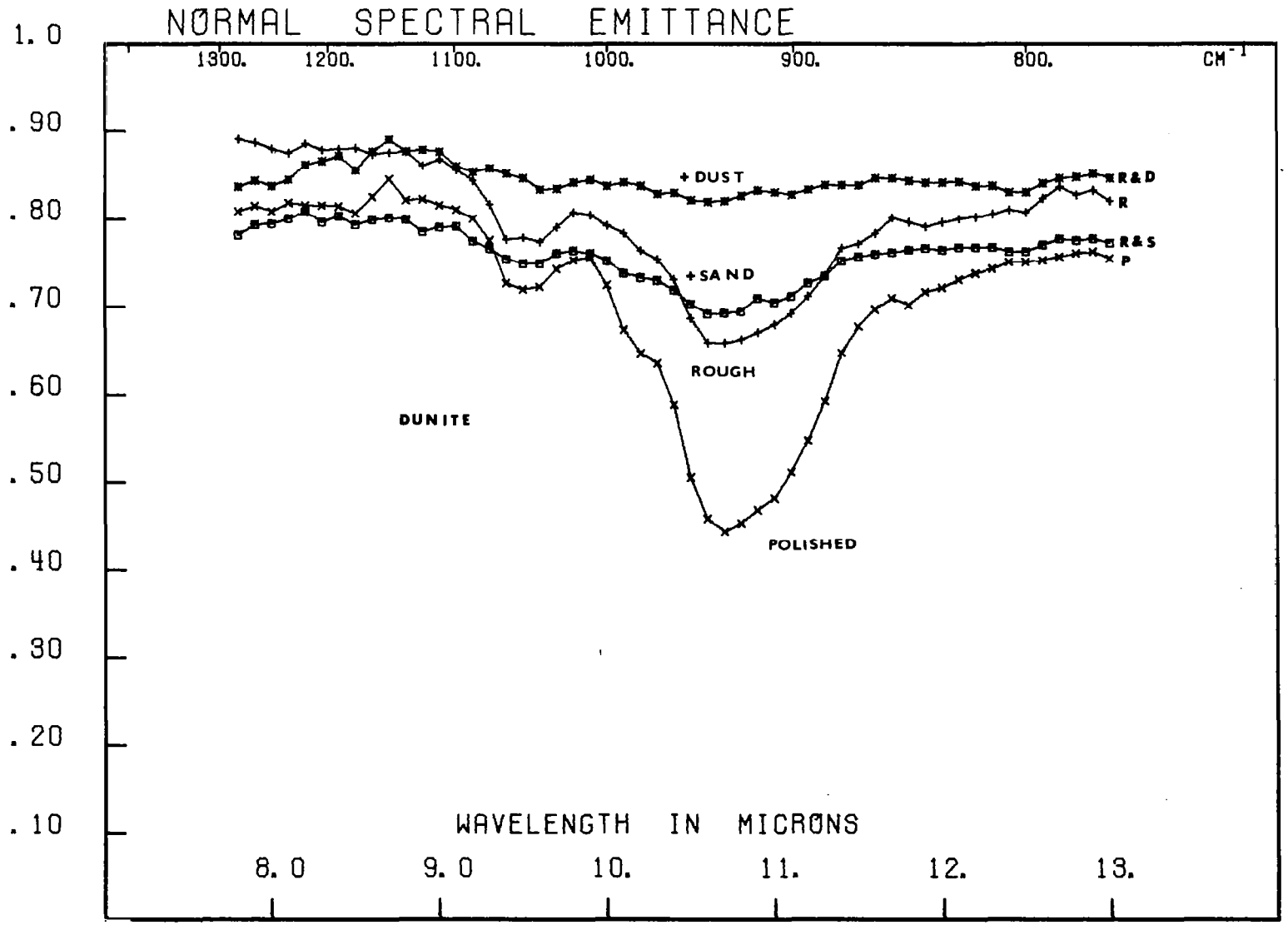

FIG. 37 NORMAL SPECTRAL EMITTANCE OF DUNITE SAMPLES AS A FUNCTION OF SURFACE ROUGHNESS AND PARTICLE SIZE. The spectral contrast disappears as the surface is roughened and declines to a minimal value when the rough surface is covered by a thin layer of sand or dust. The dust layer effectively emits as a greybody with no spectral contrast.

The average emittance of the dunite surfaces shown in Table III over the interval 8 to 13.5 μ (1250 to 740 cm^{-1}) thus approximates 0.71 to 0.84. Regardless of the manner in which the surface is prepared (rough plus dust, rough plus sand), the average emittance at 0.84 is not exceeded and then the curve is that of a greybody devoid of spectral contrast (0.02 value).

b. Particle Size

Emission curves were attempted for a dunite sand sample, 150 to 300 μ size at temperatures as low as 75°C (350°K). For a series of temperatures between 110 and 370°C (380 and 640°K) values were obtained for an emittance around 0.72. The values at 75°C were too uncertain to be more than indicative, due to the low sensitivity of the instrument used at these source temperatures. The values are listed in Table IV.

Table IV

EMITTANCE VALUES FOR DUNITE SAND (150 to 300 μ)

AT VARIOUS TEMPERATURES

Temperature		Average Emittance, (ε) (8 to 13 μ)	
°C	°K		
75	348	0.54[a]	0.87[a]
110	383	.71	.70
175	448	.79	.68
227	500	.66	---
370	643	.71	.79

[a] Energy levels are so low and the gain of the equipment is set so high that these values are indicative only.

Average emittance values calculated from reflectance data are shown in Table V.

Table V

EMITTANCE VALUES CALCULATED FROM REFLECTANCE DATA OF POLISHED SURFACES[a]

Sample	Average Emittance, (ϵ) at 77°C (350°K)	
	1 to 25 μ[b]	8 to 13 μ
Granite (3382)	0.86	0.80
Obsidian (3358)	.83	.78
Dunite (3390)	.78	.72
Meteorite ("Haven") (3408)	.81	.79

[a] Average emittance here is calculated for a blackbody energy level at 77°C (350°K) by using the relationship $(1-\rho_\lambda)$, where ρ_λ = the reflectance obtained at wavelength (λ) from a polished surface at ambient temperature.

[b] See Fig. 17.

Quartz. Figure 38 shows emission spectra over the wavelength range 7.8 to 13 μ (1280 to 770 cm^{-1}), for polished X-cut quartz, rough X-cut quartz, a sample of fine-grained siliceous chert (E_3), and for a sample of quartz sand (E_1), of a particle size range from 300 to 500 μ. Chert is a compacted fine-grained material with a slightly roughened surface and its spectrum is quite similar to that of the loosely compacted sand grains. Both closely resemble the roughened quartz surface (E_2), and all four spectra indicate the presence of the characteristic doublet at 12.5 μ (800 cm^{-1}).

In Fig. 39 the chert spectrum has been reproduced (E_2) and compared to the emittance from quartz powder (E_1) sized to contain 1 to 10 μ particles. (See photograph in Fig. 43.) The longer absorption curve (A), with peaks at 9.26, 12.5, 14.5, and 21.7 μ (1080, 800, 690, and 460 cm^{-1}), is of finely powdered quartz embedded in a potassium bromide pellet. The similarity between the chert spectrum and the absorption spectrum of quartz is marked, at least from 7.8 to 13.0 μ, although the absorption spectrum

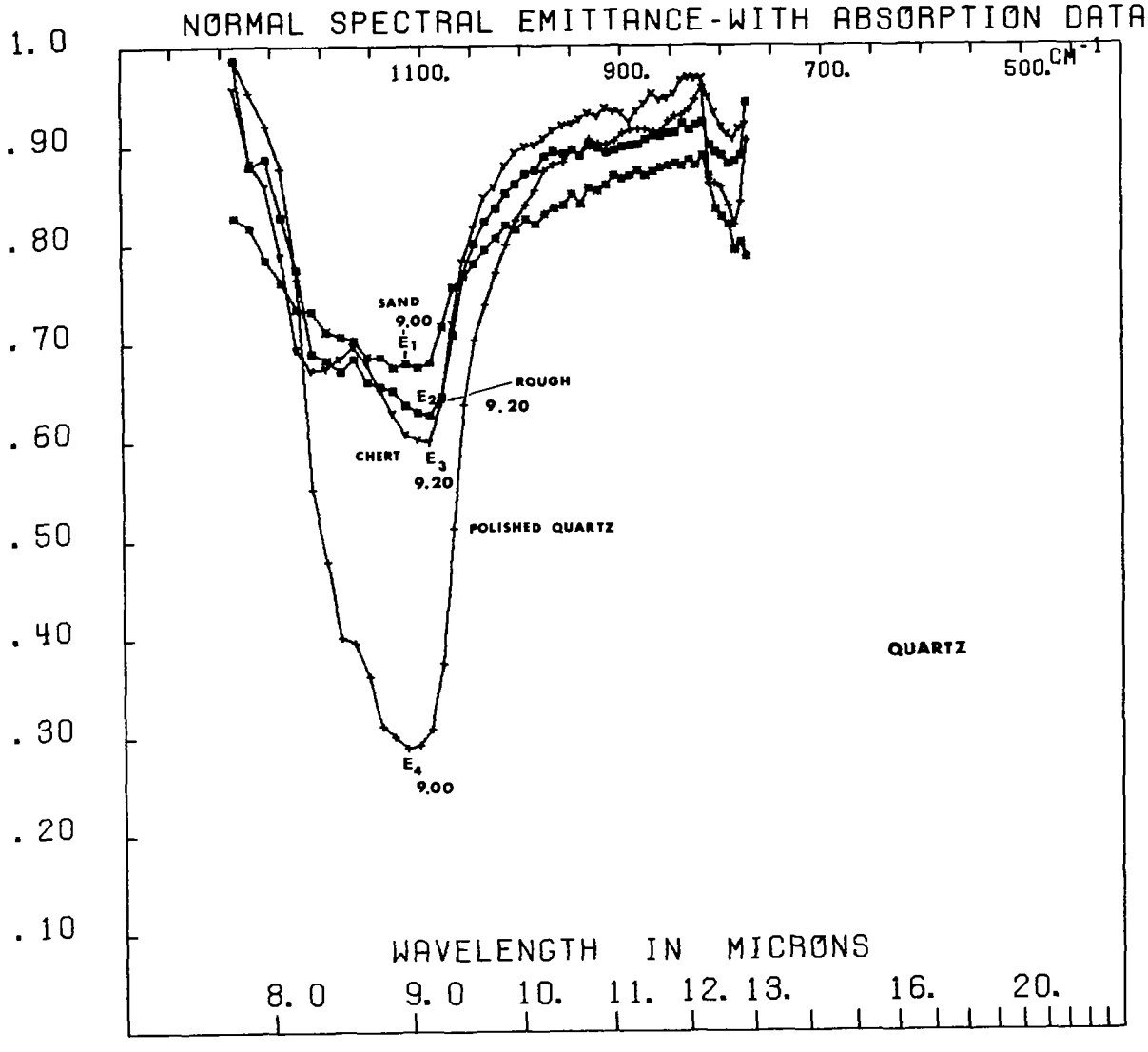

FIG. 38 NORMAL SPECTRAL EMITTANCE CURVES FOR POLISHED QUARTZ (E_4) AND FOR ROUGHENED QUARTZ (E_3), COMPARED WITH THE SPECTRA FROM A QUARTZ SAND (E_1) AND A FINE-GRAINED CHERT (E_2). All four spectra show the characteristic doublet at 12.5 μ.

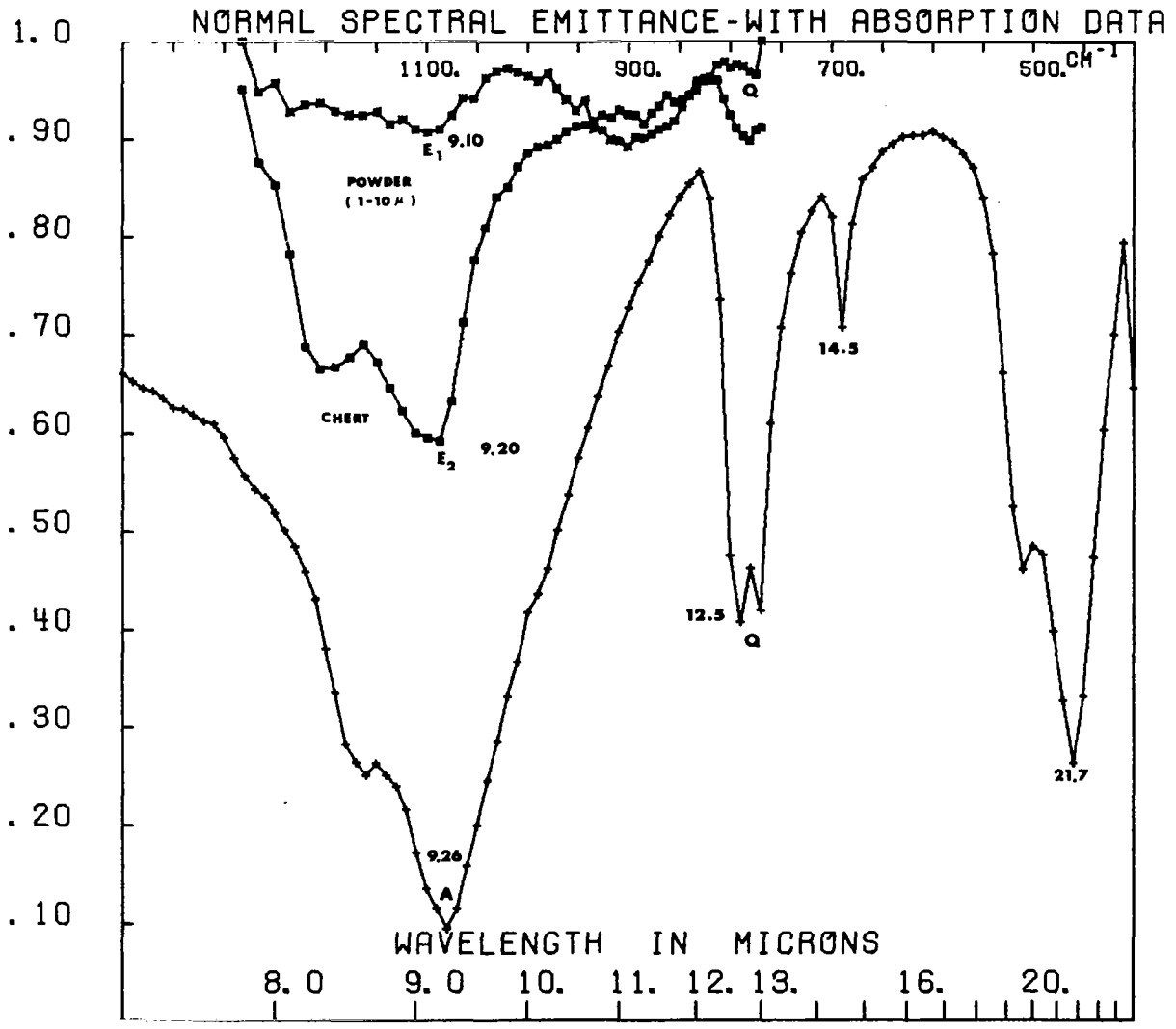

FIG. 39 NORMAL SPECTRAL EMITTANCE CURVES FOR THE CHERT SAMPLE (E_2) AND THE QUARTZ POWDER (E_1) SIZED TO CONTAIN 1 TO 10 μ PARTICLES. The absorption curve (A) of quartz is shown in the lower curve for comparison.

again is slightly displaced towards a longer wavelength. (The extended wavelength emission spectra (from 14 to 25 μ) for quartz appear in Figs. 75 and 76.

Emission spectra for dunite with a polished surface (E_1) and roughened (E_2) are compared with the reflectance spectrum (plotted as $1-\rho$) in Fig. 40. Again the correspondence between the emission and reflection spectra is clearly marked (for details see Table II).

Photomicrographs showing the range in particle sizes for the quartz samples used in these experiments are shown in Figs. 41, 42, and 43. The sample of the 25 to 45 μ sized quartz was the parent sample from which the other finer grades were separated; it still contains a small portion of very fine-grained material. The 10 to 25 μ and the 1 to 10 μ splits (Figs. 42 and 43) are much cleaner separations.

The effect of voids in the surface being examined is most interesting. In Fig. 44 two curves appear for the same quartz powder fraction (i.e., the 25 to 45 μ material*). For curve A the material was sifted into the fairy castle structures, while for curve B the same material was pressed into a pellet under about 70,000 tons psi pressure. The same curves are redrawn above and the increase in spectral "contrast" consequent upon the decrease in void space after pressing can be readily seen.

Spectral detail is also apparent in the 9.7 and 12.4 μ region (1030 and 806 cm^{-1}), after pressing. The curve for the chert sample (E_2) in Fig. 39 shows that despite its fine particle size, the lack of voids yields a marked spectral contrast in the emittance spectrum.

Three photographs (Figs. 45, 46, and 47) show stereo-pairs of fairy castle structures in quartz, dunite, and silicon carbide powders. These illustrations should be viewed through a stereoscope so that the three-dimensional effect of the fairy castle structure can be seen. It is possible, however, with the naked eye to observe on Fig. 45 that the fairy castle structure starts immediately, without forming any basal layer. The

---

* Other spectral data for the 10 to 25 μ quartz powder in sifted and in pellet form show a similar, two to three times greater, spectral contrast in the pelletized material.

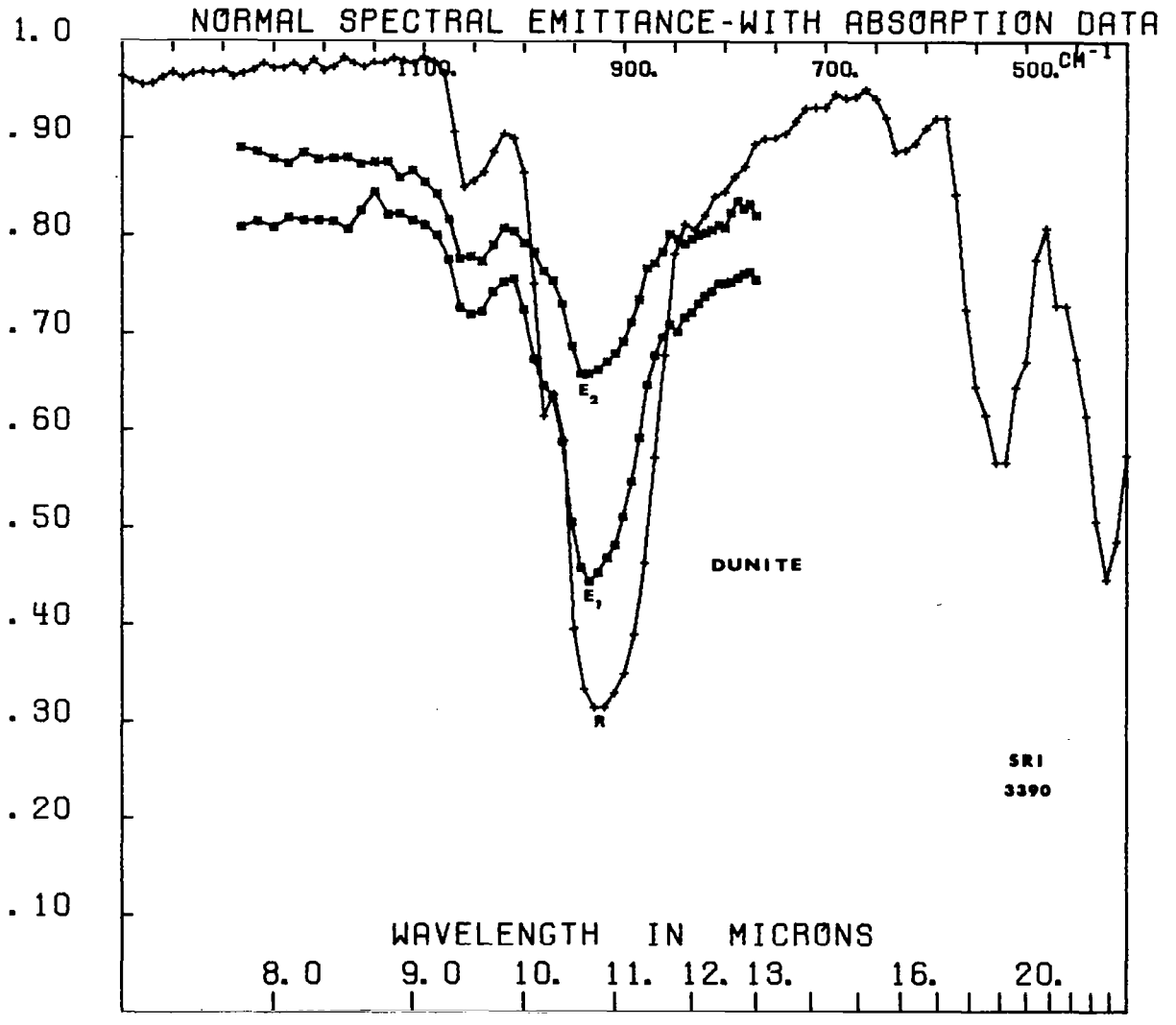

FIG. 40 NORMAL SPECTRAL EMITTANCE CURVES FOR DUNITE WITH A POLISHED SURFACE (E_1) AND IN A ROUGHENED CONDITION (E_2), COMPARED WITH THE CALCULATED EMITTANCE SPECTRUM (R) OBTAINED FROM THE REFLECTANCE DATA FROM THE POLISHED SURFACE.

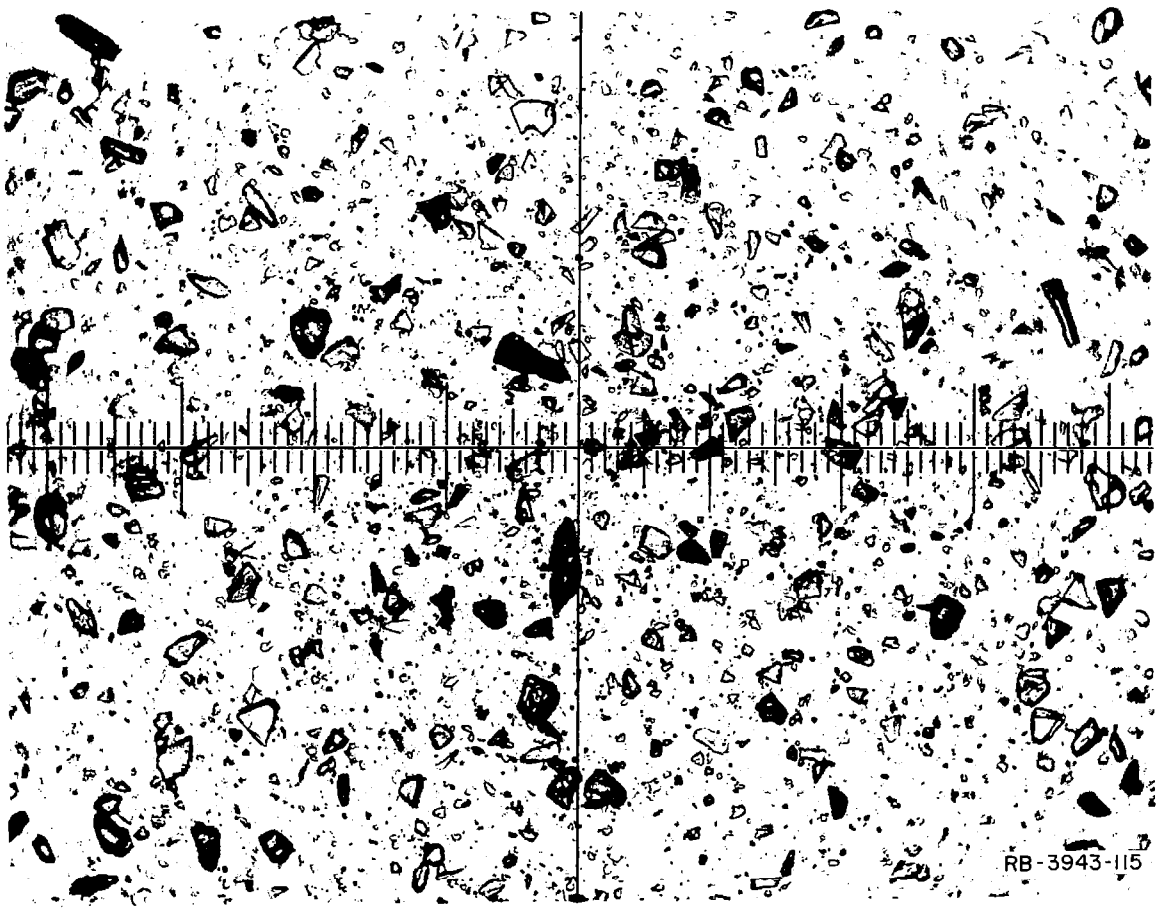

FIG. 41 PHOTOMICROGRAPH OF THE 25 TO 45 μ QUARTZ POWDERS USED IN THE EMITTANCE EXPERIMENTS. One small division equals 13.0 μ.

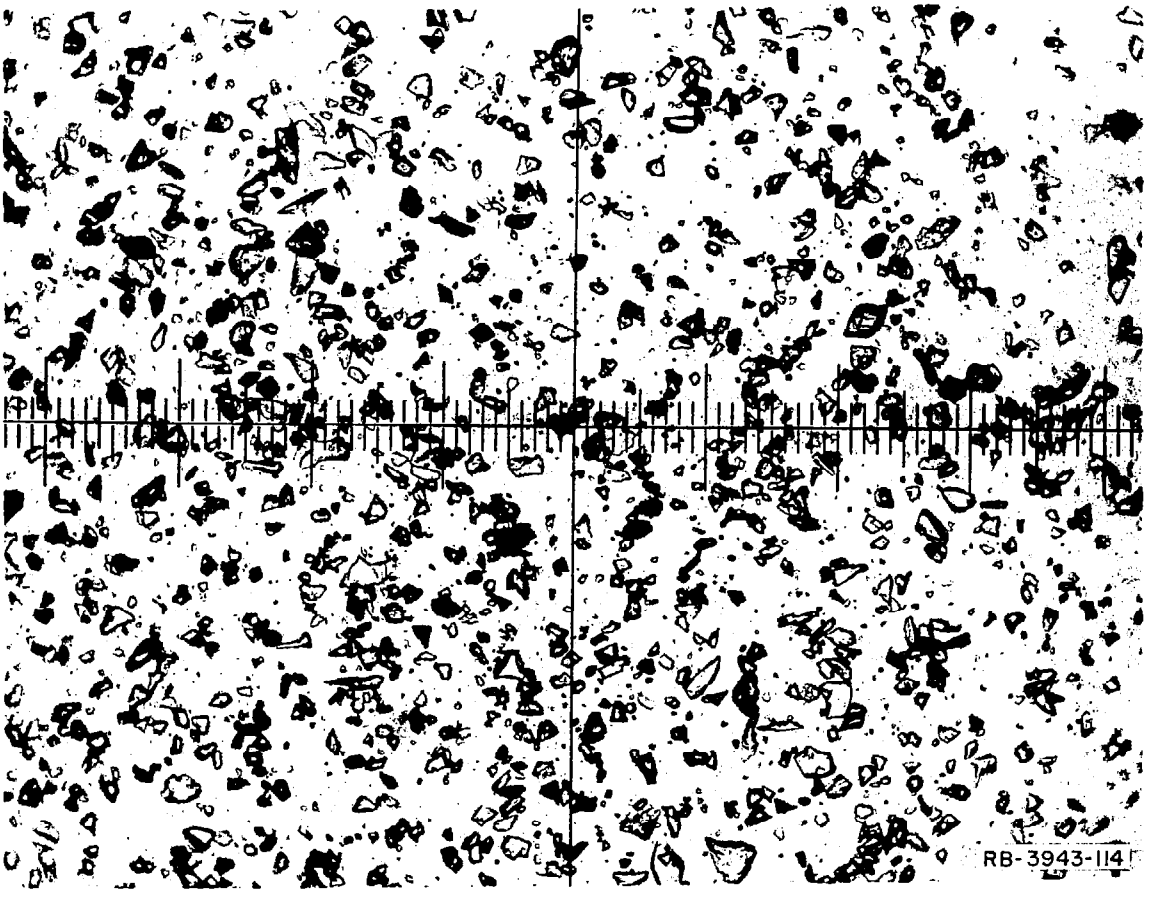

FIG. 42 PHOTOMICROGRAPH OF THE PARTICLE SIZES IN THE 10 TO 25 μ QUARTZ POWDERS. One small division equals 13.0 μ.

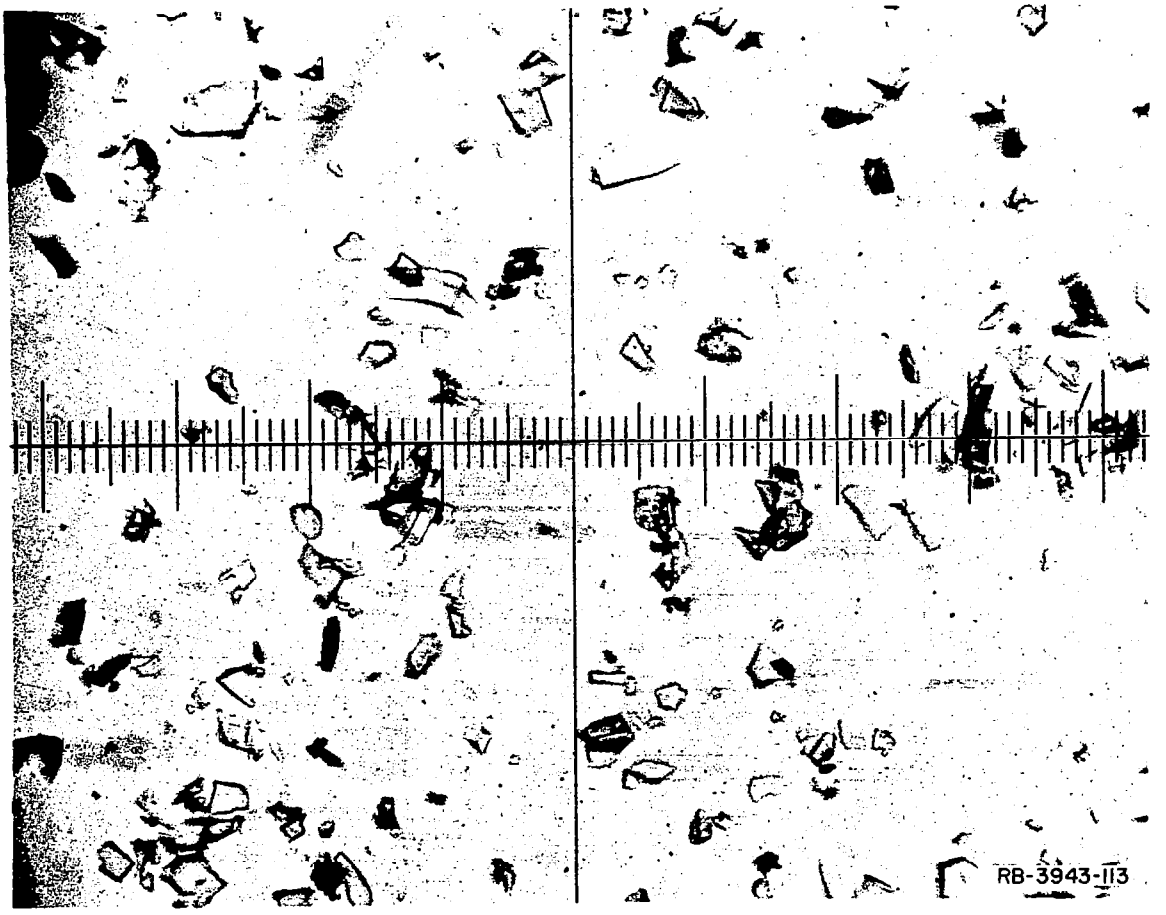

FIG. 43 PHOTOMICROGRAPH SHOWING THE PARTICLE SIZE IN THE 1 TO 10 μ QUARTZ POWDERS USED IN THE EMITTANCE EXPERIMENTS. One small division equals 2.62 μ.

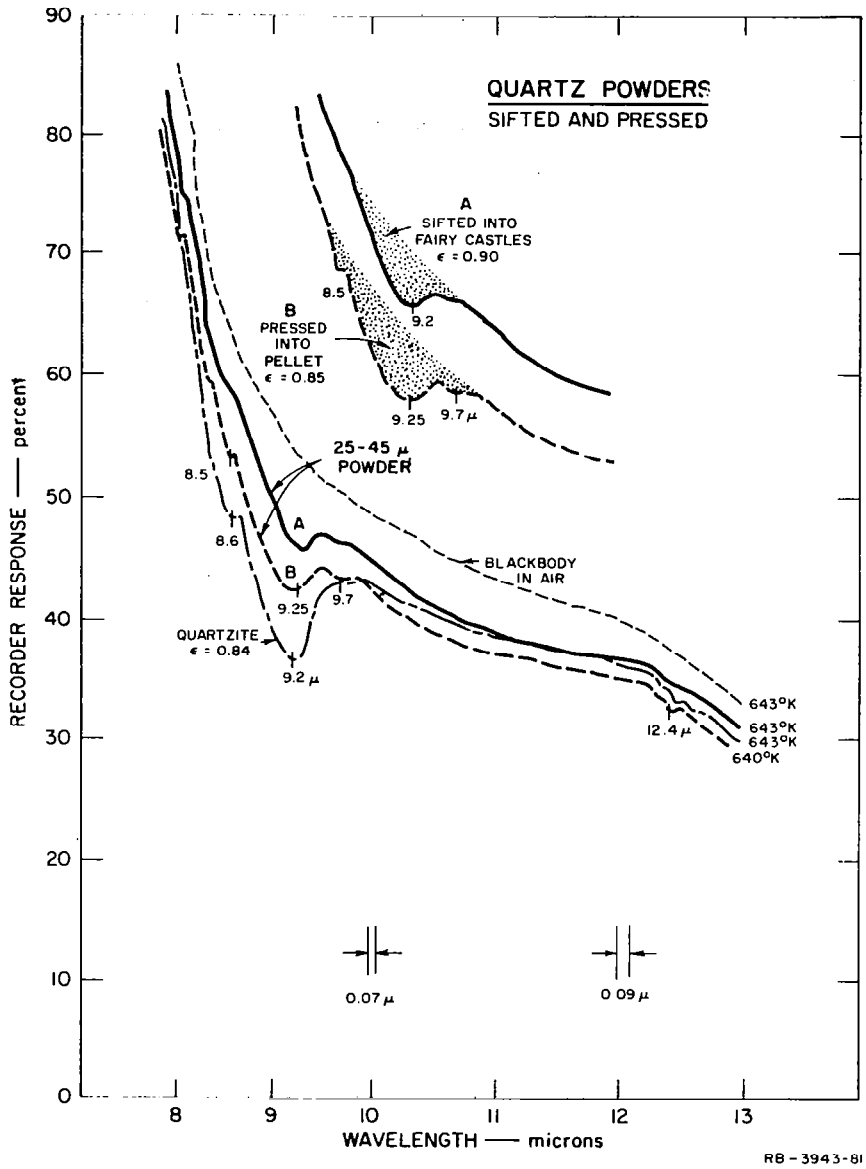

FIG. 44 EMISSION SPECTRA SHOWING THE EFFECT OF DECREASING VOID SPACE IN THE CURVES FOR QUARTZ POWDERS. The spectral contrast is doubled in the pelletized material compared to that in the fluffy, fairy castle structures.

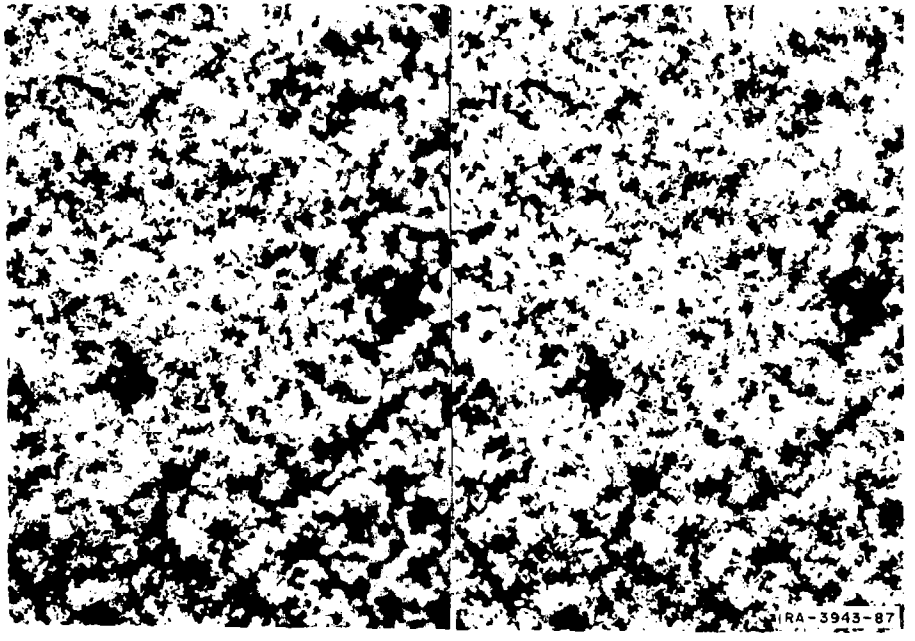

FIG. 45 STEREO-PAIR OF FAIRY CASTLE STRUCTURES IN THE 1 TO 10 μ QUARTZ POWDER. Note that the structure commences immediately without forming a basal layer. About X33. Emission spectra of this material are shown in Figs. 1-3.

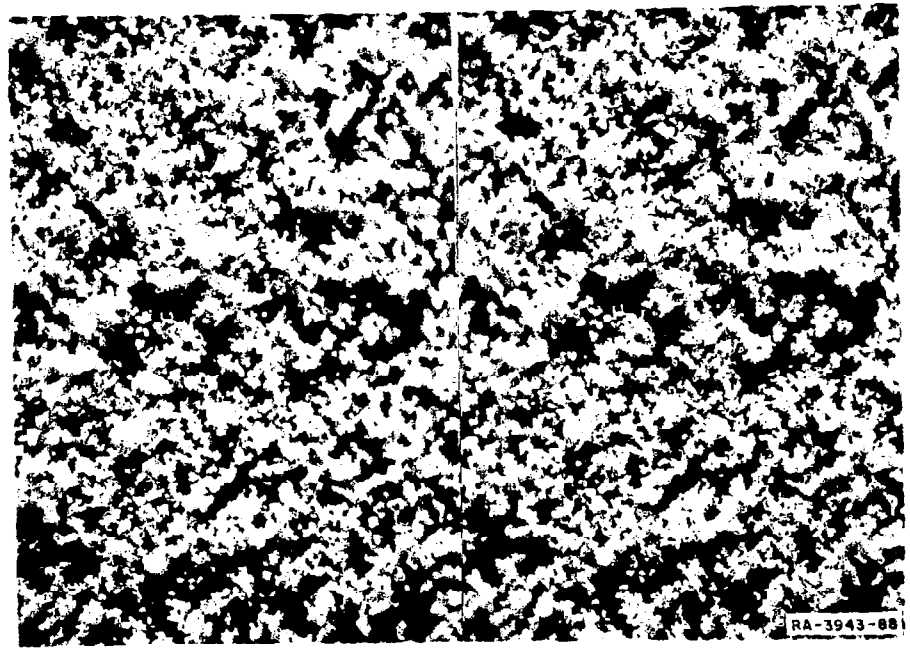

FIG. 46 STEREO-PAIR OF FAIRY CASTLE STRUCTURES WITH DUNITE POWDER OF A PARTICLE SIZE LESS THAN 10 μ. About X33. Emission spectrum of this material is shown in Fig. 48.

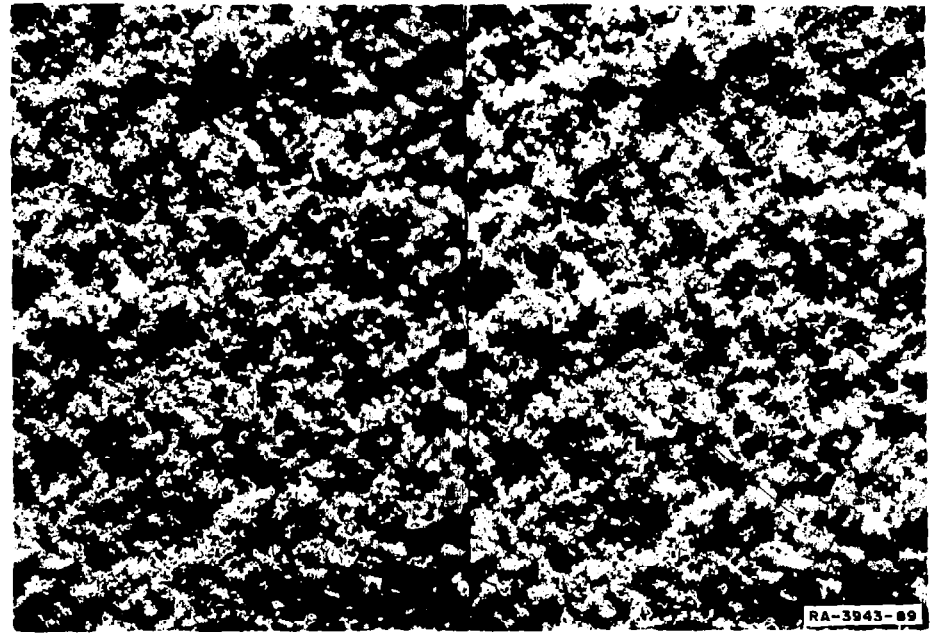

FIG. 47 STEREO-PAIR OF FAIRY CASTLE STRUCTURES IN 17 μ SILICON CARBIDE POWDER. About X33. Emission spectrum of this material is shown in Fig. 49.

electrostatic process by which these particles adhere commences immediately and the highly porous structure forms immediately on impact of the first particles. It makes no difference whether this surface is aluminium foil (conducting) or glass (nonconducting), or whether the powders are conducting (carbon black) or nonconducting (quartz or dunite)--the fairy castle structures will form as long as the particles are between 1 to 25 μ in size.

Dunite. Normal spectral emittance curves for dunite in various degrees of surface roughness and particle size are shown in Fig. 48. The polished dunite surface has a spectrum (A) with marked spectral contrast at points E_1 and E_2, and yields an emittance from 7.8 to 13.0 μ wavelength of 0.71. The roughened surface of the same specimen (B) shows a drop in the spectral contrast with an emittance of 0.80.

A grit-sized sample (over 850 μ) is shown in curve (C) compared with that of sand-sized material (150 to 300 μ) in spectrum (D). The curve for a dunite dust (40 to 80 μ size) is shown in (E) with that for a very fine-grained dunite powder (less than 10 μ) in curve (F). Spectral contrast (E_1 and E_2) may still be seen in all but the finest powder (see Table III).

Thus, as the particle size is increased from a fine powder to that of dust, sand, and grit, the average emittance drops from 0.89 to 0.80. A surface which is roughened has the same average emittance as a coarse grit, but it takes a high degree of polish to decrease this average emittance to the minimal value of 0.71.

Very fine dust (-10 μ) behaves almost as a greybody with an emittance of 0.94. Slightly coarser material shows spectral quality already and from sand-size to coarse grit (almost 1 mm in size) no marked increase appears in either the spectral quality or the emittance values as a function of size (Table III). The spectral curves resemble one another so closely as to be almost indistinguishable. We know from the data of Fig. 37 (rough dunite compared with polished dunite + sand layer) that the rough dunite (with an emittance of 0.80) shows approximately the same spectrum as 1-mm-sized dunite grains.

Spectral departures from the blackbody curve are at a maximum for polished materials. These "contrasts" decrease rapidly with even a

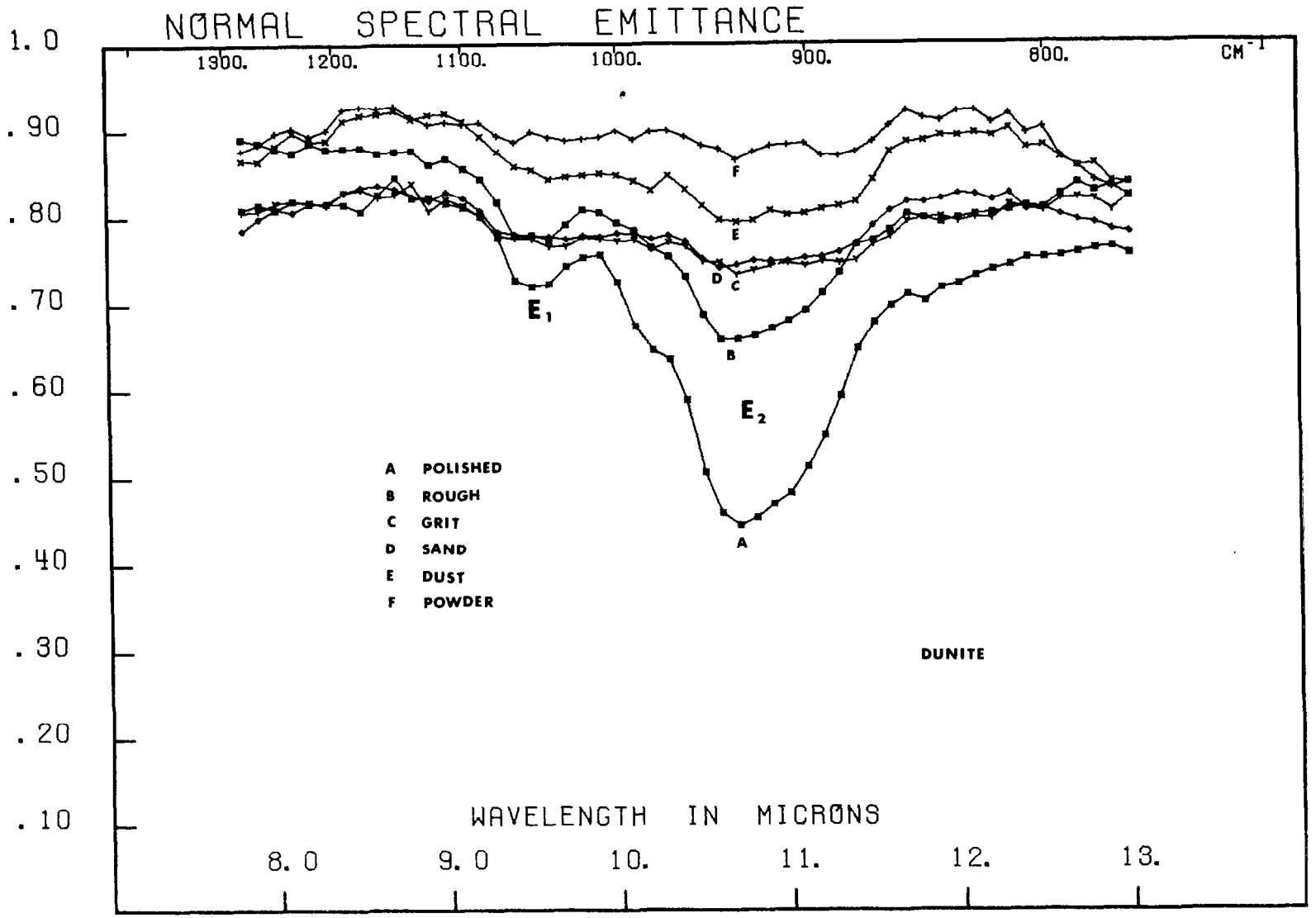

FIG. 48 NORMAL SPECTRAL EMITTANCE CURVES FOR DUNITE IN VARIOUS DEGREES OF SURFACE ROUGHNESS AND PARTICLE SIZE. Polished dunite is shown in curve (A), and with a roughened surface in curve B. A grit-sized sample (over 850 μ) is shown in curve C, with a sand-sized (150 to 300 μ) sample in curve D. The curve for a dunite dust (40 to 80 μ) is shown in curve E, and that of a very fine-grained dunite powder (less than 10 μ) is shown in curve F. Most spectra still show the contrast at points (E_1) and (E_2) despite their decreasing grain size.

slight roughening of the surface, and reach an average value of about 0.75 to 0.8 (Table II). This emittance value persists with decreasing grain size, until at about 40 to 50 μ particle size the spectral "contrasts" disappear. From 1 to 40 μ there is a close relationship with decreasing particle size. The emittance values do not change markedly and the surface emits as a greybody, with an average emittance of about 0.85 to 0.93 with the finest particle sizes. The only really fine-grained material yet studied, the alumina sample with the 200 A particles, emits as a greybody with an emittance varying between 0.90 and 0.94.

Silicon Carbide. Spectral emission curves for silicon carbide are shown in Fig. 49. These are of interest for three reasons--first, they can be obtained in a wide variety of presized fine fractions, and second, they have been used by B. Hapke[22] in some of his photometric experiments and measurements are available for these particular sizes. It is quite simple to produce the fairy castle structures by sifting these powders (see Fig. 47).

The third, and perhaps most significant reason is that they represent a silicon compound with a different bonding to that found in most rock materials, and the more usual infrared phenomena of peak shift with structural change can be readily illustrated. These powders show marked spectral contrast and this makes them ideal for studying the effects of packing. Figure 49 shows that a 17 μ powder (600 grit) departs spectrally from the blackbody curve, at 12.4 μ (808 cm^{-1}), with an average emittance over this window of only 0.93. The curve for a "minus 12 μ" powder (1000 grit) shows the same spectral contrast with an average emittance over this window also of 0.93. The curve for the 75 to 150 μ powder (240 grit) is even more marked, with a wide departure at about 12.2 μ (820 cm^{-1}), with an average emittance of 0.79. The curve for the coarsely crystalline plates shows the same maximum, but with a very low average emittance of only 0.54.

Alumina. Spectral data for alumina* (Al_2O_3) in various degrees of crystallinity appear in Fig. 50. Departures from the blackbody

---

* Extensions of the plate sapphire spectrum may be found in Fig. 77 over the wavelength range 14 to 25 μ.

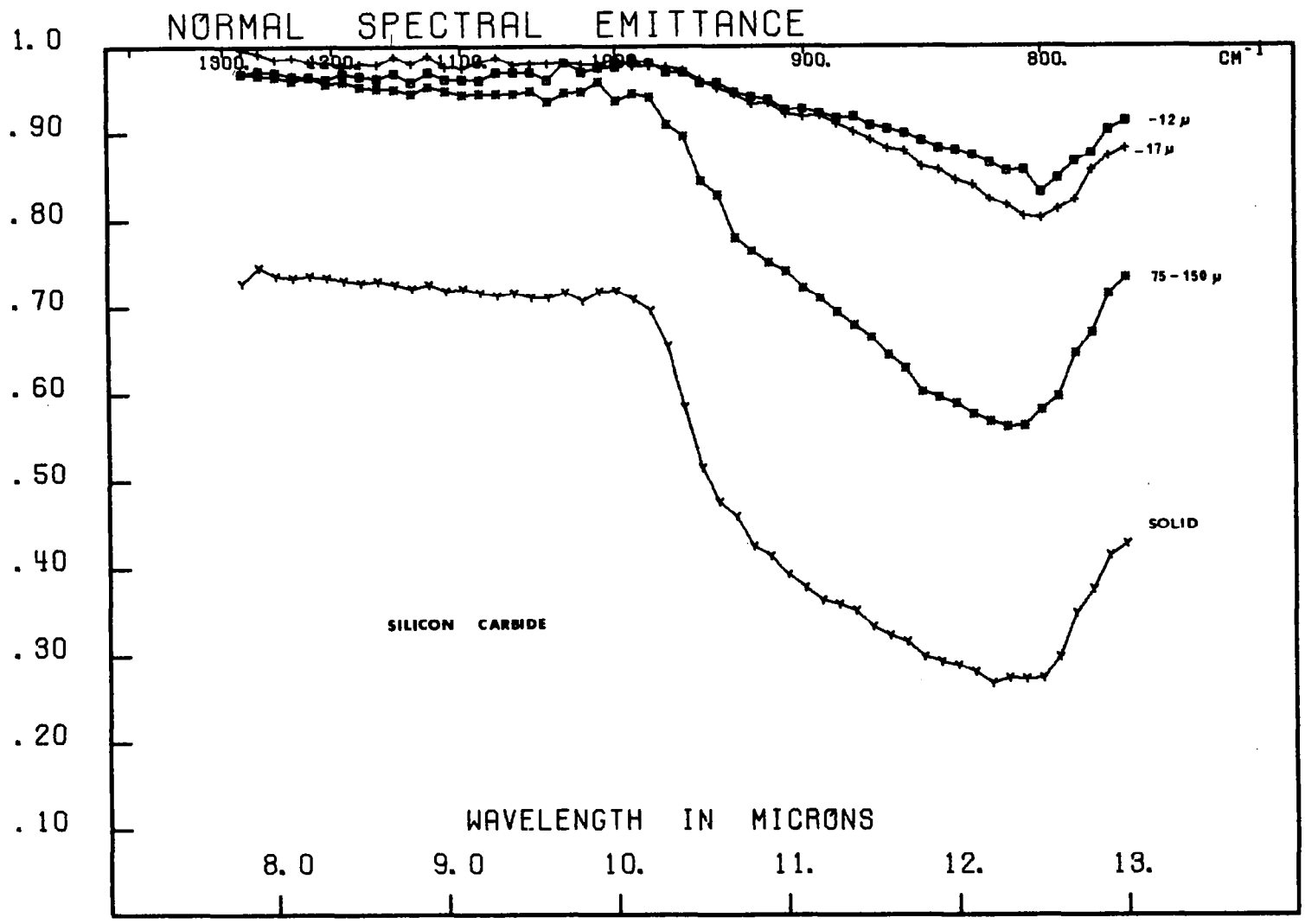

FIG. 49 NORMAL SPECTRAL EMITTANCE CURVES FOR SILICON CARBIDE (CARBORUNDUM) OF VARYING PARTICLE SIZES. The uppermost curve is shown of material with an average size of 12 μ compared with that for a material with an average size of 17 μ. The spectrum of the coarser grained (75 to 150 μ) material is shown, contrasting with that of the solid, single crystals of silicon carbide in the lowermost curve. Despite the diminished spectral contrast (with decreasing particle size) it is still possible to determine the composition from the emittance spectra of 12 μ-sized materials.

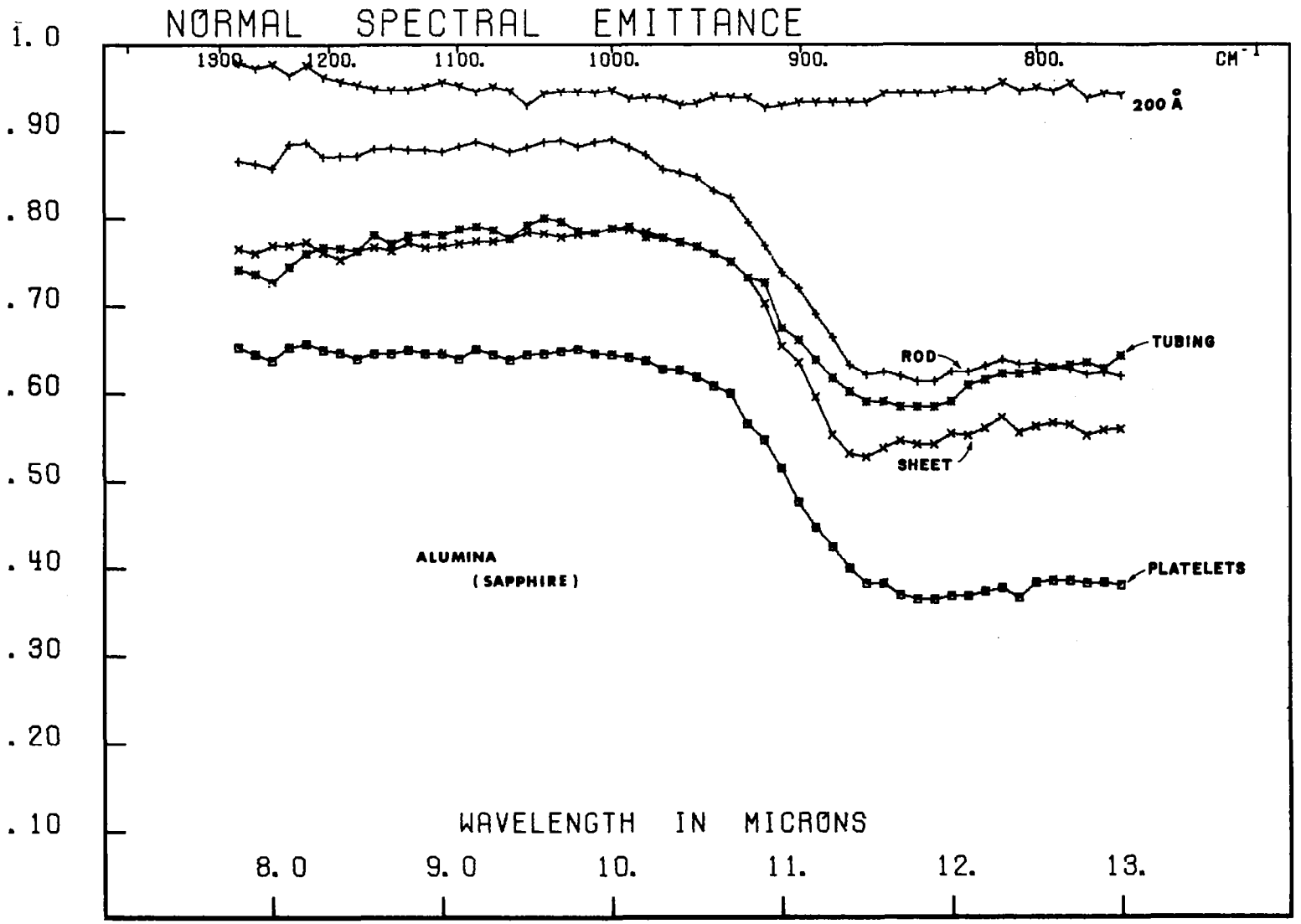

FIG. 50 NORMAL SPECTRAL EMITTANCE CURVES FOR ALUMINA (Al_2O_3) IN VARIOUS DEGREES OF CRYSTALLINITY. The uppermost curve is that of the 0.02 μ (200 A) fine-grained powder which emits as a greybody, with an emittance of almost 1.0. The single crystals of sapphire (plate or rod) show good spectral contrast, with minima in the vicinity of 12 μ. The coarser grained (and vesicular) tubing show two spectra with approximately the same spectral contrast.

curves are only significant at wavelengths longer than 10.0 μ (1000 cm^{-1}). Up to this point the two spectra trace parallel but different paths; such curves are called "greybody" curves because of the lack of spectral contrast and their departure from the emission curve of a true blackbody. In all probability all exterior surfaces are grey rather than black by these criteria, for only an enclosed hole can emit a truly blackbody radiation. As the particle size of the alumina is decreased from the sapphire plate (single crystal) to that of the sapphire rod, from that of the polycrystalline platelets which contain coarse Al_2O_3 crystals to that of the porous coarse grain tubing, and to that of the 0.02 μ (200 A) powder, the emittance curve approaches that of a blackbody.

The 0.02 μ alumina is almost a perfect blackbody (by both emittance and reflectance measurement) in the wavelength 8.0 to 25.0 μ (1250 to 400 cm^{-1}). Similar studies with quartz show comparable effects. Details of spectral contrast are apparent in the coarse-grained material, but in the very fine-grained 1 to 10 μ materials this has vanished, and the spectra closely resemble those of blackbodies.

c. Theoretical Treatment of Scattering Effects on the Emittance of Material*

The optical properties of smooth surfaces are fairly well understood and predictable. The vast majority of surfaces in the world, however, are rough to some degree. About the smoothest materials normally dealt with in the practical world are the surfaces of the lenses of optical instruments such as cameras, eyeglasses, and binoculars, or the mirrors on the walls of homes. It is commonly known that when these very smooth surfaces are scored or otherwise scratched, their optical properties change markedly. For those materials which are opaque to the passage of light the roughening of the surface is well known to reduce the reflectivity of the surface. Assuming that Kirchhoff's law is obeyed, the emittance (ϵ_λ) of a material is ($1-\rho_\lambda$) where ρ_λ is the reflectance. Hence roughening increases the emittance of a surface.

---

* This section was written by Dr. T. O. Passell (SRI), coworker on the theoretical aspects of emittance.

The problem to be discussed is that of predicting, in some quantitative fashion, the degree to which a given amount of roughness, measured in a particular way, increases the emittance of a surface. Because of the many practical problems of correctly describing a real surface, several different approaches will be discussed which have been used by various investigators. Depending on the level of knowledge about a given powdery or rough surface, one or the other of these approaches would be more appropriate. If, for example, one had a fluffy powder surface produced from sifting a dielectric powder onto a flat container, it might be very difficult to measure a particular property of this surface without destroying the surface. Perhaps the only information available about such a surface might be the fractional part of the volume taken up by particles and the particle size distribution. This surface would clearly require a theoretical approach somewhat different from that required for the surface produced by a carefully prepared layer of precision ball bearings of uniform diameter.

The problem will be discussed in three parts. First, consideration will be given to surface irregularities greater in size than the wavelength of the light being emitted. Second, surface undulations smaller than the wavelength of the light will be reviewed. Finally, the medium will be assumed to be homogeneous--whatever the nature of the surface--the discontinuities being included by calculations of their influence on the scattering coefficient.

(1) Effect of Surface Irregularities Larger than the Wavelength

Recently a series of papers has appeared giving exact numerical calculations of the emittance for cavities of various shapes.[23-28] Typical cavities for which computations have been made are cylindrical, rectangular, and V-grooves, spherical cavities truncated at various latitudes, and cylindrical holes of various depths. Vollmer[29] has verified experimentally the theoretical calculations for the thermal emittance of a cylindrical hole.

Figure 51 shows the effects of several particular cavities or grooves taken from References 23-28. As expected, the entire set of curves lies above that for a perfectly smooth surface, indicating that any cavity

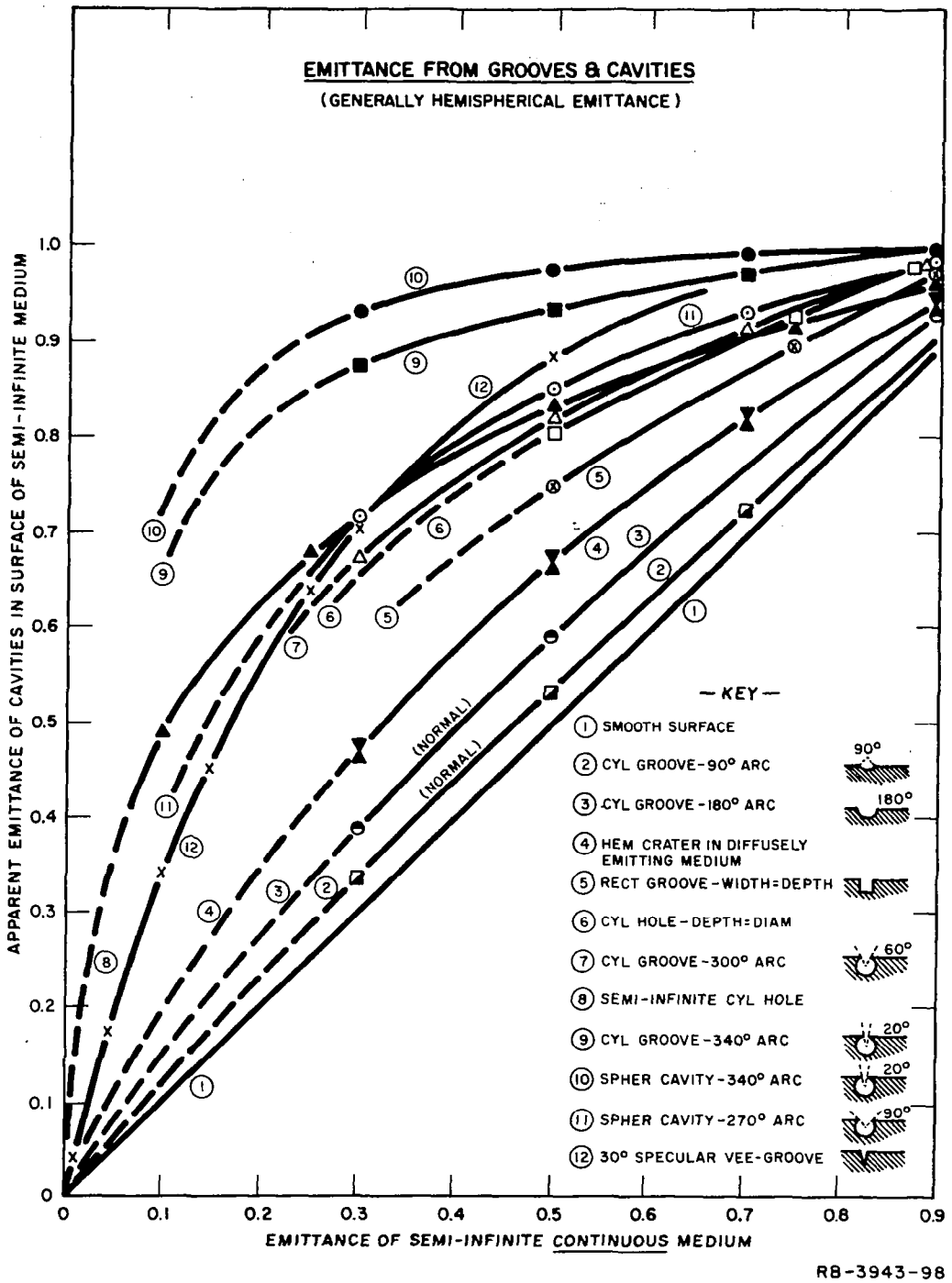

FIG. 51 EMITTANCE FROM GROOVES AND CAVITIES AS A FUNCTION OF THE GEOMETRY OF THE SURFACE. Graph shows the emittance of a semi-infinite continuous medium as a function of surface geometry, plotted against the apparent emittance of the cavities in a semi-infinite medium.

of whatever size or shape tends to blacken a surface, or in other words, to increase its emittance. Plotted in Fig. 51 is the apparent emittance of variously shaped holes in the surface of a semi-infinite medium as a function of the emittance of a semi-infinite continuous medium of the same material. The dotted portions of the curves were drawn by extrapolation from the published data points, which are shown as dots or crosses. Apparent from Fig. 51 is the somewhat greater effect of cavities for increasing the emittance of highly reflecting versus highly absorbing materials, respectively. Thus a shiny metal would undergo a greater fractional change in its emittance from a given roughening of the surface than would more highly absorbing materials.

If a given surface of interest can be described by some combination of the various cavity shapes which have been computed theoretically, Fig. 51 can be used directly to obtain the emittance, provided the emittance of the perfectly smooth material is known. It should be remembered that the cavities must be large compared to the wavelength of the radiation being considered. Hence it would not be appropriate to apply the curves of Fig. 51 to a prediction of the emittance of quartz at 9.0 μ from a quartz plate containing a groove 5 μ wide by 3 μ deep.

Giovanelli[30] gives a slightly different approach to the computation of emittance in a discontinuous medium. He has computed the reflectance of a semi-infinite medium made up of randomly distributed spherical regions of uniform absorption and scattering coefficients, $\underline{a}$ and $\underline{s}$, separated by free space. The particular calculations of Reference 30 are for diffusing spheres as opposed to specular reflecting spheres. Figure 52 shows a plot of the results tabulated in Tables I and III of Reference 30. The lower curve shows the emittance of a semi-infinite discontinuous medium made up of relatively opaque spherical particles ($ar \gg 1$), where r is the radius of the particle occupying less than 5% of the total volume, whereas the upper curve gives the same results for opaque spheres occupying 80% of the total volume. The degree of packing has only a slight effect on emittance (see also Fig. 44). For example, the change is only 20% for a material whose emissivity in the smooth state is 0.1. It will be noted, however, that the increase in emittance in going from a continuous to a discontinuous medium

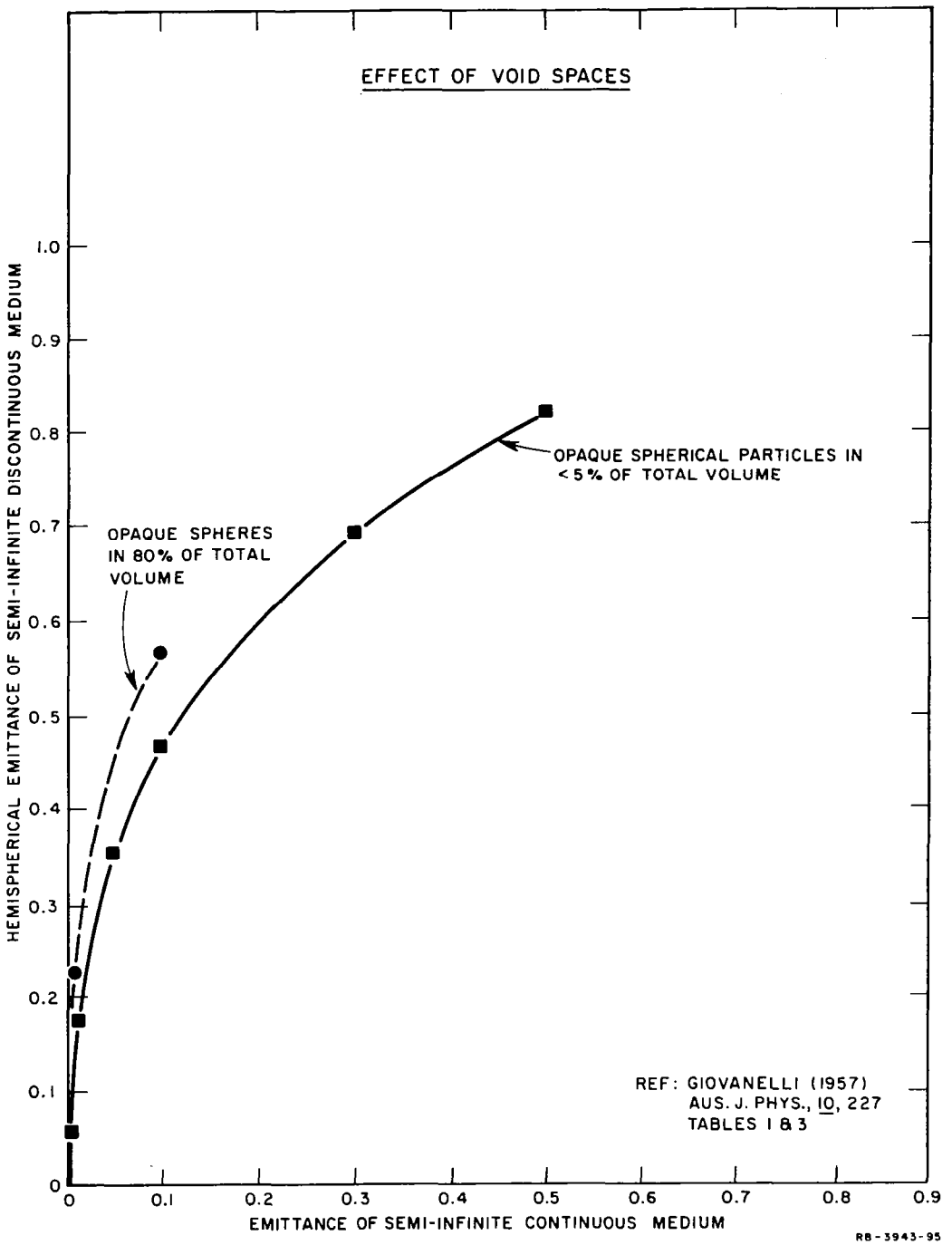

FIG. 52 EFFECT OF VOID SPACES IN A SURFACE. The emittance of a semi-infinite continuous medium is plotted against the hemispherical emittance of a semi-infinite discontinuous medium, as a function of the percentage of opaque spherical particles in the total volume. Data from Reference 30, Tables I and III. Compare with experimental data in Fig. 44.

with that same material is about a factor of 5. By comparison with Fig. 51, the results of Giovanelli indicate that the discontinuous media he describes are roughly equivalent to the results obtained for the semi-infinite cylindrical hole (Curve 8). However, the cavity calculation does not include the effects of portions of the surface away from the edge of the cavity, whereas the treatment of Giovanelli considers the entire surface.

(2) Surfaces Where Undulations Are Smaller than the Wavelength

Bennett and Porteus[31] review the problem of determining the reflectance, and hence the emittance, of a medium whose surface has irregularities which are small compared to the wavelength of the light being considered. In particular they refer to the original work of Davies[32] which is a theoretical development predicting the scattering of radar waves from rough water surfaces. Bennett and Porteus[31] have found that this theory applies also to the optical region and for both metals and dielectrics. The equations to be given below are for normally emitted radiation.

Equation (5) gives the relation between emittance of a rough surface and the emittance of the smooth surface, for conducting materials.[31]

$$\frac{1-\epsilon_{rough}}{1-\epsilon_{smooth}} = \exp[-(4\pi\sigma)^2/\lambda^2] \qquad (5)$$

where σ in Eq. (5) is the root mean square deviation of the surface from the mean surface level and λ is the wavelength of the radiation being emitted. Figure 53 shows the relation between ϵ_{rough} and ϵ_{smooth} for various values of σ/λ in the range $\epsilon_{smooth} \leq 0.9$. The ordinate, ϵ_{rough}, is an upper limit to the normal emittance since it ignores one of the terms in Davies' equation.[32] Bennett and Porteus[31] show that this term is not significant over the range of σ/λ shown in Fig. 53.

An interesting rule of thumb is apparent in the measurements of surface roughness by Bennett and Porteus.[31] The value of σ was discovered to be approximately 1/20 to 1/25 of the average particle size of the grit used in the roughening process (Ref. 31, Table 1, p.126).

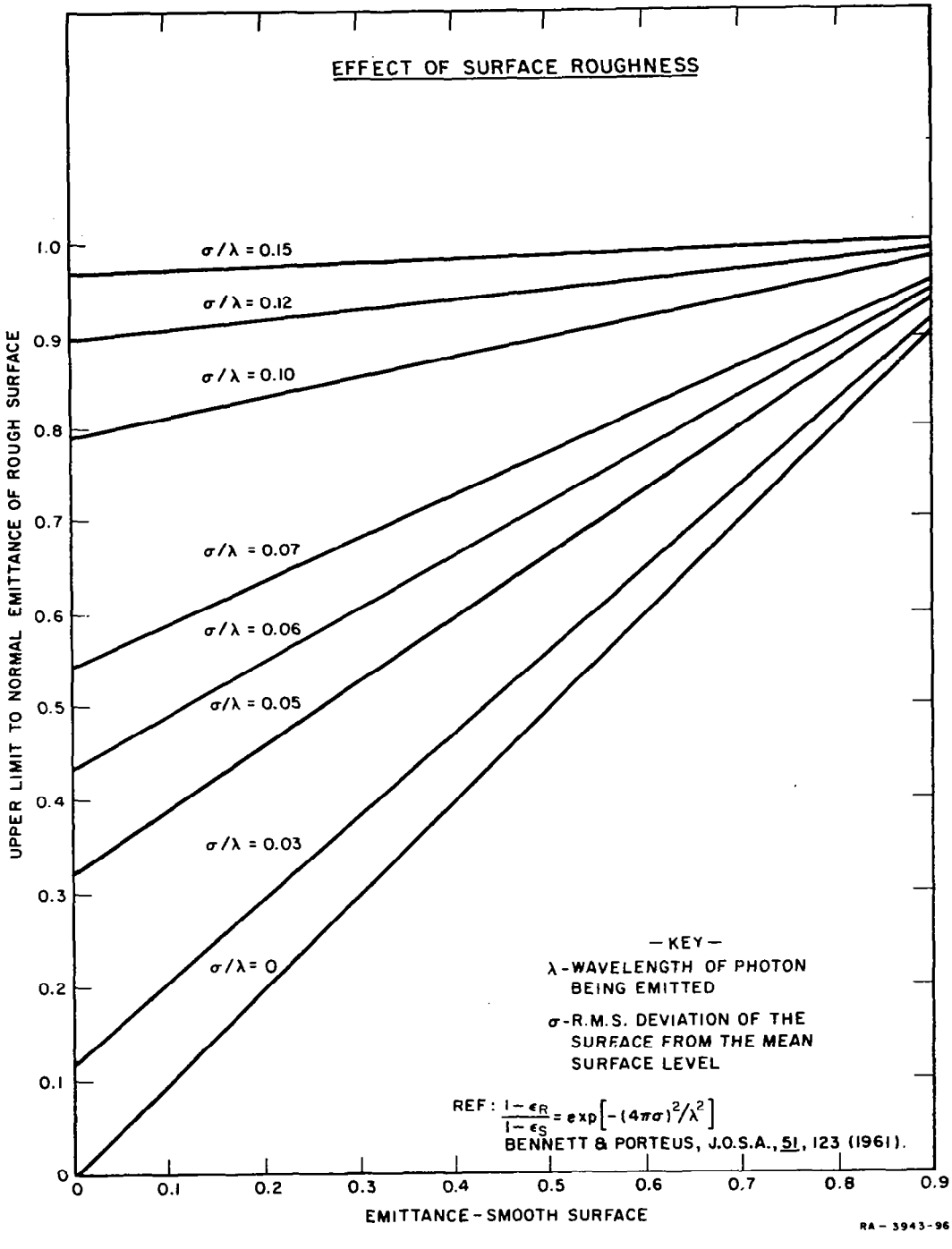

FIG. 53 EFFECT OF SURFACE ROUGHNESS ON THE EMITTANCE OF A SURFACE. Emittance of the smooth surface plotted against the upper limit to the normal emittance of a rough surface for a series of ratios of the RMS deviation from the mean surface level compared to the wavelength. Data from Ref. 31.

(3) Media Homogeneous over Few Attenuation Lengths

Schuster[33] and Hamaker[34] have treated our problem from the following standpoint. A semi-infinite medium is assumed capable of three acts: (1) emission of radiation, (2) absorption of radiation, and (3) scattering of radiation. It is further assumed that the ratio between the probability for these three events is constant throughout the region of interest. The primary variables describing the medium are s, the scattering coefficient, and a, the absorption coefficient, both in units of inverse length (cm^{-1}).

For a semi-infinite medium where t (the thickness) is large enough so that st and/or $at \gg 1$, and where s represents the coefficient for isotropic scattering, Schuster[33] gives the following equation for its diffuse emittance:

$$\epsilon = \frac{2\left(\frac{a}{a+s}\right)^{1/2}}{1+\left(\frac{a}{a+s}\right)^{1/2}} \qquad (6)$$

Hamaker[34] generalizes Eq. (6) so that scattering need not be considered isotropic (equally intense for all scattering angles). This he does by replacing s in Eq. (6) by $2s$ and redefining s as the coefficient for backscattering (scattering over angles from 90 to 180 degrees with respect to the initial direction).

Figure 54 shows how the emittance varies with the ratio s/a under both the Schuster and Hamaker definition of s. Note that a backscattering/absorption ratio of 16 is required to give an emittance of 0.3, the value at the emission minimum near 9 μ in quartz.

(4) Discussion of Emittance for Quartz near 9 μ.

At least two chief experimental results require an explanation. The first (A below) is the marked increase in normal spectral emittance at the emission minimum near 9 μ (1110 cm^{-1}) produced by sandblasting of a smooth quartz plate. A second (B) is the variation in emittance as a function of particle size for powdered samples.

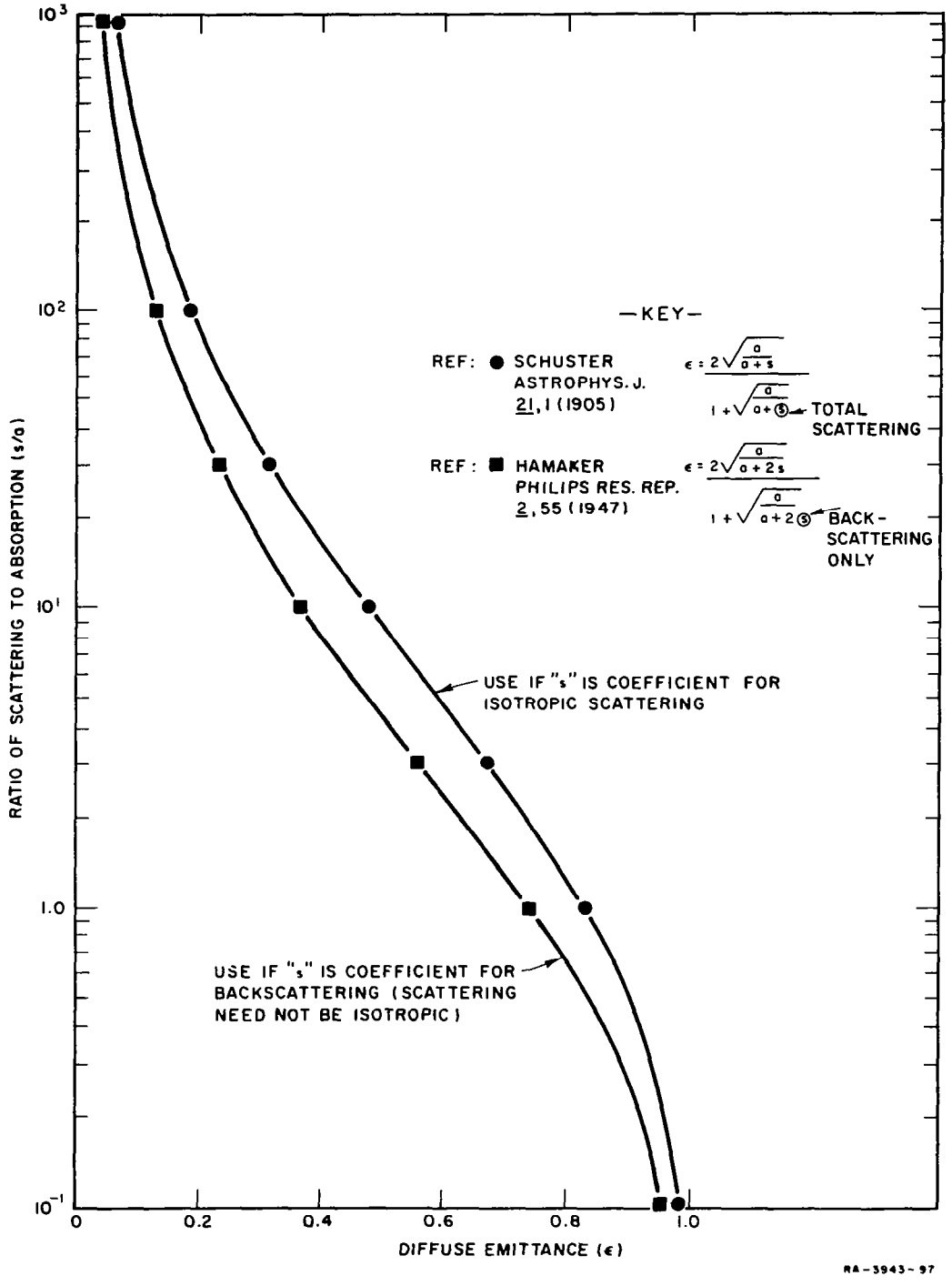

FIG. 54 DIFFUSE EMITTANCE AS A FUNCTION OF THE RATIO OF SCATTERING TO ABSORPTION. Data from Refs. 33 and 34.

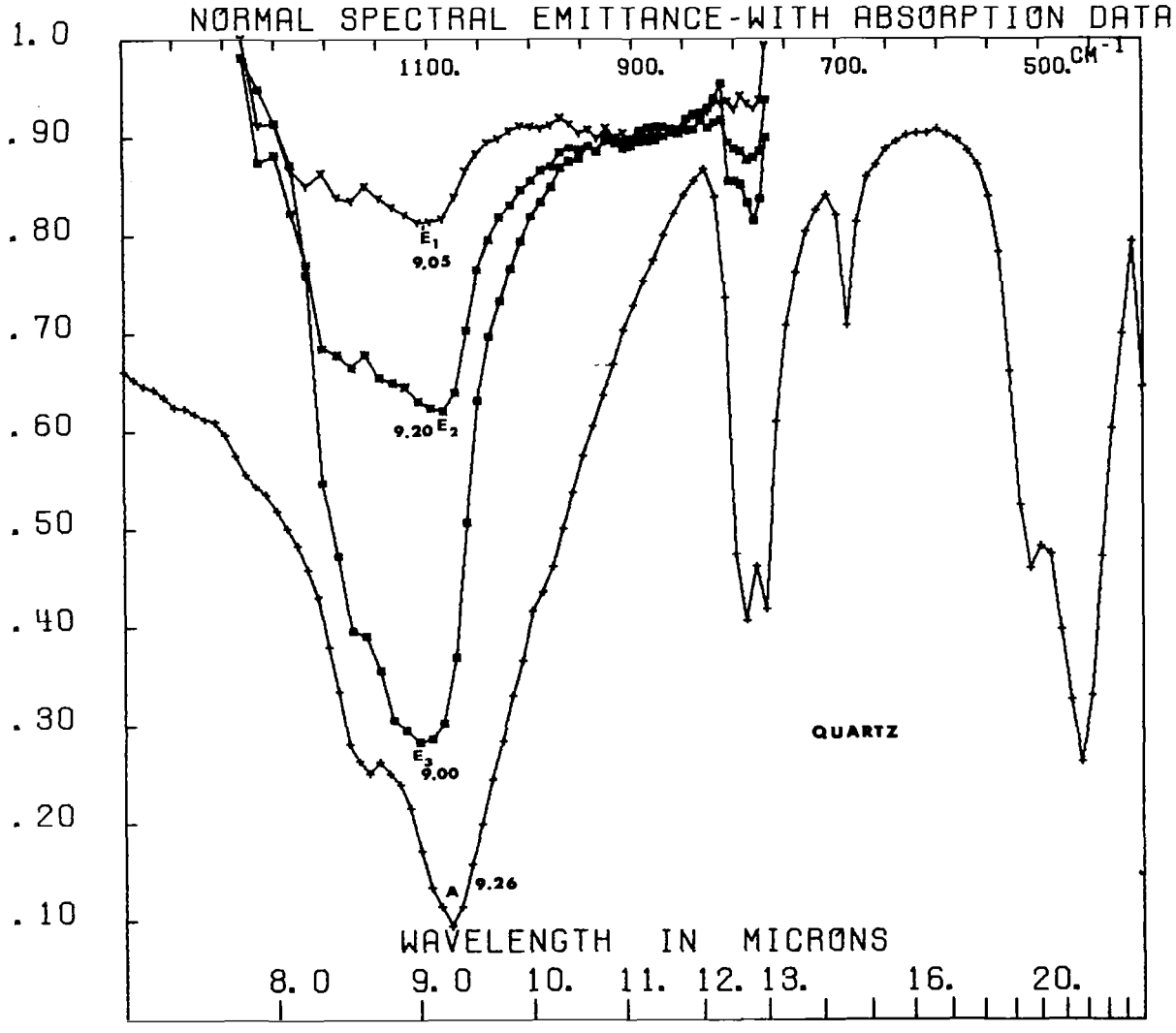

FIG. 55 NORMAL SPECTRAL EMITTANCE OF QUARTZ WITH VARIOUS SURFACE ROUGHNESSES. The emittance of a polished X-plate (E_3) is shown contrasted with that of the roughened surface (E_2). Also plotted on the diagram are the emittance spectrum of 25 to 45 μ quartz powder (E_1) and the absorption spectrum (A) of quartz.

(A) Curves E_2 and E_3 in Fig. 55 are examples of the first effect. It is seen that sandblasting the smooth surface alters the emittance at 9 μ from 0.28 (E_3) to 0.62 (E_2). Away from the emission minimum, this change in emittance decreases rapidly to an insignificant amount at 8 and 10.5 μ (1250 and 952 cm^{-1}). (Figure 2 also shows these surfaces compared with some finer powders.)

We have some information concerning the nature of the sandblasted surface (see Figs. 56-59). Notice that if most of the pits created by the sandblasting are small relative to 9 μ, but below our limit of resolution of the photograph, we can consider the problem using the information contained in Fig. 53. Assuming the initial quartz oscillator plate to be perfectly smooth, we see that a surface roughness described by $\sigma/\lambda \cong 0.065$ is required to give a change in emittance from 0.28 to 0.62. The final surface would be predicted to have a surface level which fluctuates about the mean surface level by $\sim 0.065 \times 9\ \mu$ or 0.6 μ. (This corresponds to a surface of high finish of "25 microinches", as used in the language of the machine shop.)

If the sandblasted surface* is assumed to contain pits and grooves larger than 9 μ in their characteristic dimensions, Fig. 52 or perhaps Fig. 51 may be useful as a correlating theory of emittance. For example, from Fig. 51 we see that a material whose smooth emittance is 0.28 can be changed to one of 0.62 by creating, over the entire surface, cylindrical holes with a depth-to-diameter ratio of 1.0.

In the context of Hamaker's extension of Schuster's theory shown in Fig. 54, a change in the ratio s/a from 20 to 2 is required to give the experimentally observed emittance change, which resulted from sandblasting.

Normally one expects an increase in scattering and little change in absorption in a material when the surface is roughened. Thus s/a

---

* RMS surface deviation (σ) was estimated (by a rule of thumb) to be 20 μ for the roughened quartz plate shown in Figs. 57, 58, and 59. Thus σ/λ would be 2.25 at 9.0 μ. Thus (σ) corresponds to a rough surface of about "800 microinches".

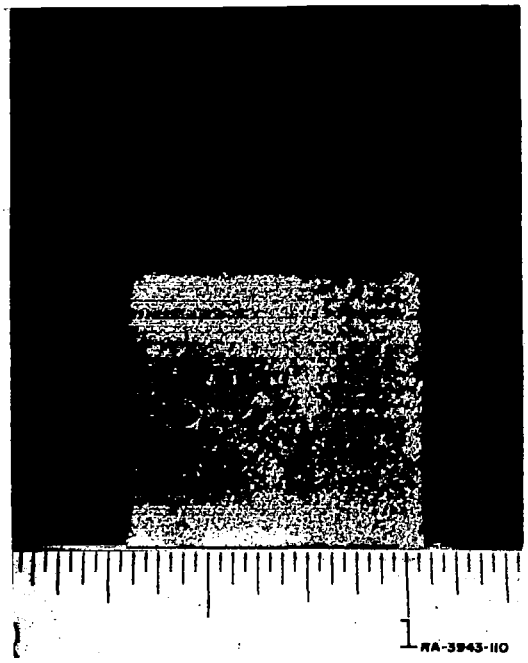

FIG. 56 PHOTOMICROGRAPH OF THE ROUGH SURFACE OF THE X-CUT QUARTZ PLATE. A plan view of the upper frosted surface. Scale is in inches.

FIG. 57 SECTION THROUGH THE X-CUT QUARTZ PLATE AS ROUGHENED, SHOWING A VIEW ACROSS A CENTRAL BREAK (VERTICALLY THROUGH FIG. 56). Left-hand half is viewed in this photograph. Scale – one small division equals 13.0 μ. Note the subsurface cracking and strains visible in this photograph.

FIG. 58 ENLARGED PLAN VIEW OF THE ROUGHENED X-CUT QUARTZ PLATE. Note the linear structure from upper left to lower right showing in the fractures and pitting. Scale – one small division equals 37.7 μ.

FIG. 59 HIGHLY ENLARGED PLAN VIEW OF THE X-CUT ROUGHENED QUARTZ PLATE. Same view as Fig. 58. Scale – one small division equals 2.62 μ. Note that many of the larger fractures and pits with concave surfaces are over 10 μ in diameter. This surface is estimated to have an RMS deviation from the surface of over 20 μ (800 microinches).

might be expected to increase and the material would decrease in emittance. However, in Figs. 2 or 55 (E_2), the only region where the emittance may have decreased is from 11 to 12 μ and 7.5 to 8.0 μ. In the context of the Hamaker-Schuster approach, it may be that the strong specular reflection property of quartz at 9 μ can be considered a scattering process. Surface roughening is expected to decrease the region of coherence and hence the specular reflection of the surface. By this means scattering is reduced.

It is not apparent how one might predict how a given roughening of the surface has affected the scattering coefficient. If the surface could be considered a set of discrete, separated, spherical particles, Rayleigh and Mie scattering theory might be applied, along with Davies'[32] theory (Fig. 53) when specular reflectance bands are involved.

The low emittance of the polished quartz plate at the reststrahlen wavelength (9.0 μ) must be due to an absorption length which is short compared to the wavelength.

If the surface is multiply fractured (as in sandblasting) so that there are many interfaces in one absorption length, then these interfaces may be treated as equivalent to the surfaces of the opaque particles of Fig. 52. The radiation is not strongly absorbed in the distance between successive reflections, but is absorbed sufficiently to consider the material as opaque. We note that a small concentration of such discontinuities can increase the effective emittance from 0.28 to about 0.7. This agrees reasonably well with the observed effect, in spite of the fact that the void and particle spaces are essentially interchanged by this new concept.

(B) The second experimental effect needing an explanation is the variation in emittance of a powder surface as a function of particular size. A complicating factor with powder surfaces is the large temperature gradient as a function of depth near the surface, for which the experimental results obtained in this work (see Figs. 1, 31, and 37) the samples were heated by a hot surface about 1 mm or so below the exposed surface. Assuming a thermal conductivity of 10^{-4} (calories)/(^{o}K-cm-sec) for these powders, the temperature gradient required to maintain a constant surface temperature at 640°K is 0.24^{o}K/μ.

If cavities in the surface extend as deep as 100 μ (as seems likely from observation of the stereo photographs in Figs. 45, 46, and 47), the bottom of such cavities would be some 24°K above the measured surface temperature. The radiation being emitted would therefore be a combination of radiation from cavities at (T + 10 to 20)°K and radiation from exposed surface at T°K.

For discussion purposes, consider a powder surface to be made up of two components: (1) clumps of particles with surface undulations of the same size as the particle diameter, and (2) cavities between the clumps whose size may or may not be related directly to the particle diameter.

If all the particles are large compared with the wavelength, Fig. 52 might be applied directly after a measurement of surface layer bulk density (to derive therefrom the fraction of the total volume occupied by the particles). Since emittance is not strongly dependent upon the packing fraction (see Fig. 44), the bulk density measurement need not be particularly precise. Since Fig. 52 is concerned with opaque particles, large relative to the wavelength, it might be well to point out that for such large particles, quartz is extremely opaque in the entire 8 to 13 μ wavelength region ($\underline{a}$ = 0.045 μ^{-1} to 0.67 μ^{-1}). (See Table VI.)

It is interesting that particle diameters $<$ 50 μ have been shown[32] to form complex structures with many cavities--the so-called "fairy castle" structure. These cavities may be controlling the emittances in the 9 μ band in finely powdered quartz. So long as the cavities are large compared with the wavelength (and this appears to be the case in Fig. 45) we can apply the appropriate cavity curves of Fig. 51. When cavities become smaller than the wavelength being emitted, they become less important and the surface may then be best treated from the standpoint of the surface roughness parameter, σ/λ, as in Fig. 53, using the particle diameter as a rough indicator of σ. If electrostatic effects are the chief cause of the expanded fairy castle structure, the cavities may become larger with decreasing particle size, rather than smaller. Hence it seems possible that the cavities always remain large relative to the wavelength for even the smallest particle sizes.

Table VI

ABSORPTION COEFFICIENTS FOR QUARTZ (X-CUT) PLATES

(After Saksena, Ref.35, Table 6)

Wavelength (μ)	Value of a (μ^{-1})
5.05	0.021
5.48	.014
5.96	.022
6.55	.019
7.0	.015[a]
7.5	.042[a]
8.0	.111[a]
(9.0)	.670[b]
10.0	.067[a]
11.0	.026[a]
12.0	.043[a]
12.3	.092[a]
12.5	.051[a]
12.6	.023[a]
12.75	.055[a]
13.0	.045[a]
14.0	.027[a]
14.4	.046[a]
15.0	.007[a]

[a] At these wavelengths the X-cut plate (0.089 mm) was too thick and was replaced by an "equivalent" V-cut plate (0.031 mm).

[b] Value estimated by SRI from absorption measurements, as in Fig. 55.

According to the absorption coefficients noted above ($\underline{a}$ = 0.045 μ^{-1} to 0.67 μ^{-1}) and if we assume scattering to be proportional to the number of interfaces between quartz and air, scattering should not override absorption until the particle size is down in the range from 1.6* to 22 μ. The scattering referred to here excludes the coherent reflection process, which is indistinguishable from scattering. Thus, if scattering rather than cavities is the controlling factor, the expected decrease in emittance should appear when the particle size decreases below 1.6 μ* (for the 9 μ wavelength region) or below 22 μ (for much of the remainder of the 8 to 13 μ region).

The assumption that scattering is proportional to the number of interfaces per unit path length is a very crude model. However, the standard approaches used for separated spherical particles (Mie and Rayleigh scattering formulae) do not appear applicable.

(5) Conclusions

It is apparent that no one theoretical approach can explain the emittance of surfaces over all the possible nonuniform distributions of matter. When the nonuniformities are regular in shape, large compared to the wavelength, and describable by some simple geometric shape such as cylinder, rectangle, V-groove, or sphere, the data summarized in Fig. 51 should give results as accurate as can be measured experimentally. Also, the instance where surface undulations are small compared with the wavelength has been theoretically treated and experimentally confirmed (see Fig. 53).

Cavities between randomly spaced spheres large with respect to the wavelength are theoretically described by Giovanelli, as shown, for example, in Fig. 52.

---

* Data are not given in Saksena's paper (Ref. 35), or in that of Wentink and Planet (Ref. 36) for fused silica for absorption coefficients within the 8 to 10 μ strongest absorption band. Values given in Table VI were estimated for absorption data on KBr pellets (Fig. 55).

The intermediate region where undulations or cavities are about the same size as the wavelength can be treated by extrapolation from the solutions for the two extreme cases solved above, perhaps interpolating between the extrapolations from each extreme. Presumably the methods of Schuster and Hamaker apply over the entire range of roughness if the roughness can be properly translated into appropriate values for the backscattering and the absorption coefficient. No simple method appears feasible for accomplishing this translation. The only one suggested was the use of optical constants or direct measurements for the absorption coefficient of the basic material and the assumption of 100% probability for isotropic scattering at each interface between a particle and air for the scattering coefficient.

The experimental results seem to show a steady rise in emittance as particle size decreases. If the materials were to be packed under pressure, one would expect an opposite trend in the particle size range $< 10\,\mu$, assuming pressing has eliminated the cavities. The cavities may be controlling the emittance for the lightly sifted fairy castle structures, the cavity characteristics being only slightly related to particle size.

It is clear that the most difficult problem in this study is to find a practical experimental method for quantitatively describing the degree of surface roughness over a wide range.

d. Experiments Designed for an Understanding of the Scattering Process

It soon became obvious that the problem of scattering of emitted infrared radiation was the most important aspect of the study. This scattering effect is perhaps best illustrated by the following example. Crystals of copper sulfate (blue vitriol) have a deep blue color. If these crystals are crushed, the depth of the blue (the "spectral contrast") is lessened by the introduction of white (broad band) light which has been scattered by the newly increased air-crystal interfaces.

When finely powdered, the blue color almost disappears in the increasing level of "white" radiation. What was originally a marked spectral absorption, producing a strong blue coloration, is replaced by a weakening

blue tinge superimposed on the white radiation. The contrast is lost. If one considers the emission from such a sample in relation to Kirchhoff's law, ($\epsilon = 1-\rho$), where ϵ is the emission and ρ is reflection, then scattering has removed the spectral contrast from both the reflection and the emission spectra. It also should have decreased the total emission from the sample by the increased total reflection, yet we know from experimental data that this is not the case (Figs. 2, 37).

In an effort to explore this phenomenon we prepared the curves shown in Figs. 60 and 61. In Fig. 60 a spectral curve was run for polished quartz and another was run for polished dunite. Then the two specimens were run at the same time, in such a manner that one-half of the energy falling on the spectrometer slit was from the quartz, and one-half was from the dunite. A solid curve, a composite of that for quartz and dunite, resulted. Thus the spectral minima for one material were not "filled in" by energy radiated from the other material. Similar but diminished effects were seen for sand-sized quartz and dunite samples; the spectral characteristics of each sample were retained in the spectra of the subsequently mixed sands.

A different approach to the scattering analysis of powders was suggested by S. Rubin (SRI). If the emission from a single grain deep in a fluffy powder structure is considered, radiation from this grain could perhaps reach the outside directly. More than likely it would be reflected off one or more adjoining grains (and perhaps pass through some finer grains) before entering the optical collection system of the spectrometer.

To test this model the following experiment was designed. The blackbody curve was run in a normal manner. A reflection attachment was placed in the beam so that the singly reflected spectrum of a quartz plate could be obtained using infrared energy from the blackbody in the usual way. (The quartz plate was maintained at ambient temperature.) A second reference attachment was then placed so that the beam reflecting off the quartz plate was itself reflected again from another quartz plate (at ambient temperature), yielding a doubly reflected spectrum.

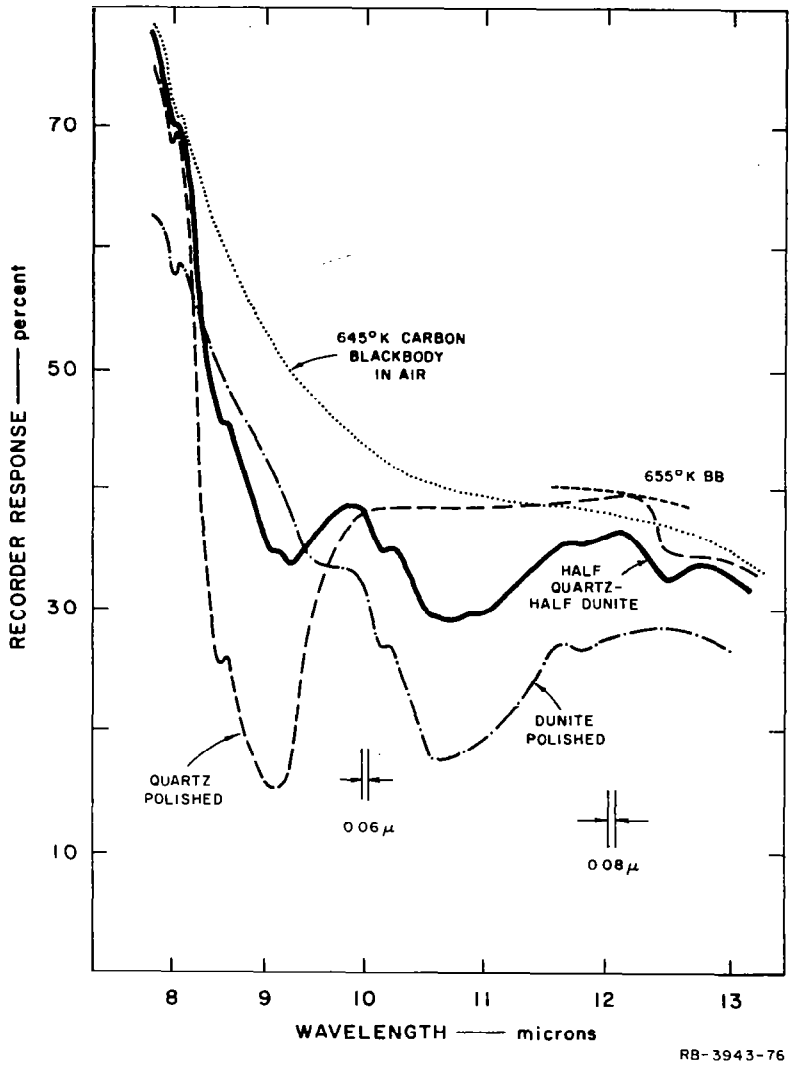

FIG. 60 SPECTRAL EMITTANCE CURVES FOR POLISHED QUARTZ (DASHED CURVE) AND FOR DUNITE (DASH-DOT), COMPARED WITH THE CURVE FOR A COMPOSITE SAMPLE (SOLID LINE). The blackbody curve for carbon black at this temperature (645°K) is shown as the dotted curve. The deviation of the quartz spectrum above the blackbody curve at 12.2 μ could be approximated by a 655°K blackbody, indicating a possible error of 10°K in the temperature determination.

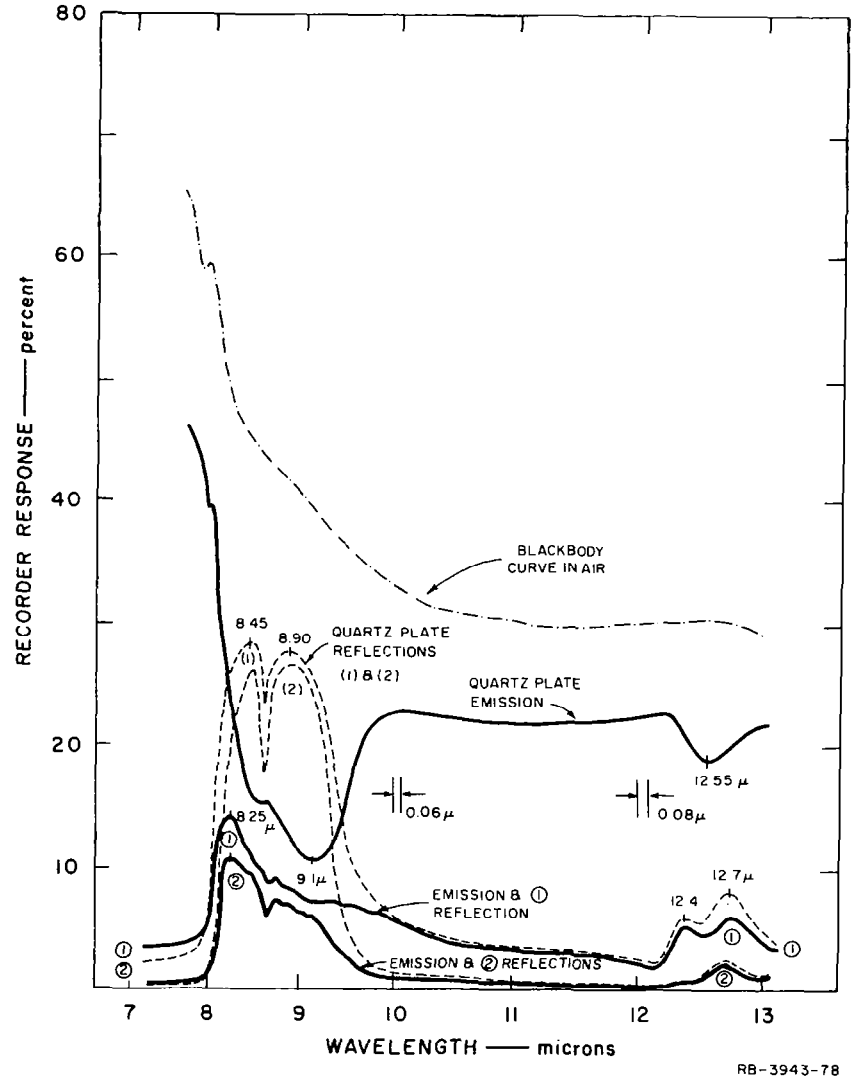

FIG. 61 SPECTRAL CURVES SHOWING THE EFFECT OF MULTIPLE REFLECTION OF 640°K QUARTZ EMISSION AFTER A SINGLE- AND DOUBLE-REFLECTION FROM ADDITIONAL QUARTZ PLATES, AT AMBIENT TEMPERATURES. The characteristic quartz emission minima are completely removed by a single reflection from another quartz surface. (Compare with Figs. 65, 66, and 67.)

These spectral reflectances are shown as dashed lines in Fig. 61, showing the characteristic, double-peak reflection maxima in the 8.45 and 8.9 μ regions (1183 and 1124 cm^{-1}). By normalizing the blackbody curve to unity at a given wavelength, the reflection efficiency can be calculated for both the singly and doubly reflected beams. These calculations are tabulated in Table VII.

Table VII

REFLECTION PERCENTAGES FOR QUARTZ PLATES

Calculations	Peak Wavelength		
	9.1 μ	8.45 μ	8.25 μ
Single-reflection efficiency	65.2%	63.5%	52.1%
Double-reflection efficiency	61.5	59.0	39.1
Recorder response - quartz emission	10	16	26
Recorder response - quartz emission with 1 reflection			
Calculated	6.5	10	14
Observed	7	11	14
Recorder response - quartz emission with 2 reflections			
Calculated	6	9	10
Observed	5.5	9	11

Without disturbing the geometrical arrangement of the two reflection attachments (with their attached quartz plates), the blackbody source was removed. A third quartz plate was used, this time for the emitting source. Thus quartz emission was singly and then doubly reflected from other quartz plates--parallel to reflection from adjoining quartz grains. The three solid spectral curves in Fig. 61 were obtained in this manner.

The curves show that the characteristic quartz emission minima are completely removed by a single reflection from another quartz surface. The second reflection merely further decreases the level of the peak. Exactly similar effects were obtained from the emission from a fused quartz plate reflected from the two other fused quartz plates. The wavelength of the

quartz radiation peak was changed markedly by these reflections, from an emission minimum of 9.1 μ (1100 cm^{-1}) to one with a peak (of reflection characteristics) centered at 8.25 μ (1212 cm^{-1}), a particularly short wavelength value for quartz. This type of problem lends itself readily to modeling on the computer as the following discussion will illustrate.

Figure 62 was taken from Final Report I (1962), page 91, where the variations in the reflectance with temperature for a Z-cut quartz plate were shown. These data came from curves by Simon and McMahon[10] and were redrawn for Final Report I. By photographically enlarging their original reflectance curves to a suitable size, it was possible to extract data points by manually digitizing at 0.1 μ intervals over the wavelength range 7.7 to 13.3 μ (1300 to 750 cm^{-1}). These were then expressed as emittance values, ϵ_λ, for the digital plotting program.

Figure 63 represents the digital plot of Simon and McMahon's original data, calculated as $\epsilon_\lambda = 1-\rho_\lambda$ and plotted linear in microns. Area computation also showed that regardless of the temperature at which Simon and McMahon's measurements were made, the average emittance (from 7.8 to 13 μ) over the temperature range 4^oK to 873^oK remained 0.72 to 0.74. Close inspection of the drawing shows that despite the striking difference between the spectrum at 4^oK and the spectrum at 873^oK, the average emittance (area under the curves) remains constant. To make this clearly visible, three of the calculated emittance curves have been replotted in Fig. 64 for data taken at 80^oK, 623^oK, and 873^oK. The spectral contrast visible at points A, B, and C clearly changes with increasing temperature, resulting in a slightly broadened peak, with an increased emittance minimum. The area under the curve, however, adjusts itself by the broadening of the major peaks and the lowering of the emittance values in the flat, greybody region between 10 and 12 μ (1000 to 850 cm^{-1}).

In the experiment designed to produce the curves of Fig. 61, the quartz plates on which single- and double-reflections of the blackbody and of the other quartz plate emission were made were kept at ambient temperature. From Fig. 62 it is clear that the temperature of the reflecting surface of quartz plays an important role in determining the spectral distribution of the reflected (and consequently calculated emittance) of the surface.

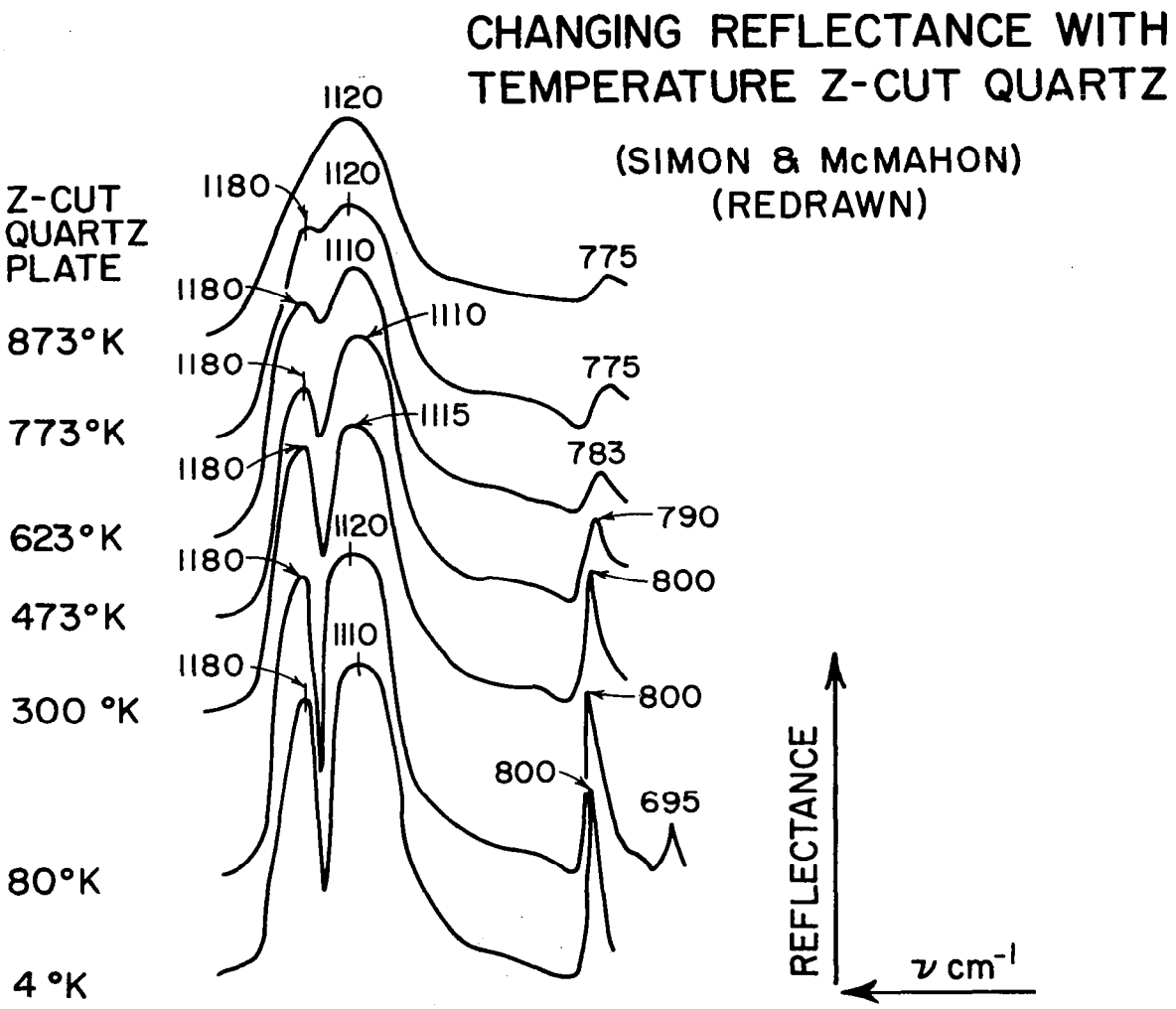

RC-3943-30R

FIG. 62 VARIATION IN REFLECTANCE WITH TEMPERATURE FOR A Z-CUT QUARTZ PLATE. The angle of incidence of radiation is 20°, and the radiation was not polarized. The curves are displaced vertically. Redrawn from Ref. 10 and replotted as Figs. 63 and 64.

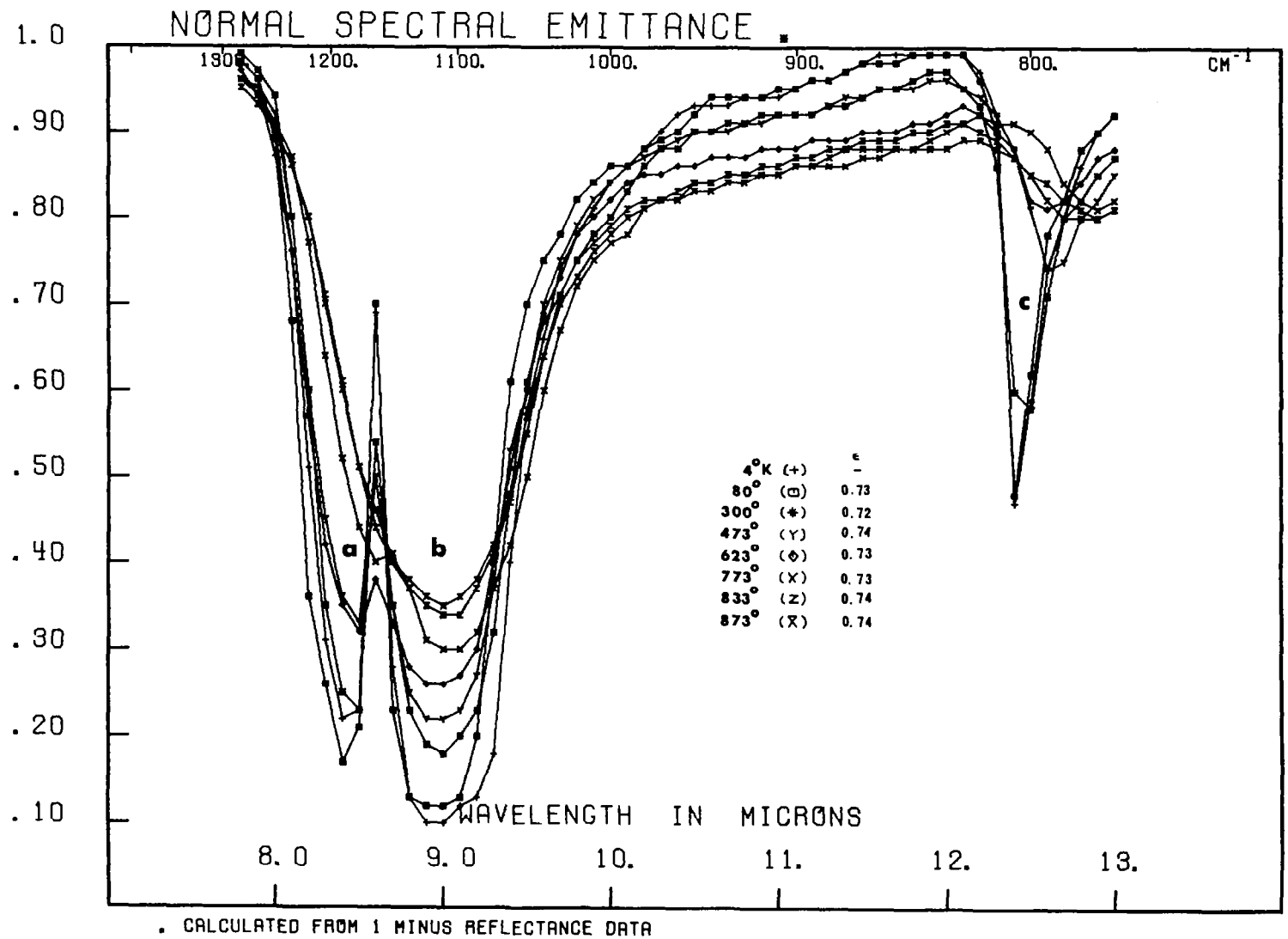

* CALCULATED FROM 1 MINUS REFLECTANCE DATA

FIG. 63 NORMAL SPECTRAL EMITTANCE CURVES, CALCULATED FROM REFLECTANCE DATA, FOR QUARTZ Z-CUT PLATE SHOWN IN FIG. 62. Despite the change in the spectral characteristics as the temperature rises from 4°K to 873°K, the emittance (area under the curves) $\epsilon_{\lambda_1-\lambda_2}$ remains constant between 0.72 and 0.74. The spectral contrast at the peaks A and C should be carefully followed as a function of temperature (see Fig. 64).

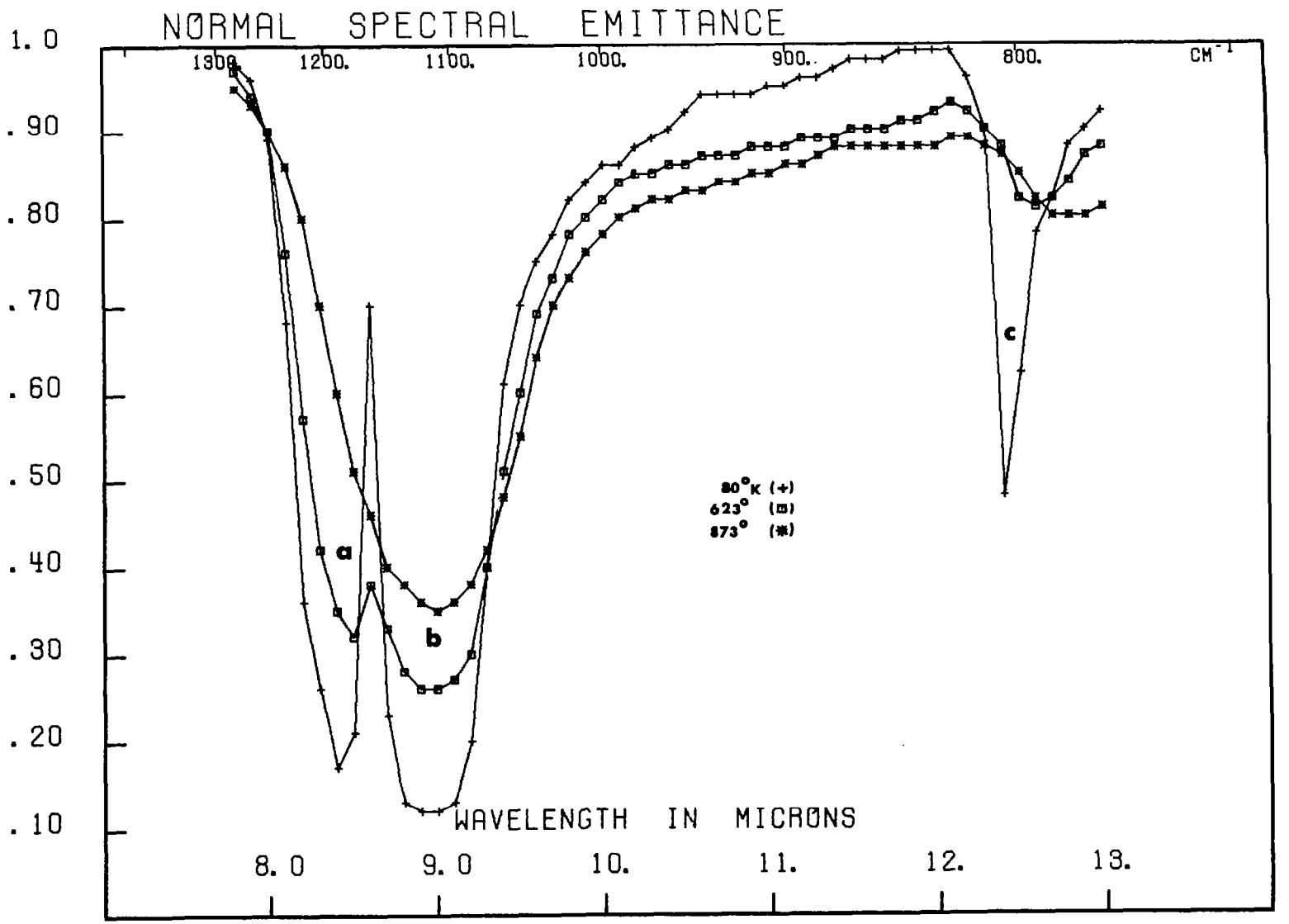

FIG. 64 NORMAL SPECTRAL EMITTANCE CURVES CALCULATED FROM REFLECTANCE DATA OF FIG. 63. Three curves have been selected for detailed examination, those of 80°, 623°, and 873°K. Spectral detail at A, B, and C should be examined carefully as a function of temperature.

A computer program was developed which allowed the reflection process of a quartz emission spectrum (quartz plate at 640°K, upper curves in Figs. 65-67) to be modeled, with allowance for "N" reflections at selected elevated temperatures. The reflection data of Simon and McMahon were used and sets of multiple reflection curves were computed and plotted. Of these, three have been selected for illustration--80°K, 623°K, and 873°K reflection, each source being at 640°K. The computer was programmed so that the radiant energy ($W_\lambda \cdot \epsilon_\lambda$) from the 640°K quartz source at 0.1 μ intervals was consecutively reflected for a total of N reflection cycles. The final* energy level after reflections (R_λ) was computed from

$$R_\lambda = W_\lambda \cdot \epsilon_\lambda (1 - \rho_\lambda)^N \qquad (7)$$

where N goes from 1 to 8. These are the lower curves in Figs. 65, 66, and 67. Striking differences appear in the 8.5, 9.0, and 12.5 μ regions (1200, 1110, and 800 cm^{-1}).

As the temperature of the reflecting surface is raised, so the reflectance spectrum changes its character from the sharply peaked, well-resolved spectrum at 80°K to the smoothly rounded spectrum of the 873°K sample. At 80°K (Fig. 65) one reflection of a quartz surface produces a radiation maximum centered at about 8.22 μ. Subsequent reflections diminish this peak but still show it as a triplet centered about 8.7 μ (1150 cm^{-1}).

Raising the temperature for the reflecting surfaces to 623°K (Fig. 66) makes the emission and the reflectance temperatures approximately identical. This could be the case for a coarsely granular specimen, the temperature being 640°K at a slight depth and 623°K at the surface.

A single reflection still creates a peak centered at about 8.4 μ (1190 cm^{-1}) but subsequent multiple reflections shift the peak to about

---

* The self-emission of the successive reflection plates was omitted from the figures, but is included in the data of Table VIII.

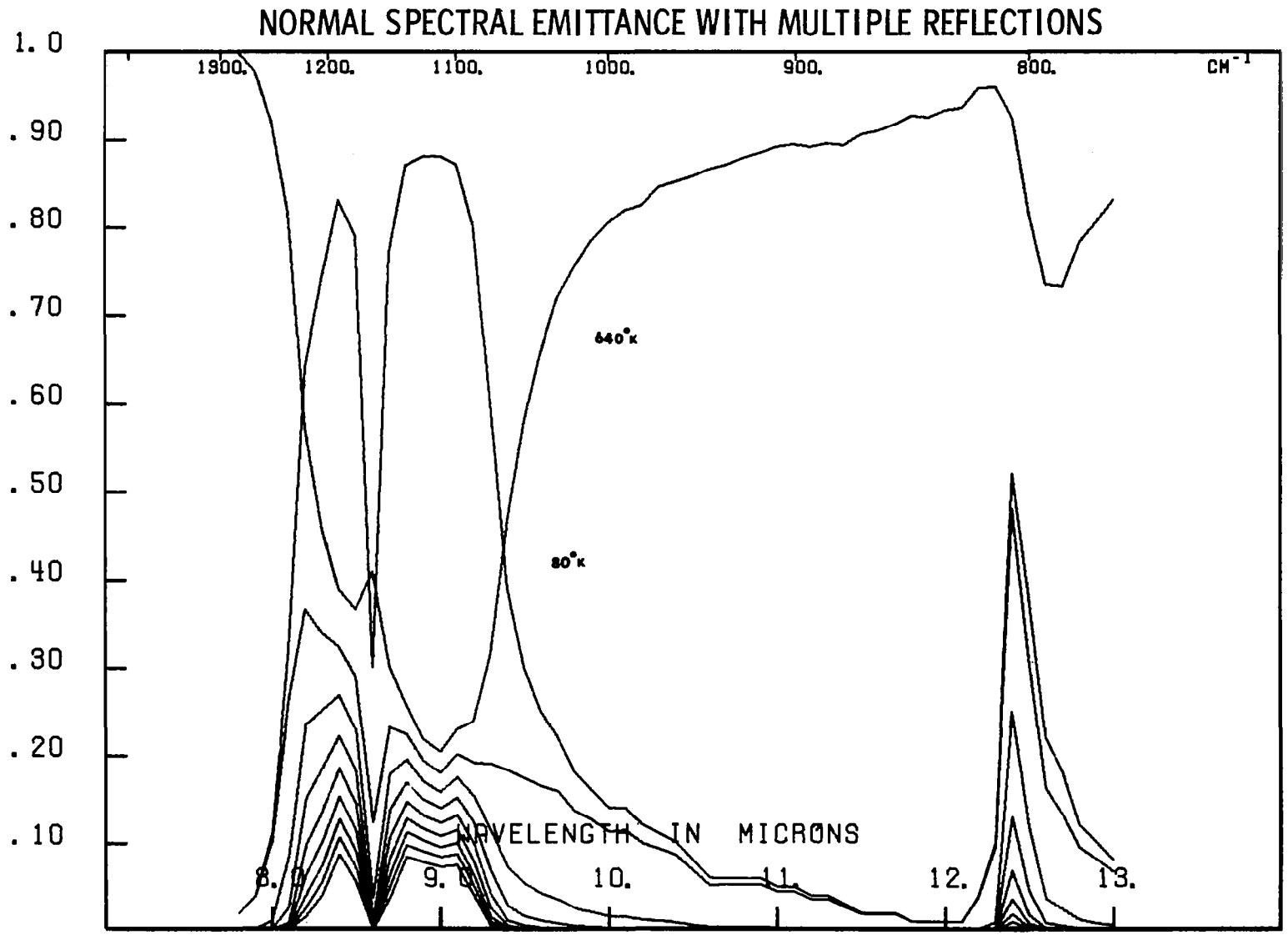

FIG. 65 NORMAL SPECTRAL EMITTANCE CURVE OF Z-CUT QUARTZ (UPPER) AT 640°K WITH MULTIPLE REFLECTIONS FROM A FURTHER Z-CUT QUARTZ PLATE AT 80°K. Successively lower curves are for N-multiple reflections (where N goes from 1 to 8).

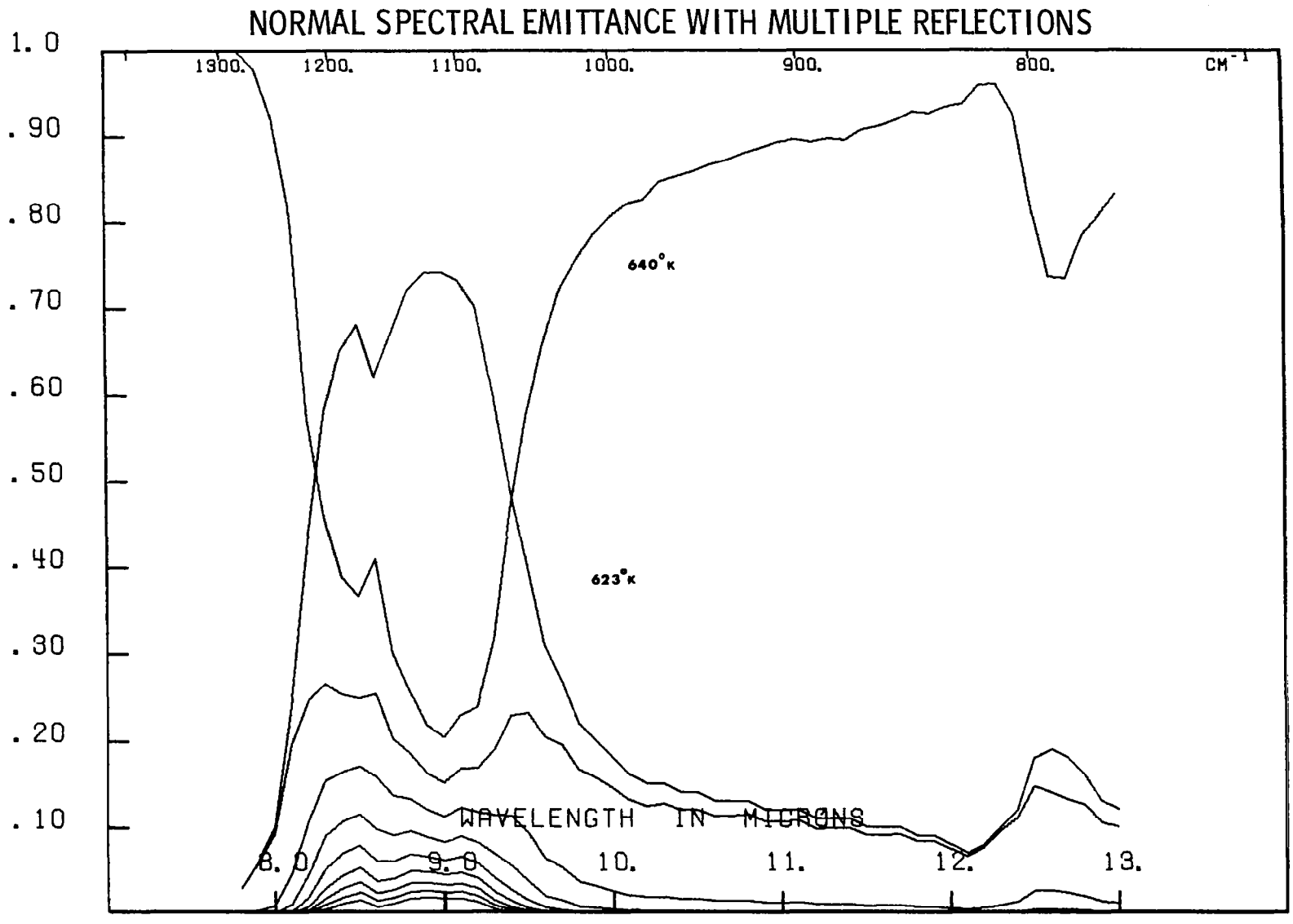

FIG. 66 NORMAL SPECTRAL EMITTANCE CURVES FOR Z-CUT QUARTZ (UPPER) AT 640°K, WITH MULTIPLE REFLECTIONS FROM A FURTHER Z-CUT QUARTZ PLATE AT 623°K. The successively lower curves are for N-multiple reflections (where N goes from 1 to 8).

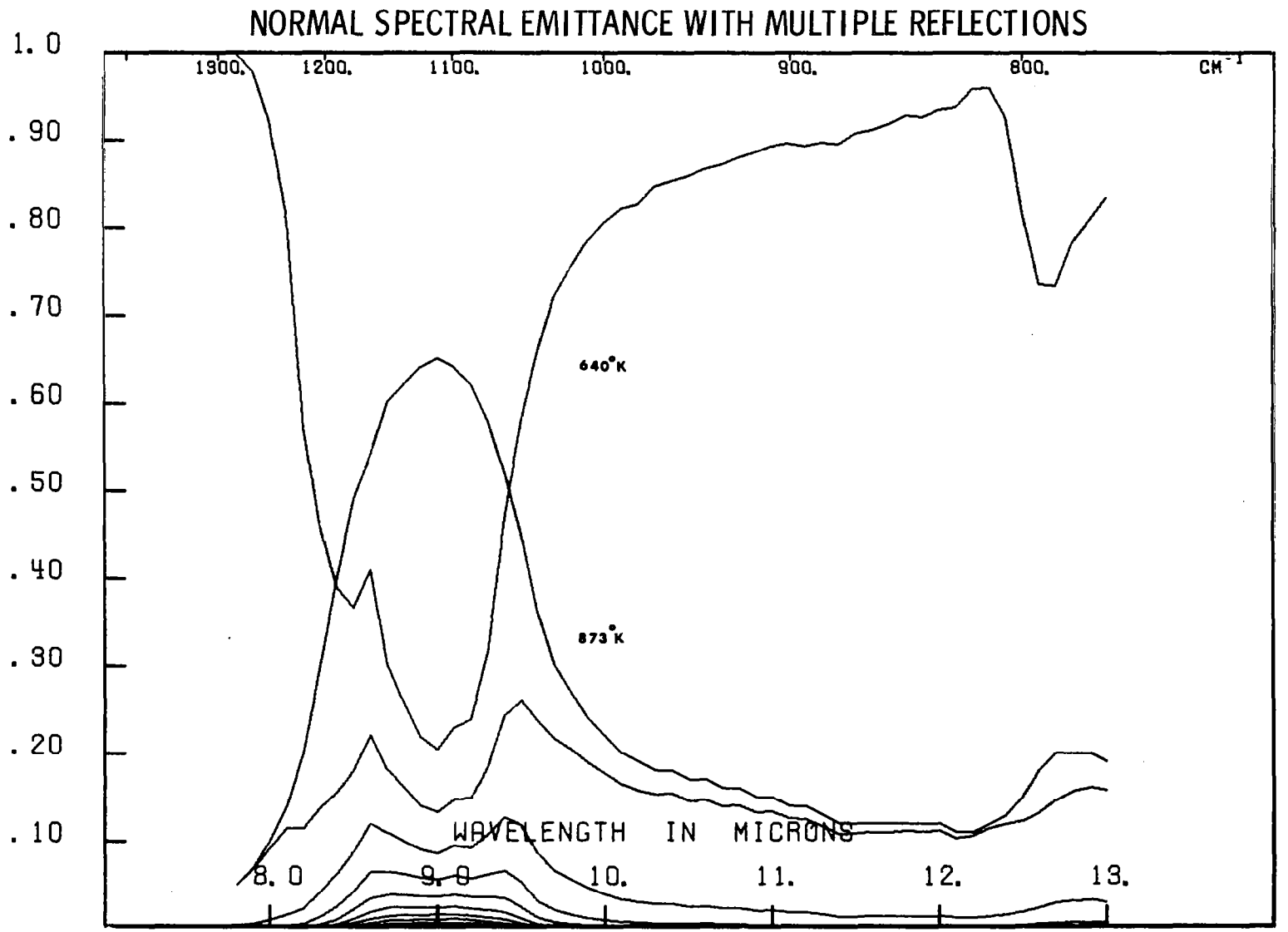

FIG. 67 NORMAL SPECTRAL EMITTANCE CURVE OF A Z-CUT QUARTZ (UPPER) PLATE AT 640°K WITH MULTIPLE REFLECTIONS FROM A FURTHER Z-CUT QUARTZ PLATE AT 873°K. Successively lower curves are for N-multiple reflections (where N goes from 1 to 8).

8.5 μ, with a slight hump at 9.3 μ (1175 and 1075 cm^{-1}). The peak at 9.6 μ rapidly decreases with multiple reflections. At 873°K (Fig. 67) the reflection spectrum changes markedly, producing a peak at 9.5 μ with the first reflection. After three consecutive reflections, the energy decreases rapidly, but is still centered around 9.0 μ (1100 cm^{-1}). As the temperature of the reflecting surface raises from 80°K to 873°K, singly or doubly reflected quartz radiation changes from a sharp maximum at 8.2 μ to a weaker maximum at 8.3 μ. The highest temperature for reflection lowers the maximum to 9.3 μ.

The model tested had a surface of quartz maintained at 640°K, covered with an aggregate of coarsely crystalline material (quartz) at a different temperature from that of the emitting surface. Another interesting model (but one not tested) would have a thermal gradient from the source to the uppermost surface and hence would have continually lowered temperatures for the reflecting surfaces. This could be approximated by a rough quartz plate overlain by a fairy castle structure, with a marked thermal gradient between the quartz and the top of the fairy castle structure. Our computer experiment shows the mathematical testing of a model which had been proposed to explain the change in emittance levels as the surface is roughened or covered with a highly porous material of the same composition.

When one considers the self-emission as well as the reflectance from these "N" plates, the emission levels rapidly approach blackbody, that is, the emittance rises to unity. This is the familiar situation in the production of blackbody radiation by multiple reflection from the walls of an enclosure--if "N" is sufficiently large, the initial value of the emittance is of little consequence. (See Table VIII.)

Table VIII.

QUARTZ EMITTANCE LEVELS FOLLOWING N-REFLECTIONS FROM SIMILAR PLATES (X-CUT)

(Same orientation, polish, and temperature)

Formula Used - Level $E^1 = E\sum_{o}^{N} (1-E)^N = 1.0$ as N increases

	At 8.0 μ	At 8.33 μ	At 9.0 μ	At 9.5 μ	At 10 μ
Emittance (E)	0.90	0.43	0.20	0.59	0.80
+ 1 reflection	.99	.67	.36	.83	.96
+ 2 reflections	.999	.81	.49	.93	.992
+ 3 reflections	--	.89	.59	.97	.998
+ 4 reflections	--	.94	.67	.99	--
+ 5 reflections	--	.97	.73	.996	--

5. Functional Groups (Anions) Other than Silicates

Rocks are often composed of functional groups (anions) other than those of the silicates, which have formed the bulk of this study. Such inorganic anion groups have strong, commonly simple, absorption spectra. Some of these were shown in Fig. 5 of this report, reproduced from Final Report I.

Strong absorptions (and hence strong reflection maxima and emission minima) occur for carbonates at 7.0 μ, nitrites at 8.1 μ (1235 cm^{-1}), nitrates at 7.25 μ (1380 cm^{-1}), phosphates at 9.5 μ (1050 cm^{-1}), and sulphates at 8.85 μ (1130 cm^{-1}), whereas all silicates show the peaks between 9 and 11 μ (1100 to 900 cm^{-1}) (see Fig. 5). To test if a peak shift would accompany changes in functional groups in emission analysis, a set of experiments was carried out to obtain the emittance spectrum of some carbonate and sulphate samples. Figure 68 shows tracings of the spectra exactly as obtained with the single-beam instrument, for a cleavage plate of calcite ($CaCO_3$) with a highly polished surface. The reststrahlen for a carbonate functional group occurs somewhere near 7 μ (1430 cm^{-1}) right in the center of the CO_2 band in air absorption, and on the wing of the H_2O bands at 6.5 μ (1540 cm^{-1}). These

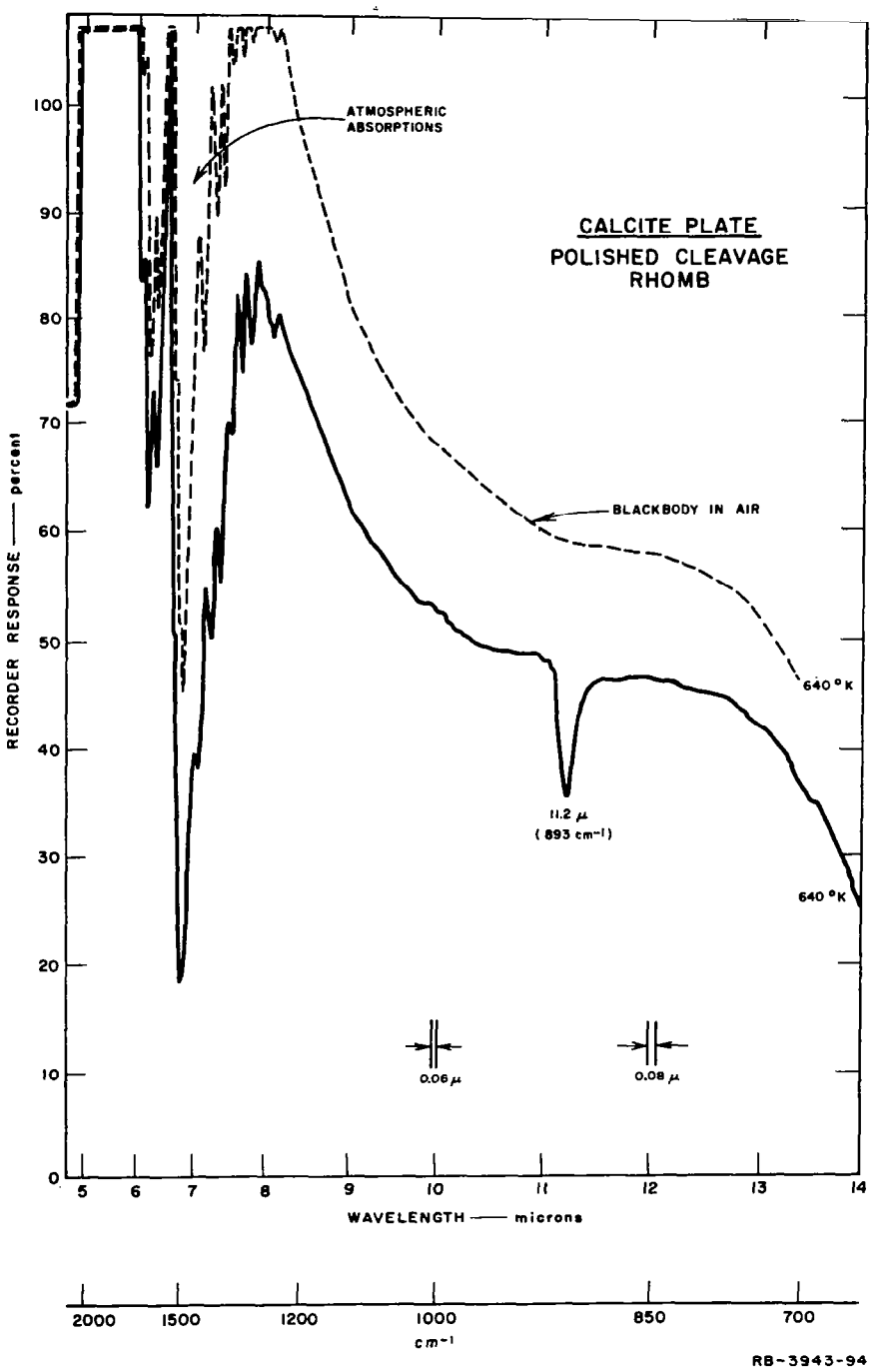

FIG. 68 DIRECT TRACING OF THE SPECTRUM OBTAINED WITH A SINGLE-BEAM SPECTROMETER FOR A CLEAVAGE PLATE OF CALCITE (WITH A HIGHLY "POLISHED" SURFACE). The spectral contrast for a carbonate material occurs in the middle of the atmospheric absorption band near 7 μ. The emittance can be calculated (with difficulty) by obtaining the ratio between the blackbody curve (dashed) and the sample curve (solid) at equal wavelength intervals, on this widely fluctuating curve.

atmospheric absorptions caused considerable problems when the two curves were digitized to obtain the emittance ratios, because of the rapidly changing spectral levels. Despite this "noise" the data have been normalized and are replotted in Fig. 69. The strong minimum is seen now at 6.70 μ (1490 cm^{-1}) with the diagnostic secondary peak at 11.30 μ (885 cm^{-1}).

In Fig. 70 the spectrum was obtained for a structural polymorph of $CaCO_3$ called aragonite. This crystal had a roughened surface but still shows the peak at 6.70 μ in its emittance spectrum. The smaller peak is shifted towards 11.50 μ (870 cm^{-1})--a shift of 0.2 μ due to the change in structural coordination of the $CaCO_3$ molecule.

The sample of magnesium-calcium carbonate, dolomite [$Ca,Mg(CO_3)$] used for Fig. 71 was dolomite rock, with a weathered and roughened surface, broken off the dolomite horizon at the base of the Rainier Tuff series, Rainier Mesa, Nevada Test Site. The roughened surface on the sample produced a smaller emittance minimum (lower spectral contrast) at 6.45 μ (1550 cm^{-1}), a shift of 0.25 μ from that of the calcium carbonate polymorphs (Fig. 71). In addition, the secondary peak at 11.20 μ (893 cm^{-1}) was shifted a distance of 0.3 μ in the same sense.

It is possible, therefore, from the emittance spectrum alone to distinguish between calcite, aragonite and dolomite rocks by spectral shifts in the 6.5 to 13.0 μ wavelengths.

Sulphate emission spectra also have been obtained by direct measurements for an anhydrite ($CaSO_4$) sand with an average grain size of 150 to 300 μ. In Fig. 72 the normal spectral emittance curves of this are shown and compared directly with that of a quartz sand of a small particle size. The reststrahlen for the $(SO_4)^{2-}$ functional group in anhydrite sand appears at 8.60 μ (1163 cm^{-1}) while that for the $(SiO_4)^{2-}$ functional group in quartz sand appears at 9.10 μ (1100 cm^{-1}), a shift of 0.5 μ obtained by direct emittance measurements at 640°K. The radiant energy plot ($\epsilon_\lambda \cdot W_\lambda$) is shown ($\times 10^4 \pi$) in Fig. 73.

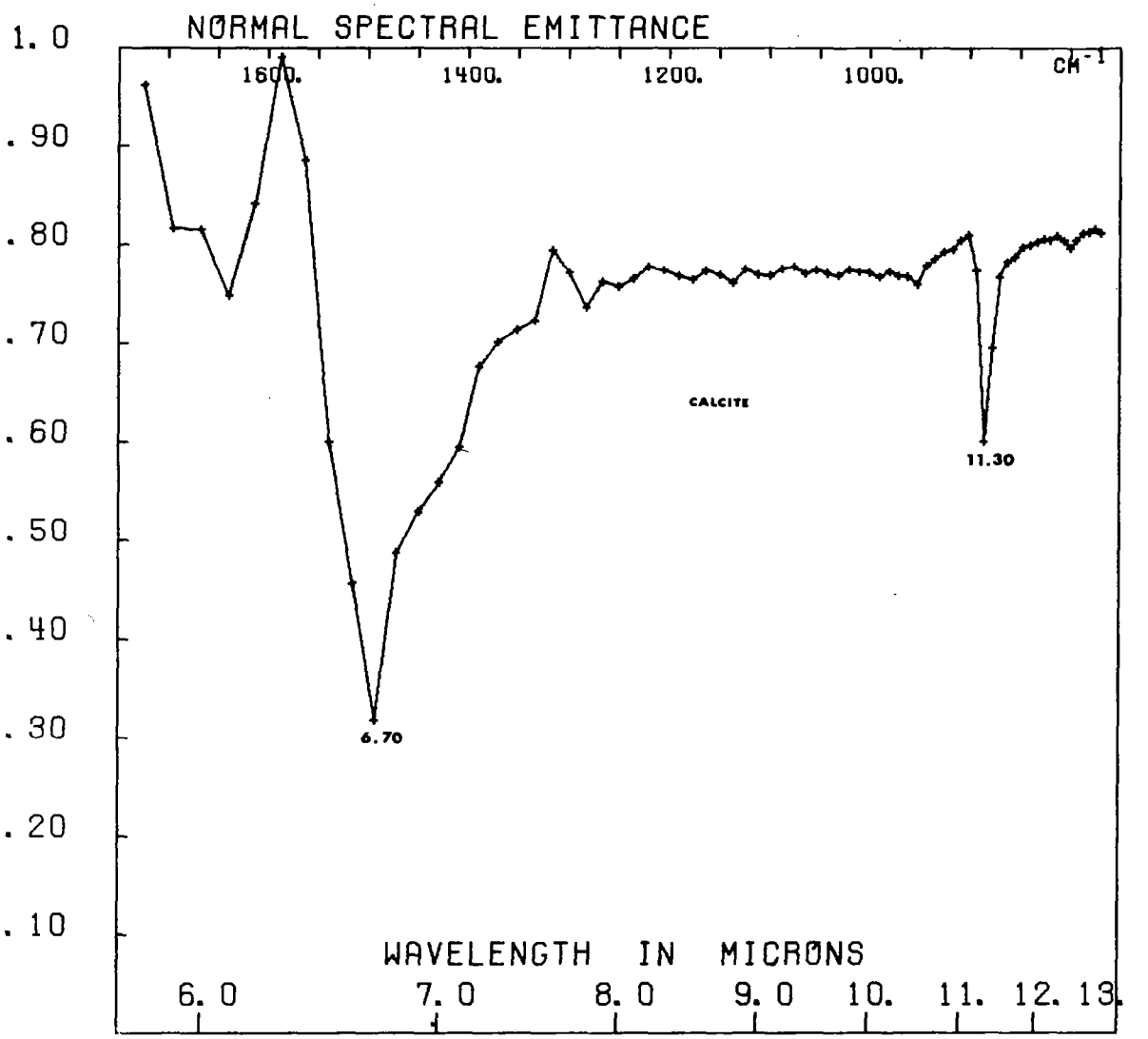

FIG. 69 NORMAL SPECTRAL EMITTANCE CURVE CALCULATED FROM RATIOS OBSERVED IN FIG. 68, FOR CALCITE ($CaCO_3$) AS A CLEAVAGE PLATE. Note the presence of two minima at 6.70 and 11.30 μ.

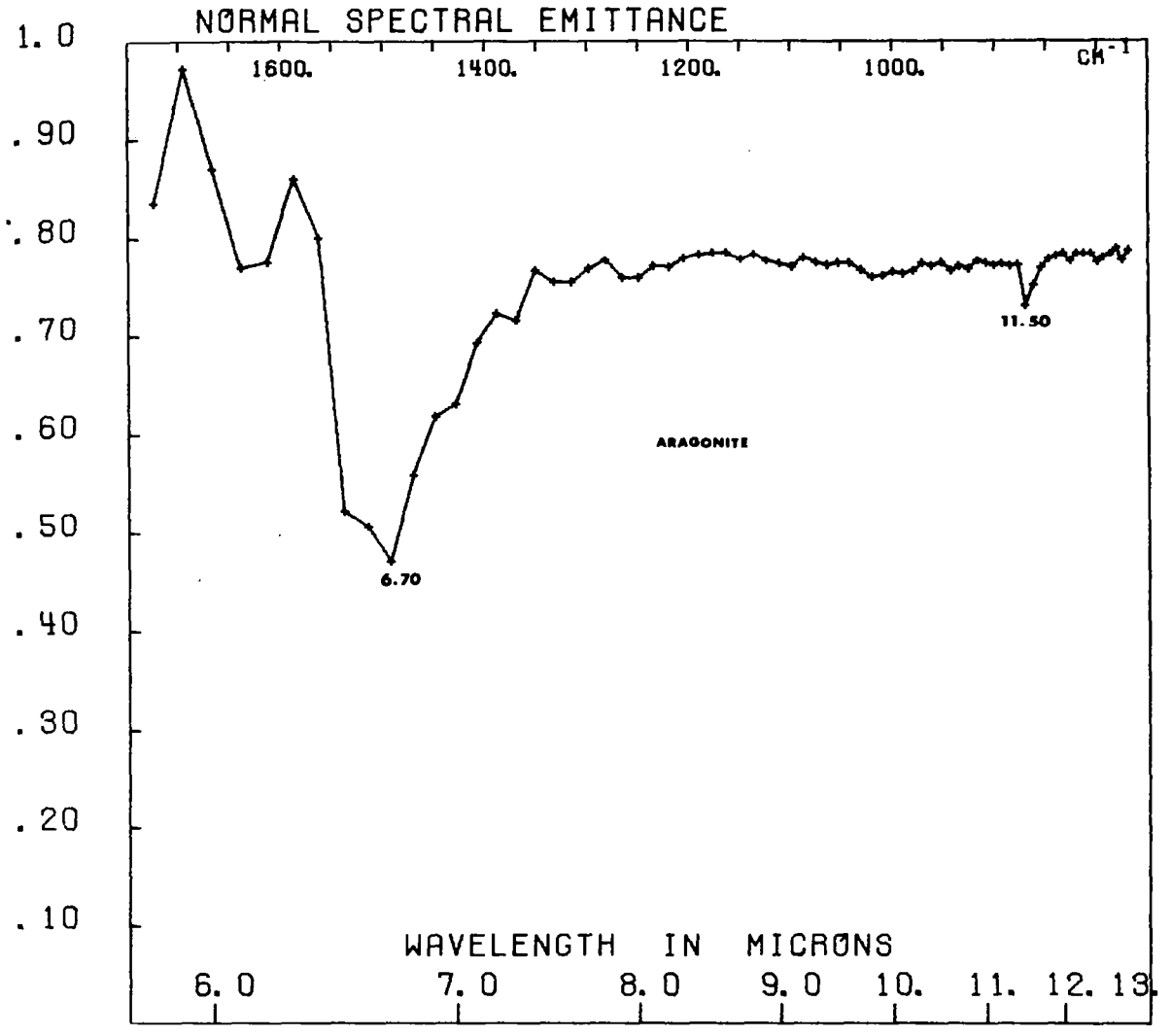

FIG. 70 NORMAL SPECTRAL EMITTANCE CURVE FOR ARAGONITE (ALSO $CaCO_3$, BUT A DIFFERENT STRUCTURAL GROUP), CALCULATED IN THE MANNER OF DATA FROM FIG. 68. Note specifically the two emission minima at 6.70 and 11.50 μ, shifted from the position for the other polymorph of $CaCO_3$, calcite.

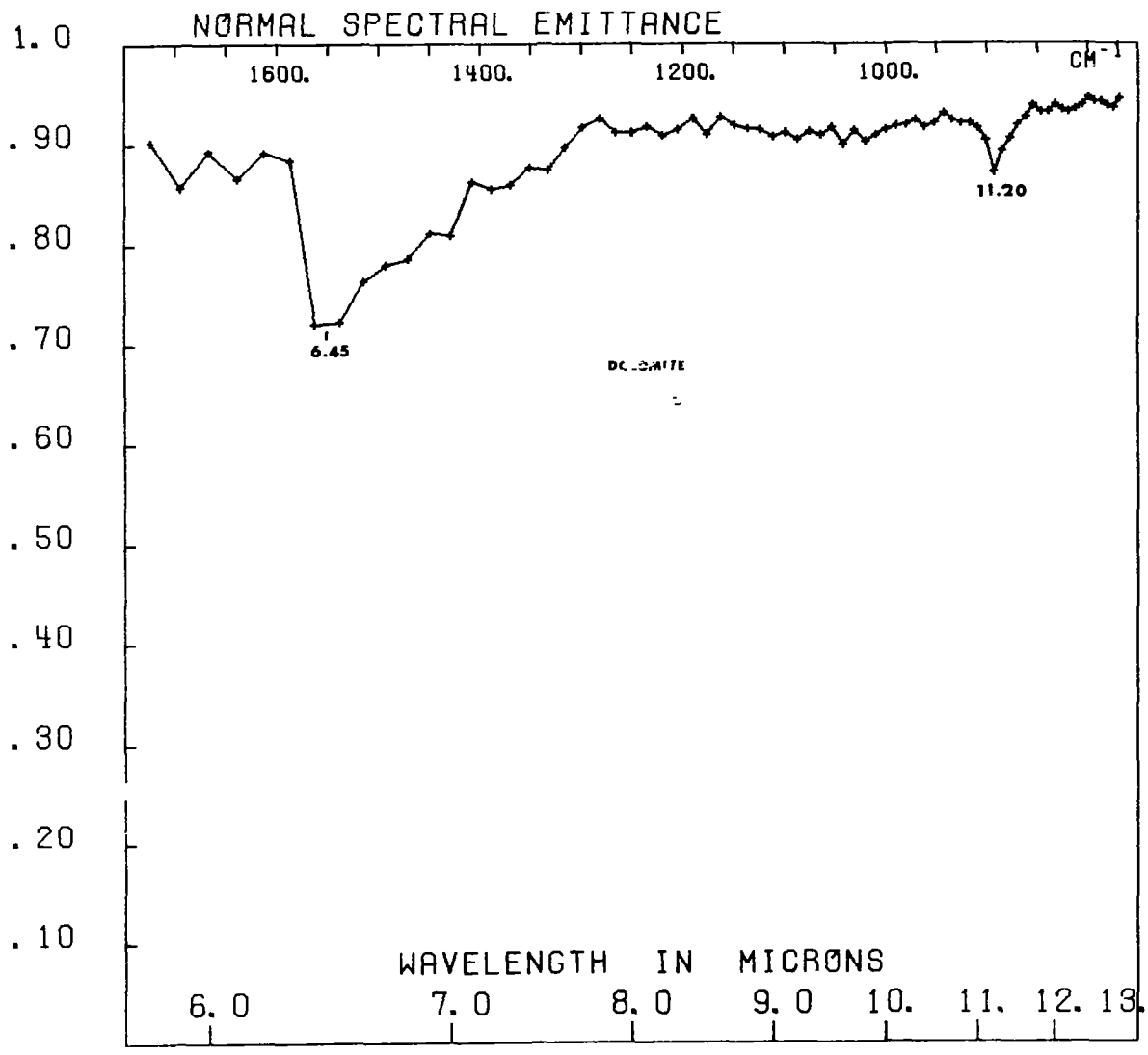

FIG. 71 NORMAL SPECTRAL EMITTANCE CURVE FOR DOLOMITE, [Ca, $Mg(CO_3)$]. The sample was a rough-surfaced, natural rock outcrop of the dolomite from which a chip was taken for the measurements. The roughened surface has resulted in decrease of the minimum at 6.45 μ and 11.20 μ. Note the change in the wavelength of these two minima with composition as shown in Figs. 69 and 70.

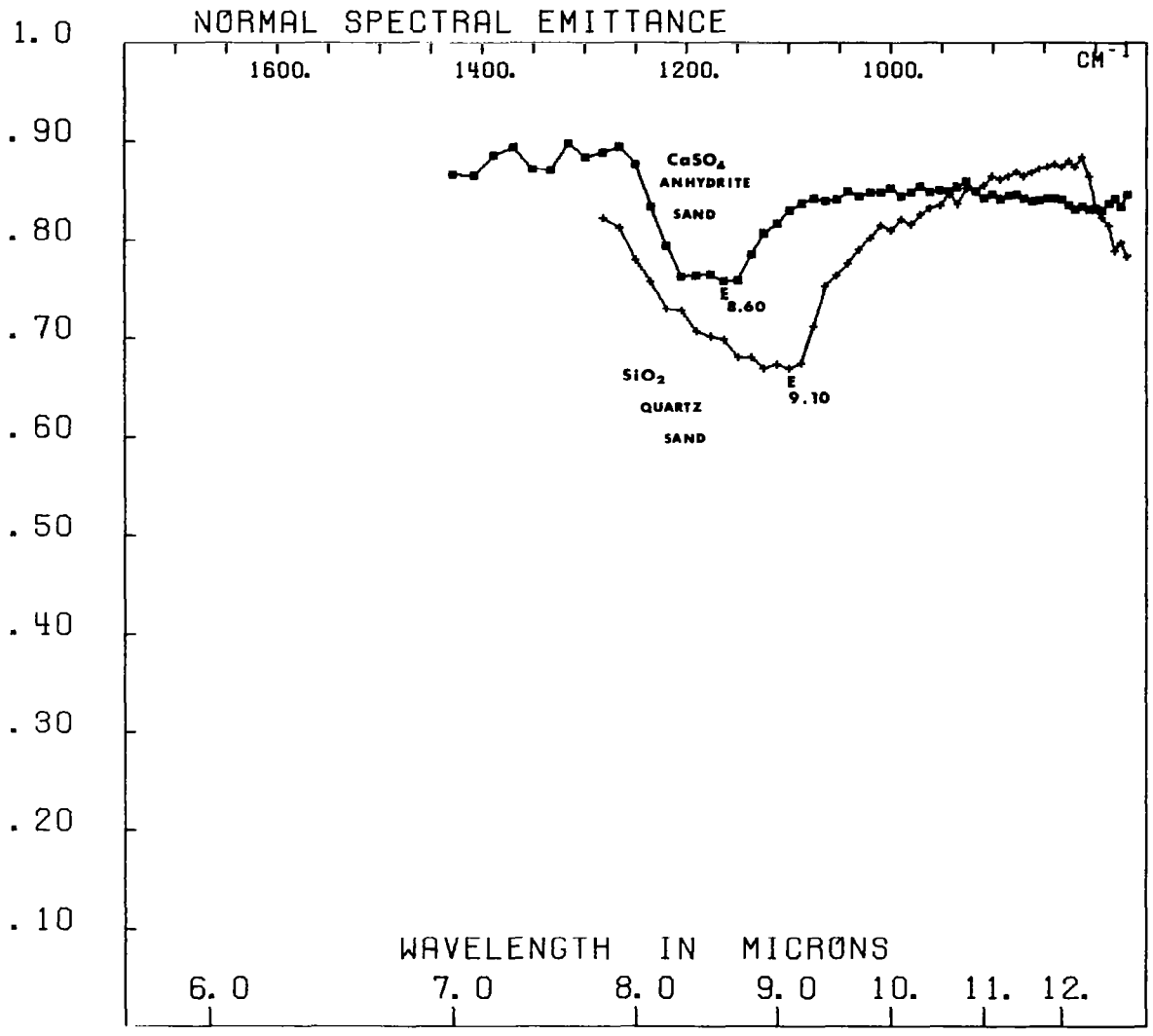

FIG. 72 NORMAL SPECTRAL EMITTANCE OBTAINED FOR SAND-SIZE SAMPLES OF ANHYDRITE ($CaSO_4$) AND QUARTZ (SiO_2) SANDS. Note the emission minima are displaced from that of the anhydrite (8.60 μ) to that of the quartz (9.10 μ), a distance of 0.5 μ.

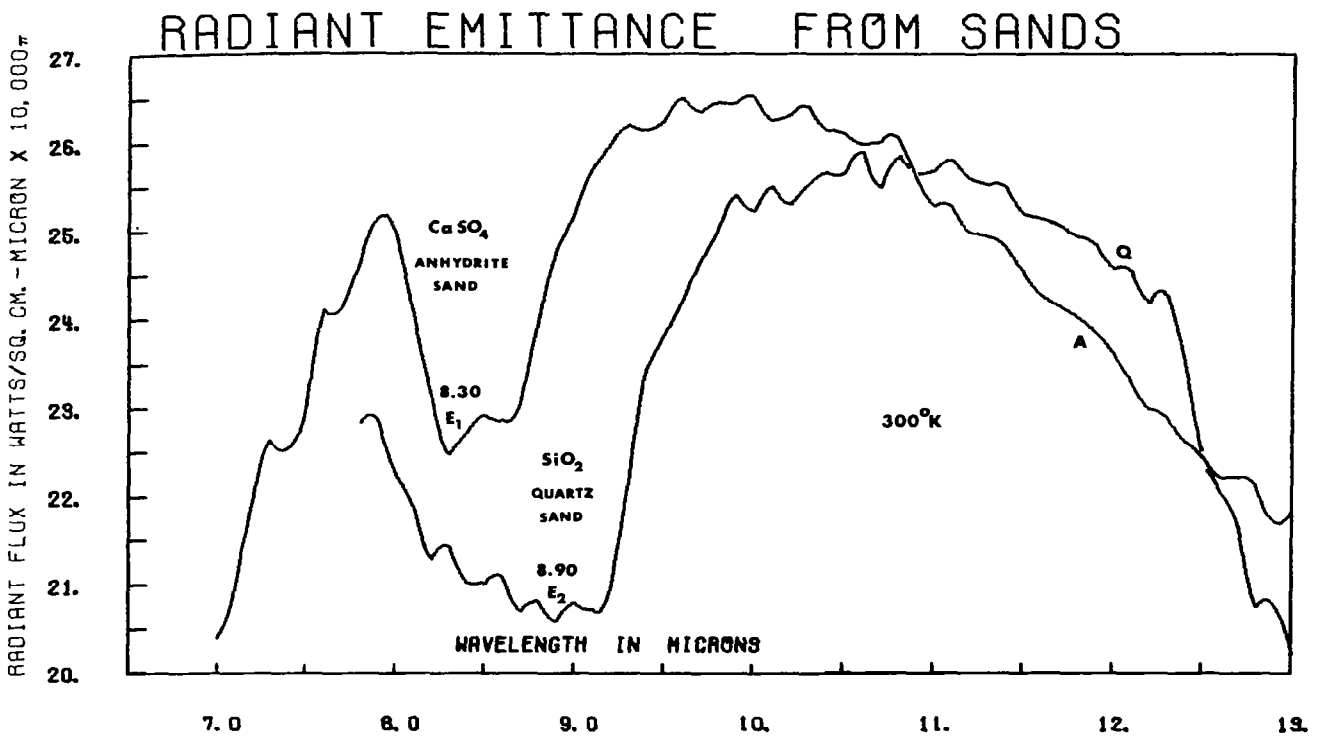

FIG. 73 RADIANT EMITTANCE FROM ANHYDRITE AND QUARTZ SANDS PLOTTED AS A FUNCTION OF WAVELENGTH. Same data as Fig. 72, plotted on a radiant flux format. Note that the emission minimum of the anhydrite (E_1) is now at 8.30 μ, and that for the quartz sand (E_2) is at 8.90 μ, shifted from the minimal positions shown on Fig. 72 as a result of a change away from a normalized format. The shift in the emittance minima is 0.6 μ, approximately that shown in Fig. 72. Note also that numerical values of the ordinate have been multiplied by ($10^4 \cdot \pi$).

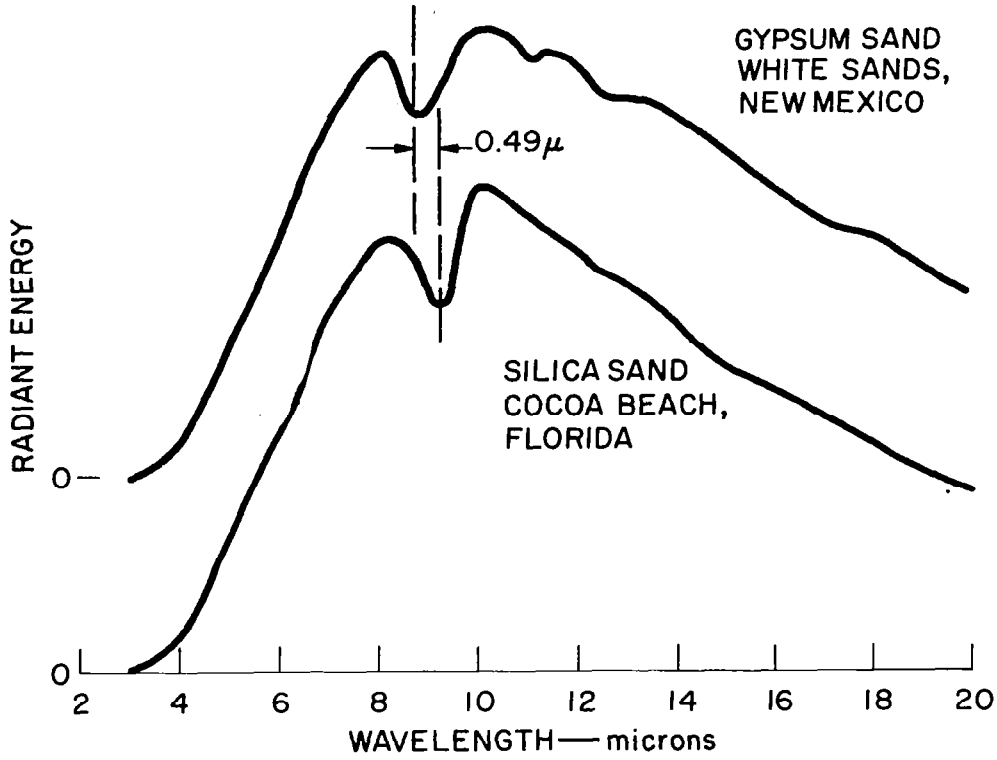

FIG. 74 EMITTANCE SPECTRA OBTAINED FOR GYPSUM AND SILICA SAND (QUARTZ) OBTAINED BY BELL AND OTHERS[37,38] BY DIRECT EMITTANCE MEASUREMENTS USING MOBILE SPECTROMETERS. The format of presentation is identical with that of Fig. 73.

Figure 74 shows emission curves for gypsum and silica sand as observed in the field at ambient temperatures (300°K) by Bell and others,[37,38] in New Mexico and in Florida. The figure is directly comparable with Fig. 73. These measurements indicate that finely divided gypsum sand at White Sands, New Mexico, and quartz sand at Cocoa Beach, Florida, each gave significant and different deviations from the blackbody radiation curves. The data were obtained with mobile spectrometers operated at night (to minimize reflected sunlight from the source) with the source several hundred feet to several thousand feet from the instrument. The radiation was collected by telescopic optics mounted in front of the spectrometer. The close correlation between the emission minimum found by Bell, et al, for gypsum and for silica (a difference of 0.49 μ), and those found in the laboratory in our direct emission experiments, of 0.50 μ lend considerable credence to this method for operational use under either terrestrial or lunar conditions.

Bell's data were attenuated by the spectral signal of the atmosphere. Corrections had to be made to remove these effects from their signals. Their spectra, extending from 3 to 20 μ, needed considerable correction for the marked absorptions at 2.7, 7.0, and 15 to 20 μ bands (see Figs. 84 and 85).

6. Longer Wavelength (15 to 25 μ) Studies

To produce the required wavelength characteristics, spectrometers are designed to use prisms or gratings as their dispersing media, depending on the particular material from which the prism is made (NaCl, KBr, CsBr, KI) or the particular grating interval (various values of lines per inch, blaze angle). It is common to use the NaCl prism in the wavelength range from 2.5 to 15.0 μ (4500 to 667 cm^{-1})and the KBr prism in the wavelength range from about 12 to 25 μ (from 833 to 400 cm^{-1}). If it is desired that a still longer wavelength range be investigated, a CsBr prism is used out to 35 or 40 μ (280 or 250 cm^{-1}).

Many of the reflectance and absorption spectra of silicates have shown a second fundamental Si-O stretching vibration in the vicinity of 20 to 22 μ (500 to 450 cm^{-1}). These may be seen in Figs. 34 and 35. To investigate this region by direct emission, experiments were designed so that the wavelength range from 14 to 25 μ could be investigated (715 to 400 cm^{-1}). Fig. 75 shows the direct emittance measurements for quartz plates in both the X-cut (E_1) and Z-cut (E_2) configurations. The E_1 spectrum has an emission minimum at 20.5 μ (488 cm^{-1}), whereas the Z-cut quartz plate (E_2) shows a stronger doublet with a peak at 21.7 μ (460 cm^{-1}). A direct parallel to this can be seen from Figs 7 and 13 for the calculated emittance curve for X-cut quartz obtained by reflectance measurements, showing a sharp peak close to 20 μ (500 cm^{-1}). The X- and Y-cut plates show peaks at 20.2 μ (496 cm^{-1}) but the Z-cut plate shows a doublet with peaks at 21.2 and 21.5 μ (472 and 460 cm^{-1}), paralleling Fig. 75. The direct emission measurements on roughened X-cut quartz (E_2) and fused quartz (E_1) are shown in Fig. 76, in which little difference appears between the spectra of these particular materials in this wavelength.

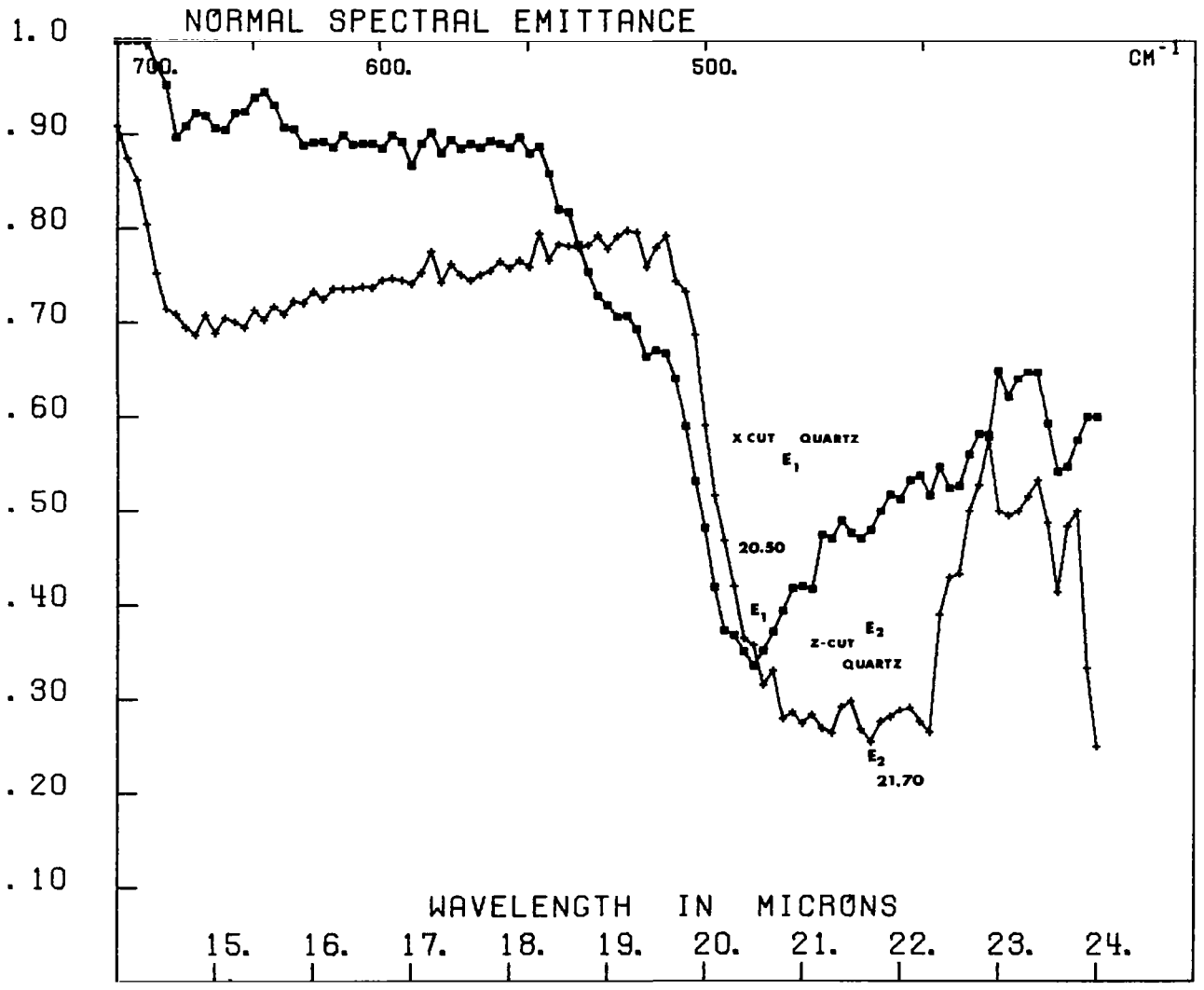

FIG. 75 NORMAL SPECTRAL EMITTANCE FOR X-CUT AND Z-CUT QUARTZ PLATES IN THE LONGER WAVELENGTH REGION FROM 14.0 TO 24.0 μ. Emittance minima for X-cut quartz (E_1) appear at 20.50 μ, and that for a Z-cut (E_2) quartz plate appears centered around 21.70 μ.

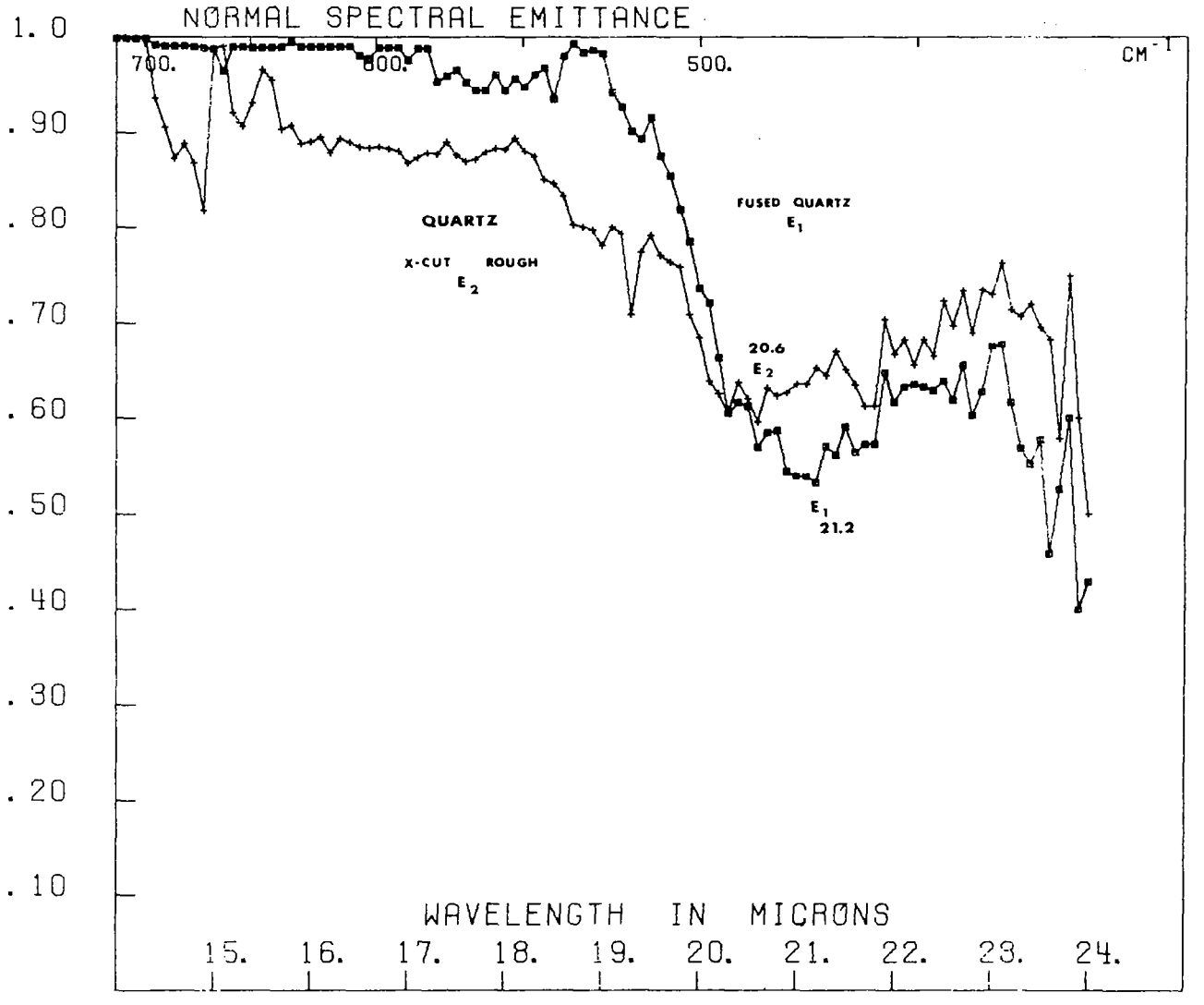

FIG. 76 NORMAL SPECTRAL EMITTANCE CURVES FOR FUSED QUARTZ (E_1) AND ROUGHENED X-CUT QUARTZ (E_2) MATERIALS, IN THE LONGER WAVELENGTH REGION FROM 14.0 TO 24.0 μ. The fused quartz shows a minimum of emittance (E_1) at 21.20 μ, while that of the roughened quartz X-cut plate shows an emittance at 20.60 ...

The emission spectrum for the sheet sapphire sample is shown in Fig. 77 for this wavelength range. The spectrum shows two minima, occuring at 17.0 μ (590 cm^{-1}) and 22.30 μ (448 cm^{-1}). The emission minima reported in Fig. 50 for the various particle sizes of Al_2O_3, therefore, continue to reach a minimum value at the 17.0 μ peak (E_1).

All these spectra show rapid (noise) oscillations. Any infrared signal is markedly attenuated by atmospheric absorptions, and these are extremely numerous between 15 and 25 μ (see Fig. 68). As a consequence, it is often difficult to exactly determine the emittance value when digitizing these rapidly changing curves. This is a more marked problem using a single-beam instrument in this wavelength region.

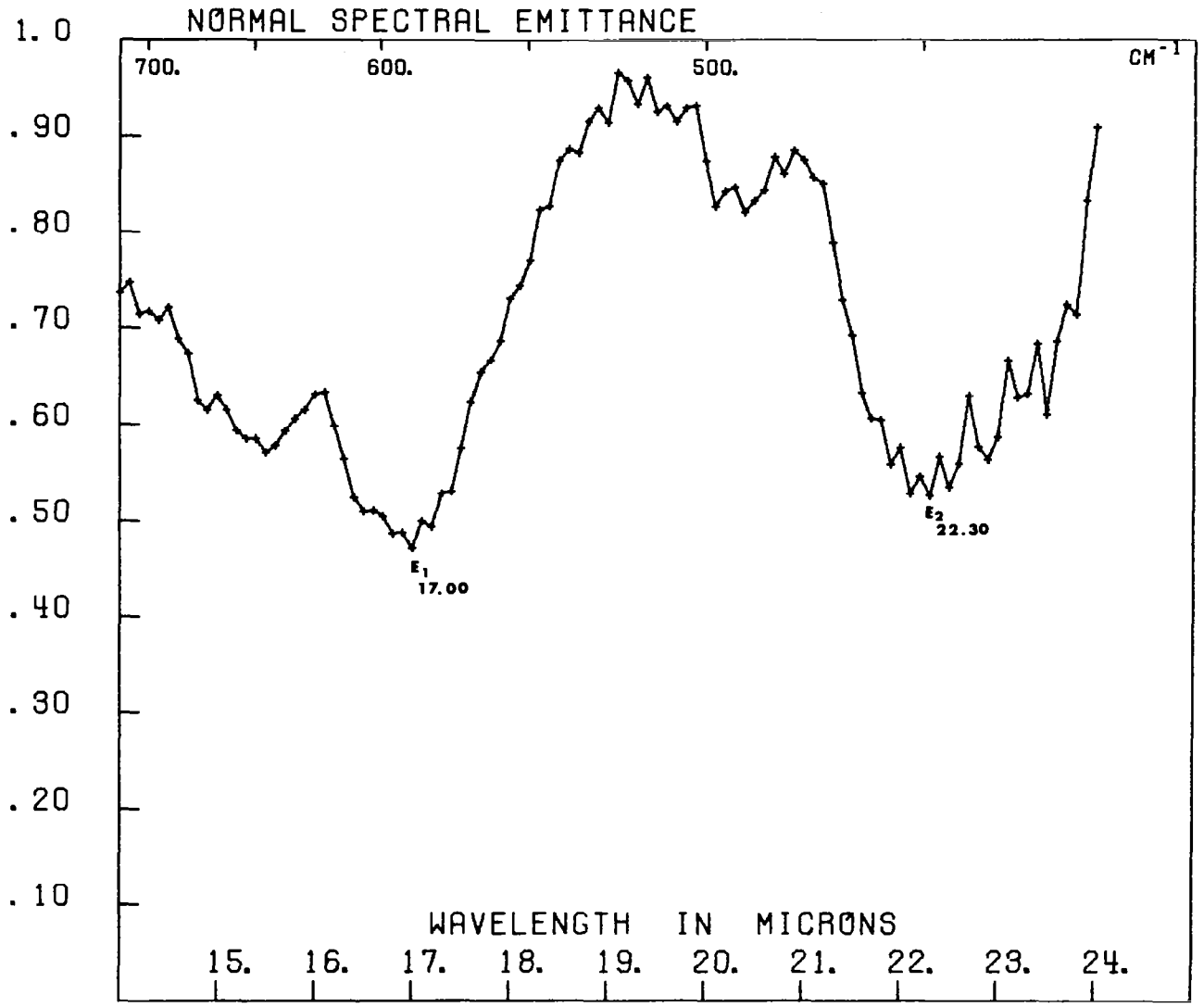

FIG. 77 NORMAL SPECTRAL EMITTANCE FOR A SAPPHIRE (Al_2O_3) SHEET, IN THE LONGER WAVELENGTH RANGE FROM 14.0 TO 24.0 μ. Two emittance minima are shown at 17.00 (E_1) and 22.30 (E_2) μ for this material, contrasting in wavelength with those of the SiO_2 materials shown in the preceding figures.

IX COMBINED TECHNIQUES

A. Results of Studies on Stony Meteorites (Chondrites)

Dr. Carleton Moore of the Arizona State University furnished samples of chondritic (stony) meteorites for study by emission, reflection, and absorption analyses. Characteristics of these chondrites are listed in Tables IX-XI.

Reflection analyses were made on two samples of the Farmington meteorite (Farmington-A and Farmington-B). Direct emission analyses were performed on the two sides of a specimen of Leedey chondrite (Leedey-1 and Leedey-2) and on the two sides of a further Farmington specimen (Farmington-1 and Farmington-2).

Table IX

CHARACTERISTICS OF CHONDRITES USED FOR ANALYSIS

Bruderheim,	Alberta, Canada. Fell March 4, 1960. A hypersthene chondrite (see attached modal analysis).
Farmington,	Washoe Co., Kansas. Fell June 25, 1890. A polymict brecciated black hypersthene chondrite.
Haven,	Reon Co., Kansas. Found 1950. A veined crystalline chondrite.
Ladder Creek,	Greeley Co., Kansas. Found 1937. A crystalline spherical chondrite.
Leedey,	Dewey Co., Oklahoma. Fell Nov. 25, 1943. White chondritic stone.

Table X

BRUDERHEIM MODAL ANALYSIS

Mineral	Modal Weight (%)	
Pyroxene	42.26	(hypersthene En_{78}, with substantial CaO)
Olivine	40.67	(Fo_{78})
Feldspar	0.36	(An_5 - high temperature form)
Apatite and Merrillite	0.35	
Metallic	7.60	
Troilite	6.71	
Chromite	0.85	
Holes	1.21	

Table XI

ELECTRON PROBE ANALYSIS OF CHONDRITIC MINERALS

$\frac{Fe}{Fe + mg}$ mol %

Sample	In Olivine	In Pyroxene
Bruderheim	23.8 (25)[a]	20.7
Farmington	23.8 (24)[a]	20.8
Ladder Creek	22.6 (24)[a]	21.0

[a] Values obtained by B. Mason, using x-ray methods.

The emission, reflection, and absorption curves are shown for Bruderheim, Leedey, Haven, and Ladder Creek stony meteorite (chondrite) materials in Figs. 78-81.

In Fig. 78 emission curves have been shown for the Leedey chondrite as duplicate runs (Leedey-1 and Leedey-2). The peak postions of the emission minima are at 10.7 and 10.8 μ respectively (935 and 926 cm^{-1}). The absorption curve for Bruderheim chondritic material is shown in the lower curve, with a major absorption peak in the vicinity of 11 μ. The minimum value is at 11.24 μ (890 cm^{-1}). A small amount of detail is shown between 14 and 17 μ with a secondary maximum of absorption showing at approximately 20 μ (490 cm^{-1}).

A reflection curve for the Haven chondrite is shown in Fig. 79, with a pattern similar to that of the Bruderheim chondrite represented in the lower absorption curve. Haven shows a reflection peak near 11 μ, with a local minimum at 10.75 μ (930 cm^{-1}). The 20 μ peak on the absorption spectrum is also indicated by a reflection peak at 19.6 μ (510 cm^{-1}). These two curves are remarkably similar although the absorption peaks are displaced again to the longer wavelength in every case.

Simon [40] (page 152) has discussed this change in peak wavelength in detail, and concludes that:

> "The maxima of the reflection curves do not indicate exactly the frequency of the vibrational bonds because both the real and the imaginary parts of a complex refractive index contribute to the reflectivity in the region of strong dispersion. This effect is particularly strong in the Si-O-Si vibrational bond of crystalline quartz and the correct frequency has to be obtained by determining separately the two components of the index, e.g., by measuring reflectivity at two angles of incidence; by means of this method the Si-O-Si bond-stretching vibration in quartz has been located at 1065 cm^{-1}."

Two samples of the Farmington chondrite are shown in Fig. 80 (Farmington-B in reflection, and Farmington-2 in emission). The emission minimum of 11.3 μ (885 cm^{-1}) closely resembles that of the reflection peak with a minimum of 11.24 μ (890 cm^{-1}) and the absorption spectrum for the Ladder Creek chondritic material with a local minimum of 11.36 μ

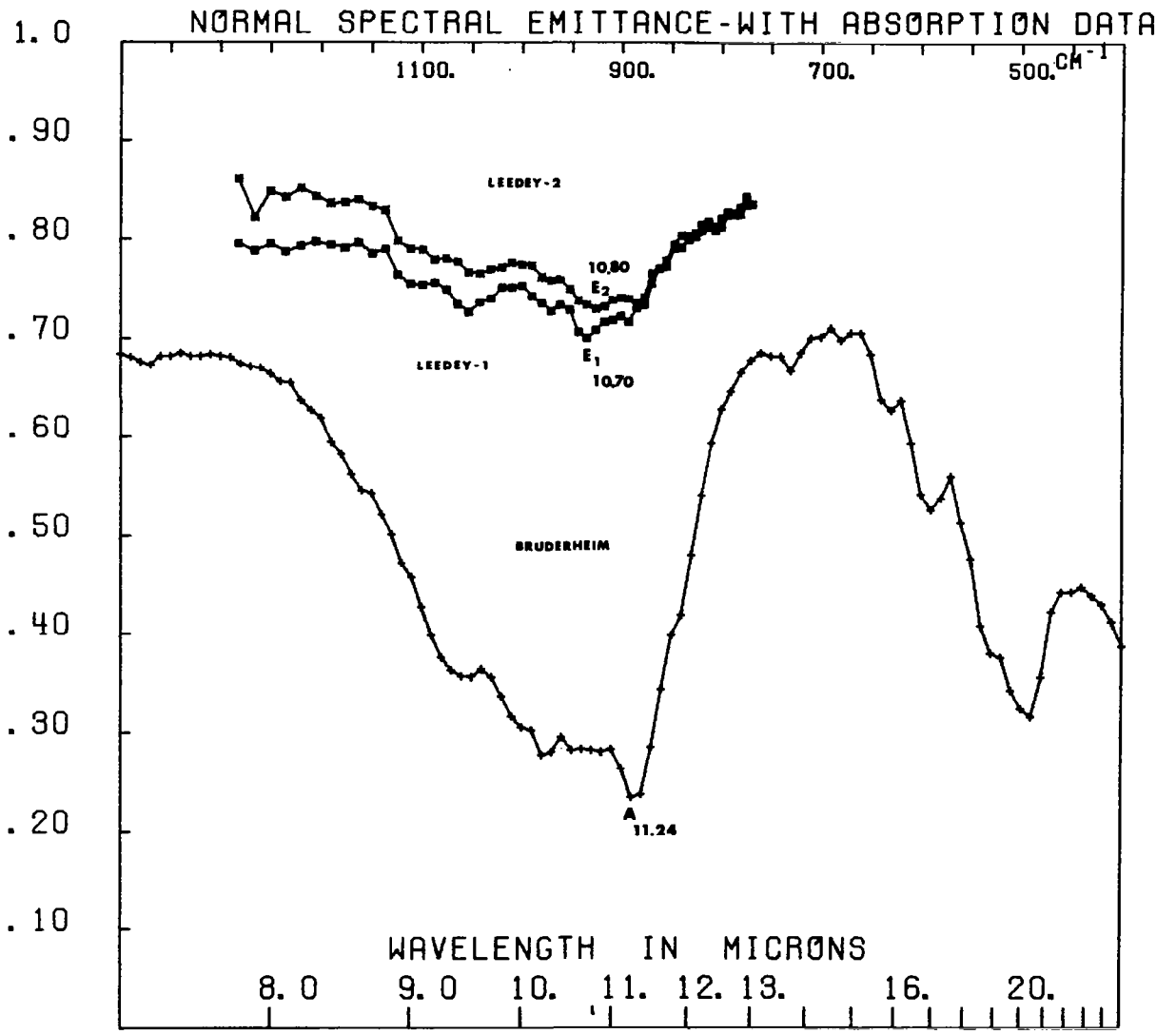

FIG. 78 NORMAL SPECTRAL EMITTANCE CURVES FOR METEORITIC MATERIALS. Emittance spectra shown for Leedey chondrite with minima at (E_1) 10.70 μ and (E_2) 10.80 μ for the two surfaces of this material. The lower curve (A) is that of the absorption spectrum for Bruderheim chondrite, with an absorption maximum at 11.24 μ, considerably displaced to longer wavelengths than those shown in the emittance spectra.

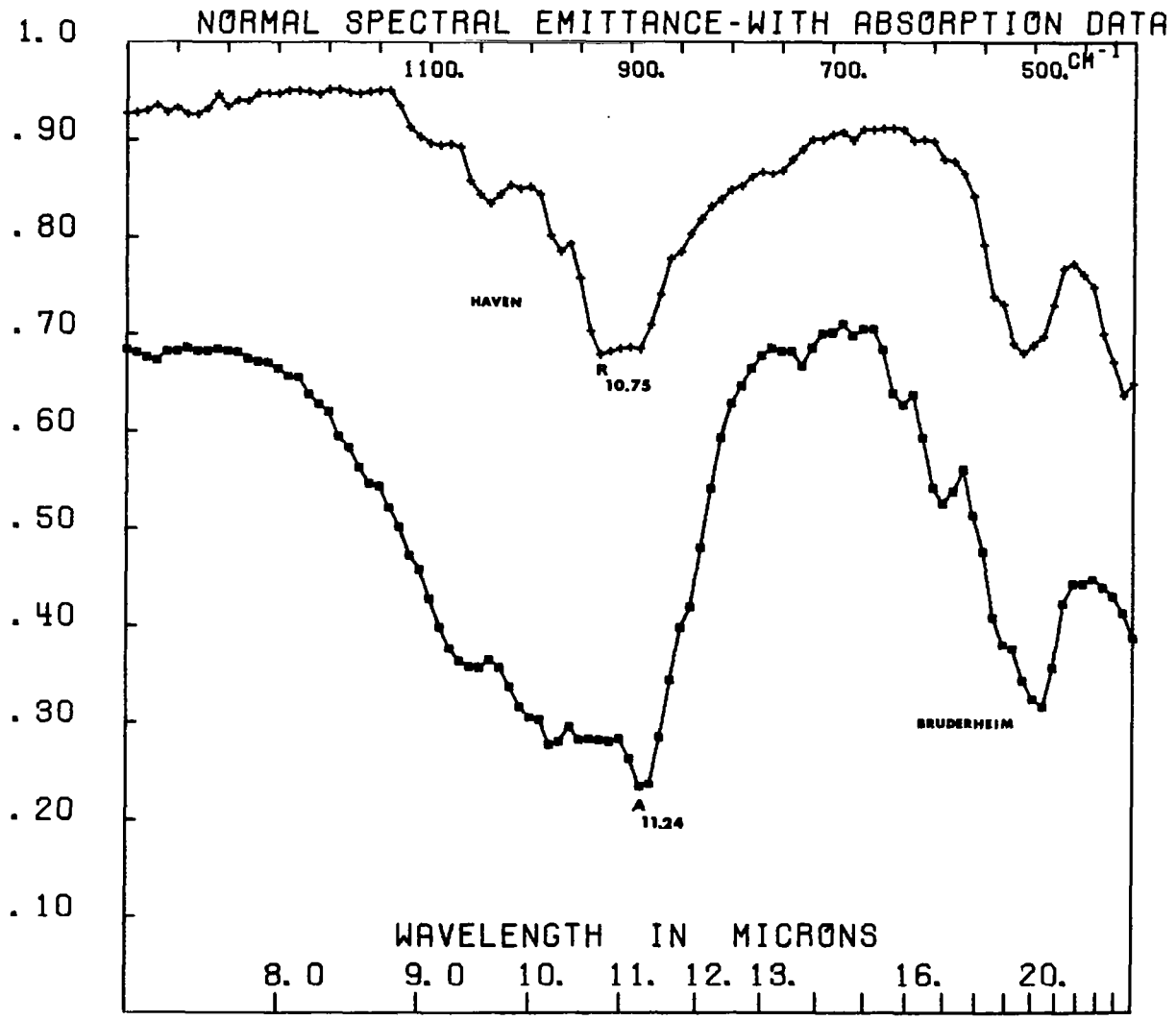

FIG. 79 CALCULATED NORMAL SPECTRAL EMITTANCE CURVE OF REFLECTANCE DATA FROM HAVEN CHONDRITE (R) WITH AN EMITTANCE MINIMUM AT 10.75 μ, COMPARED WITH THE ABSORPTION SPECTRUM (A) FOR BRUDERHEIM CHONDRITE.

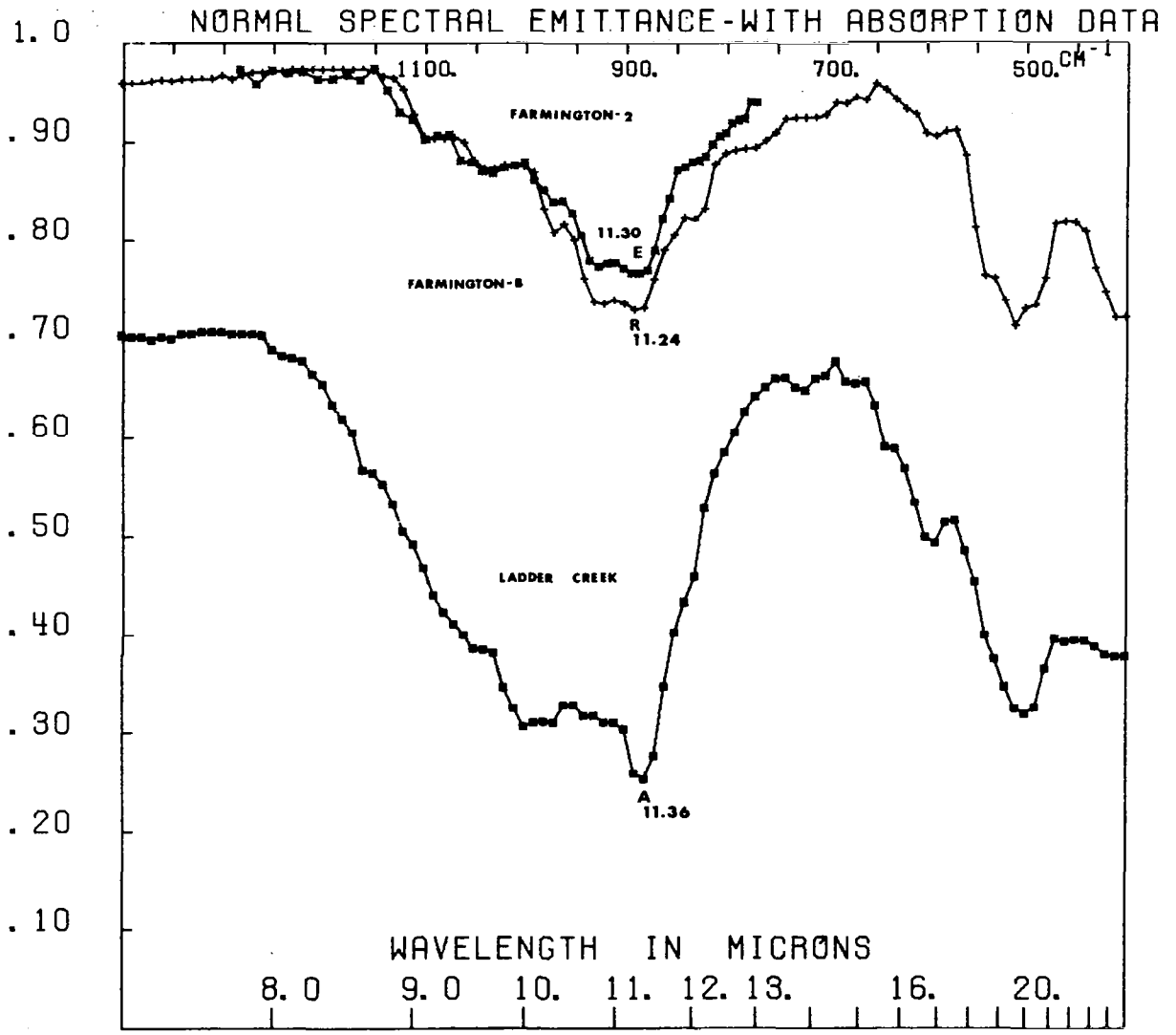

FIG. 80 NORMAL SPECTRAL EMITTANCE CURVE OF FARMINGTON CHONDRITE SAMPLE (SIDE 2) WITH AN EMITTANCE MINIMUM (E) AT 11.30 μ, COMPARED WITH THE EMITTANCE CURVE CALCULATED FROM REFLECTANCE DATA (R) FOR FARMINGTON-B SAMPLE, AT 11.24 μ. The lower curve is the absorption spectrum (A) for the Ladder Creek chondrite, with an absorption maximum at 11.36 μ.

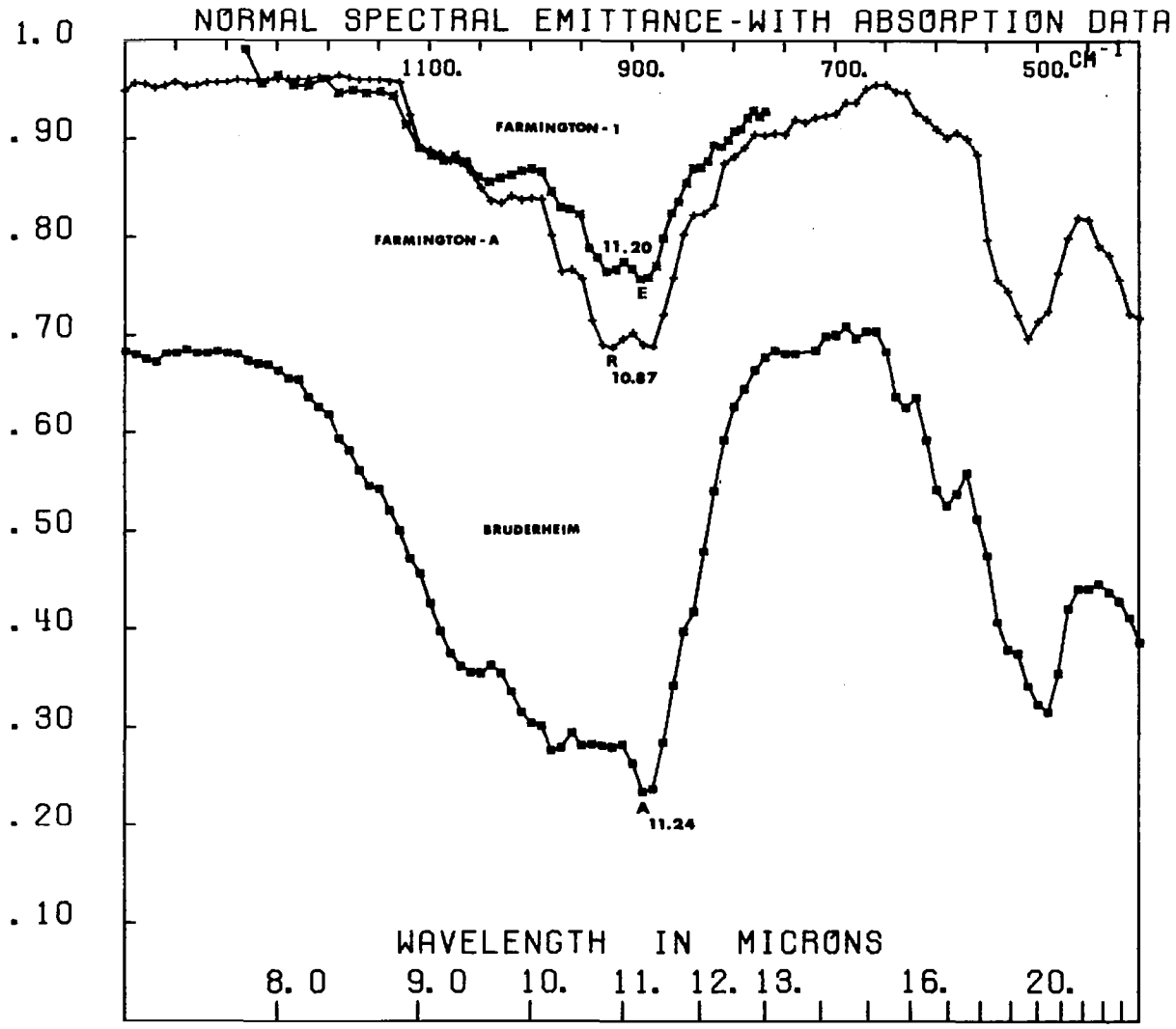

FIG. 81 NORMAL SPECTRAL EMITTANCE CURVE FOR FARMINGTON CHONDRITE (SIDE 1) WITH AN EMITTANCE MINIMUM (E) AT 11.20 μ, COMPARED WITH FARMINGTON-A SAMPLE WITH AN EMITTANCE MINIMUM CALCULATED FROM REFLECTANCE (R) AT 10.87 μ. The lowermost curve is that of the absorption spectrum (A) for Bruderheim chondrite, with an absorption maximum at 11.24 μ.

(880 cm^{-1}). The long wavelength range peaks at approximately 20 μ (500 cm^{-1}) in both the reflection and the absorption curves. There is a remarkably close correlation between the three types of infrared spectra for these three samples.

Two other samples of Farmington (Farmington-A and a repeat emission spectrum, Farmington-1) show closely similar spectra (Fig. 81) with peaks at 11.20 μ (893 cm^{-1}) for the emission curve and 10.87 μ (922 cm^{-1}) for the reflection curve. The absorption spectrum for Bruderheim is again included to show the close similarity in the spectra between these different chondrites.

B. Studies on Rock Samples

Figure 82 shows the reflection and emission spectra for a sample of quartz monzonite porphyry (SRI 3582) obtained from the HARDHAT area of the Nevada Test Site. The emission spectrum again emphasizes the lower wavelength portion of the spectrum (8 to 9 μ), showing a lower emittance than that of the reflection spectrum. The curves are remarkably similar and show that the spectra of this rock differ markedly from those of the preceding meteorites, which had peaks in the vicinity of 10.8 to 11 μ (920 to 900 cm^{-1}).

Emission, reflection, and absorption curves are shown for the dunite specimen (SRI 3390) in Fig. 83. The lowermost curve (A) is the absorption spectrum of powdered material embedded in a KBr disc, and shows its absorption maximum at 11.23 μ (890 cm^{-1}). A considerable number of other peaks are apparent in the spectrum which are faithfully reproduced in both the reflectance spectra and (within the wavelength of the data) in the emission spectrum. The reflection spectrum (R) has a maximum at 10.80 μ (926 cm^{-1}); the emission spectra for polished dunite (E_2) and for rough dunite (E_1) both show emission minima at 10.70 μ (935 cm^{-1}). The similarity between the four spectra (for the peaks labeled with the # symbol) is remarkable. The peaks on the absorption spectrum are again displaced to longer wavelengths, but are the same in number and intensity as those shown on the other types of spectra. By comparison of Figs. 83 and 82, the large separation in the wavelength between the minima of the

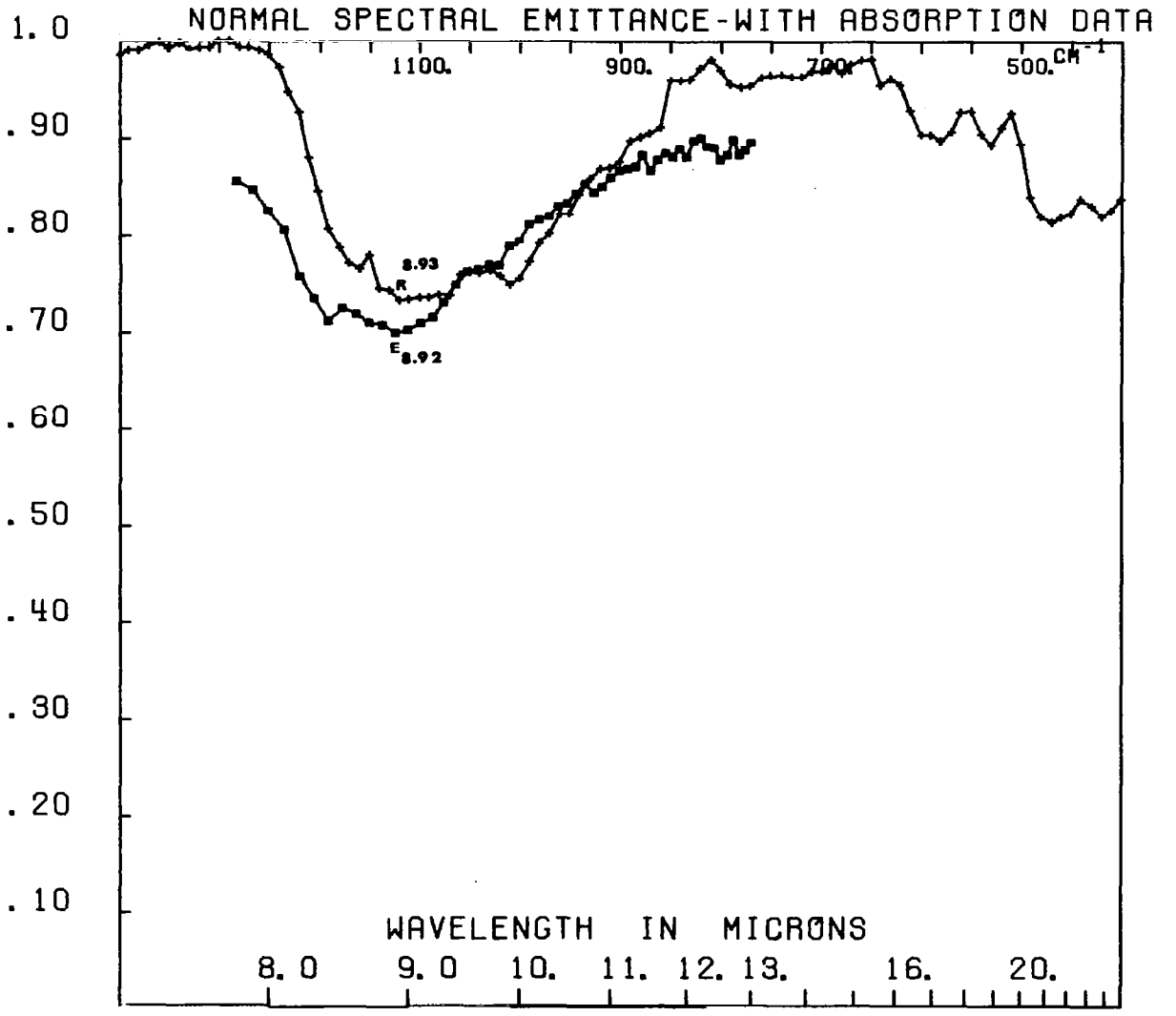

FIG. 82 NORMAL SPECTRAL EMITTANCE FOR A SAMPLE OF HARD HAT QUARTZ MONZONITE PORPHYRY (SRI 3582) WITH AN EMITTANCE MINIMUM (E) AT 8.92 μ. The calculated emittance curve from the reflectance data (R) has an emittance minimum at 8.93 μ, closely comparable to that obtained by the direct emission measurements.

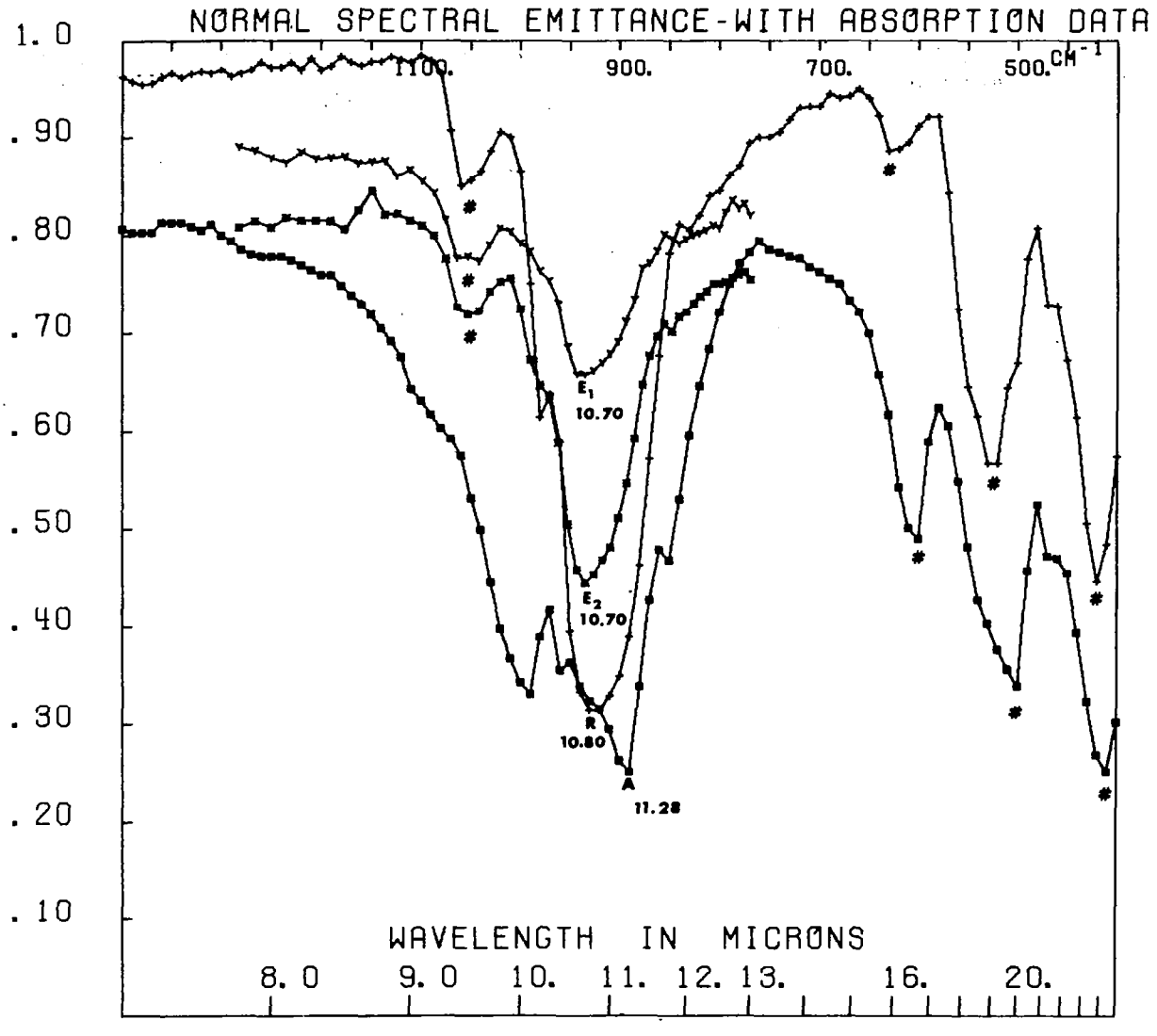

FIG. 83 NORMAL SPECTRAL EMITTANCE CURVES FOR DUNITE. The spectrum obtained from the polished specimen (E_2) has an emittance minimum at 10.70 μ, closely comparable to that obtained for the roughened surface (E_1) at 10.70 μ. The uppermost curve is that of the calculated emittance spectrum obtained from reflectance data (R) with an emittance minimum at 10.80 μ. All three curves show spectral peaks in common (* symbol) at approximately 9.5, 10.7, 16, 19, and 23 μ. The lowermost curve is that of the absorption spectrum (A) for the same material, showing the displacement of the absorption maximum again to a longer wavelength (11.28 μ).

quartz monzonite porphyry (at 9 μ) and those of the dunite (at 10.9 μ), (1110 to 918 cm^{-1}), can be established—a shift of over 1.9 μ (almost 200 cm^{-1} at this point).

C. Studies on the Rock Suite Supplied by the U.S. National Museum (Appendix A)

The suite of 29 standard rock samples were received from the U.S. National Museum. Full chemical and some mineralogical analyses are available for most of the suite, and it has been possible to prepare infrared absorption, reflection, and emission spectra for all of the samples.

Emission curves were prepared on the existing rough surface (see photographs in Figs. 18, 19, and 20). The samples were then polished and reflection spectra were obtained, after which the excess material was prepared for absorption spectra. The polished samples will be returned to the National Museum after study so that a standardized file can be kept at the Museum.

The curves and the descriptive data from the Museum appear in Appendix A. Most of the text concerning the curves appears in the figure captions; reference should be made to the appendix for this material.

The appendix is a study complete in itself. It illustrates the three analysis methods applied to a typical set of terrestrial igneous and metamorphic rocks. The emission data are particularly useful because the samples had the form and surface roughness which may be expected in operational situations (see Table II).

X ATMOSPHERIC ATTENUATION OF INFRARED RADIATION

It has long been realized that the atmosphere strongly attenuates infrared radiation, in the wavelength range from the visible to the far infrared. These attenuations are usually a series of complete absorption bands separated by "relatively transparent" sections called "windows." Many studies tried to evaluate these attenuations, as a function of distance along a sea level path,[13] as a function of altitude, and as a function of the carbon dioxide and the water vapor content.

Detailed attenuation data for the infrared wavelengths of interest to this study (from 7 to 25 μ, 1400 to 400 cm^{-1}) are scarce and difficult to obtain in their original form. The work of Taylor and Yates,[13] is perhaps the most outstanding of these studies, and Fig. 84 has been prepared from their attenuation spectra. These were based on the transmission of a blackbody source (a searchlight) across Chesapeake Bay over a sea-level path of 1000 feet, 3.4 miles, and 10.1 miles under various atmospheric conditions. Although these data are only correct for the time of the experiment—the weather conditions, CO_2 and water vapor contents, temperature, relative humidity, etc.,—so few compilations of spectral data are available that these are important. Obviously, to be correct they should be reestablished at the time of any experiment.

For the purposes of this evaluation of the method we have used the data of Taylor and Yates, as shown in Fig. 84. The data were digitized at 0.1 μ intervals and used for the radiant energy computations. For every sample, computed at 0.1 μ wavelength, we have taken the 375°K energy level and derived the attenuation of the energy as seen after the 3.4-mile path. This is the central curve of Fig. 84. For the longer wavelength we used the only available information that could be found, that of Taylor and Yates[13] for a 1000-foot path length from 14 to 25 μ. We have also recomputed the attenuation data and used them as an example of the Lagrangian interpolation in Fig. 85. We have suppressed the data points in this particular figure, although it could have been prepared with the

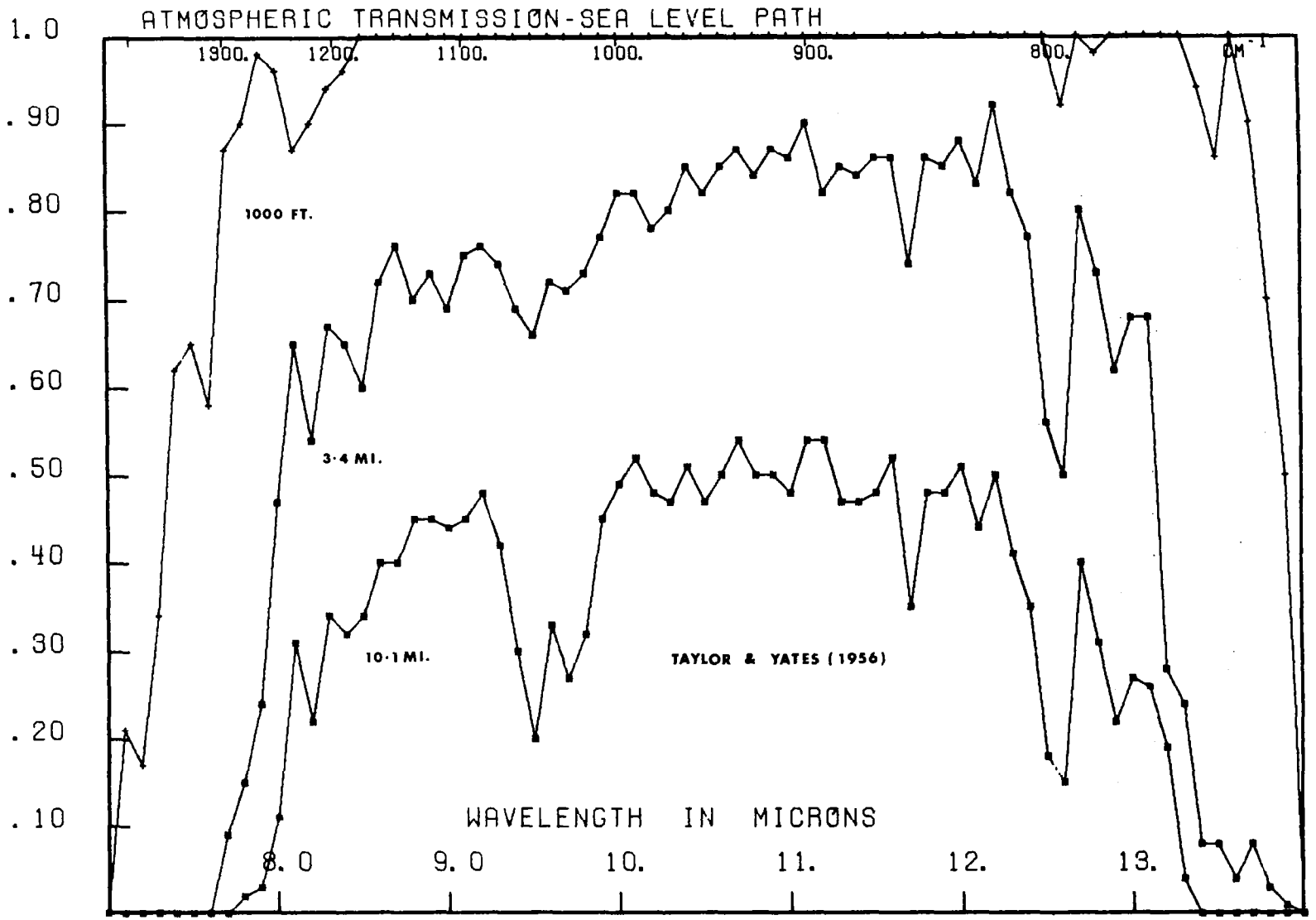

FIG. 84 ATMOSPHERIC TRANSMISSION OVER A SEA-LEVEL PATH AS A FUNCTION OF WAVELENGTH, FROM 7 TO 14 μ. *Data from Taylor and Yates.*[13] *Curves obtained by manually digitizing their continuous (analog) spectra, at 0.1 μ intervals (symbols as shown). Curves are shown for 1000 feet, 3.4 miles, and 10.1 miles sea-level path.*

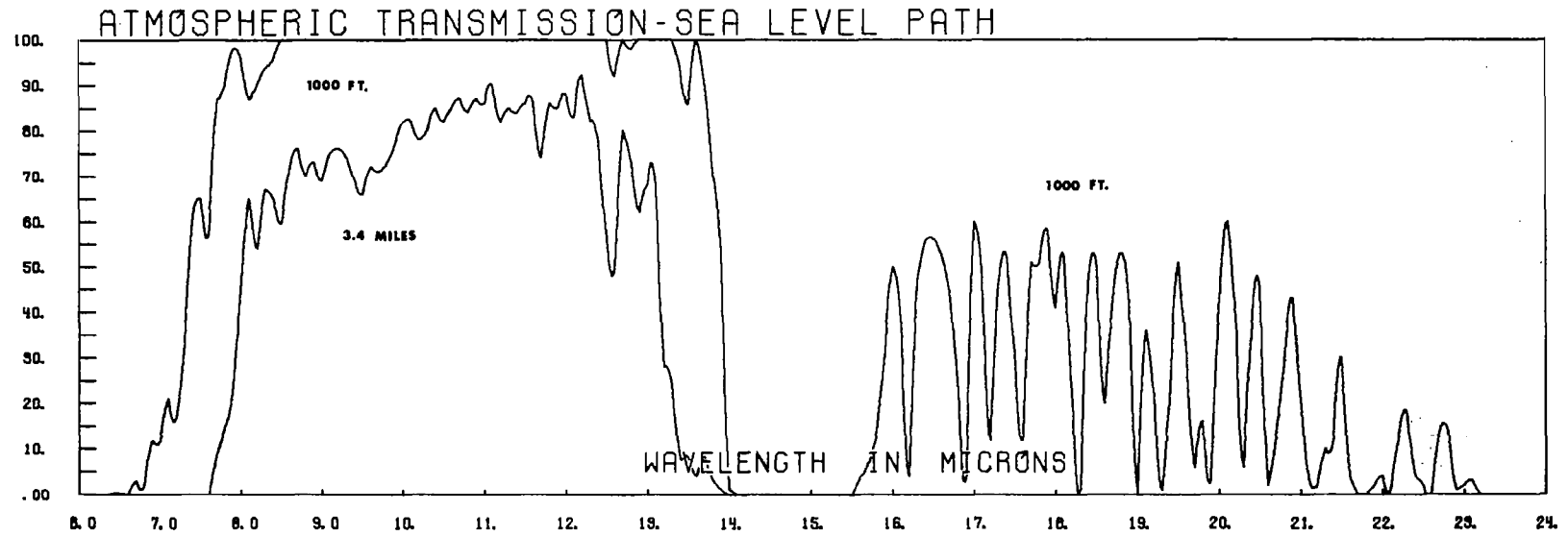

FIG. 85 ATMOSPHERIC TRANSMISSION ON A SEA-LEVEL PATH AS A FUNCTION OF WAVELENGTH, FROM 6 TO 24 μ. Same data as Fig. 84 but smoothed with a second-order Lagrangian interpolation between the data points. Uppermost curve is that of the 1000-foot path length and is continued from 15.5 to 23.3 μ. The lower curve is that of the 3.4-mile path length, which only shows transmission between 7.5 and 14 μ.

same symbols shown as on the preceding diagram. Smooth curves would have passed through the data points. The curves shown in Fig. 86 represent data obtained originally from Altschuler[4] and replotted by van Tasse and Simon[42]. The data represent the attenuation of a blackbody signal as seen from a balloon-borne instrument, at a 100,000-foot altitude with a line-of-sight at 60° to the zenith overhead. Comparison with the curves in Figs. 84 and 85 shows that the same peaks are present, although greatly diminished in their intensity. The section of interest to this present study, from 7 to 13 μ and from 13 to 25 μ, is stippled. The peaks of ozone (O_3) appear strongly at 9.6 and 9.8 μ and again on the flanks of the strong CO_2 band at 15 μ. The maximum absorption, however, due to ozone at this point is only 20% of the signal.

Figure 87 shows the emittance curves for a 400°K blackbody, solid line, and the same blackbody when seen through the atmospheric ozone at 9.6, 9.8, and 14 μ. This represents the attenuation due to the <u>total mass</u> of the ozone in the atmosphere and approximates 80% of the signal, in contrast with the data shown in Fig. 86.

The significance of this particular diagram, however, lies in the emittance spectrum of the tektite at 400°K, calculated from the reflectance spectrum obtained in 1962 (Final Report I). A tektite source at 400°K, radiating from the lunar surface, seen through the atmospheric ozone has an attenuated signal. It would be difficult to extract from this signal the information as to these characteristics of the source. If this was recorded from the balloon at 100,000-foot altitude, the depth of the peak due to atmospheric ozone would be considerably lessened (to 25%) and it might be possible to decipher whether the composition were that of the tektite or of a meteorite. A source of tektite composition has an emission minimum at 9 μ, whereas a meteoritic chondrite composition, or a dunite, or serpentine had its emission minimum in the vicinity of 11 μ, outside the attenuation of the atmospheric ozone. It is therefore highly important that one observe the lunar radiation from as high as possible in the atmospheric pile, preferably outside the effects of the ozone band entirely.

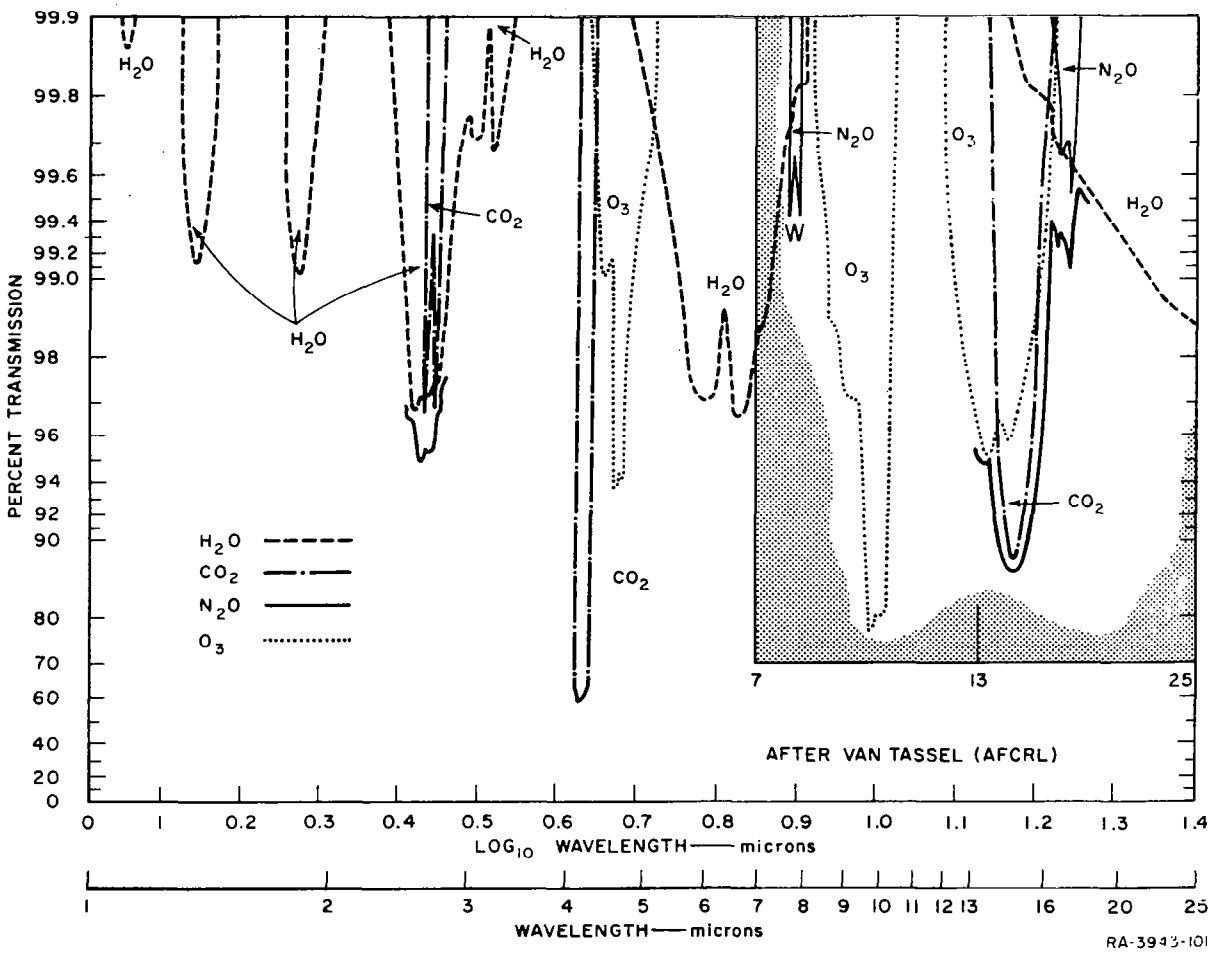

FIG. 86 TRANSMISSION SPECTRA AS A FUNCTION OF WAVELENGTH FOR AN INFINITE LENGTH SLANT-PATH AT A ZENITH ANGLE OF 60°, FROM A 100,000-FOOT ALTITUDE. *Data taken originally from Altschuler's data*[41] *and modified by* van Tassell[42] for balloon-borne instrumentation, observing planetary objects. Stippled area indicates the region of interest to this study.

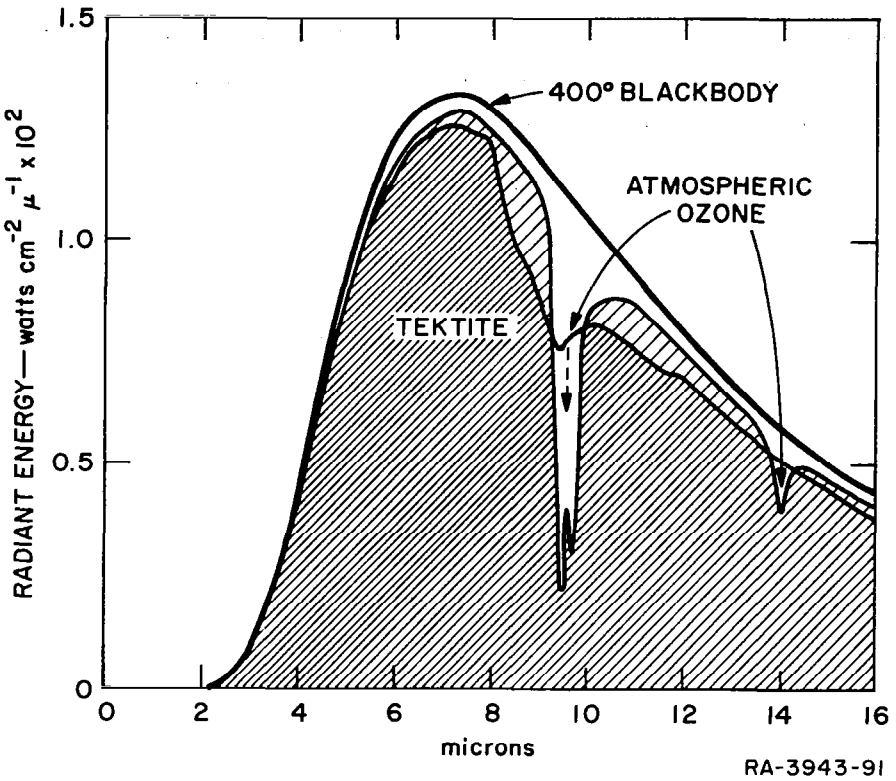

FIG. 87 HEMISPHERICAL EMITTANCE CURVES FOR A 400°K BLACKBODY (SOLID LINE), AND THE SAME BLACKBODY WHEN SEEN THROUGH THE TOTAL ATMOSPHERIC OZONE (WITH ABSORPTION AT 9.6, 9.8, AND 14 μ). Attenuation at this point is approximately 80% of the signal, in contrast with the data shown in Fig. 86. The lower double-striped spectrum is that of a tektite composition, if emitting on the lunar surface at 400°K, and showing how its characteristic spectrum would be masked by the attenuation of the atmospheric ozone.

ACKNOWLEDGMENTS

The writer wishes to acknowledge his indebtedness to several persons who were of great assistance during these studies.

Dr. Thomas O. Passell, co-worker on the project, wrote the section entitled "A Theoretical Treatment of Scattering Effects on the Emittance of Materials." In addition, his technical contributions and discussions aided the investigation immeasurably.

Dr. Sylvan Rubin gave advice and direction during the project and edited the manuscript from a technical viewpoint.

Mr. Charles Brabant provided the computational programming and developed the plot routine to the required format, so that the output could be used in this report as text-figure originals.

All of the SRI reflectance spectra and the absorbance measurements were made by Elizabeth Lawler, whose help at all stages was gratefully appreciated, particularly when the data had to be manually digitized.

The 10 reflectance spectra of our powdered samples were performed by J. T. Bevans of Space Technology Laboratories (STL) and have been included here as Figs. 11, 12, and 13. These data are highly valued and the assistance of STL in obtaining them for us was most beneficial. Dr. Eugene Burns, also of STL, has been a coworker with the author on several papers and his participation continues to be a rewarding association.

Samples of meteoritic chondrites were obtained from Carleton Moore, Arizona State University, for use in these studies. Their ready availability for studies of this type is most helpful.

The 29 rock samples from the U.S. National Museum formed the backbone of the work and were extremely useful.

PRESENTATION OF PROFESSIONAL PAPERS

A. One technical paper was presented at the Lunar Surface Materials Conference in Boston on May 23, 1963. It was written jointly with Dr. Burns of Space Technology Laboratories (STL) and was entitled "Feasibility of Remote Compositional Mapping of the Lunar Surface -- Effects of Surface Roughness."

Dr. Burns' contributions to the paper include an analysis of the total reflectance data on powdered samples and further development of the operational parameters, such as those imposed by the consideration of a particular orbital spacecraft. Other contributions were made by the STL staff. In particular, the excellent data from the total reflectance studies on powdered rock by J. T. Bevans represent a definite contribution to the understanding of the scattering properties of fine powder.

B. A paper containing some of the emittance data was presented by R. J. P. Lyon at the Sixth Annual Spectroscopy Conference in Denver on August 12, 1963. This was jointly prepared with Dr. Eugene A. Burns and was titled "Mineral Analysis by Thermally Emitted Infrared Radiation."

C. The third joint paper treats in greater detail the subject of an earlier note to the Editor of Nature. It is entitled "Errors in the Measurement of the Lunar Temperature; Integrated Emissivities of Materials Suspected to Comprise the Lunar Crust," and contains work performed by R. J. P. Lyon and E. A. Burns at SRI during the 1962 contract period.

D. Another paper written jointly with Dr. Eugene A. Burns and entitled "Instrumentation for a Mineralogical Satellite" was presented by Dr. Burns at the XIV International Astronautical Congress at Paris, France, on September 30, 1963.

REFERENCES

1. Hunt, J. M., Wisherd, P., and Bonham, L. C., Infrared Absorption Spectra of Minerals and other Inorganic Compounds, Anal. Chem. 22, 1478-1497 (1950)

2. Hunt, J. M. and Turner, D. S., Determination of Mineral Constituents of Rocks by Infrared Spectroscopy, Anal. Chem. 25, 1169-1174 (1953)

3. Tuddenham, W. M. and Lyon, R. J. P., Relation of Infrared Spectra and Chemical Analysis for some Chlorites and Related Minerals, Anal. Chem. 31, 377-380 (1959)

4. Tuddenham, W. M. and Lyon, R. J. P., Infrared Techniques in the Identification and Measurement of Minerals, Anal. Chem. 32, 1630-41 (1960)

5. Lyon, R. J. P., Tuddenham, W. M., and Thompson, C. S., Quantitative Mineralogy in 30 Minutes, Econ. Geol. 54, 1047-1055 (1959)

6. Coblentz, W. W., Investigation of Infrared Spectra, Pub. 65, Carnegie Institute of Washington, 1906

7. Coblentz, W. W., Selected Radiation from Various Solids, II, Nat. Bur. Standards (US) Bull, 6, 301 (1901)

8. Pfund, A. H., The Identification of Gems, J. Opt. Soc. Amer., 35, 611-614 (1945)

9. McMahon, H. O., Thermal Radiation Characteristics of Some Glasses, Jour. Am. Ceram. Soc. 34, 91-6 (1950)

10. Simon, J. and McMahon, H. O., Study of the Structure of Quartz, Cristobalite, and Vitreous Silica by Reflection in Infrared, Jour. Chem. Phys. 21, 23-30 (1953)

11. Gardon, R., The Emissivity of Transparent Materials, J. Am. Ceram. Soc. 39, 278-285 (1956)

12. Lyon, R. J. P., Evaluation of Infrared Spectrophotometry for Compositional Analysis of Lunar and Planetary Soils, Stanford Research Institute, Project No. PHU-3943, Final Report, under Contract No. NASr-49(04), Sept. 1962; now TN D-1871, NASA Technical Note published April 1963

13. Taylor, H. H. and Yates, H. W., NRL Report 4759, published also as PD 121199 (May 11, 1956); also J. Opt. Soc. Am. 47, 233 (1957)

14. Miller, F. A. and Wilkins, C. H., Infrared Spectra and Characteristic Frequencies of Inorganic Ions, Anal. Chem. 24, 1253-94 (1952)

15. Sevchenko, N. A., and Florinskaya, V. A., The Reflection and Transmission Spectra of Various Modifications of Silicon Dioxide in the Wavelength Region 7-24 μ, (in Russian), Doklad, Akad. Nauk USSR, 109, 1115 (1956)

16. Kruse, P. W., McGlauchlin, L. D., and McQuistan, R. R., Elements of Infrared Technology: Generation, Transmission and Detection. J. Wiley and Sons, N. Y., N. Y., 448 (1962)

17. Hapke, B. and H. Van Horn, Photometric Studies of Complex Surfaces, with Applications to the Moon, J. Geophys. Research, 68, 4545-4570 (1963)
See also Hapke, B., A Theoretical Photometric Function for the Lunar Surface, J. Geophys. Res., 68, 4571-4586 (1963)

18. Nell, C. B. and Robinson, G. G., Measurement of Thermal-Radiation Properties of Temperature Control Surfaces in Space, in Measurement of Thermal Radiation Properties of Solids, ed. J. C. Richmond, NASA SP-31, 193, (1963)

19. Kern, C. D., Desert Soil Temperatures and Infrared Radiation Received by TIROS III, J. Atmos. Sci., 20, 175 (1963)

20. Buettner, K. J. K., and Kern, C. D., Infrared Emissivity of the Sahara from TIROS Data, Science, 142, 671 (1963)

21. Lyon, R. J. P. and Burns, E. A., Analysis of Rocks by Reflected Infrared Radiation, Econ. Geol., 58, 274 (1963)

22. Hapke, B., Photometric and Other Laboratory Studies Relating to the Lunar Surface, Proc. 1963 Lunar Surface Symposium, J. Salisbury and P. Glasser, Ed., Academic Press, in preparation

23. Sparrow, E. M., Radiant Absorption Characteristics of Concave Cylindrical Surfaces, J. Heat Transfer, Trans. ASME, Series C, 84, 283 (1962)

24. Sparrow, E. M., L. U. Albers, and E. R. G. Eckert, Thermal Radiation Characteristics of Cylindrical Enclosures, J. Heat Transfer, Trans. ASME, Series C 84, 73 (1962)

25. Sparrow, E. M., and V. K. Johnson, Absorption and Emission Characteristics of Diffuse Spherical Enclosures, J. Heat Transfer, Trans. ASME, Series C, 84, 189 (1962)

26. Sparrow, E. M., and J. L. Gregg, Radiant Emission from a Parallel Walled Groove, J. Heat Transfer, Trans. ASME, Series C, 84, 271 (1962)

27. Sparrow, E. M., and L. U. Albers, Apparent Emmissivity and Heat Transfer in a Long Cylindrical Hole, J. Heat Transfer, Trans. ASME, Series C, 82, 253 (1960)

28. Hollands, K. G. T., Directional Selectivity, Emittance, and Absorptance Properties of Vee Corrugated Specular Surfaces, J. Solar Energy 7, No. 3, 108 (1963)

29. Vollmer, J. V., Study of the Effective Thermal Emittance of Cylindrical Cavities, J. Opt. Soc. Amer. 47, 926 (1957)

30. Glovanelli, R. G., Radiative Transfer in Discontinuous Media, Austr. J. Phys. 10, 227 (1957)

31. Bennett, H. E., and J. O. Porteus, Relation Between Surface Roughness and Specular Reflectance at Normal Incidence, J. Opt. Soc. Amer. 51, 123 (1961)

32. Davies, H., The Reflection of Electromagnetic Waves from Rough Surface, Proc. Inst. Elec. Engrs. 101, 209 (1954)

33. Schuster, A., Radiation from a Foggy Atmosphere, Astrophys. J. 21, 1 (1905)

34. Hamaker, H. C., Radiation and Heat Conduction in Light Scattering Material, Philips Research Reports 2, 55-67 (1947), see also pages 103-111, 112-125, and 420-425 of same journal volume

35. Saksena, B. D., The Infrared Absorption Spectra of α-Quartz Between 4 and 15 μ, Proc. Phys. Soc., 72, 9 (1958)

36. Wentink, T. Jr., and Planet, W. G., Jr., Infrared Emission Spectra of Quartz, J. Opt. Soc. Am., 51, 595 (1961)

37. Bell, E. E., and Eisner, I. L., Infrared Radiation from the White Sands at White Sands National Monument, New Mexico, J. Opt. Soc. Am., 46, 303-4 (1956)

38. Bell, E. E. Eisner, I. L. Young, J. B. Abolins, A. and Oetjen, R. A., Infrared Techniques and Measurements, Ohio State Research Foundation, Final Engineering Report, Contract 33(616)3312, p. 105 (ASTIA - AD 151221), 1957

39. Duke, M., Maynes, D., and Brown, H., The Petrography and Chemical Composition of the Bruderheim Chondrites, J. Geophys. Research 66, 3557 (1961)

40. Simon, I., Structure of Neutron-Irradiated Quartz and Vitreous Silica, J. Am. Ceram. Soc. 40, 152 (1957)

41. Altschuler, T., Atmospheric Tranmission of Infrared, G. E. Report R. 59ELC115, Cornell U., Ithaca, New York (1960)

42. van Tassell, R., and Simon, I., Reflection and Emittance Spectra, in Proceedings of the 1963 Lunar Surface Materials Symposium, ed. J. Salisbury and P. Glasser, Academic Press (in press) (1963).

APPENDIX A

INFRARED SPECTRA OF SAMPLES PROVIDED BY THE U. S. NATIONAL MUSEUM

A suite of 29 rock samples was received from the U. S. National Museum following the request of Dr. William Fischer, Theoretical Geophysics Branch, U. S. Geological Survey, Washington, D. C.

Each sample has been analysed by three different techniques - emission, reflection and absorption - and the infrared spectra have been recorded. The records were then manually digitalized at 0.1 micron - (or at 10 cm^{-1}) intervals, normalized by a computer and plotted by a digital plotter, all three on the same plate.

Descriptive material for each specimen was provided by the U. S. National Museum, and the computed average emittances, reflectances and transmittances were added from the computational material.

The figure texts generally describe the type of surface used for the normal spectral emittance measurements. All surfaces were highly polished before the spectral reflectance measurements. These were made at an angle of 30° with the normal to the polished surfaces using the 120° - prism reflection attachment. Transmission measurements were made through a KBr pellet, in which the crushed sample was embedded at the 0.15% level - the standard analytical method.

USNM 1391
(SRI 3556)

Buffalo Peaks, Park Co., Colo.

OPAL

C. W. Cross.

Occurrence From clay in saddle between main peak and eastern spur from it.

Analysis by W. F. Hillebrand.

Sp. gr. 2.023
H = 5.5

Insol. SiO_2	=	0.710
Sol. SiO_2	=	96.706
Loss by ign.	=	2.584
		100.000

IR Spectra	Averaged over this range
Emittance	Not Run
Reflectance	$1-\rho = 0.92$ (1400 - cm^{-1})
Transmittance (un-normalized)	$\tau = 0.48$ (1400 - cm^{-1})

CR-100

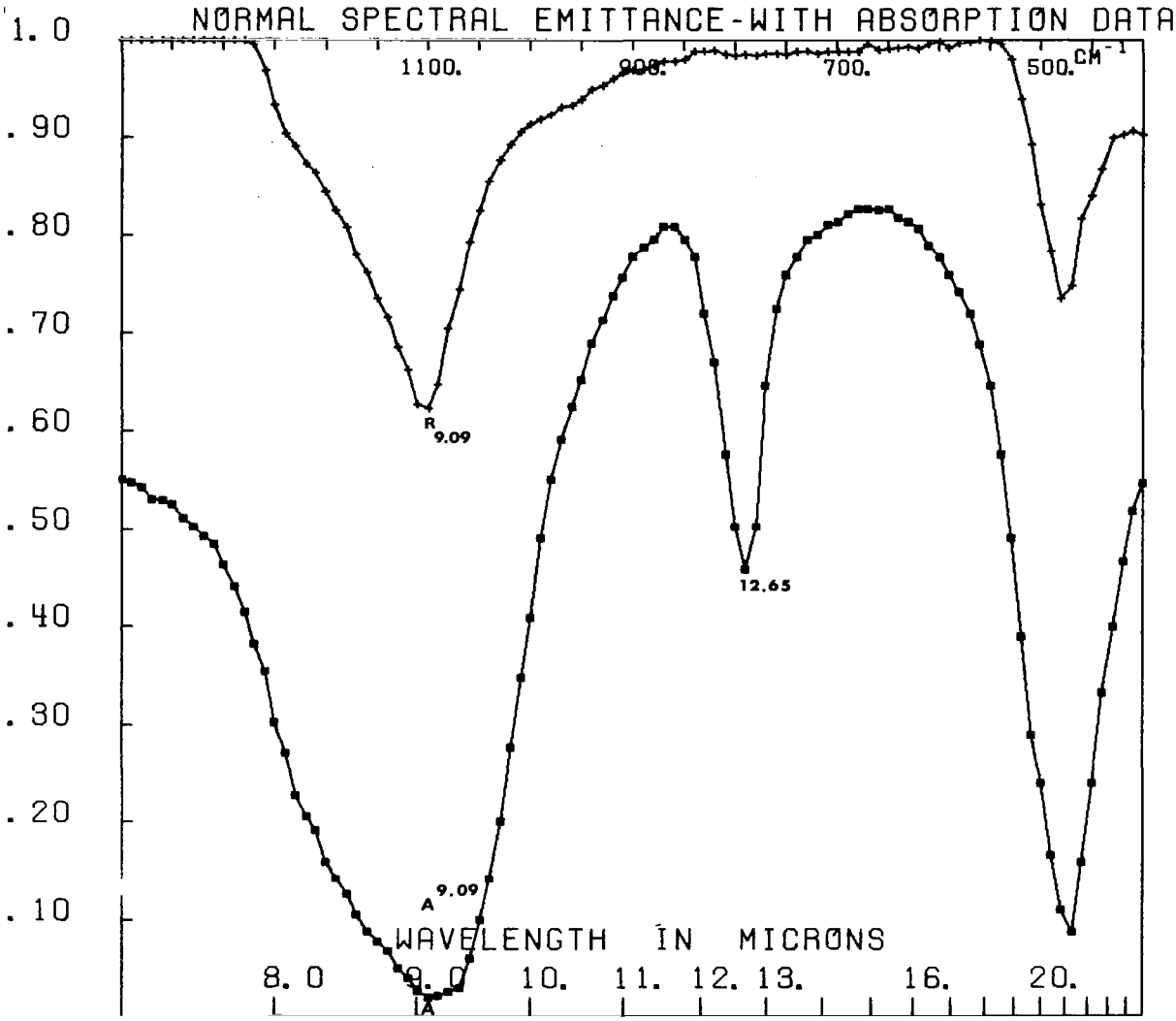

FIG. A-1 OPAL (USNM 1391) NORMAL SPECTRAL EMITTANCE – WITH ABSORPTION DATA
Emittance spectrum not prepared, reflectance (R) from polished surface normalized and shown as $(1 - \rho)$, absorption (A) spectrum from a KBr pellet preparation shown as an unnormalized plot of transmission (%T). Note 12.65μ peak does not appear on reflection spectrum, while fundamentals at 9.09 and 21.3μ show clearly.

USNM 82 (SRI 3549) — Lassen Peak, California

DACITE Lassennose No. 40 W.T.p. 176 (Diller) L.H.W.

Structure	Porphyritic.	Phen. << grm.
	Phenocrysts.	Rounded or broken.
	Groundmass.	Vitreous, fibrous, pumiceous.
Constituents	Phenocrysts.	Plagioclase (andesine) > quartz x hornblende, x biotite, hypersthene, augite.
	Groundmass.	Clear glass swarming with acicular colorless crystallites, grains of the phenocrysts, spherulitic patches.
	Accessories.	Magnetite, apatite.
Noteworthy	Groundmass, analysis shows much silica.	
Comment	A typical dacite.	
Occurrence	Lava	
Literature	Diller, J. S., Bull. U.S.G.S. 150, p. 217. Baron von Richthofen, Nat. Sys. Vol. Rocks, p. 16. Hague & Iddings, Am. Jour. Sci. 3d, Vol. 26, 1883, p. 231. 234, 235.	

Analysis of dacite, Lassen Peak, California
Bull. 150, p. 218, (3) W. F. Hillebrand, analyst

SiO_2	68.72	SrO	0.03
TiO_2	0.31	BaO	0.07
Al_2O_3	15.15	MgO	1.28
Cr_2O_3	None	K_2O	2.78
Fe_2O_3	1.16	Na_2O	4.26
FeO	1.76	Li_2O	Trace
MnO	0.11	H_2O	0.74
CaO	3.30	P_2O_5	0.09

Total - 99.76

IR Spectra	Averaged over this range	
Emittance	$\epsilon = 0.91, 0.93$	(1280 - 770 cm^{-1})
Reflectance	$1-\rho \doteq 0.94$	(1400 - 400 cm^{-1})
Transmittance (un-normalized)	$\tau = 0.54$	(1400 - 400 cm^{-1})

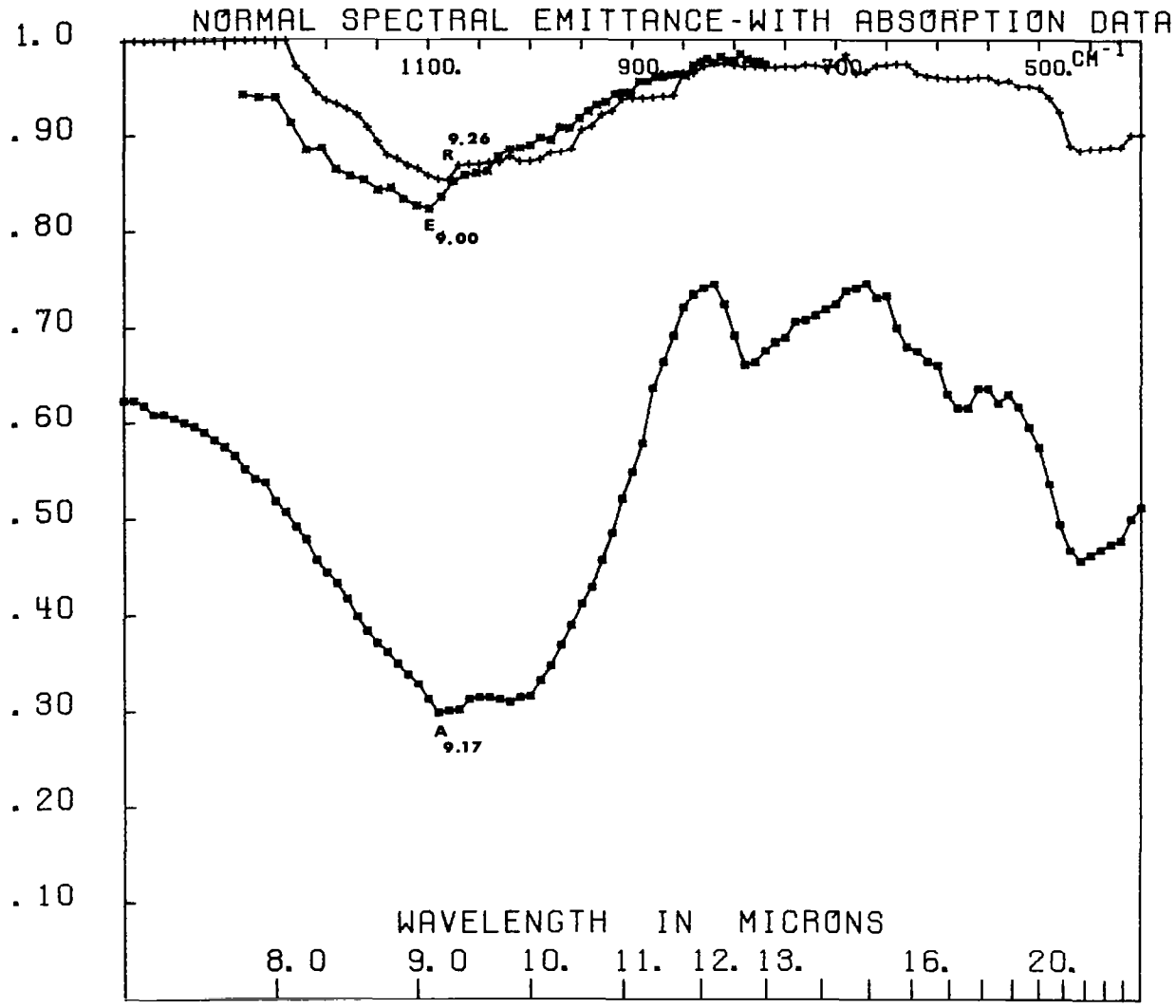

FIG. A-2 DACITE (USNM 82) NORMAL SPECTRAL EMITTANCE – WITH ABSORPTION DATA
Emittance (E) observed between 7.8 and 13.0μ and normalized. Reflectance (R) and absorption (A) observed from 1400 to 400 cm^{-1} (7.143 to 25μ).

USN 158
(SRI 3548)

Variety: Granitite.
Ockerthal, Hartz Mts.
(Stürtz Coll. Cross)

GRANITE

Structure	Granular.	Coarse. Micrographic.
Constituents	Chief.	Orthoclase > quartz > plagioclase > biotite.
	Accessory.	Magnetite > zircon.
	Secondary.	Chlorite > epidote > muscovite
Noteworthy	Beautiful micrographic intergrowth of quartz and orthoclase.	
Literature	See lit. of 157, also Lossen, Erläut. z. Blatt Harzgerode, geol. sp. Karte Pr.	
Analysis	None	

IR Spectra	Averaged over this range	
Emittance	ε = 0.88, 0.90	(1280 - 770 cm^{-1})
Reflectance	$1-\rho$ = 0.85	(1400 - 400 cm^{-1})
Transmittance (un-normalized)	τ = 0.54	(1400 - 400 cm^{-1})

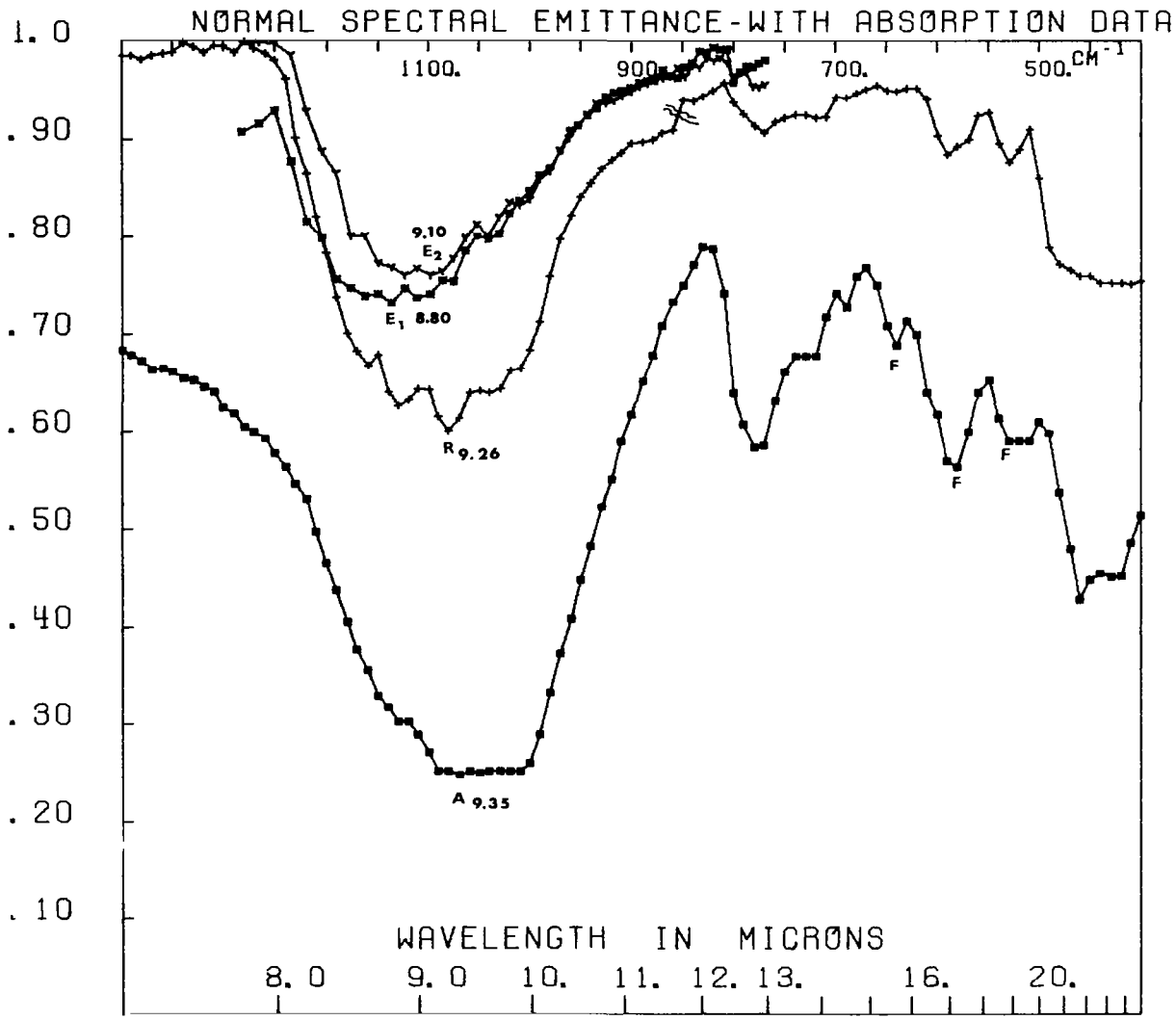

FIG. A-3 GRANITE (USNM 158) NORMAL SPECTRAL EMITTANCE – WITH ABSORPTION DATA
Emittance spectra (E_1 and E_2) show slightly different minima. Break in (R) at 850 cm^{-1} (11.85μ) is at the NaCl-KBr optics change during reflectance measurements.

USNM 377
(SRI 3552)

Aschaffenburg, Spessart Mts., Bavaria

GRANITE-GRAPHIC

(Stürtz Coll. Cross)

Structure	Pegmatitic or graphic
Constituents	Chief. Orthoclase > quartz >> muscovite
Noteworthy	Structure.
Literature	Klem, G., Erlauterung zu Blatt Schaaf-Aschaffenburg der geologischen Karte der Grossherzogthum Hessen. Darmstadt. 1894.

IR Spectra	Averaged over this range	
Emittance	ϵ = 0.87, 0.88	(1280 - 770 cm^{-1})
Reflectance	$1-\rho$ = 0.92	(1400 - 400 cm^{-1})
Transmittance (un-normalized)	τ = 0.54	(1400 - 400 cm^{-1})

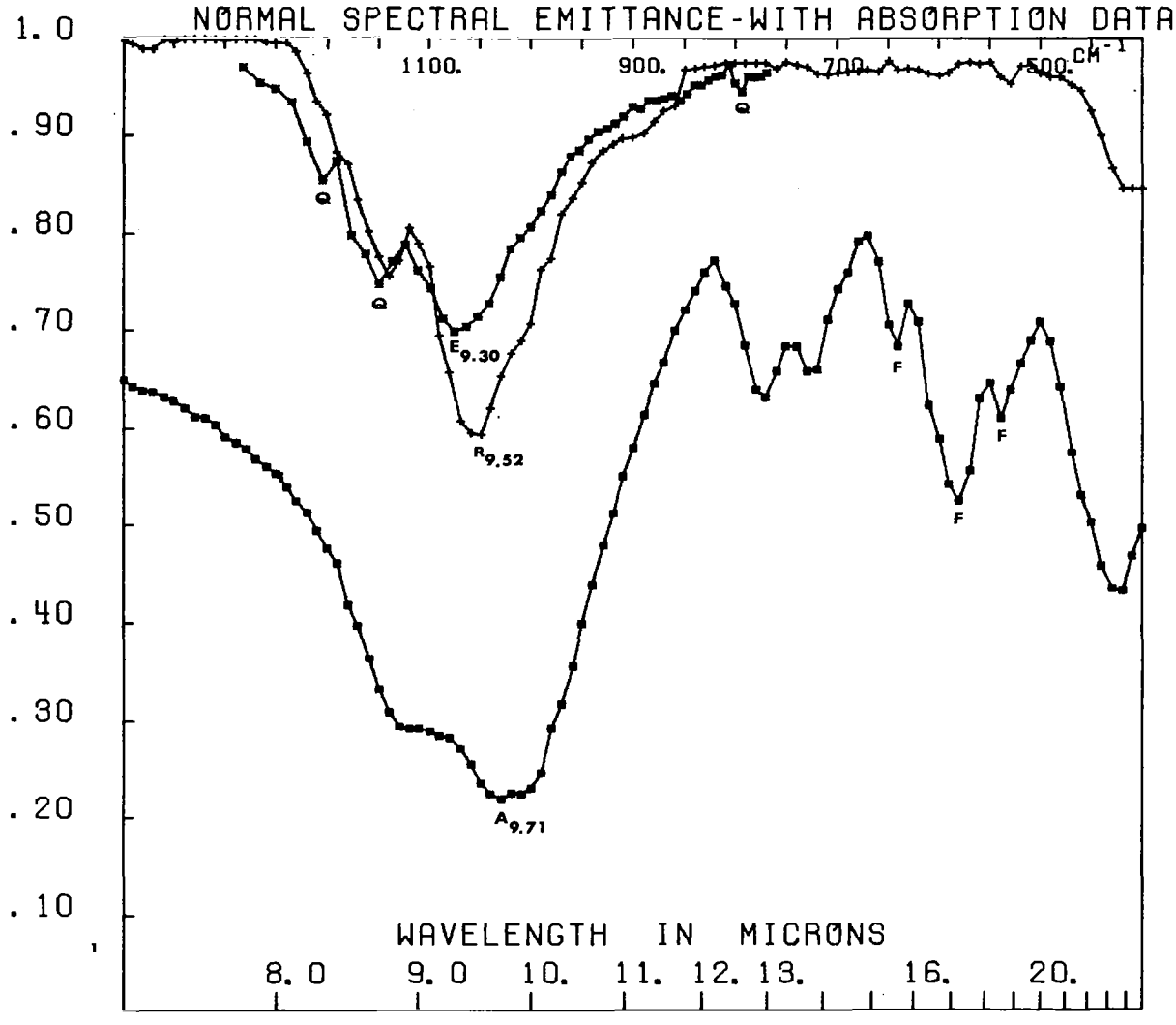

FIG. A-4 GRAPHIC GRANITE (USNM 377) NORMAL SPECTRAL EMITTANCE – WITH ABSORPTION DATA. Note the peaks (Q) due to quartz in the emittance (E) and reflectance (R) spectra – only the emittance spectrum shows the doublet at 790 cm^{-1} (12.65μ) due to quartz. Feldspar (F) peaks show in the absorption spectrum (A).

USNM 1924
(SRI 3558)

About 1 mile NE of Rumsey Mt., near center of Philipsburg quadrangle, Mont.

PYROXENE APLITE (Amadorose) (Calkins, F.C.)

Texture: Hypidiomorphic-granular.

Constituents: Chief. Soda lime feldspar > quartz > alkali feldspar > scapolite > pyroxene.
Accessory. Titanite, hornblende, apatite, zircon.

Noteworthy: Scapolite probably original. Interstitial feldspar probably soda-rich anorthoclase.

Literature: Emmons, W. H. and Calkins, F. C., P.P.U.S.G.S. No. 78, p. 120-126.

Occurrence: Small stock.

Analysis by W. F. Hillebrand, p. 124.

SiO_2	68.00
Al_2O_3	16.33
Fe_2O_3	.26
FeO	.70
MgO	1.41
CaO	5.90
Na_2O	6.20
K_2O	.38
H_2O-	0.06
H_2O+	.25
TiO_2	.43
ZrO_2	.02
P_2O_5	.22
Cl	.13
F (High ?)	.07
S	.01
MnO	.02
BaO	.03
SrO	.03
	100.45
Less O for Cl and F --	.06
	100.39

Norm.

Quartz	19.98
Orthoclase	2.22
Albite	50.30
Anorthite	16.68
Halite (NaCl)	0.47
Diopside	7.75
Hypersthene	1.06
Magnetite	.46
Apatite	.67
Ilmenite	.61
Fluorite	.16
	99.79

IR Spectra

	Averaged over this range	
Emittance	$\epsilon = 0.85$	(1280 - 770 cm^{-1})
Reflectance	$1-\rho = 0.86$	(1400 - 400 cm^{-1})
Transmittance (un-normalized)	$\tau = 0.53$	(1400 - 400 cm^{-1})

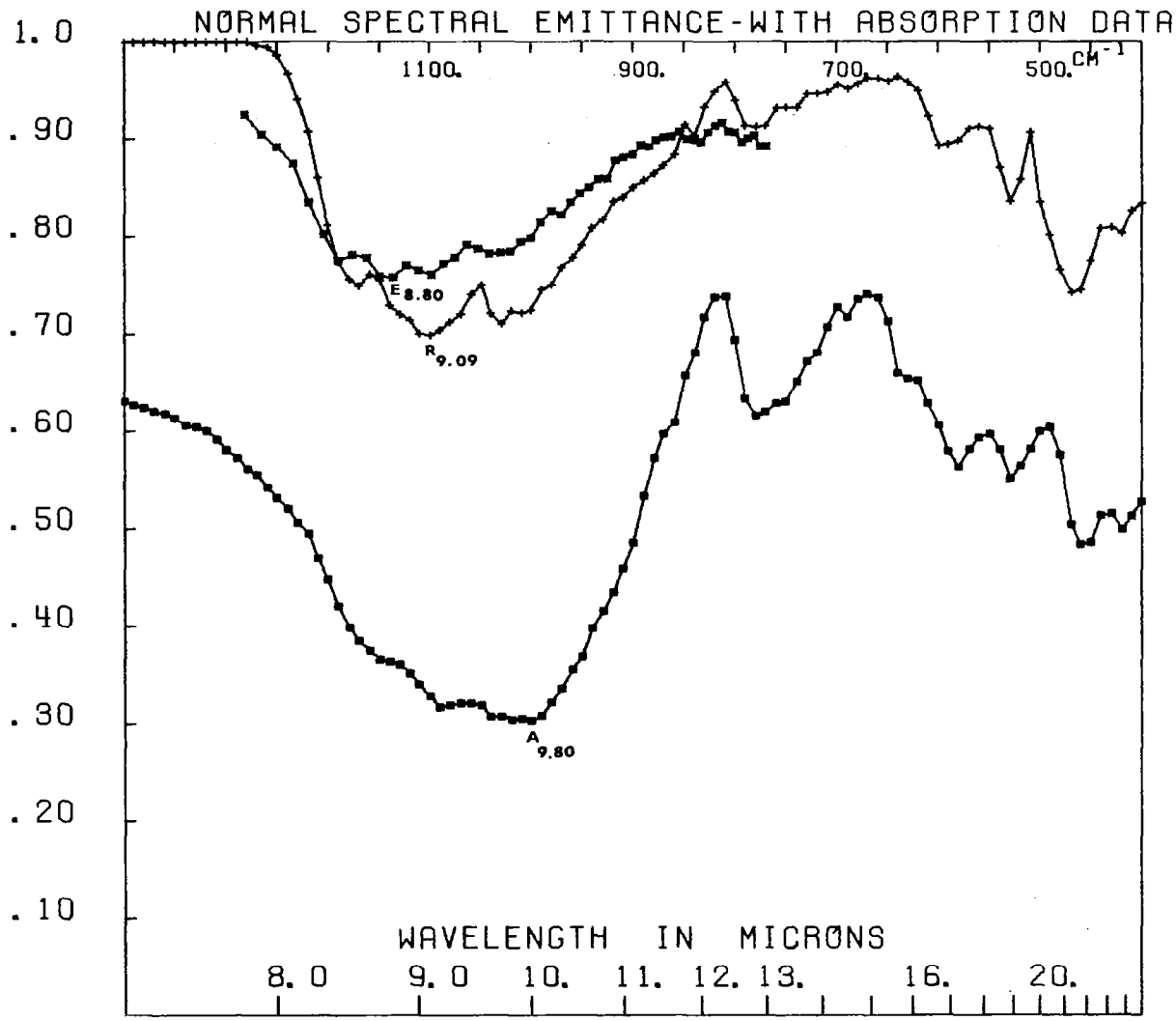

FIG. A-5 PYROXENE APLITE (USNM 1924) NORMAL SPECTRAL EMITTANCE – WITH ABSORPTION DATA. Note peak shift of minimum from emittance (E) at 1135 cm^{-1} (8.80μ) to that of reflectance (R) at 1100 cm^{-1} (9.09μ). Actually peaks are multiple and a different peak becomes the minimum.

USNM 59 (SRI 3541) — Mono Lake, Mono Co., Calif.

RHYOLITIC PUMICE. Toscanose No. 67 W.T.p. 167 (Lindgren)

Structure	Porphyritic.	Phenocrysts < groundmass.
	Phenocrysts.	Large
	Groundmass.	Isotropic. Vesicular.
Constituents	Phenocrysts.	Plagioclase, pyroxene grains, biotite.
	Groundmass.	Pure glass, with biotite and feldspar microlites. Accumulations of opacite grains.
Noteworthy	Stringy structure of glass, threadlike gas inclusions.	
Literature	Lindgren, W., Bull. U.S.G.S., 150, p. 148	

Analysis p. 149, W. H. Melville.

	Percent
Loss	2.06
SiO_2	67.39
Al_2O_2	15.99
Fe_2O_3	0.56
FeO	1.99
CaO	1.63
MgO	0.77
K_2O	4.80
Na_2O	4.74
Total	99.93

Norm.

Q	15.5
or	28.4
ab	39.8
an	8.1
hy	5.2
mt	0.7

IR Spectra	Averaged over this range
Emittance	ϵ = 0.84 (1280 - 770 cm^{-1})
Reflectance	Not Run
Transmittance (un-normalized)	τ = 0.47 (1400 - 400 cm^{-1})

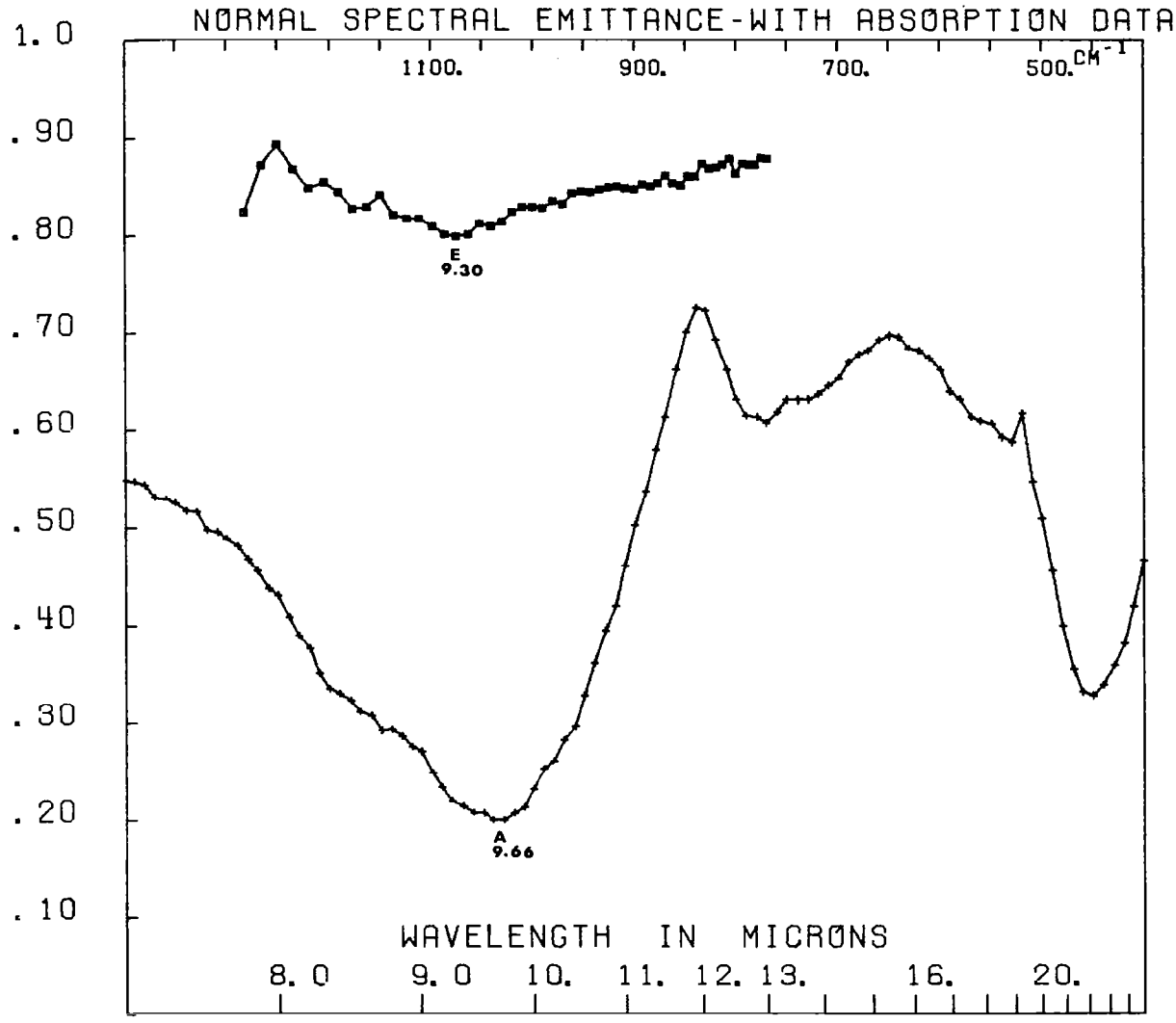

FIG. A-6 PHYOLITE PUMICE (USNM 59) NORMAL SPECTRAL EMITTANCE – WITH ABSORPTION DATA. Due to the porous nature of this rock a polished surface could not be prepared; therefore there is no reflectance spectrum.

USNM 605
(SRI 3587)

North of Twin Creek,
Pike's Peak District, Colo.
(Pike's P. Coll. No. 2155)

GRANITE-GNEISS Kallerudose No. 4 W.T.p. 154

Structure	Gneissic.	Fine-granular to porphyritic
Constituents	Chief.	Microcline x quartz > orthoclase, microperthite > biotite
	Accessory.	Fluorite, sphene, apatite
Noteworthy	Fluorite	
Comment		
Occurrence		
Literature	Mathews, E. B., "The granitic rocks of the Pikes Peak quadrangle" - J. G. Vol. VIII pp. 214-240, 1900.	

Analysis by W. F. Hillebrand

SiO_2	66.90	BaO	.14
TiO_2	.43	MgO	.31
Al_2O_3	14.86	K_2O	5.02
Fe_2O_3	.93	Na_2O	5.56
FeO	3.41	Li_2O	.06
MnO	.15	H_2O at 110°	.16
CaO	1.23	H_2O above 110°	.31
SrO	none	P_2O_5	.12
		F	1.00
			100.59
		Less O	.42
			100.17

IR Spectra	Averaged over this range	
Emittance	ϵ = 0.82, 0.88	(1280 - 770 cm^{-1})
Reflectance	$1-\rho$ = 0.87	(1400 - 400 cm^{-1})
Transmittance (un-normalized)	τ = 0.51	(1400 - 400 cm^{-1})

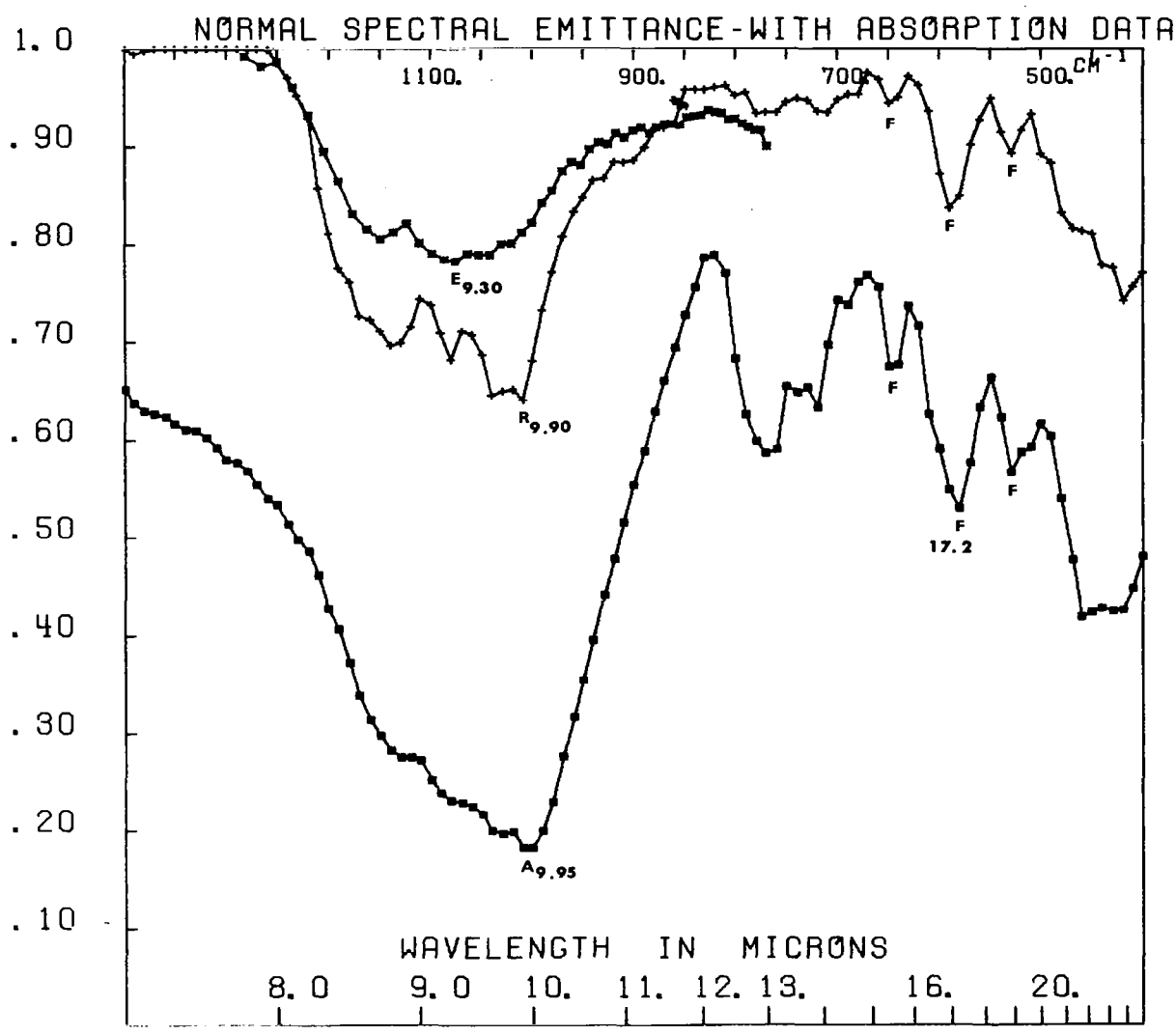

FIG. A-7 GRANITE GNEISS (USNM 605) NORMAL SPECTRAL EMITTANCE – WITH ABSORPTION DATA. Reflectance (R) and absorption spectra emphasize the longer wavelength (1010 cm^{-1}; 9.90μ) peak in the multiple minima bands, compared with the emittance (E) spectrum. Three feldspar (F) peaks appear centered around 580 cm^{-1} (17.2μ).

USNM 70
(SRI 3547)

Game Ridge, near Rosita,
Custer Co., Colo.

TRACHYTE — Phlegrose No. 7 W.T. p. 194 (Cross)

Structure	Porphyrytic	phenocrysts < ground mass
	Phenocrysts	variable in size
	Groundmass	holocrystalline, fluido - "trachytic" poikilitic
Constituents	Phenocrysts	sanidine > oligoclase > biotite
	Groundmass	orthoclase > quartz > oligoclase
	Accessories	magnetite dust, limonite, apatite, zircon

Comment — Nearly a typical trachyte (W.C.) Strikingly similar to trachyte Drachenfels. (W.C.)

Occurrence — Surface mass

Literature — Cross, W., U.S.G.S. Bull. 150, p. 181
Proceed. Colo. Sci. Soc. V. II, p. 233-237; V. III, p. 269-279. 17 Annual Rept. U.S.G.S., Pt. II, 1896, p. 263-403.

Compare — Same as spec. no. 524

Analysis p. 182 by L. G. Eakins

		Norm	
SiO_2	66.03		
Al_2O_3	18.49	Q	10.5
Fe_2O_3	2.18	or	35.0
FeO	.22	ab	44.0
MnO	Tr	an	4.7
CaO	.96	C	1.7
MgO	.39		
K_2O	5.86	hy	1.0
Na_2O	5.22	mt	0.7
H_2O	.85	hm	1.8
P_2O_5	.04		
CO_2	Tr		
Total	100.24		

Sp. gr. 29°C = 2.59

IR Spectra	Averaged over this range	
Emittance	ϵ = 0.84, 0.86	(1280 - 770 cm^{-1})
Reflectance	$1-\rho$ = 0.94	(1400 - 400 cm^{-1})
Transmittance (un-normalized)	τ = 0.51	(1400 - 400 cm^{-1})

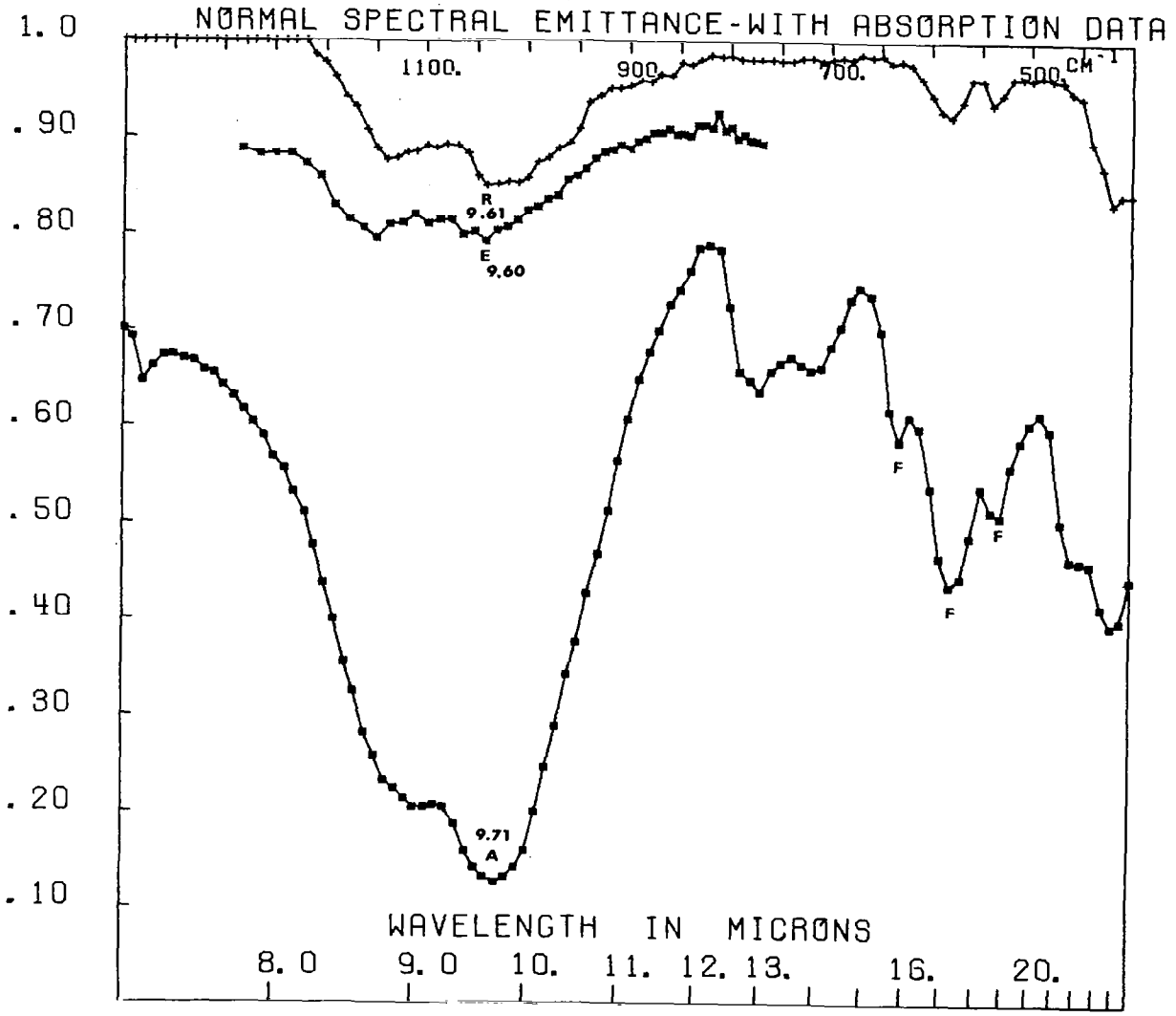

FIG. A-8 TRACHYTE (USNM 70) NORMAL SPECTRAL EMITTANCE – WITH ABSORPTION DATA. Peaks at about 750 cm^{-1} (13.3μ) again do not show on the reflectance (R) spectrum, although the feldspar (F) peaks at 570 cm^{-1} (17.5μ) may be observed in reflection.

USNM 631
(SRI 3557)

Grorud, near
Christiania, Norway.

QUARTZ-SYENITE
Var: Nordmarkite Nordmarkose No. 17. W.T.p. 197.

Structure	Granular.	Miarolitic.
Constituents	Chief.	Alkali-feldspar (microperthitic orthoclase, microcline)>>quartz>biotite>green hornblende.
	Accessory.	Titanite, apatite, iron ores, zircon, allanite(?).

Noteworthy Large titanites. Typical miarolitic structure. Normal type of the great Nordmarken mass, this rock covering several hundred square miles of wild, wooded country in the Christiania region. Quarried as a building stone. Specimen is from the general neighborhood of the altered Silurian. (L.V.P.)
Quartz albite and orthoclase in miarolitic cavities. (F.L.R.)

Occurrence Laccolithic or batholithic mass.

Literature Brogger. Zeitschr. fur Kryst. vol. 16, 1890, p. 54-62.

Analysis p. 54, No. II, by G. Forsberg.

		Norm	
SiO_2	65.20		
TiO_2 & ZrO_2	.46	or	35.0
Al_2O_3	17.45	ab	48.2
Fe_2O_3 / FeO	3.60	ne	5.4
MgO	.75	ac	1.4
CaO	1.40	di	5.9
Na_2O	6.90	ol	2.4
K_2O	5.88	il	0.9
H_2O	.50		
	100.14		

IR Spectra	Averaged over this range	
Emittance	$\epsilon = 0.86$	(1280 - 770 cm^{-1})
Reflectance	$1-\rho = 0.85$	(1400 - 400 cm^{-1})
Transmittance (un-normalized)	$\tau = 0.54$	(1400 - 400 cm^{-1})

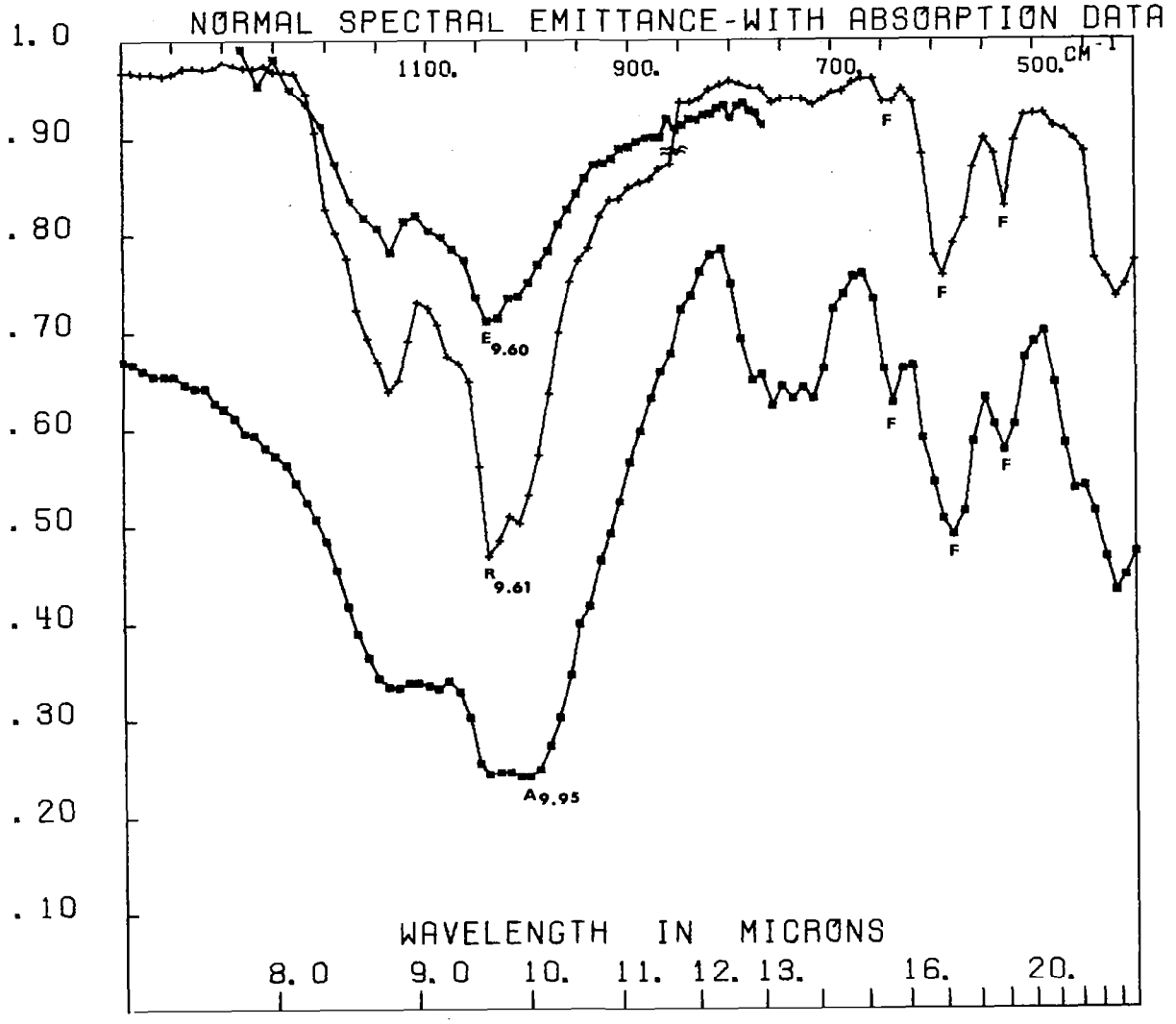

FIG. A-9 QUARTZ SYENITE (USNM 631) NORMAL SPECTRAL EMITTANCE – WITH ABSORPTION DATA. Excellent example with clearly resolved spectral peaks in the results from each technique. Spectral detail at 750 cm^{-1} (13.3μ) is weakly present even in the reflectance (R) curve.

USNM 1331 San Jose, Tamaulipas, Mexico.
(SRI 3542)
ANDESITE (Monzonite-Porphyry) (Laurvikose) Geo. I. Finley. J.

Structure	Holocrystalline porphyritic. Phenocrysts $\gtrless$ groundmass.	
	Phenocrysts.	Hypidiomorphic.
	Groundmass.	Hypidiomorphic granular.
Constituents	Phenocrysts.	Orthoclase > labradorite > augite > hornblende > quartz.
	Groundmass.	Feldspar, augite, hornblende, quartz.
	Accessory.	Pyrite, apatite; zircon rare.
	Secondary.	Epidote, chlorite, sericite.
Noteworthy		
Comment	Called "Andesite" by Finley. It is his San Narcisco type.	
Occurrence	Laccolith.	
Literature	Annals N.Y. Academy of Science, Vol. XIV, pp. 248-295.	

Analysis by Finley.

SiO_2	62.31
Al_2O_3	18.63
Fe_2O_3	2.38
FeO	1.33
MgO	.60
CaO	5.91
Na_2O	4.97
K_2O	3.52
H_2O-	.16
H_2O+	.07
P_2O_5	.07
Li_2O	
	99.95

IR Spectra	Averaged over this range	
Emittance	$\epsilon = 0.77$	(1280 - 770 cm^{-1})
Reflectance	$1-\rho = 0.86$	(1400 - 400 cm^{-1})
Transmittance (un-normalized)	$\tau = 0.53$	(1400 - 400 cm^{-1})

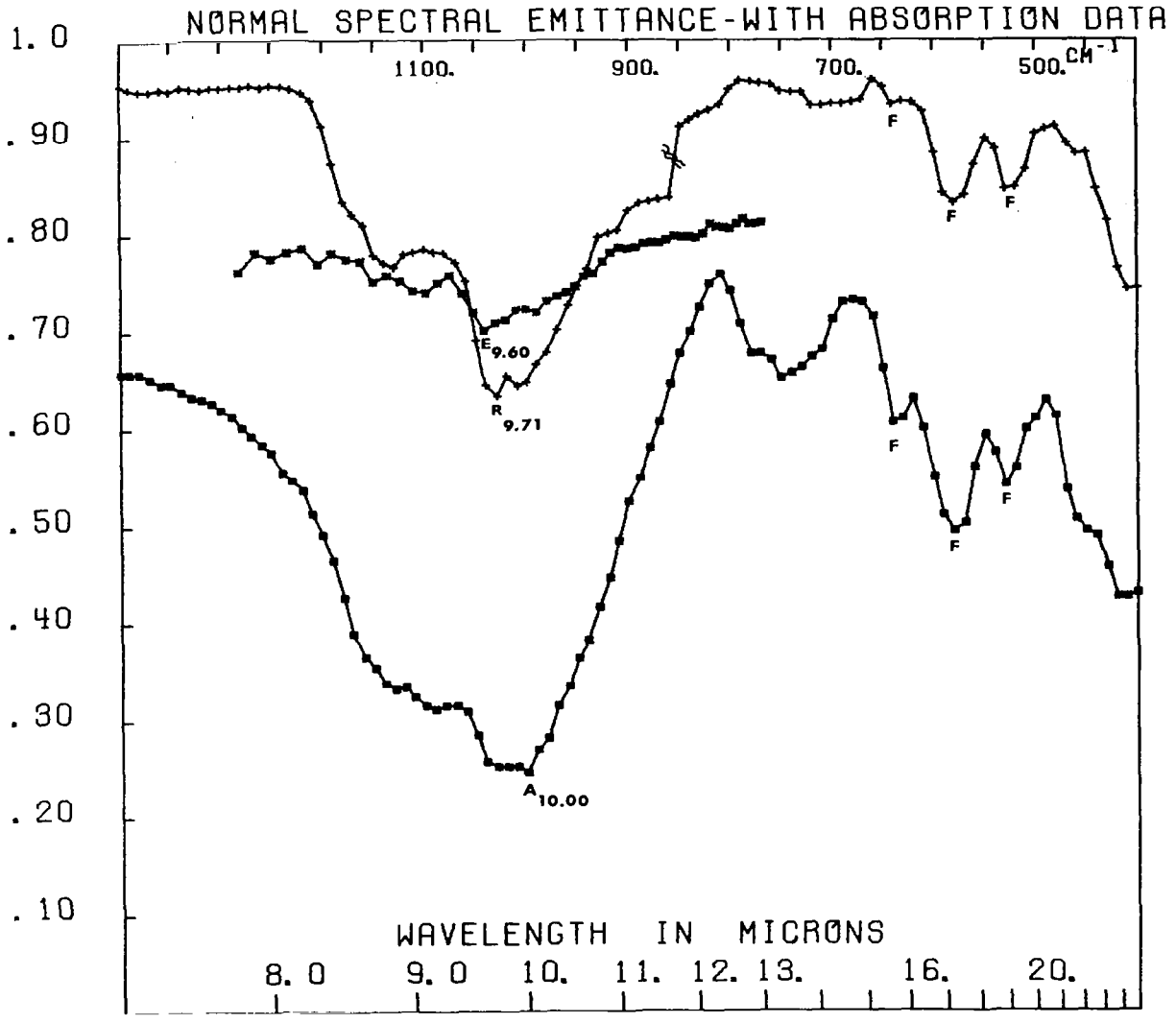

FIG. A-10 ANDESITE (MONZONITE PORPHYRY) (USNM 1331) NORMAL SPECTRAL EMITTANCE – WITH ABSORPTION DATA. Break at 850 cm^{-1} (11.75μ) is due to NaCl-KBr prism change during reflectance (R) measurement.

USNM 77 Litchfield, Kennebec County, Maine
(SRI 3555)

NEPHELITE SYENITE (Elaeolite syenite) (Bayley) L.H.W.
Nordmarkose No. 1, W.T.p. 194

Structure		Hypidiomorphic granular, granitic.
Constituents	Chief.	Albite > microcline and orthoclase > nephelite > biotite (lepidomelane) > cancrinite
	Accessory.	Sodalite, zircon? flakes of lepidomelane
Noteworthy	Microcline-microperthite, dull color of nephelite due to inclusions, mosaic of feldspar and cancrinite. Lepidomelane (analyzed) Albite " Cancrinite " Sodalite " Zircon "	
Occurrence	Boulders.	
Literature	Bayley, W. S., Bull. U.S.G.S. 150, p. 201, Plate XXIX, p. 204 Bull. Geol. Soc. Am. Vol. III, p. 231.	
Compare	949 L. G. Eakins, analyst. Analysis: Nephelite-syenite, Bull. 150, p.208.	

SiO_2	-	60.39
Al_2O_3	-	22.51
Fe_2O_3	-	.42
FeO	-	2.26
MnO	-	.08
CaO	-	.32
MgO	-	.13
K_2O	-	4.77
Na_2O	-	8.44
H_2O	-	.57
CO_2	-	Trace

Bulletin 150 also contains analyses of albite of nephelite-syenite, nephelite of nephelite-syenite, lepidomelane of nephelite-syenite, cancrinite of nephelite-syenite, sodalite of nephelite-syenite, zircon of nephelite-syenite, albite of nephelite-syenite, and microcline and orthoclase from nephelite-syenite.

IR Spectra	Averaged over this range	
Emittance	ϵ = 0.88, 0.91	(1280 - 770 cm^{-1})
Reflectance	$1-\rho$ = 0.92	(1400 - 400 cm^{-1})
Transmittance	τ = 0.49	(1400 - 400 cm^{-1})

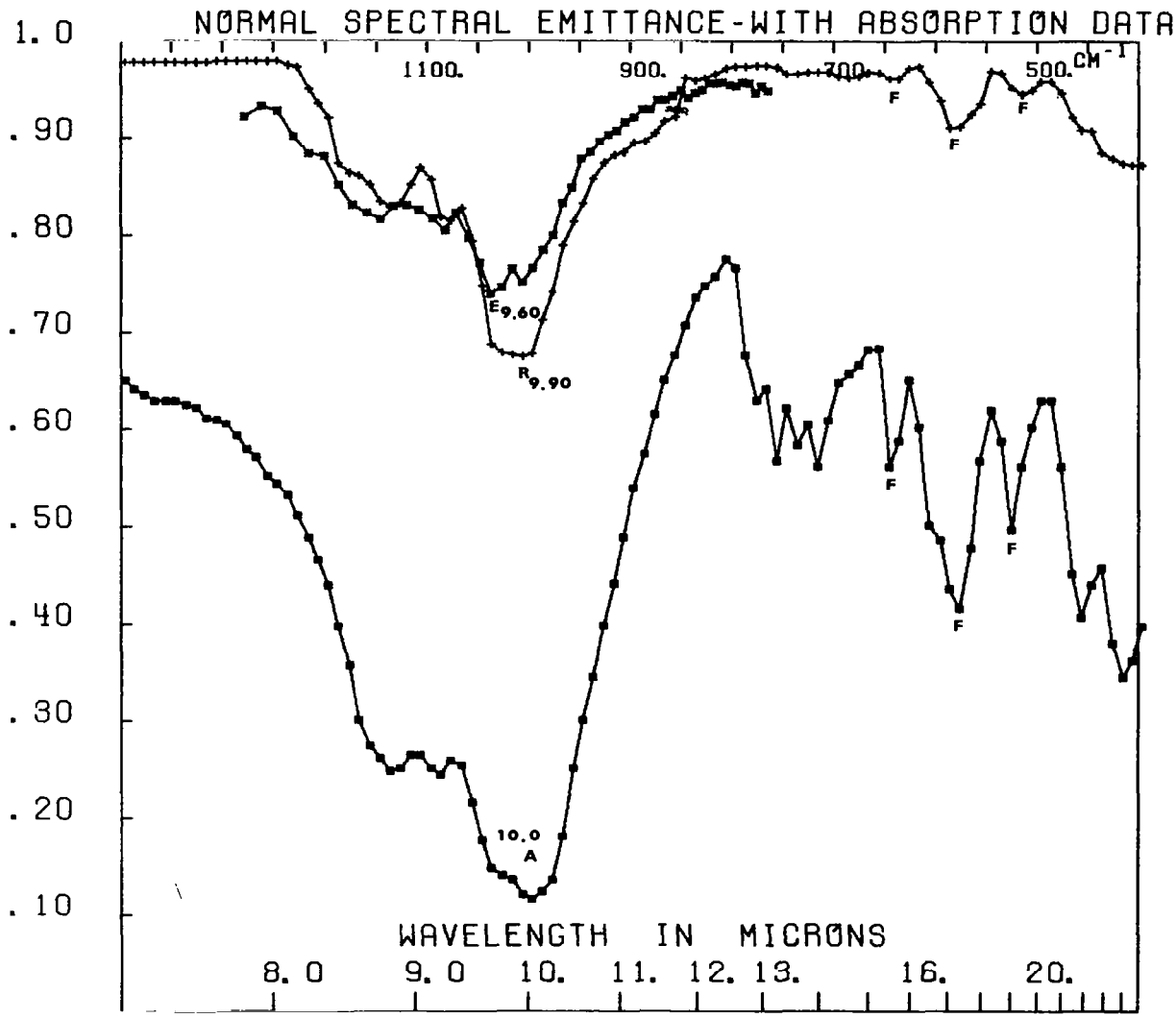

FIG. A-11 NEPHELINE SYENITE (USNM 77) NORMAL SPECTRAL EMITTANCE – WITH ABSORPTION DATA. Emittance (E) spectrum again emphasizes the lower wavelength (1042 cm^{-1}; 9.60μ) peak in the multiple minima.

USNM 101
(SRI 3546)

Snag Lake Cinder Cone,
Lassen Co., California

QUARTZ-BASALT Andose No. 52 W.T. p. 276 (Diller) L. H. W.

Structure	Subporphyritic.	Vesicular.
	Phenocrysts.	Small, Broken.
	Groundmass.	Microlitic, semiopaque
Constituents	Phenocrysts.	Plagioclase > pyroxene (hypersthene, augite) > olivine > quartz.
	Groundmass.	Globulitic, microlites of plagioclase, and still smaller undeterminable ones with grains of magnetite.
	Accessories.	Magnetite, picotite?

Noteworthy: Picotite? Inclusions in olivine as small coffee brown isotropic? crystals. Quartz as constituent. "Shell of augite and glass surrounding quartz, which is sometimes wholly resorbed by magma and its place marked by a group of granular augite." J. S. D.

Comment: In section this reaction rim is shown about cavity, the quartz having been lost in grinding.

Occurrence: Lava flow about 200 years old.

Literature: Diller, J. S., Bull. U.S.G.S. 150, p. 252.
Plate XXXVII, p. 254, quartz with rims of glass and augite.
Bull. U.S.G.S. No. 79.

Analysis quartz-basalt from Snag Lake lava field, Lassen County, California, U.S.G.S. Bulletin 150, p. 253, W. F. Hillebrand, analyst

SiO_2	57.25	BaO	0.03
TiO_2	0.60	MgO	6.74
Al_2O_3	16.45	K_2O	1.57
Fe_2O_3	1.67	Na_2O	3.00
FeO	4.72	Li_2O	None
MnO	0.10	H_2O	0.40
CaO	7.65	P_2O_5	0.20
SrO	Trace	Total	100.38

IR Spectra	Averaged over this range	
Emittance	ϵ = 0.72, 0.72	(1280 - 770 cm^{-1})
Reflectance	$1-\rho$ = 0.92	(1400 - 400 cm^{-1})
Transmittance	τ = 0.50	(1400 - 400 cm^{-1})

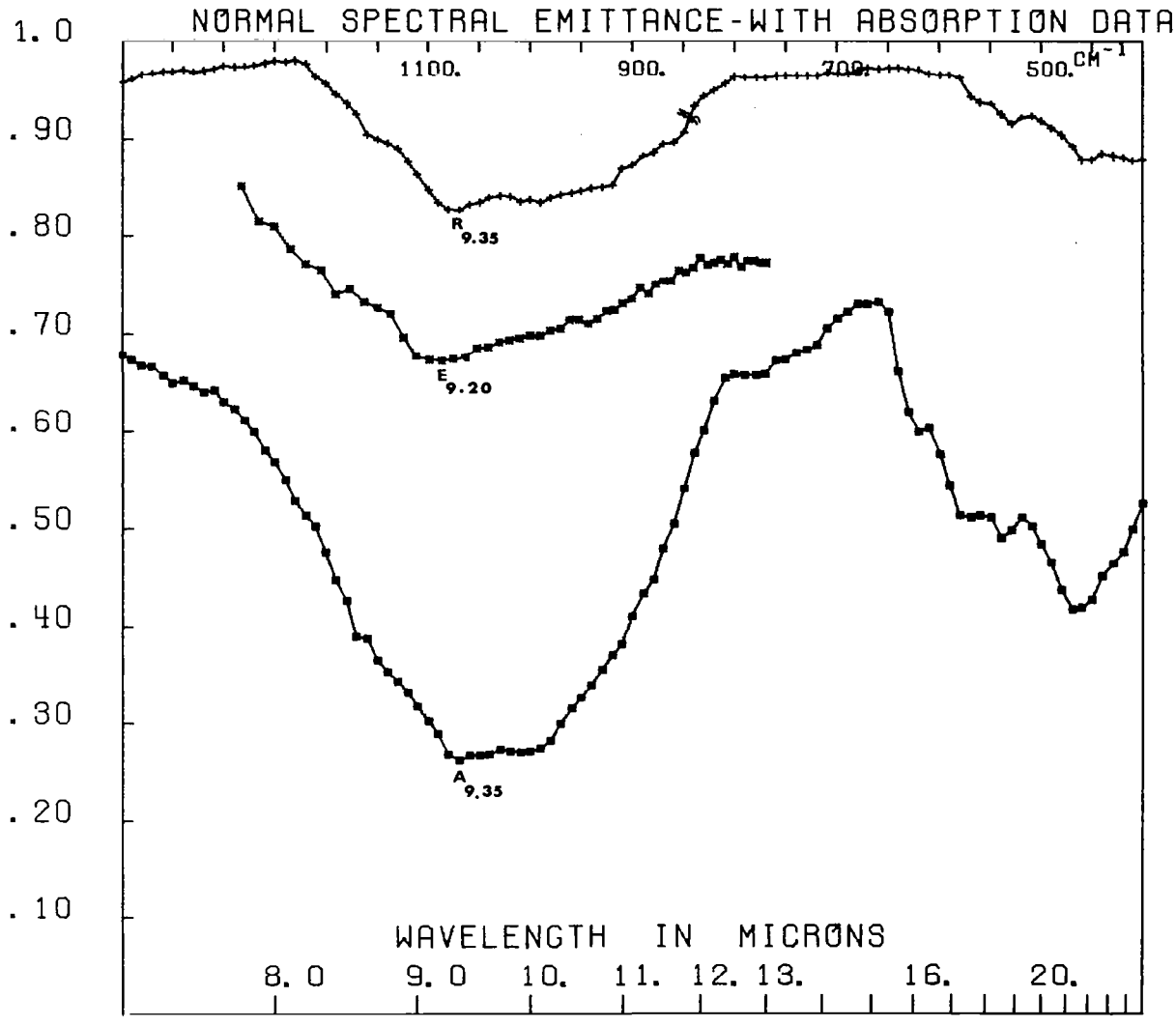

FIG. A-12 QUARTZ BASALT (USNM 101) NORMAL SPECTRAL EMITTANCE – WITH ABSORPTION DATA. Noteworthy low wavelength for the major peak (1075 cm^{-1}; 9.30μ) compared with the low SiO_2 content of the analysis.

USNM 86
(SRI 3550)

N.E. shoulder of Buffalo Peak
Park County, Colo.

HYPERSTHENE-ANDESITE Andose No. 55 W.T.p. 277 (Cross) L. H. W.

Structure	Porphyritic.	Phenocrysts > < groundmass.
	Phenocrysts.	Very small.
	Groundmass.	Vitreous, Microlitic.
Constituents	Phenocrysts.	Labradorite > hypersthene > augite, magnetite
	Groundmass.	Glassy base, plagioclase and augite microlites, magnetite particles.
Noteworthy	Brown glass inclusions in plagioclase. Hypersthene.	
Occurrence	Lava flow.	
Literature	Cross, W., Bull. U.S.G.S. 150, p. 224. Bull. U.S.G.S. No. 1.	

Analysis of hypersthene-andesite from Buffalo Peak, Colorado, Bull. 150, W. F. Hillebrand, analyst, pp. 226, 227.

I.

SiO_2	56.19
Al_2O_3	16.12
Fe_2O_3	4.92
MnO	4.43
CaO	7.00
BaO	Trace
SrO	Trace
MgO	4.60
Na_2O	2.96
K_2O	2.37
H_2O	1.03
P_2O_5	.27
Cl	.02
Total	99.91

Sp. gr. at 16°C., 2.742

II.

Analysis of hypersthene of hypersthene-andesite

SiO_2	51.70
Al_2O_3	1.72
Fe_2O_3	0.30
FeO	17.99
MnO	0.36
CaO	2.87
MgO	25.09
	100.03

IR Spectra	Averaged over this range	
Emittance	ϵ = 0.78, 0.78	(1280 - 770 cm^{-1})
Reflectance	$1-\rho$ = 0.87	(1400 - 400 cm^{-1})
Transmittance (un-normalized)	τ = 0.49	(1400 - 400 cm^{-1})

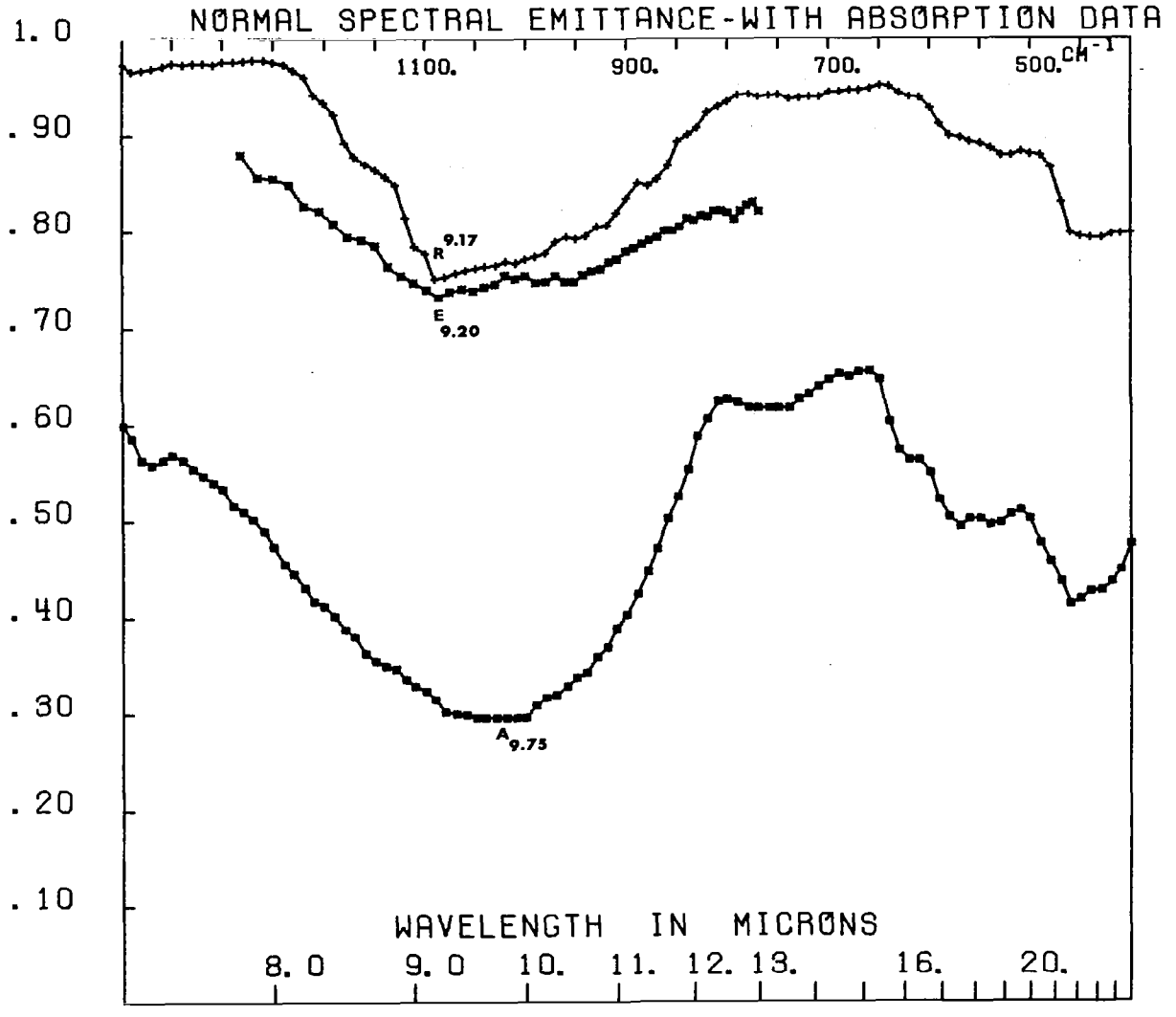

FIG. A-13 HYPERSTHENE ANDESITE (USNM 86) NORMAL SPECTRAL EMITTANCE – WITH ABSORPTION DATA. Compare with glassy equivalent in Fig. A-14. It would be difficult to decide which was the more crystalline from their spectra, but this difficulty also appears in their petrographic descriptions.

USNM 371
(SRI 3551)

Bagonya, Hungary

HYPERSTHENE-ANDESITE

(Stürtz Coll. Cross)

Vitrophyre

Structure	Vitrophyric.	Eutaxitic
Constituents	Phenocrysts	Plagioclase > hypersthene
	Groundmass	Microlitic-glass
	Accessory	Iron-ore, apatite
Noteworthy	Eutaxitic structure	
Comment	Fresh and interesting rock	
Occurrence		
Literature	Rosenbusch, Mikros. Phys. Vol. II, p. 898, 899. Zirkel, Lehrb. d. Petrog., Vol. II, p. 822.	

IR Spectra	Averaged over this range	
Emittance	$\varepsilon = 0.83$	(1280 - 770 cm^{-1})
Reflectance	$1-\rho = 0.91$	(1400 - 400 cm^{-1})
Transmittance (un-normalized)	$\tau = 0.47$	(1400 - 400 cm^{-1})

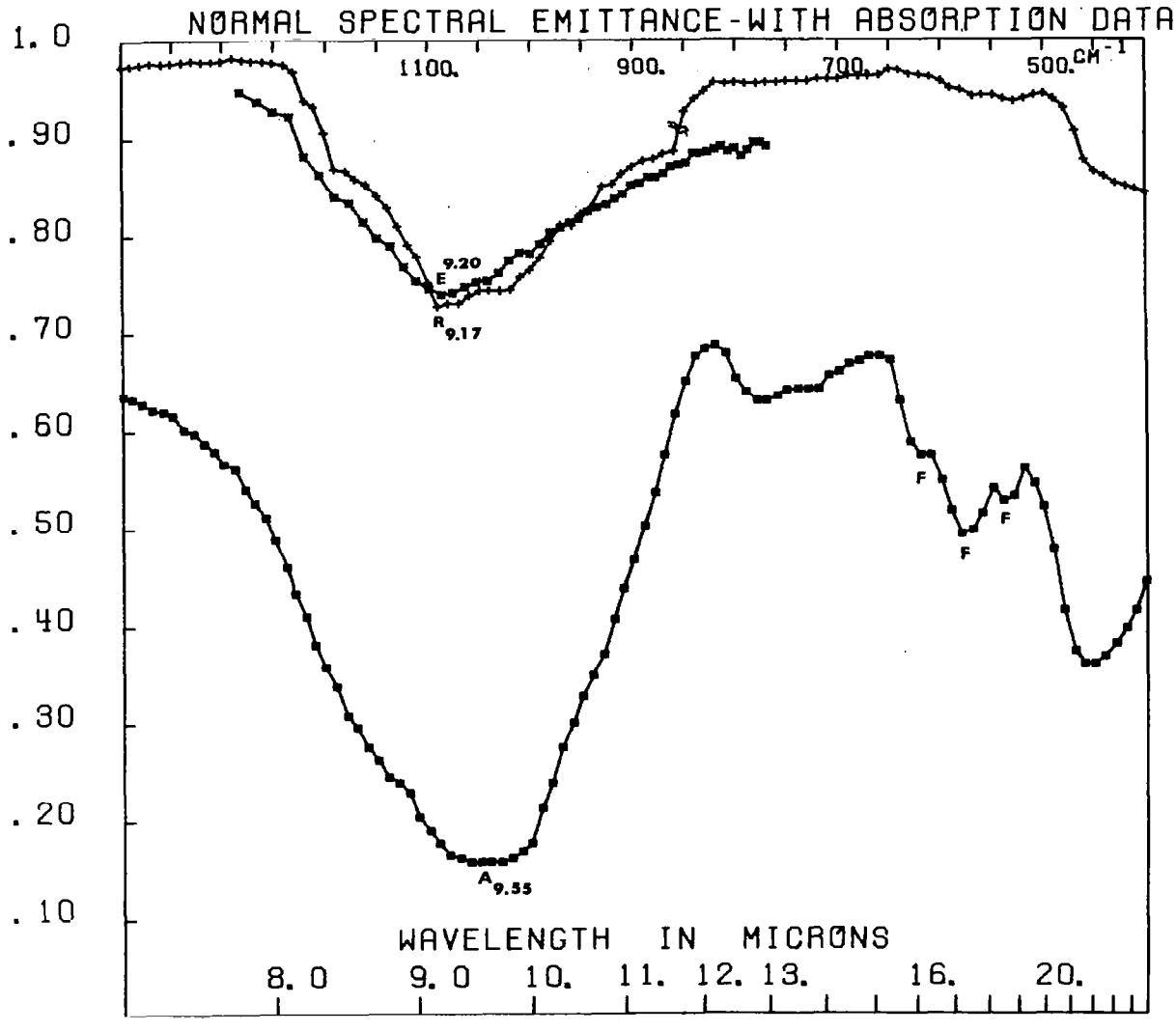

FIG. A-14 HYPERSTHENE ANDESITE VITROPHYRE (USNM 371) NORMAL SPECTRAL EMITTANCE – WITH ABSORPTION DATA. Compare with crystalline equivalent in Fig. A-14. Feldspar (F) peaks appear.

USNM 758
(SRI 3553)

By trail to North Valley,
4-1/2 mi. S. of Table Mt.,
Plumas Co., Cal.
(H. W. Turner)

QUARTZ-DIORITE Camptonose No. 24 W.T.p. 321.

Structure Hypidiomorphic-granular. Fine.

Constituents
Chief. Hornblende, feldspar, quartz.
Accessory. Apatite, iron ore, titanite (Undet. yellow mineral. Secondary (?)
Secondary. Epidote, chlorite.

Noteworthy

Comment Amphibole is an aluminous variety - not actinolite. (H. W. T.)

Occurrence Dike (?)

Literature Turner, H. W., 17th Ann. Rept. U.S.G.S., Pl. I, pp. 574-575 (817 S.N.)
Bidwell Bar Folio.

Analysis by W. F. Hillebrand

SiO_2	54.64	SrO	trace
TiO_2	.61	BaO	.05
Al_2O_3	12.09	MgO	11.86
Fe_2O_3	1.81	K_2O	1.01
FeO	5.03	Na_2O	2.35
NiO	.05	Li_2O	trace
MnO	.13	H_2O at 100°	.12
CaO	7.74	H_2O above 100°	2.44
		P_2O_5	.08
			100.01

IR Spectra

	Averaged over this range	
Emittance	ϵ = 0.91, 0.92	(1280 - 770 cm^{-1})
Reflectance	$1-\rho$ = 0.85	(1400 - 400 cm^{-1})
Transmittance (un-normalized)	τ = 0.59	(1400 - 400 cm^{-1})

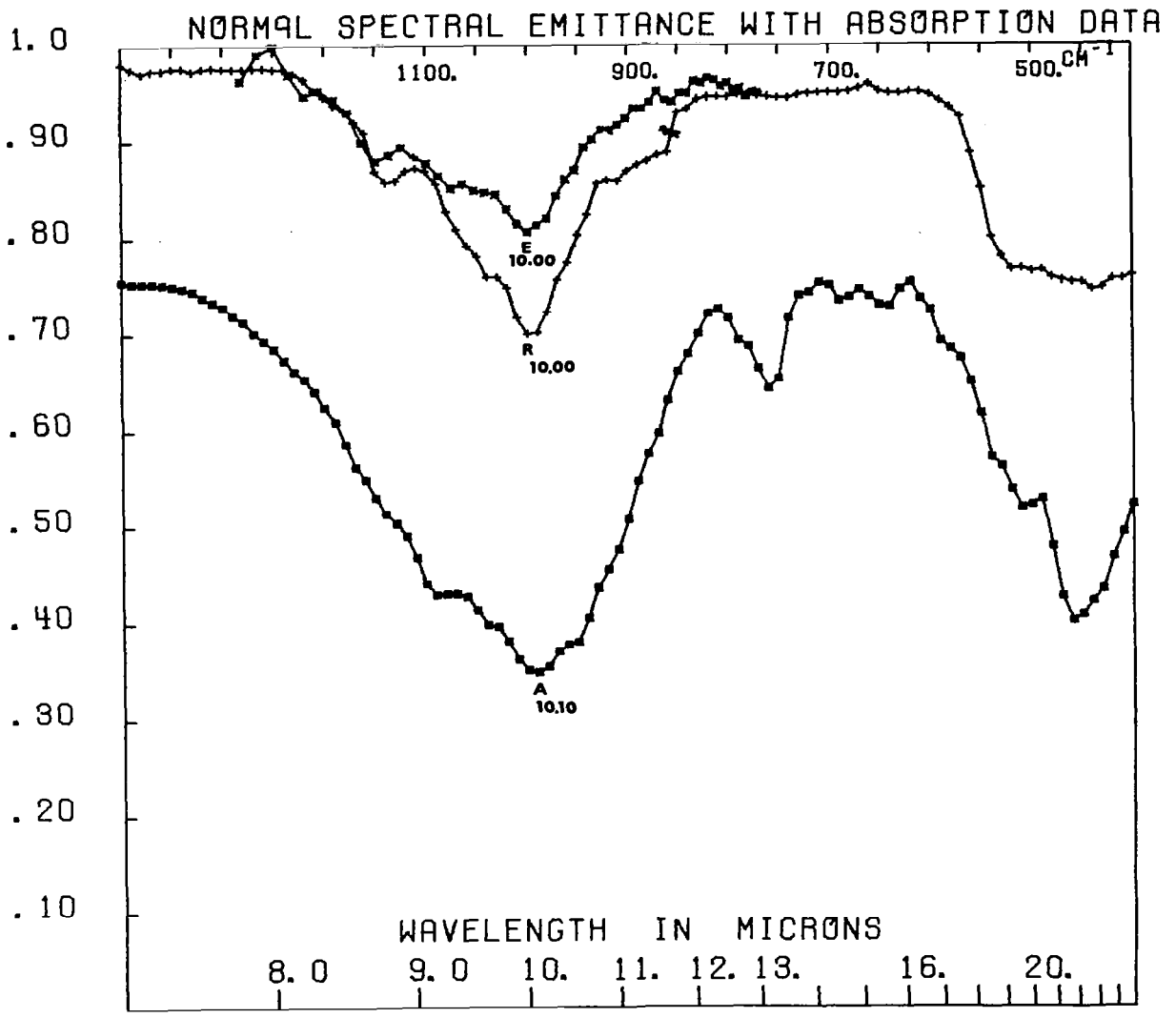

FIG. A-15 QUARTZ DIORITE (USNM 758) NORMAL SPECTRAL EMITTANCE – WITH ABSORPTION DATA. Excellent example of spectral coincidence between the three techniques. Feldspar peaks at 570 cm^{-1} (17.5μ) do not appear in the spectra of this specimen.

USNM 529
(SRI 3559)

E. Slope of Mt. Fairview
Rosita Hills,
Custer Co., Colorado.

AUGITE-DIORITE ("Fairview diorite")
orthoclase facies.)
Akerose No. 14 W.T.p. 260.

Structure	Porphyritic.	Phenocrysts < groundmass.
	Phenocrysts.	Not sharply marked off from groundmass.
	Groundmass.	Holocrystalline, granular.
Constituents	Chief.	Labradorite > orthoclase > augite > hornblende > biotite.
	Accessory.	Apatite, magnetite.
Noteworthy	Contrast with olivinitic facies, 526. Interlocking of the constituent minerals.	
Comment	Apatite unusually abundant.	
Occurrence	Dike-like mass in volcanic complex.	
Literature	Cross, W., Proc. Colo. Sci. Soc. 1887, pp. 245-248. 17th An. Rept. U.S.G.S. Pt. II, pp. 281-295.	

Analysis by L. O. Eakins.

SiO_2	53.80
TiO_2	.43
Al_2O_3	20.13
Fe_2O_3	3.57
FeO	2.65
MnO	.29
CaO	5.60
MgO	2.26
K_2O	4.49
Na_2O	5.20
H_2O	.90
P_2O_5	.56
	99.86

IR Spectra	Averaged over this range	
Emittance	$\epsilon = 0.85$	(1280 - 770 cm^{-1})
Reflectance	$1-\rho = 0.88$	(1400 - 400 cm^{-1})
Transmittance (Un-normalized)	$\tau = 0.53$	(1400 - 400 cm^{-1})

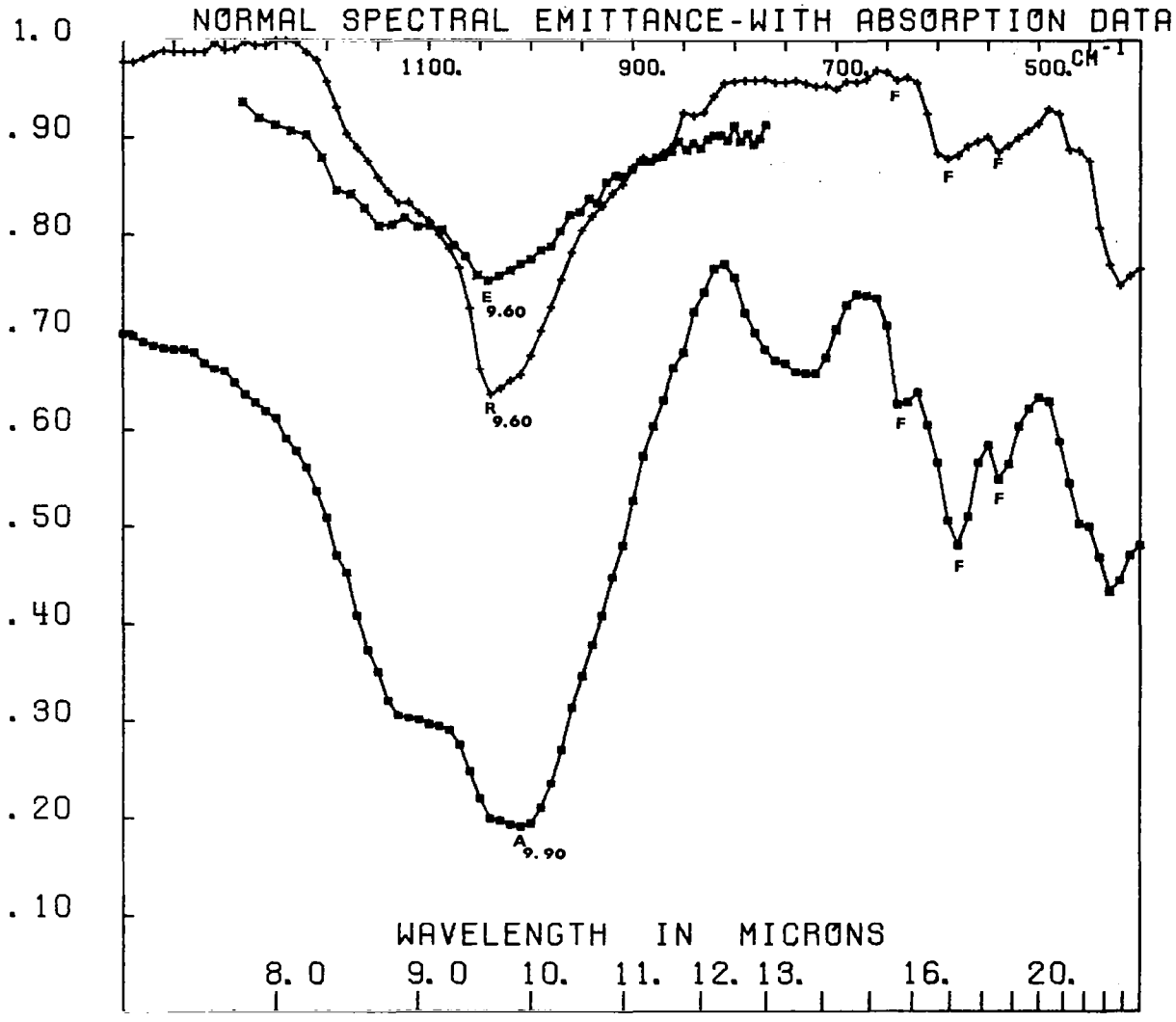

FIG. A-16 AUGITE DIORITE (USNM 529) NORMAL SPECTRAL EMITTANCE – WITH ABSORPTION DATA. Exact correlation between methods as to peak position. Note that the peak in (A) at 730 cm^{-1} (13.7μ) does not appear in the reflectance (R) spectrum, but feldspar (F) detail at 570 cm^{-1} (17.5μ) may be seen in both spectra.

USNM 109
(SRI 3584)

Granite Falls, Yellow Medicine County, Minn.

GARNETIFEROUS GABBRO Bandose No. 6 W.T.p. 247 (Bayley)

Structure Hypidiomorphic granular.

Constituents

Chief. Plagioclase > augite (diallage) > garnet > quartz.

Accessory. Magnetite (pyrite)

Inclusions Quartz, biotite, apatite, plagioclase, magnetite, chlorite, calcite, augite, hornblende, liquid.

Noteworthy Large cellular garnets, with inclusions of quartz (which include mica, apatite and dust), plagioclase, biotite, magnetite, apatite and liquid.
Secondary? origin of these inclusions, as shown by their arrangement in lines which are continuous in the surrounding substance.
Plagioclases fissured and with curved extinction show pressure.
Plagioclase inclusions: flakes of chlorite, opaque substances, magnetite dust, nests of calcite, apatite, augite, hornblende and large magnetites.
Diallage sometimes shows hornblende and magnetite grains and a fibrous cleavage around the altered edge.
Diallage sometimes wholly altered to hornblende.

Literature Bayley, W. S., Bull. U.S.G.S. 150, p. 282.
Plate XXXVIII, p. 278.

Analysis p. 286, by H. N. Stokes.

	Percent
SiO_2	52.31
Al_2O_3	18.35
Fe_2O_3	5.90
FeO	11.06
CaO	7.33
MgO	1.00
K_2O	.49
Na_2O	2.90
Loss	.35
Total	99.69

IR Spectra	Averaged over this range	
Emittance	$\epsilon = 0.81$	(1280 - 770 cm^{-1})
Reflectance	$1-\rho = 0.84$	(1400 - 400 cm^{-1})
Transmittance (un-normalized)	$\tau = 0.50$	(1400 - 400 cm^{-1})

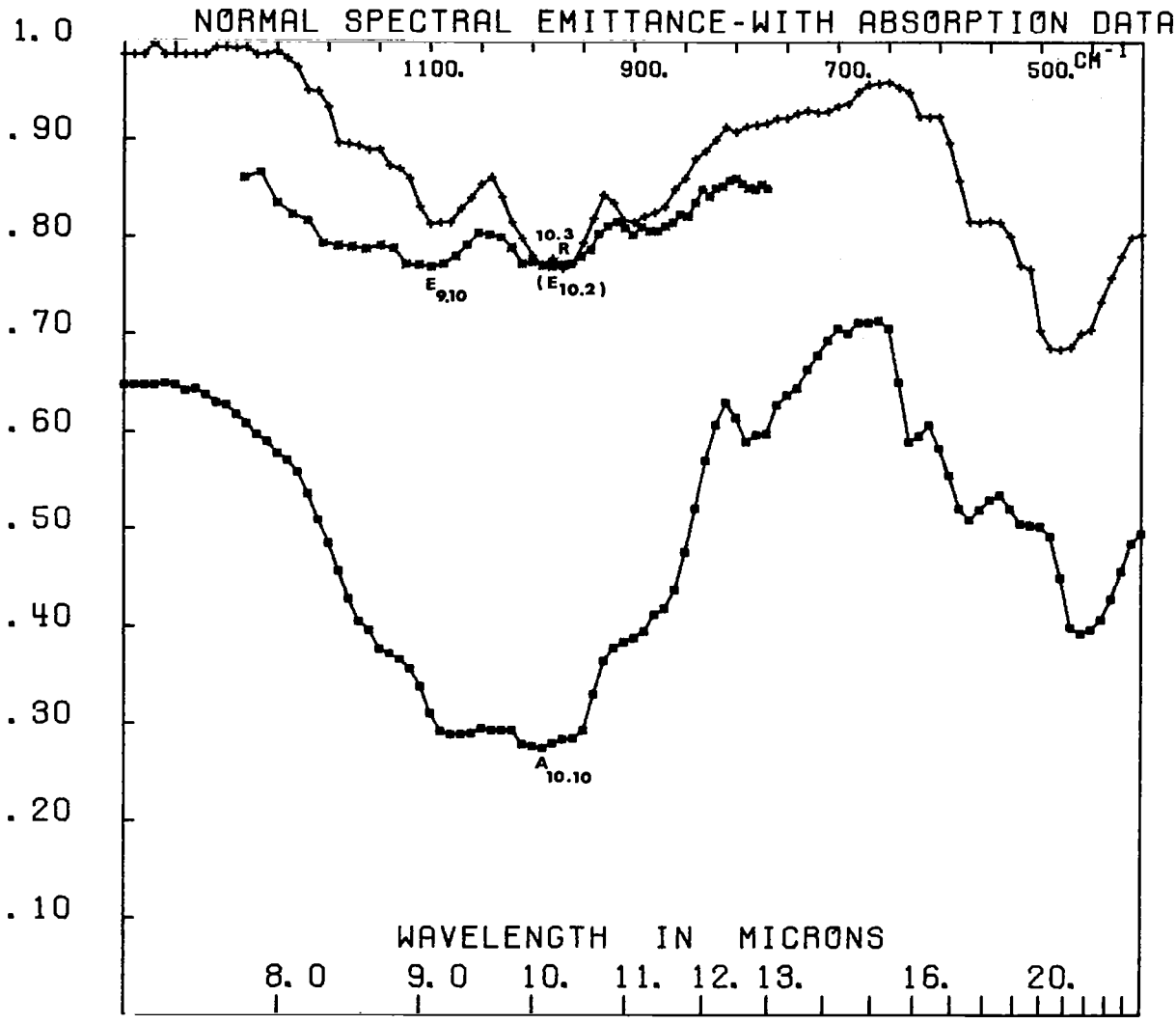

FIG. A-17 GARNETIFEROUS GABBRO (USNM 109) NORMAL SPECTRAL EMITTANCE – WITH ABSORPTION DATA. Emittance (E) spectrum again emphasizes the shorter wavelength (1100 cm^{-1}; 9.10μ) peak in the multiple band minima. Band in (A) at 770 cm^{-1} (13.0μ) may be present in the emittance (E) data, but is absent in the reflectance (R) curve.

USNM 199
(SRI 3592)

Stony Mountain, near
Mt. Sneffels, Ouray Co.,
Colo.

GABBRO (Augite Diorite)

Hessose No. 16. W.T. p. 288 (Misc. Coll. 522 Cross)

Structure: Granular. Medium.

Constituents: Chief. Plagioclase (labradorite) > augite > quartz x orthoclase > biotite x eustatite?

Accessory. Apatite, titanite, iron ore.

Secondary. Hornblende (after pyroxene).

Comment: Orthorhombic pyroxene not identified with certainty; is mostly altered.

Occurrence: Intrusive stock.

Literature: Cross, W., Proc. Colo. Sci. Soc. Vol. V, p. 231.
Cross, W., Telluride Folio, U.S.G.S.

Analysis: by L. G. Eakins.

SiO_2	52.05
Al_2O_3	17.96
Fe_2O_3	4.09
FeO	6.33
MnO	.43
CaO	8.64
MgO	5.03
K_2O	1.61
Na_2O	2.99
H_2O above 100^0	.97
P_2O_5	.31
	100.41

Specific gravity 2.891 at 13.5°C.

IR Spectra	Averaged over this range	
Emittance	$\epsilon = 0.84$	(1280 - 770 cm^{-1})
Reflectance	$1-\rho = 0.88$	(1400 - 400 cm^{-1})
Transmittance (un-normalized)	$\tau = 0.53$	(1400 - 400 cm^{-1})

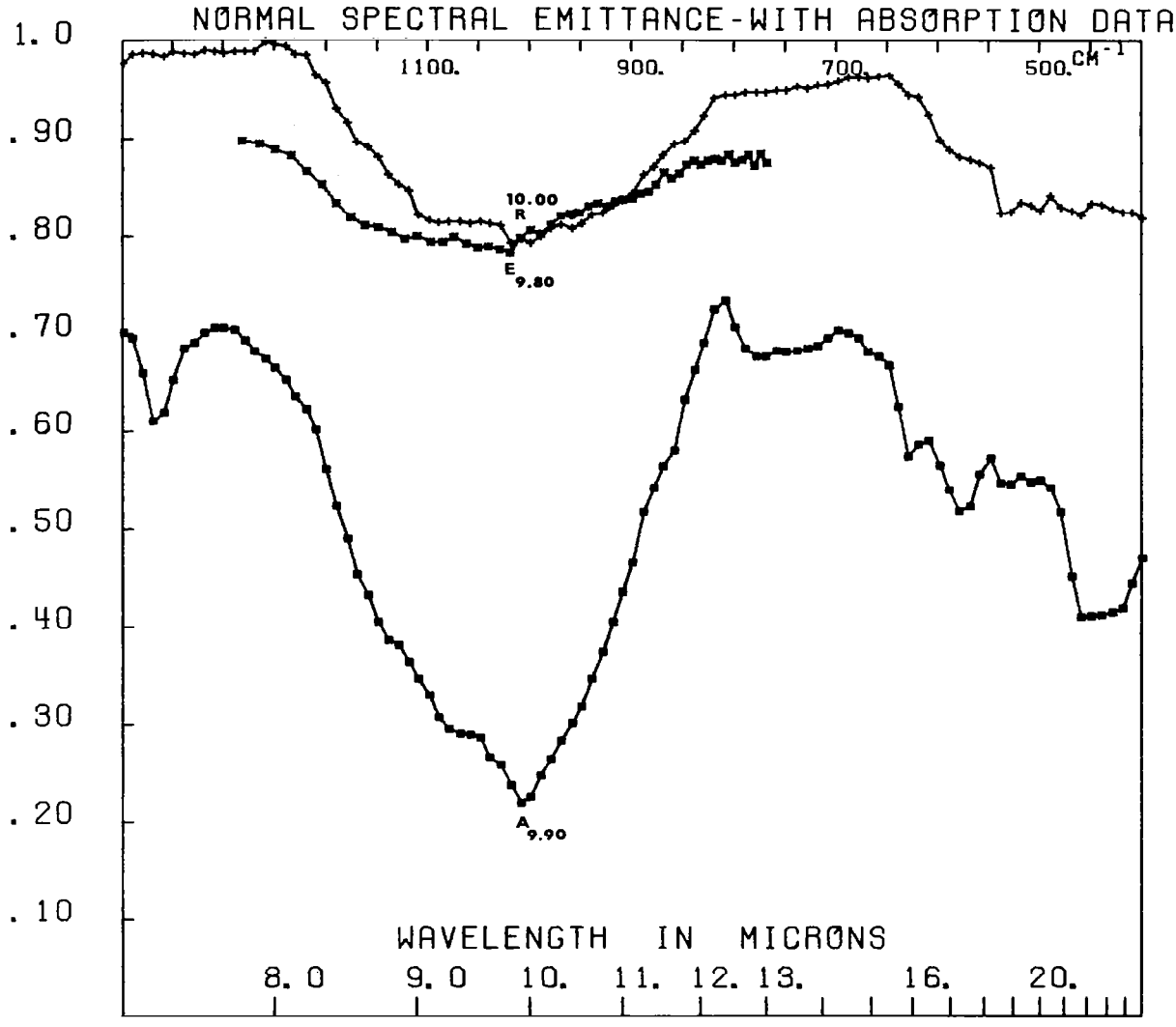

FIG. A-18 AUGITE DIORITE (GABBRO) (USNM 199) NORMAL SPECTRAL EMITTANCE – WITH ABSORPTION DATA. Peak in absorption spectrum (A) at 1370 cm^{-1} (7.3μ) is from the KBr pellet. Detail at 500 cm^{-1} (20μ) differs between absorption (A) and reflectance (R) and may be due to a local sampling problem (on the polished surface).

USNM 1585
(SRI 3554)

Shaft alongside High Line track, 3/8 mi. South of National Hotel, Cripple Creek Dist., Colo.

SCHIST

Sansome.

Texture	Schistose.	
Constituents	Chief.	Muscovite > quartz > sillimanite.
	Accessory.	Altered plagioclase and orthoclase; magnetite, biotite, chlorite, apatite.
Noteworthy	Sillimanite.	
Occurrence		
Literature	Geol. Cripple Creek, U.S.G.S. P.P. 54, p. 51.	

Analysis by W. T. Schaller.

SiO_2	51.88
Al_2O_3	23.86
Fe_2O_3	7.24
FeO	1.89
MgO	1.43
CaO	.21
Na_2O	.68
K_2O	5.55
TiO_2	.76
P_2O_5	.07
Loss on ignition	6.05
	99.62

IR Spectra	Averaged over this range	
Emittance	ϵ = 0.84, 0.96	(1280 - 770 cm^{-1})
Reflectance	$1-\rho$ = 0.88	(1400 - 400 cm^{-1})
Transmittance (un-normalized)	τ = 0.54	(1400 - 400 cm^{-1})

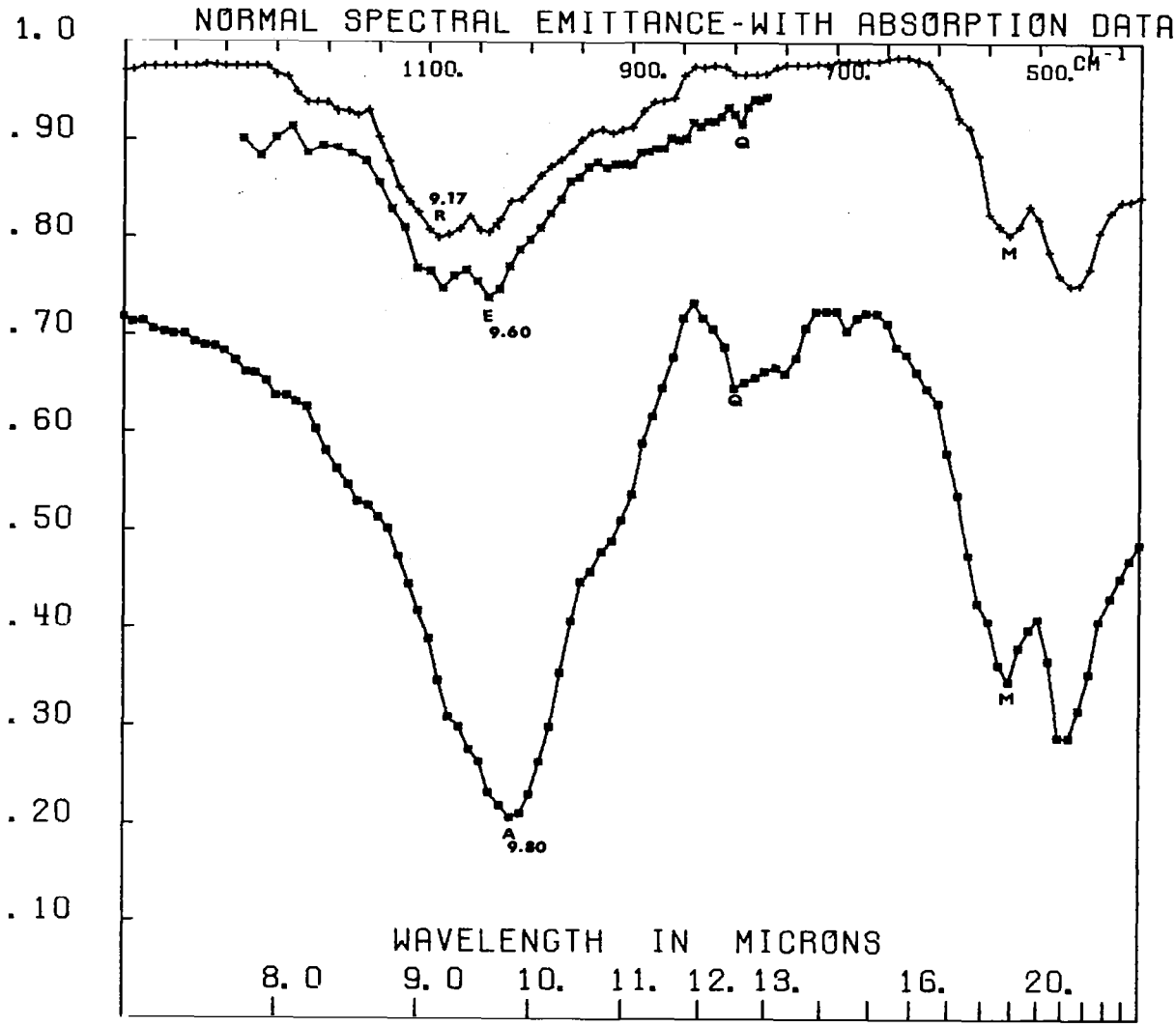

FIG. A-19 SCHIST (MUSCOVITE-QUARTZ) (USNM 1585) NORMAL SPECTRAL EMITTANCE – WITH ABSORPTION DATA. Both emittance (E) and reflectance (R) spectra showed variations in duplicate runs, as one run was taken with the slits parallel to, instead of across, the linear fabric of the schist. There was a good correlation between spectra produced by all techniques. Quartz (Q) peak occurs in (A) at 800 cm^{-1} (12.5μ). The (Q) peak at 800 cm^{-1} in (E) may also be real. A mica (M) peak is shown at 530 cm^{-1} (18.8μ).

USNM 106
(SRI 3591)

West Rock,
New Haven, Conn.

DIABASE (Pirsson) L. H. W.

Structure Holocrystalline, hypidiomorphic, "ophitic".

Constituents

Chief. Plagioclase (labradorite-andesine) x pyroxene (two kinds: light, undetermined; brown = augite) >> orthoclase (biotite).

Accessory. Apatite, magnetite, ilmenite.

Secondary. Serpentine, chlorite?

Noteworthy Alteration of light pyroxene to serpentine, dark pyroxene is fresh, ophitic structure with augite glass or chlorite-like substance. Intersertal microperthite of quartz and orthoclase. Ilmenite

Comment Normal diabase.

Occurrence Intrusive sheet or lava flow.

Literature

Pirsson, L. V., Bull. U.S.G.S. 150, p. 267.
Hawes, G. W., Am. Jour. Sci. 3d Vol. 9, 1875, p. 185.
Hovey, E. O., Am. Jour. Sci. Vol. 38, 1889, p. 361.

Analysis of diabase from West Rock, New Haven, Conn., Bull. 150, p. 272, Hawes, analyst.

SiO_2	51.78
TiO_2	1.41
Al_2O_3	12.79
Fe_2O_3	3.59
FeO	8.25
MnO	.44
CaO	10.70
MgO	7.63
Na_2O	2.14
K_2O	.39
Ignition	.63
P_2O_3	.14
Total	99.89

IR Spectra	Averaged over this range	
Emittance	$\epsilon = 0.83$	(1280 - 770 cm^{-1})
Reflectance	$1-\rho = 0.89$	(1400 - 400 cm^{-1})
Transmittance (un-normalized)	$\tau = 0.56$	(1400 - 400 cm^{-1})

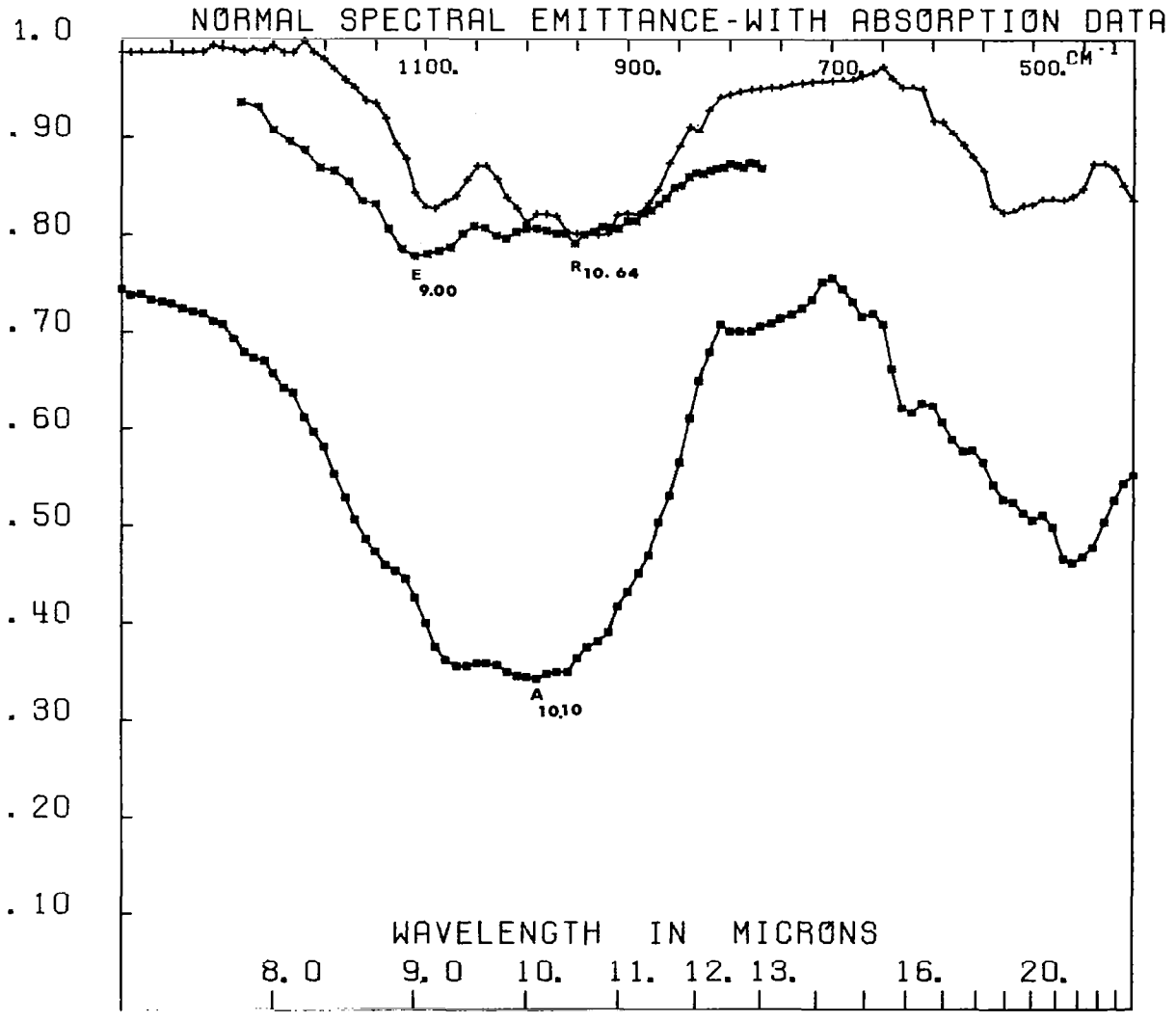

FIG. A-20 DIABASE (USNM 106) NORMAL SPECTRAL EMITTANCE – WITH ABSORPTION DATA. Emittance (E) spectrum emphasizes shorter wavelength (1110 cm^{-1}; 9.00μ) peak in the multiple band; otherwise all 3 methods can be correlated.

USNM 102
(SRI 3540)

Watchung Mountain,
Orange, N. J.

BASALT Auvergnose No. 10 W.T. p. 331 (J. P. Iddings) L. H. W.

Structure: Subcrystalline, hypidiomorphic.

Constituents:
- Chief. Pyroxene (malacolite) > placioclase (labradorite, anorthite?) > olivine (altered)
- Secondary. Serpentine, prehnite? chlorite.
- Base. Remnants of a glass base with globulites and microlites, mostly of augite with grains of magnetite.

Noteworthy: Decomposition of olivines to serpentine; decomposed olivines within pyroxenes. Decomposition of feldspar to prehnite?
Dark reddish intersticial substance not described.

Occurrence: Sheet in redstone (Juratrias) of New Jersey.

Literature: Iddings, J. P., Bull. U.S.G.S. 150, p. 254.
Am. Jour. Sci. 3d Vol. 31, 1886, p. 321.

Analysis of basalt from Watchung Mountain, New Jersey, Bull. No. 150, p. 255, L. G. Eakins, analyst.

SiO_2	- - - -	51.36	MgO	- - - -	7.97
Al_2O_3	- - - -	16.25	K_2O	- - - -	1.06
Fe_2O_3	- - - -	2.14	Na_2O	- - - -	1.54
FeO	- - - -	8.24	H_2O	- - - -	1.33
MnO	- - - -	.09	CO_2	- - - -	----
NiO	- - - -	.03			
CaO	- - - -	10.27	Total	- - - -	100.28

IR Spectra	Averaged over this range	
Emittance	$\epsilon = 0.69$	(1280 - 770 cm^{-1})
Reflectance	$1-\rho = 0.86, 0.88$	(1400 - 400 cm^{-1})
Transmittance (un-normalized)	$\tau = 0.49$	(1400 - 400 cm^{-1})

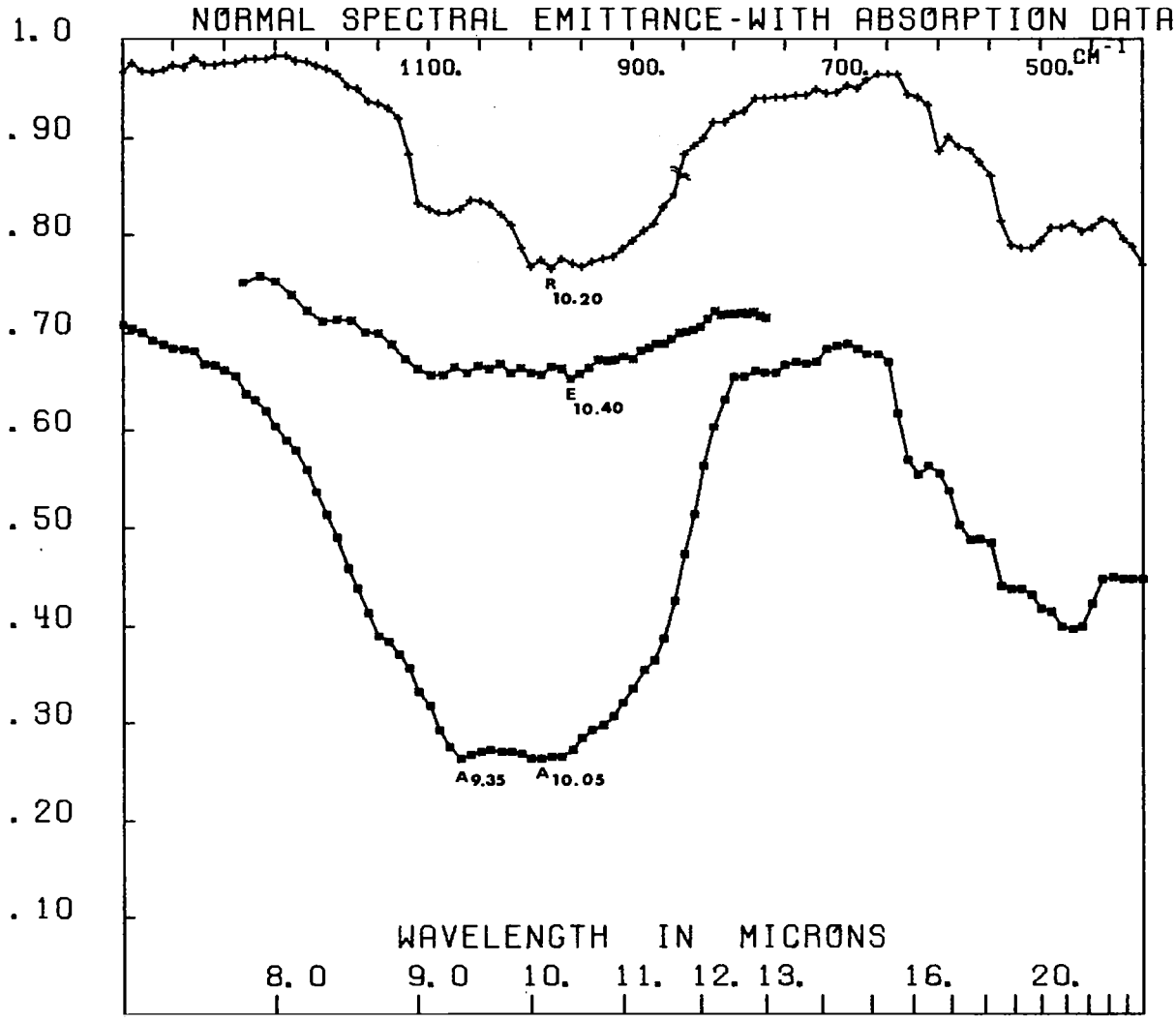

FIG. A-21 BASALT (USNM 102) NORMAL SPECTRAL EMITTANCE – WITH ABSORPTION DATA. Compare with Fig. A-22, for a sample with a higher plagioclase feldspar (F) content.

USNM 535
(SRI 3590)

North Table Mountain,
Golden, Jefferson Co., Colorado
(Denver Coll. No. 939)

PLAGIOCLASE-BASALT Shoshonose No. 20. W.T.p. 269

Structure	Porphyritic.	Phenocrysts < groundmass.
	Phenocrysts.	Well marked off from groundmass.
	Groundmass.	Holocrystalline. Imperfect intersertal.
Constituents	Phenocrysts.	Augite > plagioclase (labradorite).
	Groundmass.	Plagioclase > augite > orthoclase (?) > magnetite
	Accessory.	Apatite.
	Secondary.	Serpentine (after olivine?)
Noteworthy	Relatively high potash in chem. analysis. Peculiar plagioclase phenocrysts.	
Comment	No olivine seen in sections. (F.L.R.)	
Occurrence	Submarine lava-flow.	
Literature	Cross, W., Monog. XXVII, U.S.G.S. pp. 307-308	

Analysis by L. G. Eakins

SiO_2	49.69
TiO_2	.85
Al_2O_3	18.06
Fe_2O_3	2.64
FeO	6.19
MnO	.13
CaO	8.24
MgO	5.73
K_2O	3.90
Na_2O	2.99
P_2O_5	.81
Cl	.13
H_2O	.91
	100.27

IR Spectra	Averaged over this range	
Emittance	ϵ = 0.86, 0.89	(1280 - 770 cm^{-1})
Reflectance	$1-\rho$ = 0.90	(1400 - 400 cm^{-1})
Transmittance (un-normalized)	τ = 0.49	(1400 - 400 cm^{-1})

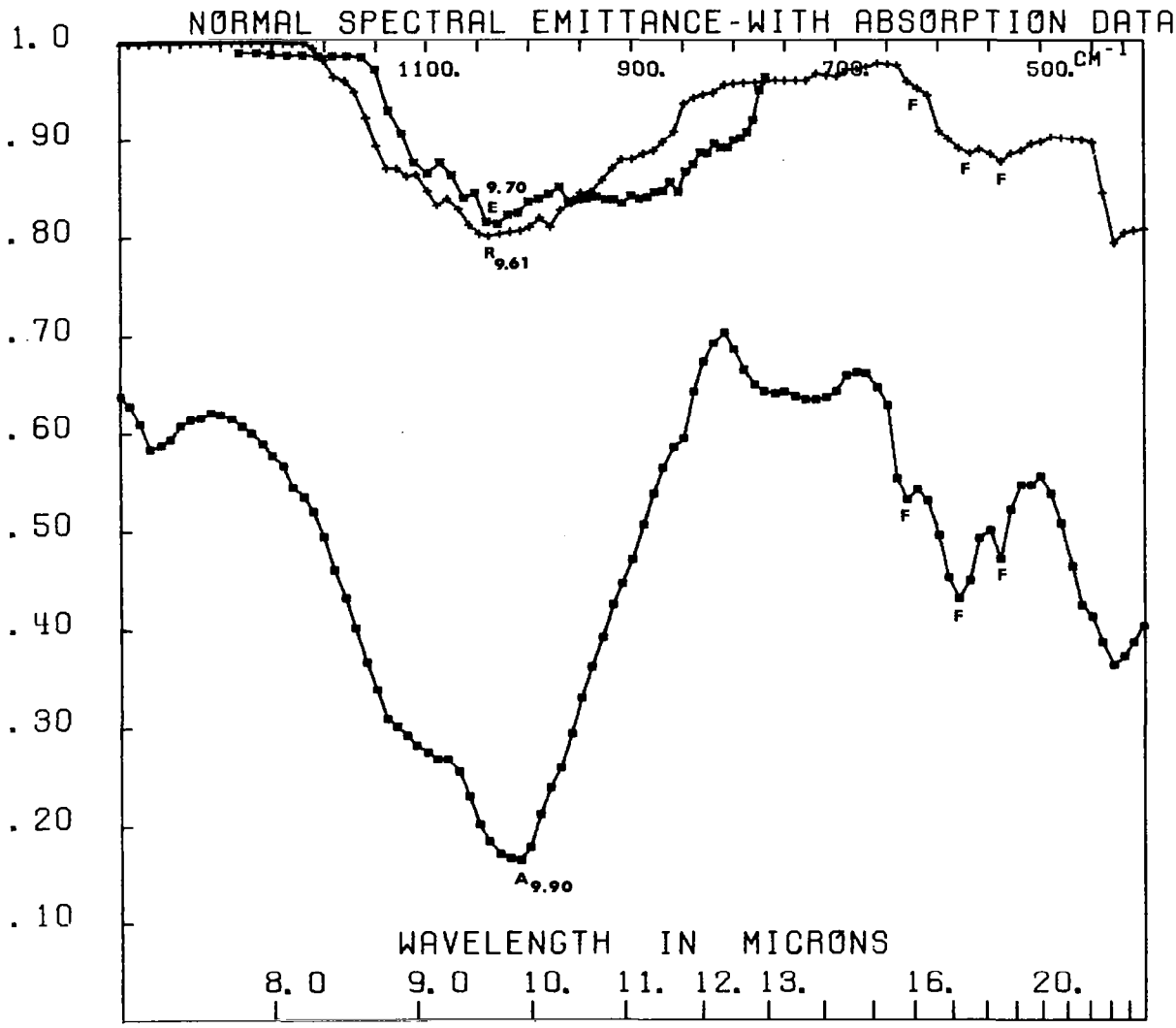

FIG. A-22 PLAGIOCLASE BASALT (USNM 535) NORMAL SPECTRAL EMITTANCE – WITH ABSORPTION DATA. Compare with Fig. A-21 for sample with lower feldspar (F) content. Extra crystalline material results in sharpened spectral contrasts.

USNM 1499
(SRI 3594)

East side Highwood Gap,
Highwood Mts., Mont.

LEUCITE-MONCHIQUITE (Monchiquose) Weed and Pirsson. J.

Texture	Porphyritic	Phenocrysts $\gtrless$ groundmass
	Phenocrusts	Short thick prisms and cross section
	Groundmass	Dark holocrystalline
Constituents	Phenocrysts	Augite > analcite > leucite > olivine
	Groundmass	Augite, iron ore, analcite; probably no glass
	Accessory	Magnetite > apatite
	Secondary	Ferruginous serpentine around olivine
Noteworthy	Analcite	
Occurrence	Dike	
Literature	Pirsson, Highwood Mts., Bull. 237, U.S.G.S. p. 149	

Analysis by H. W. Foote

SiO_2	47.82	TiO_2	.67
Al_2O_3	13.56	P_2O_5	1.10
Fe_2O_3	4.73	SO_3	Trace
FeO	4.54	Cl	.04
MgO	7.49	MnO	Trace
CaO	8.91	BaO	.16
Na_2O	4.37	SrO	.21
K_2O	3.23	Li_2O	
H_2O-) H_2O+)	3.37		100.20
		Less O =	.01
			100.19

IR Spectra	Averaged over this range	
Emittance	ϵ = 0.84	(1280 - 770 cm^{-1})
Reflectance	$1-\rho$ = 0.90	(1400 - 400 cm^{-1})
Tranmittance (un-normalized)	τ = 0.50	(1400 - 400 cm^{-1})

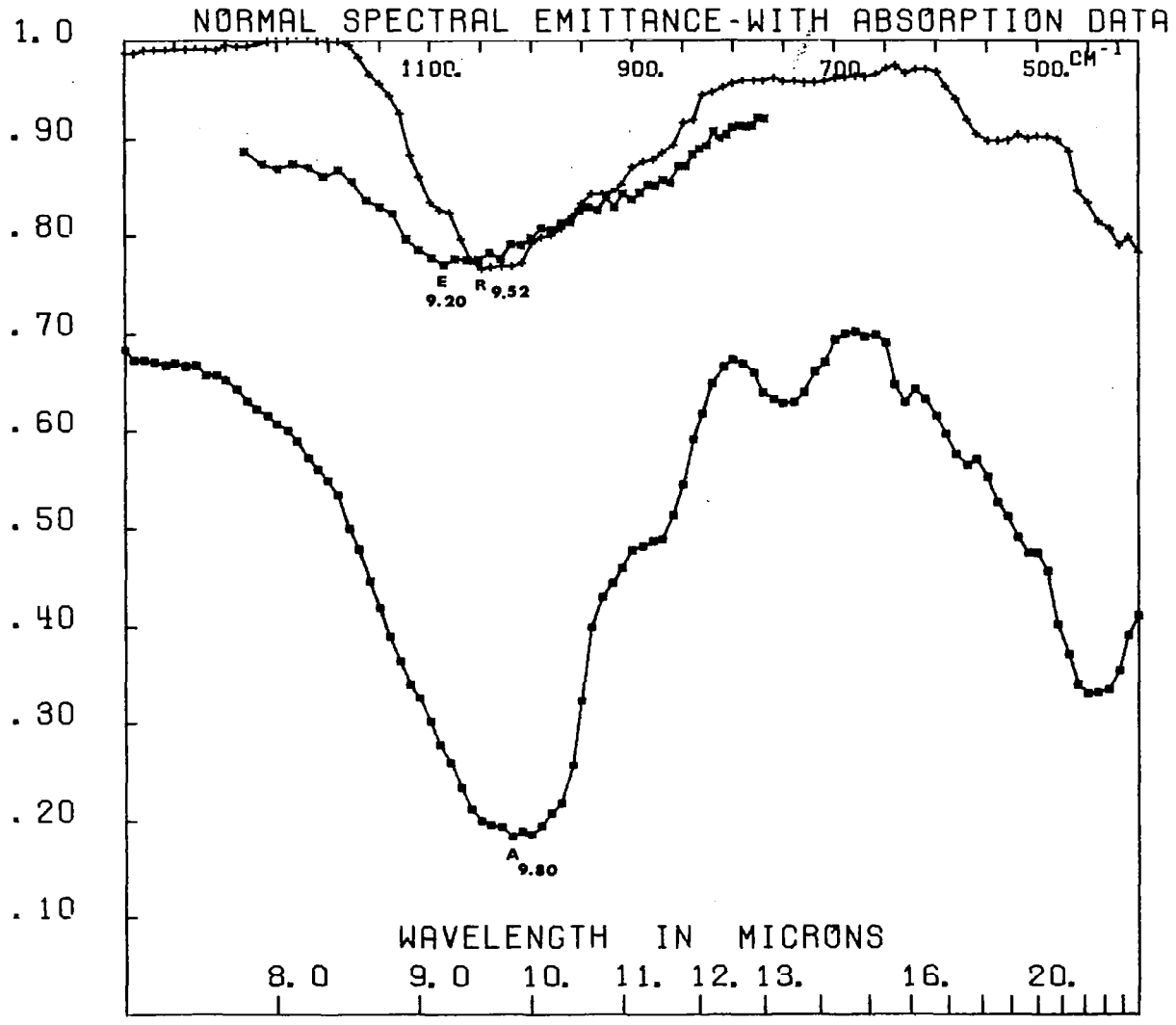

FIG. A-23 MONCHIQUITE (USNM 1499) NORMAL SPECTRAL EMITTANCE – WITH ABSORPTION DATA. Emittance (E) emphasizes shorter wavelength (1085 cm^{-1}; 9.20μ) peak of the multiple band. Peak at 750 cm^{-1} (13.3μ) only appears in the absorption (A) data.

USNM 143
(SRI 3586)

Franklin,
Baltimore Co., Md.

HORNBLENDE-GABBRO-GNEISS (Gabbro Diorite((Iddings)

Structure: Parallel arrangement

Constituents: Chief. Hornblende > feldspar (anorthite Ab_1An_8)
Accessory. Apatite, pyrite, sphene, minute epidotes, zoisite.

Noteworthy: Zoisite. Hornblende sometimes opaque with inclusions of minute black needles of magnetite.

Comment: A metamorphic gabbro.

Literature: Iddings, J. P. (Abstract from G. H. Williams) Bull. U.S.G.S. 150, p. 367.
Williams, G. H., Bull. U.S.G.S. No. 28, 1886, p. 27, 32.

Analysis: Feldspar Analysis, p. 368, W. S. Bayley

	Percent
SiO_2	45.06
Al_2O_3	35.69
CaO	18.30
Na_2O	.95
Total	100.00

Specific gravity, 2.74

Analysis p. 369, by Leroy McCay

	Percent
SiO_2	46.85
TiO_2	.30
Al_2O_3	20.02
Fe_2O_3	2.30
FeO	4.60
MnO	Trace
MgO	10.16
CaO	13.84
Na_2O	1.32
K_2O	Trace
P_2O_5	Trace
H_2O	.88
Total	100.27

Sp. gr., 2.996

IR Spectra	Averaged over this range	
Emittance	ϵ = 0.79, 0.82	(1280 - 770 cm^{-1})
Reflectance	$1-\rho$ = 0.84	(1400 - 400 cm^{-1})
Transmittance (un-normalized)	τ = 0.52	(1400 - 400 cm^{-1})

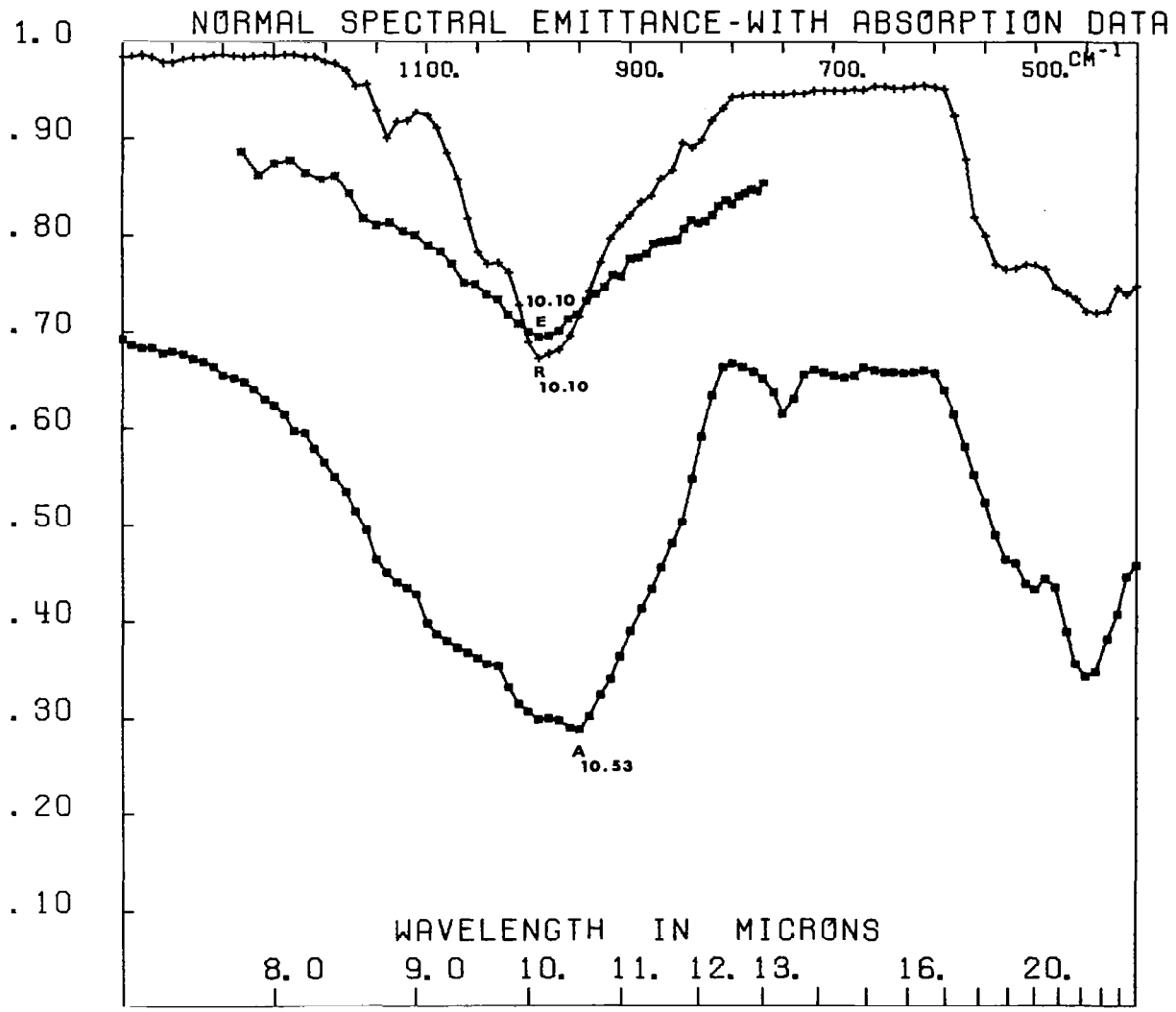

FIG. A-24 HORNBLENDE GABBRO GNEISS (GABBRO DIORITE) (USNM 143) NORMAL SPECTRAL EMITTANCE – WITH ABSORPTION DATA. Peak at 750 cm^{-1} (13.3μ) only appears in the absorption (A) data. Local point at 950 cm^{-1} (10.53μ) increases the main absorption trough; otherwise correlation between techniques is close.

USNM 111
(SRI 3588)

Sudbrook Park, Baltimore Co., Maryland

PERIDOTITE (Fedispathic Peridotite) (Iddings) L.H.W.

Structure: Porphyritic character.

Constituents: Chief. Bronzite and diallage, X olivine >> feldspar (bytownite)
Accessory. Hornblende sometimes.
Secondary. Serpentine, magnetite, scolecite, bastite (?)

Noteworthy: Olivine altered to serpentine and magnetite.
Porphyritic character in this class of rocks, with olivine in the ground mass indicating that it is here the youngest instead of the oldest constituent as is generally the case.
Bronzite altered to serpentine. Bright polarizing spots in bronzite due to intergrowth of diallage.
Minute fibres of bastite (?)
Occurrence of feldspar. Reactionary rimes of amphibole around bytownite. Unusual alteration to probable scolecite.

Comment: The feldspar composes about 5% of the rock.

Occurrence: Dikes

Literature: Iddings, J. P., (abstract from G. H. Williams) Bull. U.S.G.S. 150, p. 288, and Bull. 28, p. 43.

Analysis of peridotite from Sudbrook Park, Baltimore County, Maryland; Bull. No. 150, p. 290, Dr. Leroy McCay, analyst.

SiO_2	41.00	CaO	10.08
Al_2O_3	7.58	MgO	23.59
Fe_2O_3	5.99	Na_2O	.52
FeO	4.63	CO_2	3.62
MnO	Trace	H_2O	4.73
		Total	101.74

Spec. gravity, 2.989.

IR Spectra	Averaged over this range	
Emittance	$\epsilon = 0.88$	(1280 - 770 cm^{-1})
Reflectance	$1-\rho = 0.84$	(1400 - 400 cm^{-1})
Transmittance (un-normalized)	$\tau = 0.55$	(1400 - 400 cm^{-1})

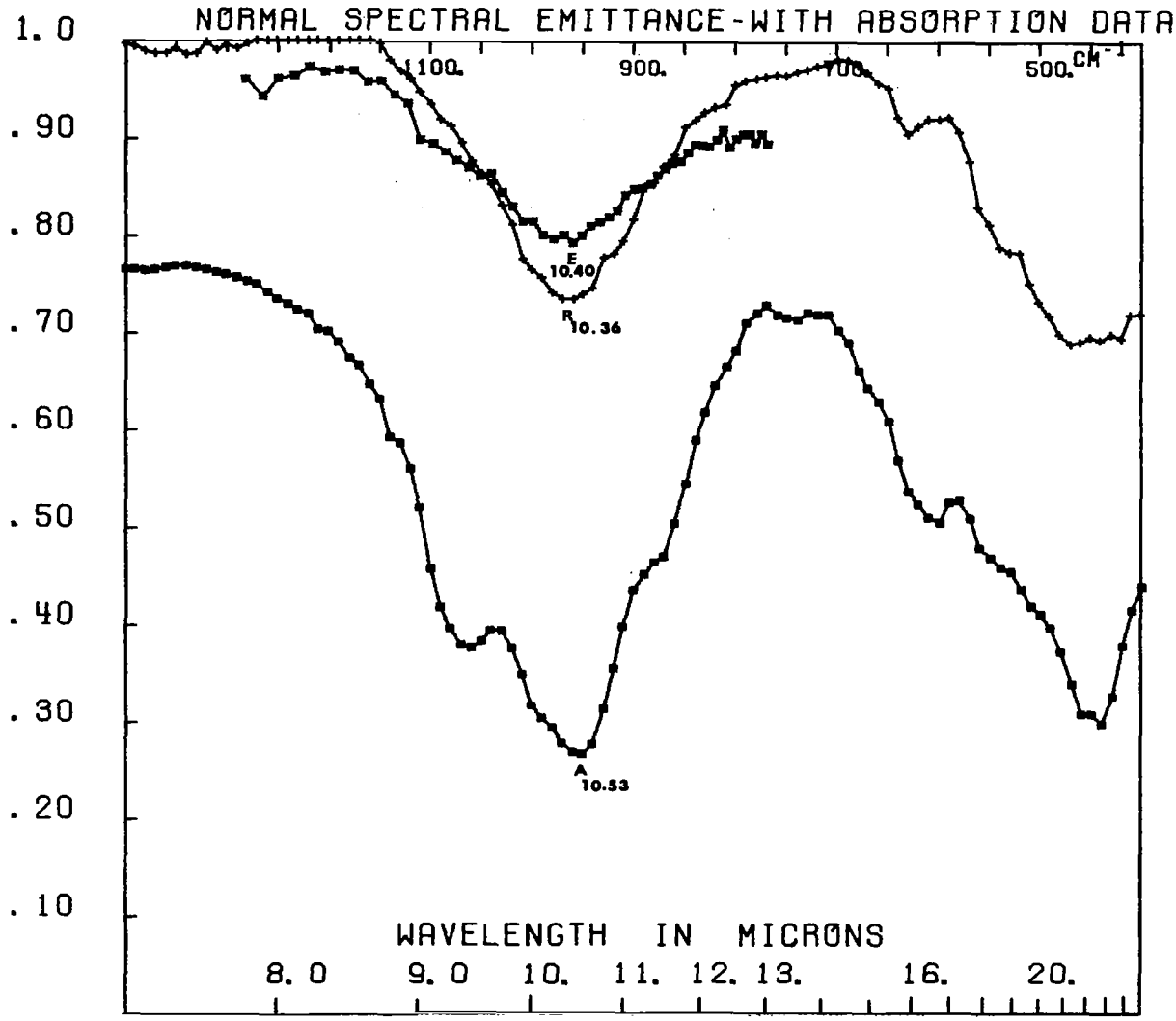

FIG. A-25 PERIDOTITE (USNM 111) NORMAL SPECTRAL EMITTANCE – WITH ABSORPTION DATA. Spectra show excellent correlation between techniques.

USNM 1734
(SRI 3585)

Big Timber Creek,
Crazy Mountains, Montana

OLIVINE GABBRO (IV. 2^2. 1^2. 2.) J. E. Wolff

Constituents Labradorite (?), brown hornblende, augite, olivine, and magnetite.

Literature U.S.G.S. Bull. 228, p. 139, Anal. "O"
U.S.G.S. Bull. 419, p. 82.

[Record was made from such information as was furnished when the collection was transferred in 1923. M. W. Moodey.]

Analysis by W. F. Hillebrand.

SiO_2	40.42	H_2O- 110°	.45
Al_2O_3	9.98	H_2O+ 110°	1.17
Fe_2O_3	9.83	TiO_2	2.51
FeO	10.67	P_2O_5	.63
MgO	11.56	MnO	.25
CaO	10.78	BaO	.05
Na_2O	1.26	SrO	.02
K_2O	.60	Li_2O	trace
		(CaNi)O	.02
			100.20

IR Spectra	Averaged over this range	
Emittance	$\epsilon = 0.83$	(1280 - 770 cm^{-1})
Reflectance	$1-\rho = 0.87$	(1400 - 400 cm^{-1})
Transmittance (un-normalized)	$\tau = 0.57$	(1400 - 400 cm^{-1})

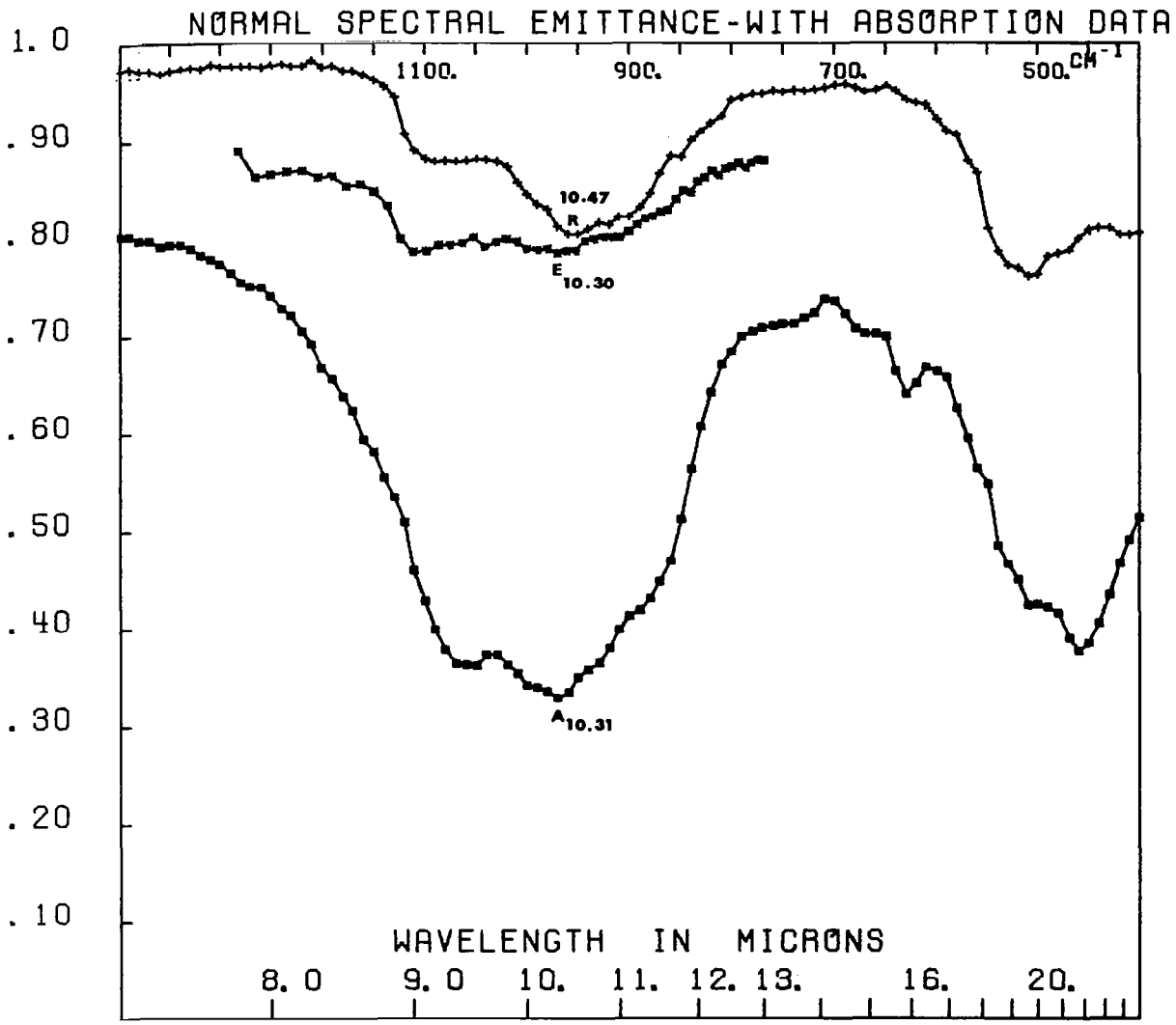

FIG. A-26 OLIVINE GABBRO (USNM 1734) NORMAL SPECTRAL EMITTANCE – WITH ABSORPTION DATA. Emittance (E) shows short wavelength emphasis; otherwise methods show comparable spectral results.

USNM 1065
(SRI 3583)

Tom Nunn's Hill, S.S.W. of Uvalde,
Uvalde quadrangle, Texas.

NEPHELITE-BASALT

(T. W. Vaughan)
(Uvaldose, U.S.G.S.B. 228, p. 72)

Structure	Porphyritic.	Phenocrysts < groundmass.
	Groundmass.	Fine-grained with idiomorphic augite.
Constituents	Phenocrysts.	Olivine > augite.
	Groundmass.	Augite > nephelite x magnetite > apatite.
	Secondary.	Serpentine from olivine.

Noteworthy

Comment Olivine is the only megascopic phenocryst.

Occurrence

Analysis by W. F. Hillebrand. U.S.G.S. Bull. 168, p. 62, Analy. "G"

SiO_2	40.32			
Al_2O_3	9.46	including Cr_2O_3	P_2O_5	.68
Fe_2O_3	4.75		Cl	.05
FeO	7.48		F	.04
MgO	18.12		S	.01
CaO	10.55		Cr_2O_3	included in Al_2O_3 above
Na_2O	2.62		NiO	.06
K_2O	1.10		MnO	.25
H_2O-	.57		BaO	.06
H_2O+	1.25		SrO	.03
TiO_2	2.66		Li_2O	trace
ZrO_2	None		SO_3	.03
				100.09
			Less O	.03
				100.06

Sp. gr. 3.148 at 19°

IR Spectra	Averaged over this range	
Emittance	$\epsilon = 0.90$	(1280 - 770 cm^{-1})
Reflectance	$1-\rho = 0.85$	(1400 - 400 cm^{-1})
Transmittance	$\tau = 0.49$	(1400 - 400 cm^{-1})

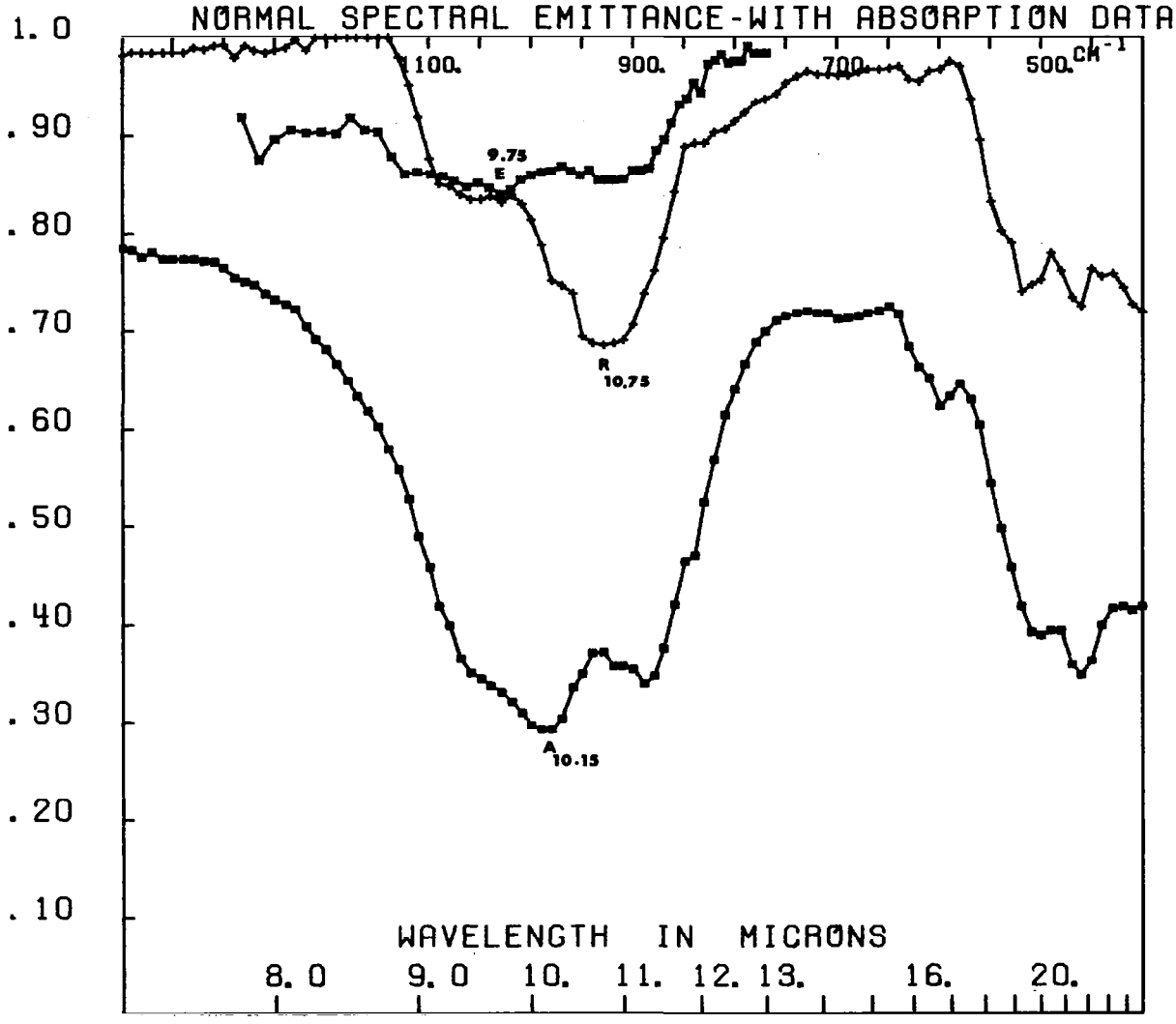

FIG. A-27 NEPHELINE BASALT (USNM 1065) NORMAL SPECTRAL EMITTANCE – WITH ABSORPTION DATA. Long wavelength peak (at 900 cm^{-1}; 11.1μ) is emphasized by the reflectance (R) peak at 930 cm^{-1} (10.75μ). Emittance (E) spectrum shows both peaks.

USNM 145
(SRI 3539)

Greenville, Plumas County, California

SERPENTINE

Structure	Irregularly fibrous.
Constituents	Chief. Serpentine. Accessory. Magnetite > chromite
Noteworthy	Serpentine, chromite. The "bar structure" of the serpentine shows its probable origin from pyroxene.
Comment	Probably derived from gabbro.
Occurrence	Irregular mass apparently erupted between slates. Quartz porphyry and granite.
Literature	Diller, J. S., Bull. U.S.G.S. 150, p. 372.

Analysis p. 374, by W. H. Melville.

	Percent
Loss	12.70
SiO_2	39.14
Al_2O_3	2.08
Fe_2O_3	4.27
FeO	2.04
CaO	Trace
MgO	39.84
K_2O	-----
Na_2O	-----
Chromite	0.11
Total	100.18

IR Spectra	Averaged over this range	
Emittance	$\epsilon = 0.87$	(1280 - 770 cm^{-1})
Reflectance	$1-\rho = 0.83$	(1400 - 400 cm^{-1})
Tranmittance (un-normalized)	$\tau = 0.47$	(1400 - 400 cm^{-1})

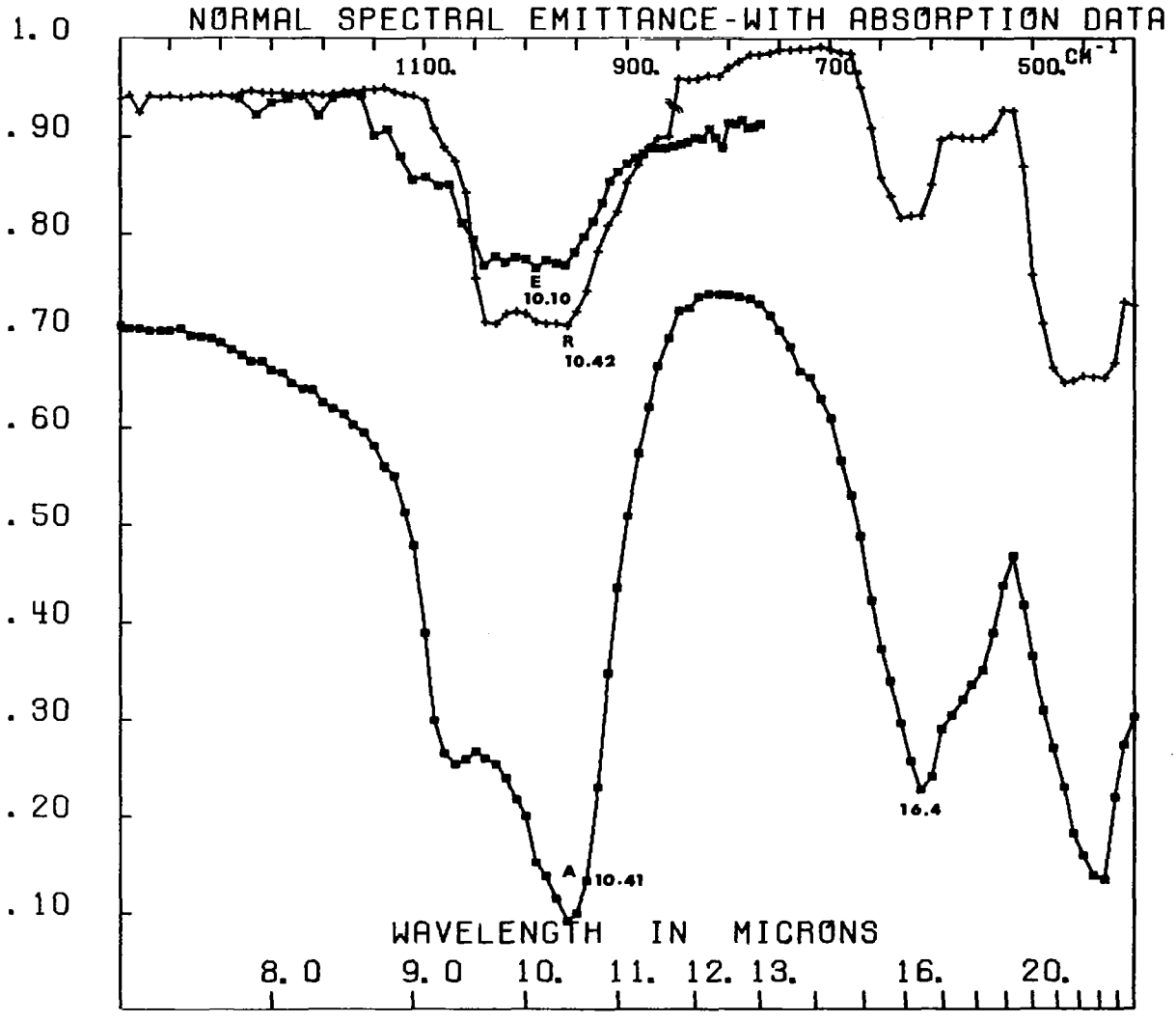

FIG. A-28 SERPENTINE (USNM 145) NORMAL SPECTRAL EMITTANCE – WITH ABSORPTION DATA. Good correlation between methods, except emittance (E). Spectrum shows the 990 cm^{-1} (10.10μ) peak locally stronger in the multiple band. Peak at 610 cm^{-1} (16.4μ) is characteristic of Mg-silicate (serpentine).

USNM 296
(SRI 3589)

Dewitt, near Syracuse, N.Y.

LIMBURGITE

(Darton and Kemp) L.H.W.

Structure	Porphyritic.	Phenocrysts < groundmass.
	Phenocrysts.	Altered, irregular.
	Groundmass.	Holocrystalline.
Constituents	Phenocrysts.	Olivine (altered) > biotite, augite rare.
	Groundmass.	Biotite > augite devitrified glass?
	Accessory.	Magnetite, apatite, perovskite.
	Secondary.	Serpentine, calcite, some magnetite, perhaps some biotite.
Noteworthy	Perovskite,	olivine altered to magnetite and serpentine.
Comment	Much altered rock. Peridotite? Biotite and augite. Phenocrysts not in this slide.	
Occurrence	Dike in Salina formation.	
Literature	Darton and Kemp, Am. Jour. Sci. 3d Vol. 49, p. 456.	

Analysis p. 461 by H. Stokes. (Bull. 168, p. 38)

SiO_2	36.80	Na_2O	.17
Al_2O_3	4.16	Cr_2O_3	.20
Fe_2O_3	-----	P_2O_5	.47
FeO	8.33	CO_2	2.95
TiO_2	1.26	Cl	----
MnO	.13	F	----
NiO	.09	SO_3	.06
CoO	-----	S	.95
CaO	8.63	H_2O below 110°	.51
BaO	.12	H_2O above 110°	6.93
SrO	Trace		100.22
MgO	25.98		
K_2O	2.48	O = S	.47
			99.75

IR Spectra	Averaged over this range	
Emittance	$\epsilon = 0.82$	(1280 - 770 cm^{-1})
Reflectance	$1-\rho = 0.86$	(1400 - 400 cm^{-1})
Transmittance (un-normalized)	$\tau = 0.53$	(1400 - 400 cm^{-1})

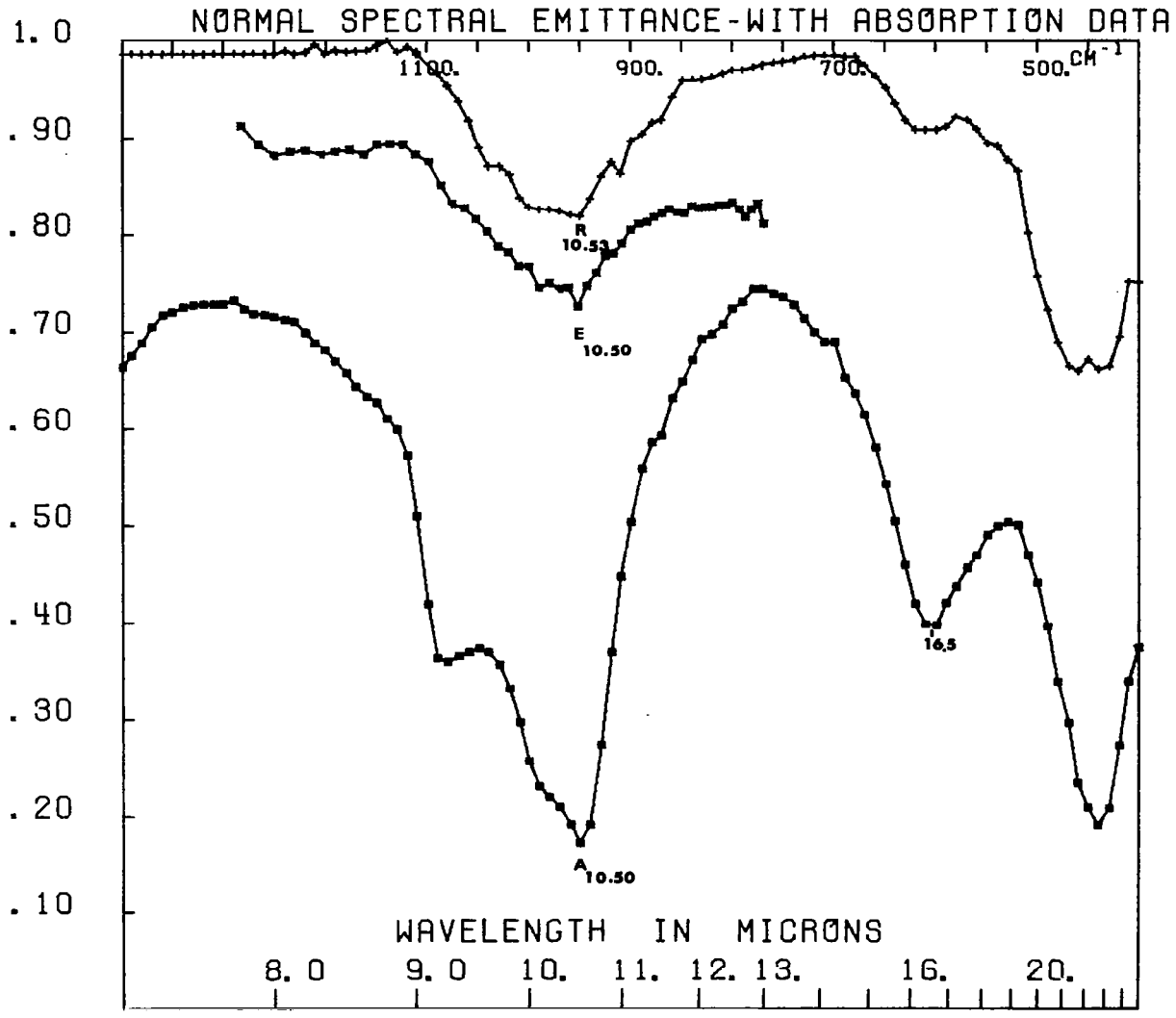

FIG. A-29 LIMBURGITE (USNM 296) NORMAL SPECTRAL EMITTANCE – WITH ABSORPTION DATA. Closely resembles serpentine of Fig. A-28. Excellent correlation between techniques. Peak at 605 cm^{-1} (16.5μ) is again present.

APPENDIX B

ROCK SURFACES: RADIANT ENERGY PLOTS

The radiant flux (W_λ, in watts/sq.cm-micron), emitted normally within each spectral increment (0.1 micron, was calculated for a set of samples. Ten temperatures of the sample source were used — 150, 200, 250, 300, 325, 350, 375, 400, 450 and 500°K.

The energy level (W_λ), obtained from the Planck radiation formula, was multiplied by the normal spectral emittance (ϵ_λ) obtained in the course of these studies. This flux level ($\epsilon_\lambda \cdot W_\lambda$) at 375°K has been called "normal spectral emittance — radiant flux in watts/sq.cm-micron" on the figures of Appendix B and C. The numerical values were multiplied by 10,000 to obtain suitable levels.

This terminology is incorrect. The numerical values as plotted are more correctly hemispherical spectral radiant flux and should be reduced by a factor of $1/\pi$ to yield the normal spectral radiant flux emitted per unit solid angle. The units then would be watts/sq.cm-micron-steradian.

The ordinate scale factor is thus 10,000 π rather than 10,000 .

The curves were obtained by these calculations, the uppermost curve being the level of radiant energy at 375°K (lunar noon temperature) given by the radiation law. The middle curve indicates that portion of the energy emitted from the sample.

The lowermost curve was computed by multiplying the sample emittance curve by the attenuation (α_λ) recorded by Taylor and Yates (1956) for the atmosphere in a sea level path length of 3.4 miles. This ($\epsilon_\lambda \cdot W_\lambda \cdot \alpha_\lambda$) curve then represents that portion of the radiant energy of the sample at 375°K which would be seen by an instrument 3.4 miles away under the conditions of Taylor's and Yates' original experiment.

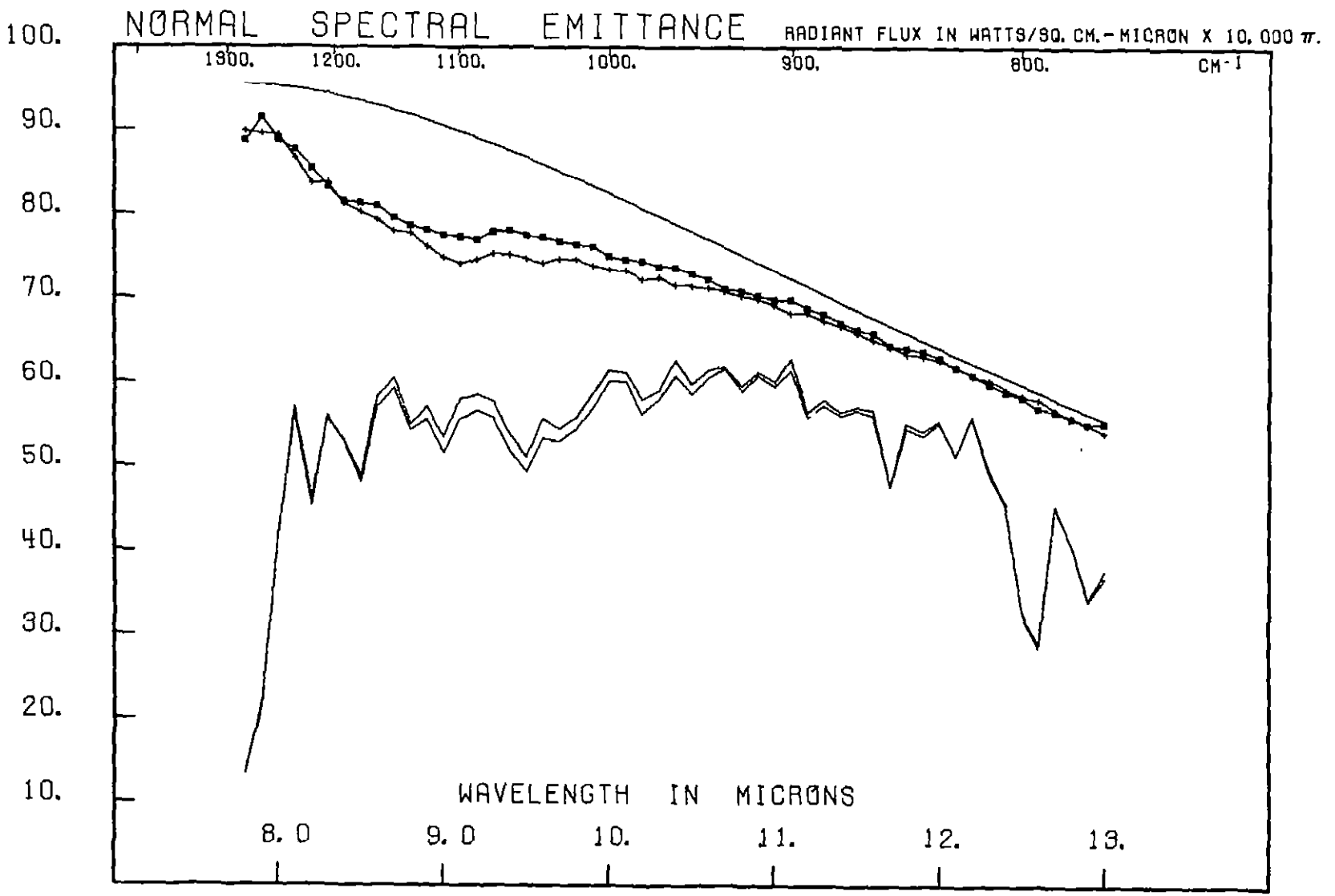

FIG. B-1 DACITE (USNM 82) NORMAL SPECTRAL EMITTANCE – RADIANT FLUX IN WATTS/SQ. CM-MICRON × 10,000 π.
Duplicate runs but both were of sawn surfaces.

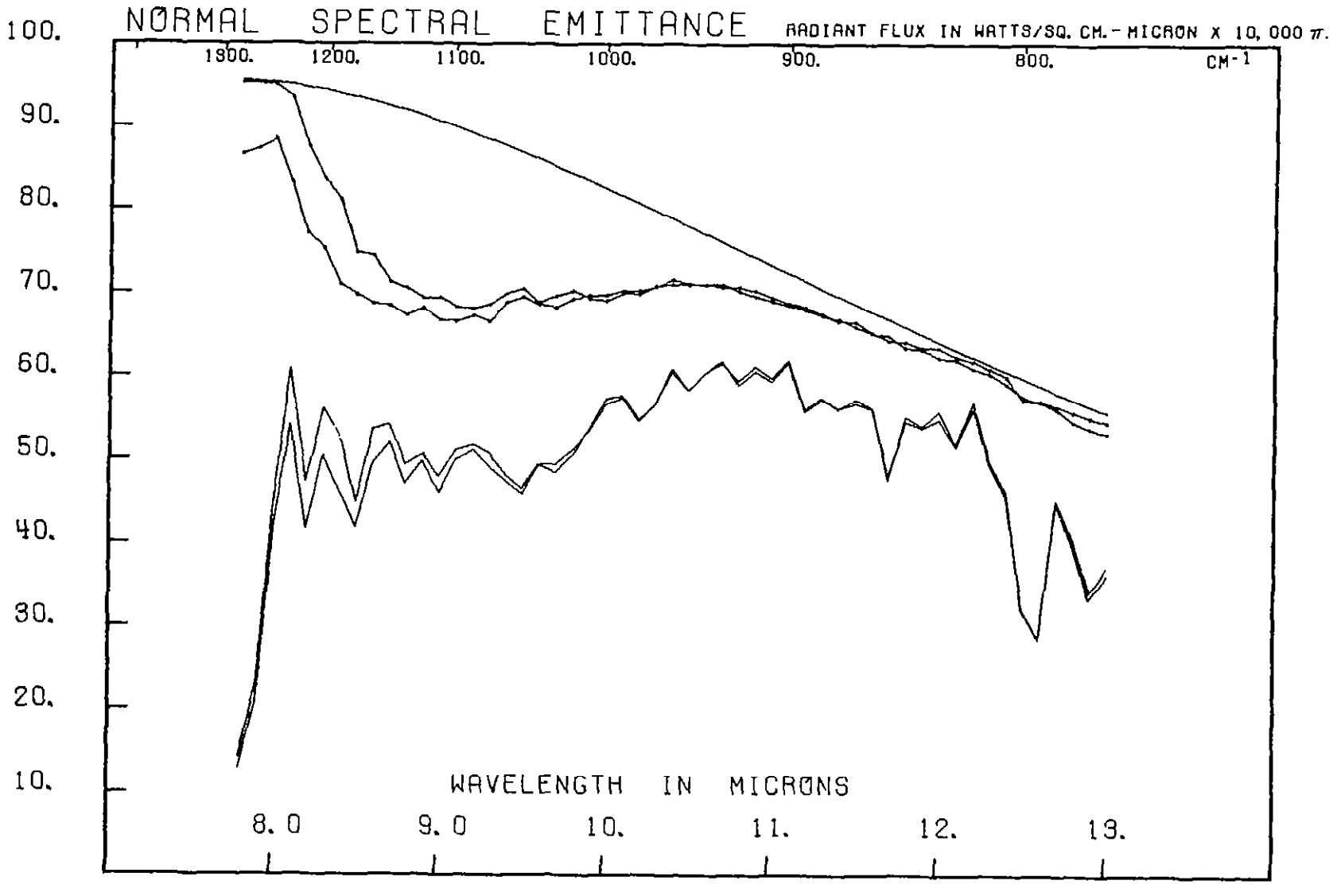

FIG. B-2 GRANITE (USNM 158) NORMAL SPECTRAL EMITTANCE – RADIANT FLUX IN WATTS/SQ. CM-MICRON × 10,000 π.
Rough surfaces, naturally broken.

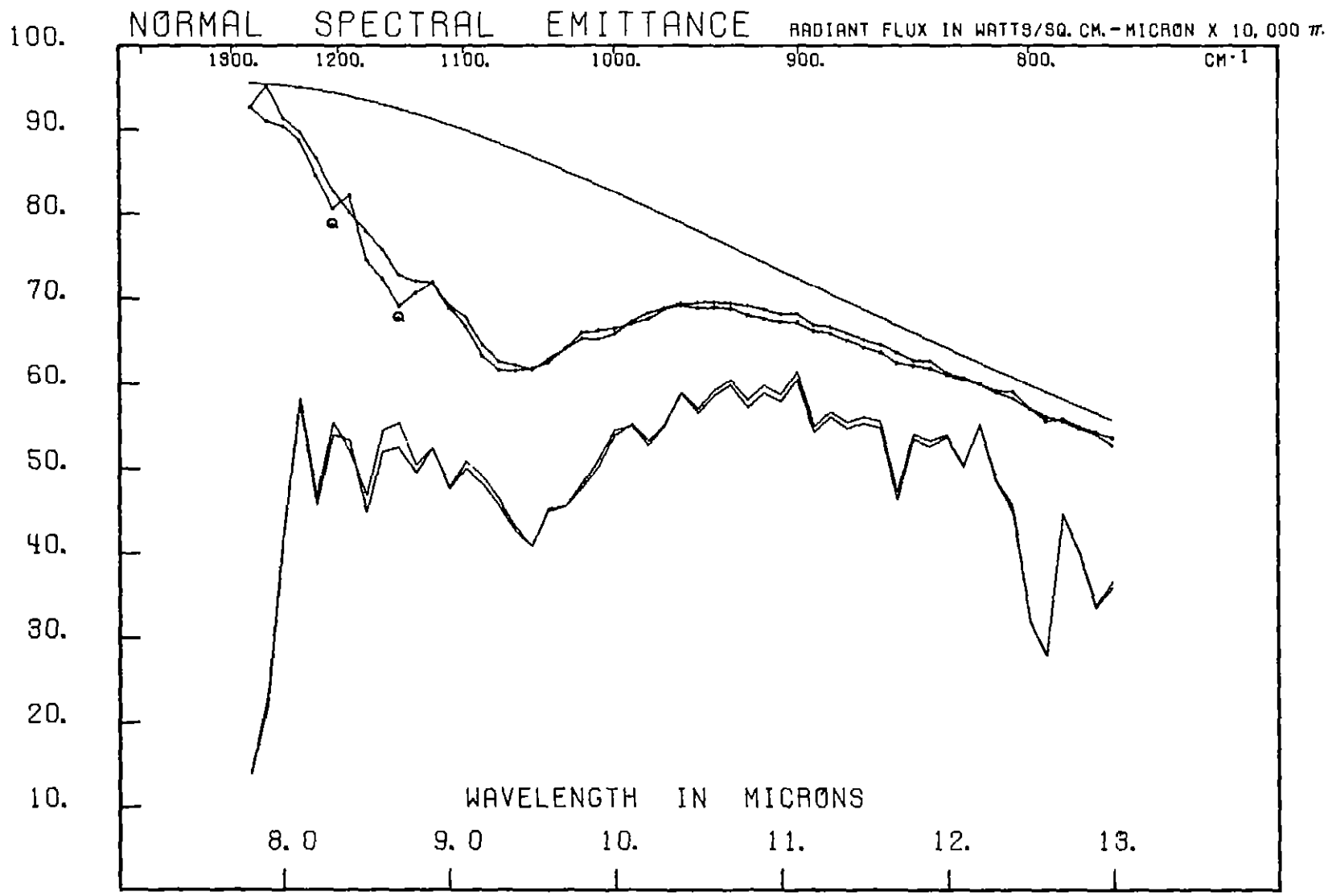

FIG. B-3 GRAPHIC GRANITE (USNM 377) NORMAL SPECTRAL EMITTANCE – RADIANT FLUX IN WATTS/SQ. CM-MICRON × 10,000 π. One spectrum was parallel with the graphic structure, the other was run across the grain (and shows peaks due to quartz Q). *Both were rough, naturally broken surfaces.*

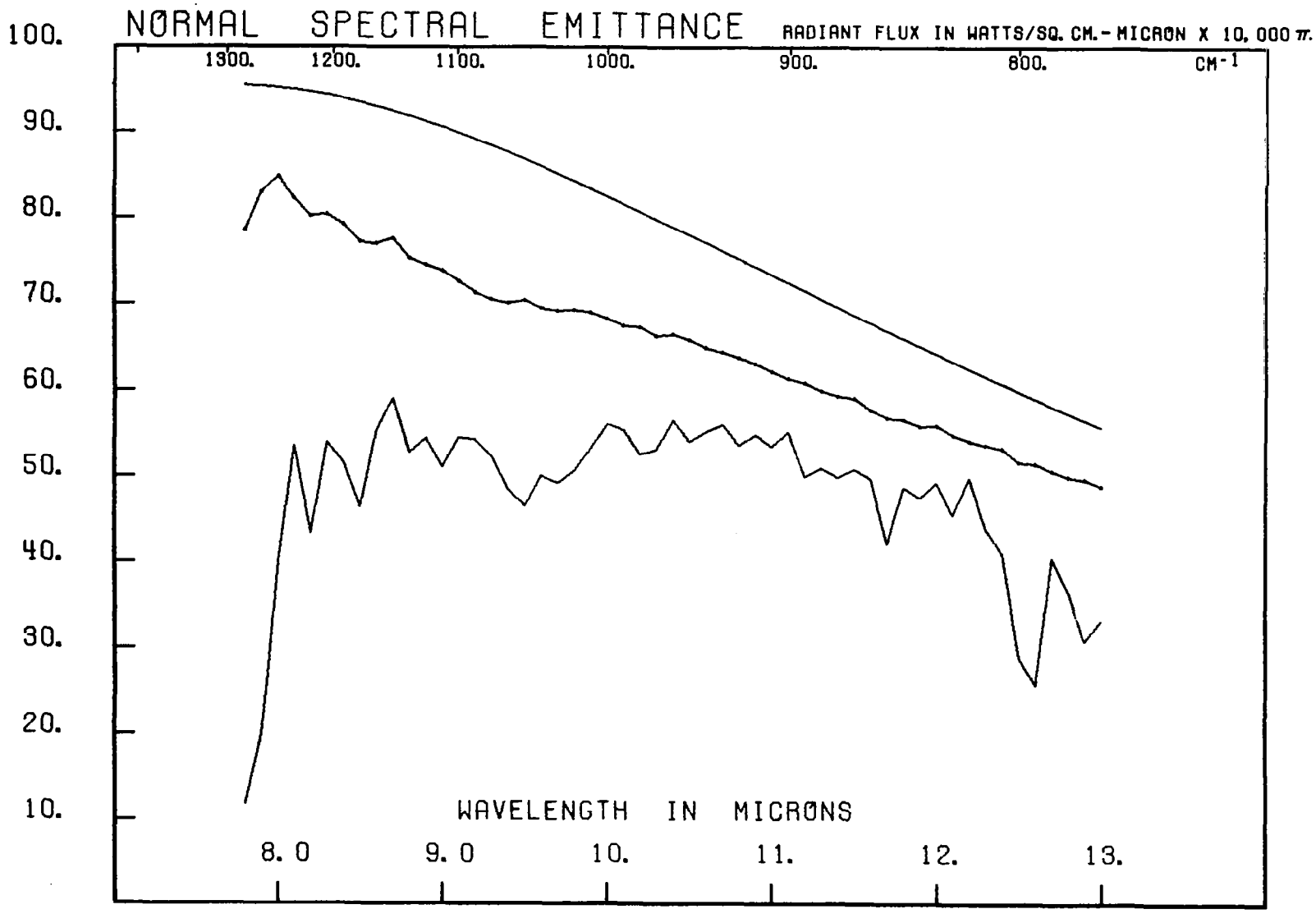

FIG. B-4 RHYOLITE PUMICE (USNM 59) NORMAL SPECTRAL EMITTANCE – RADIANT FLUX IN WATTS/SQ. CM-MICRON × 10,000 π.
Sawn, but highly porous friable surface used.

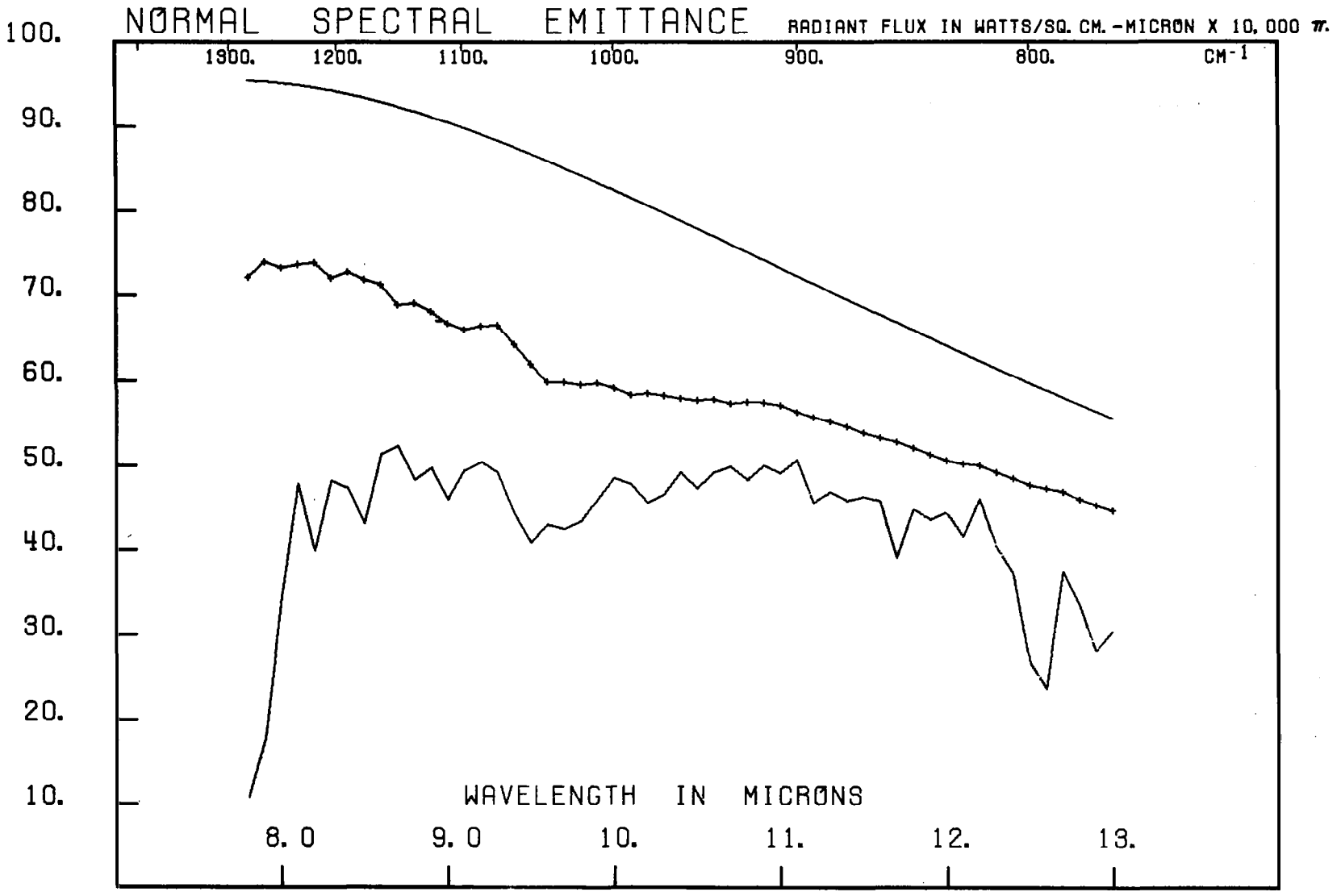

FIG. B-5 ANDESITE (MONZONITE PORPHYRY) (USNM 1331) NORMAL SPECTRAL EMITTANCE – RADIANT FLUX IN WATTS/SQ. CM-MICRON × 10,000π. Rough, broken, natural surface used.

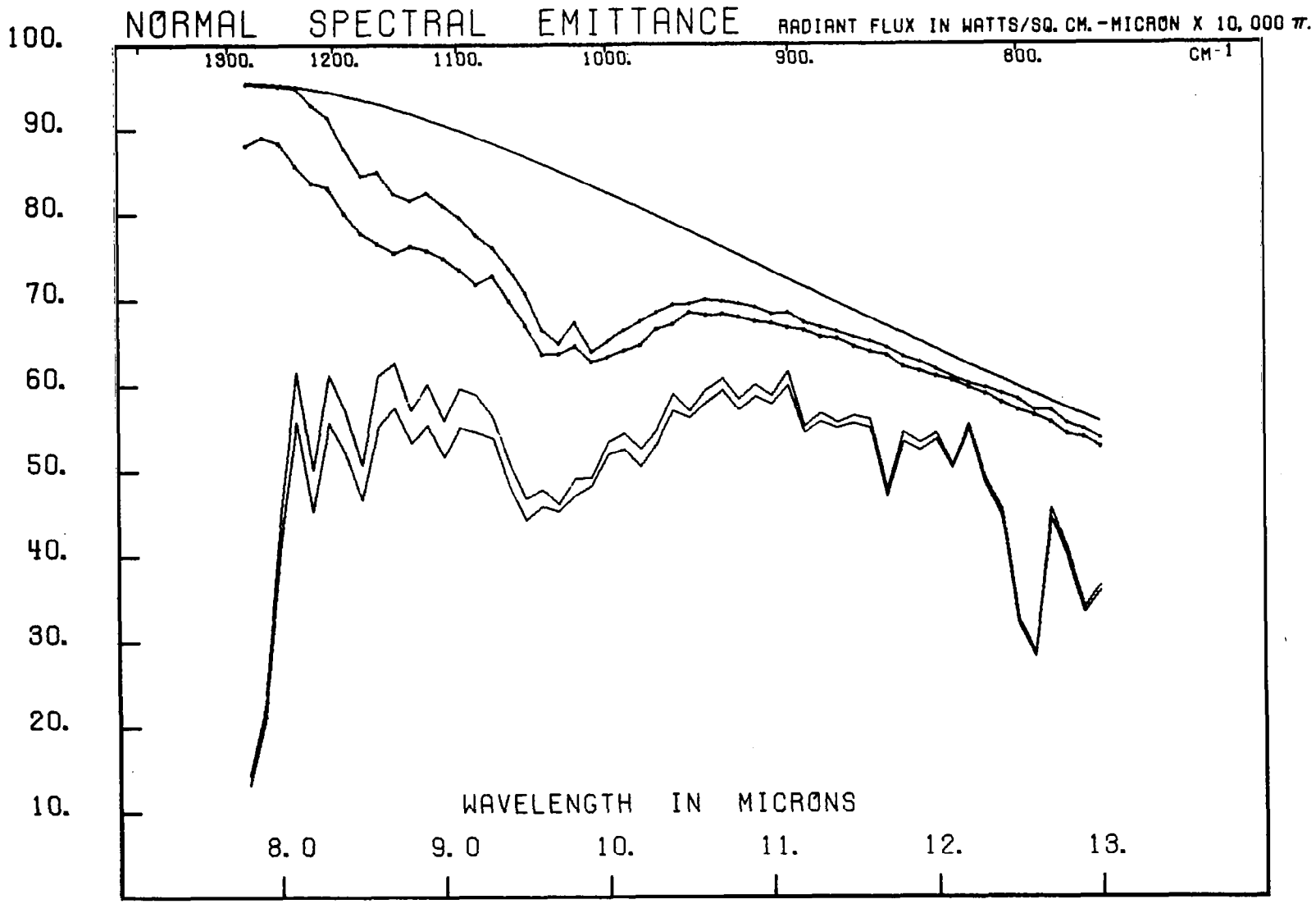

FIG. B-6 NEPHELINE SYENITE (USNM 77) NORMAL SPECTRAL EMITTANCE – RADIANT FLUX IN WATTS/SQ. CM-MICRON × 10,000 π.
Rough broken surface used, with repeated duplicate runs and with changed surface orientations.

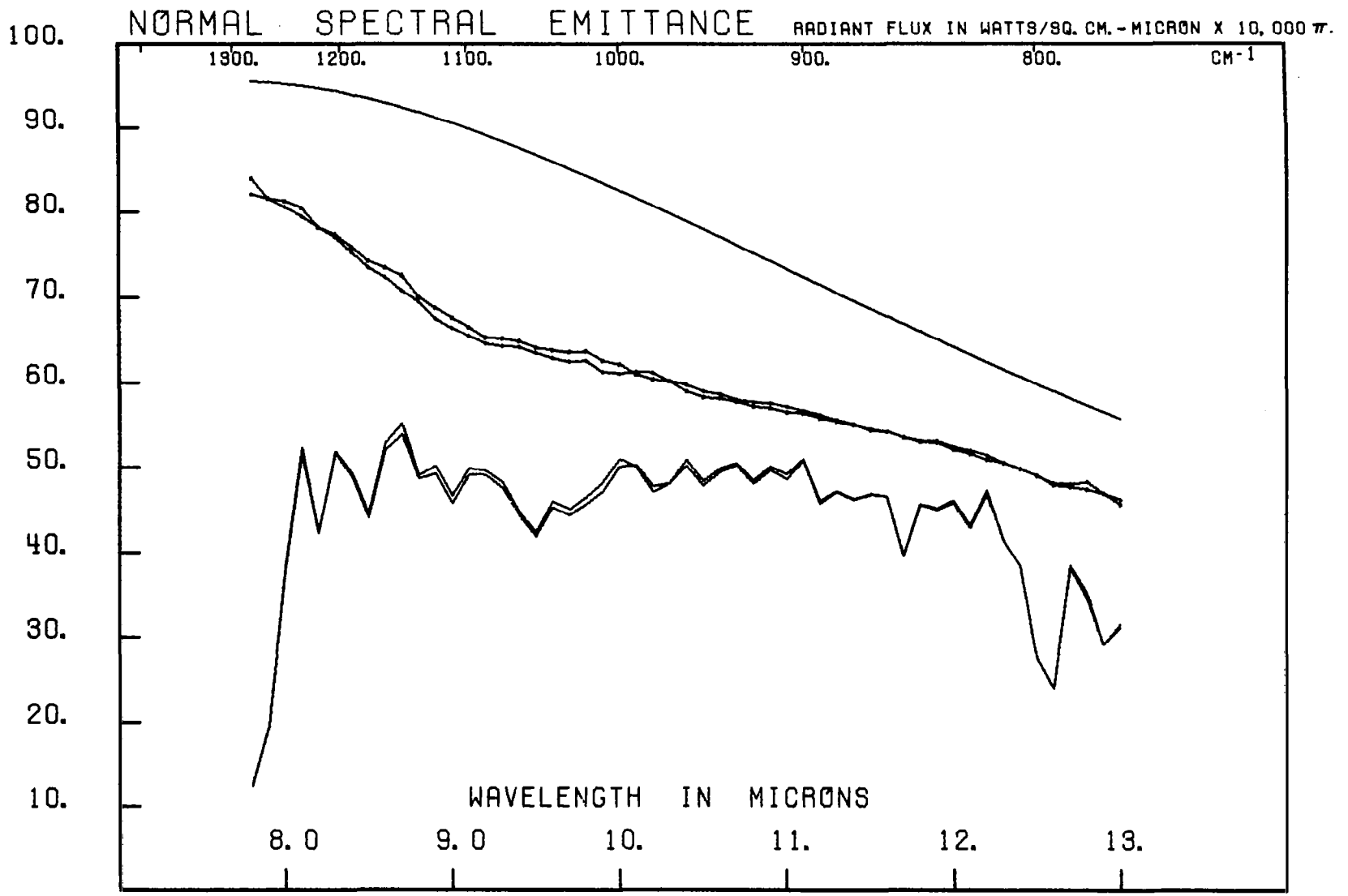

FIG. B-7 HYPERSTHENE ANDESITE (USNM 86) NORMAL SPECTRAL EMITTANCE – RADIANT FLUX IN WATTS/SQ. CM – MICRON × 10,000π. Duplicate runs using a sawn surface.

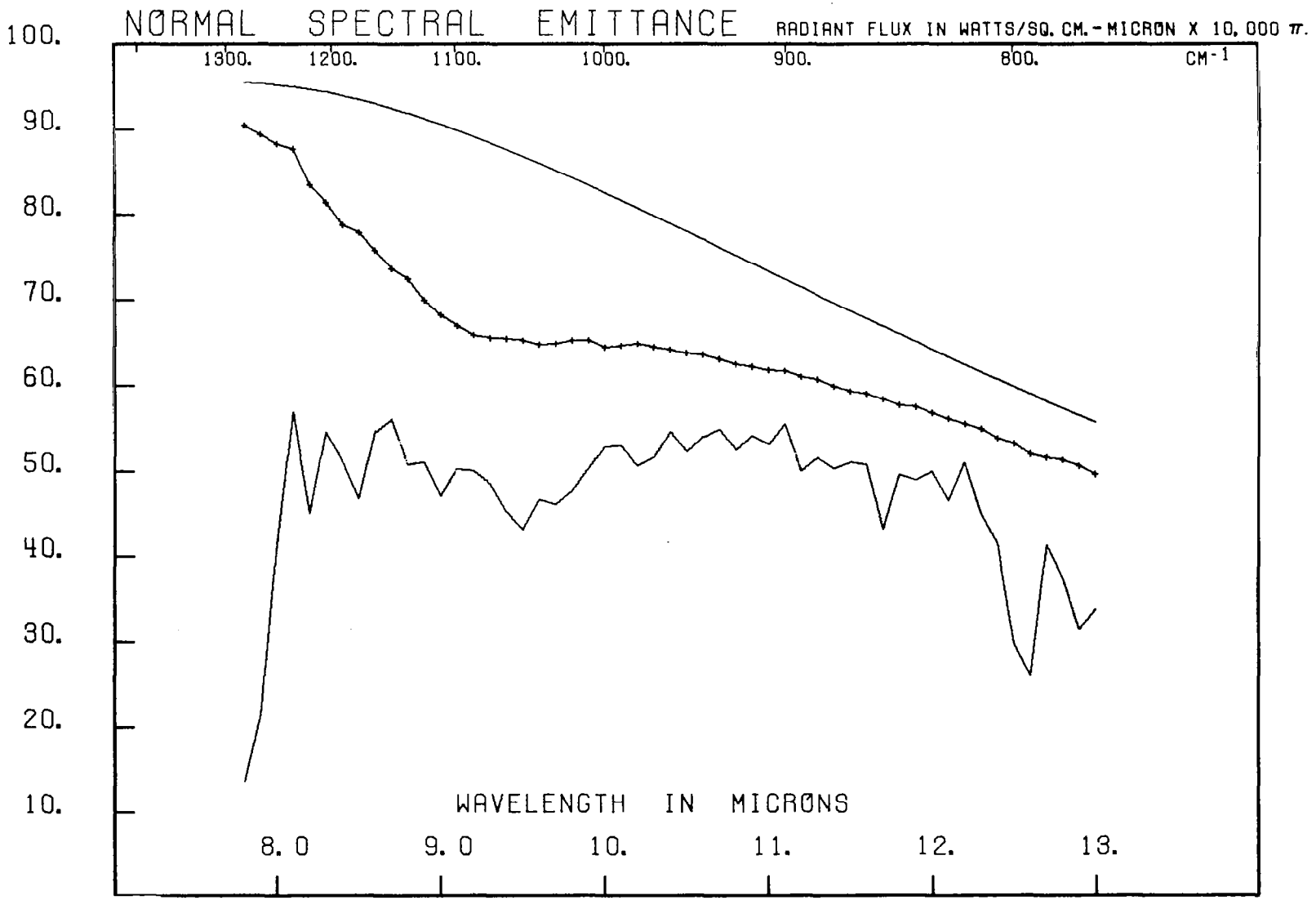

FIG. B-8 HYPERSTHENE ANDESITE VITROPHYRE (USNM 371) NORMAL SPECTRAL EMITTANCE – RADIANT FLUX IN WATTS/SQ. CM-MICRON × 10,000π. Rough, broken side heated.

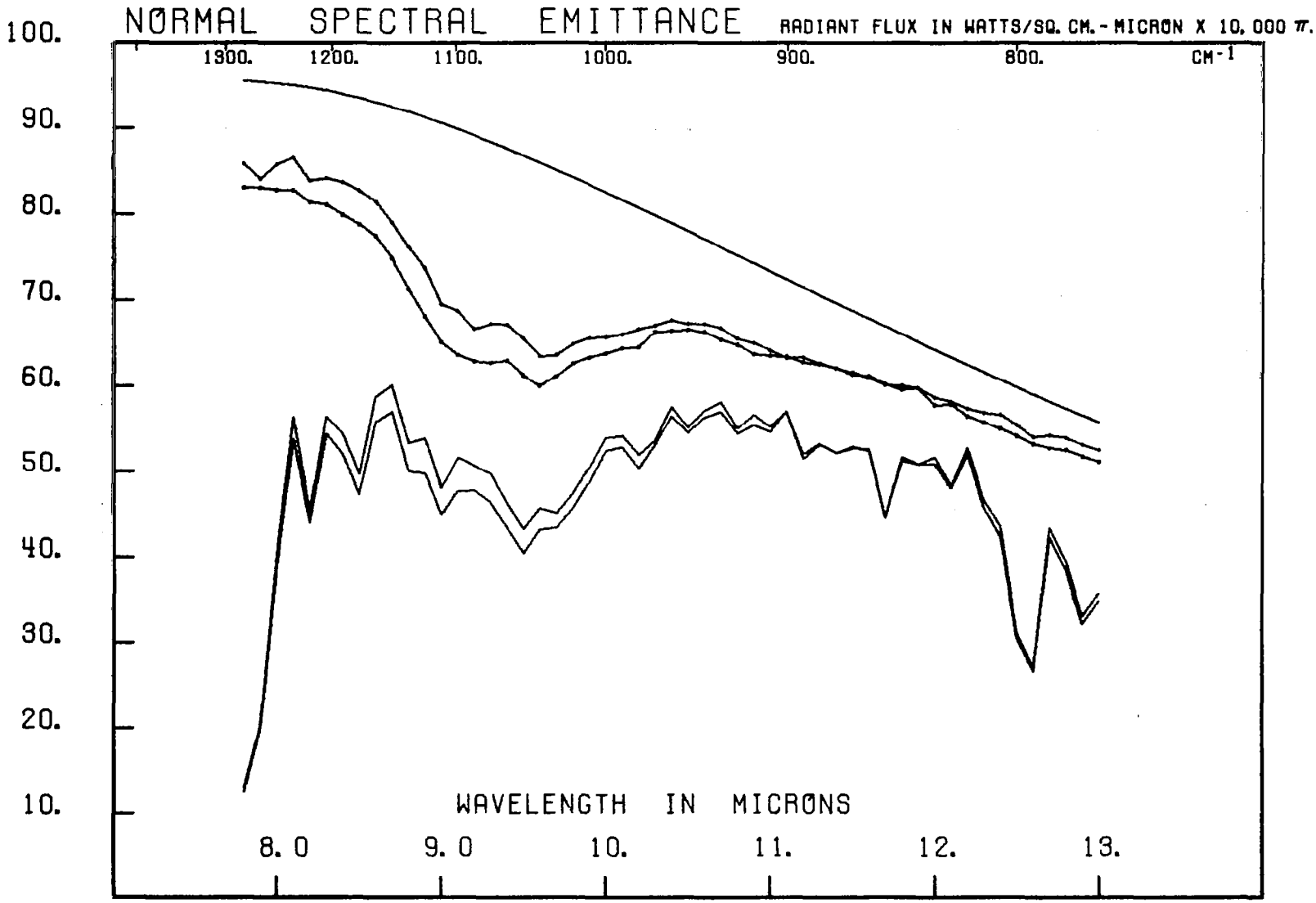

FIG. B-10 SCHIST (MUSCOVITE-QUARTZ), (USNM 1585) NORMAL SPECTRAL EMITTANCE – RADIANT FLUX IN WATTS/SQ. CM-MICRON × 10,000π. Rough broken surfaces heated in duplicate runs – one parallel with the schistosity, and one at right angles to it.

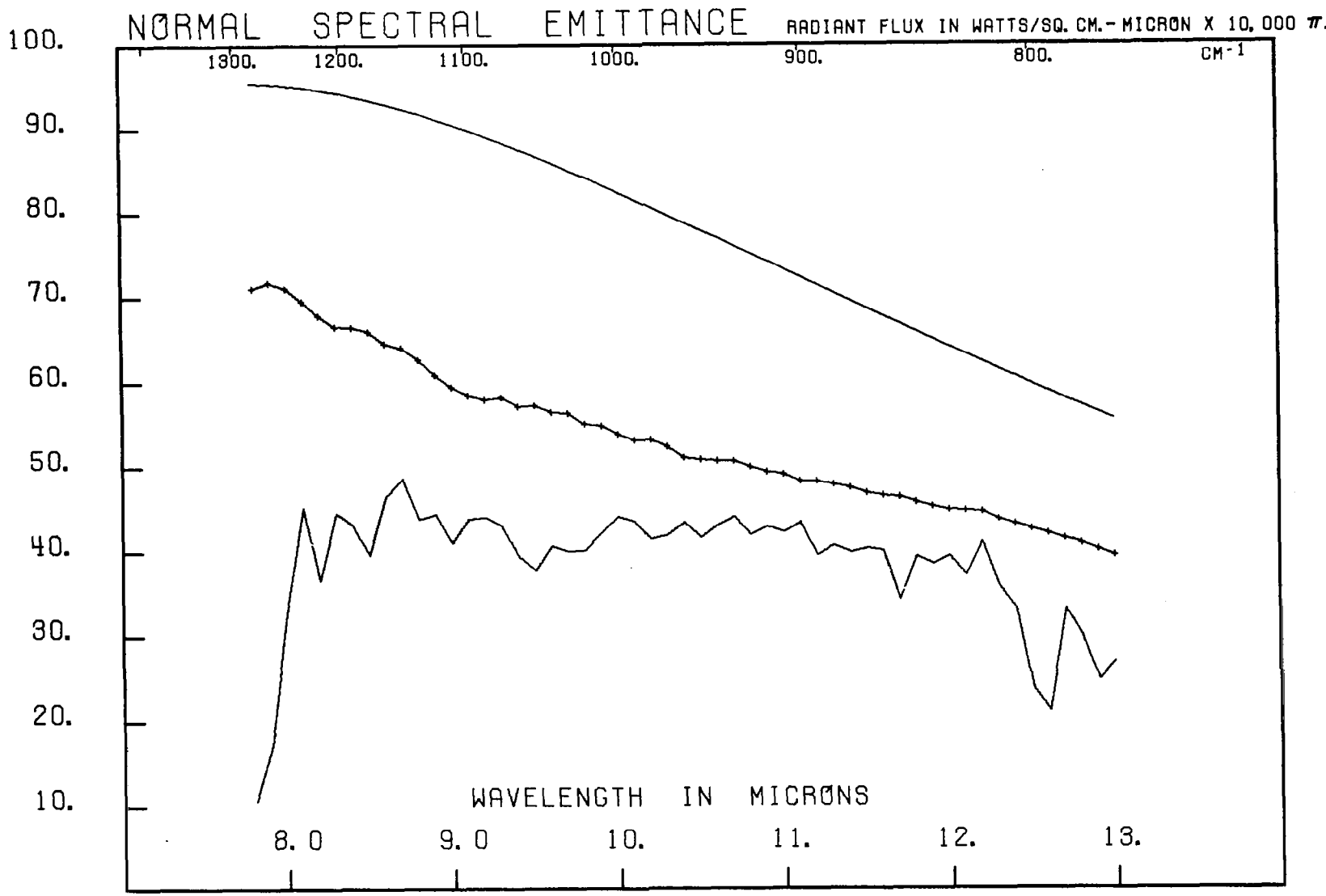

FIG. B-11 BASALT (USNM 102) NORMAL SPECTRAL EMITTANCE – RADIANT FLUX IN WATTS/SQ. CM-MICRON × 10,000 π.
Rough broken surface as received was used.

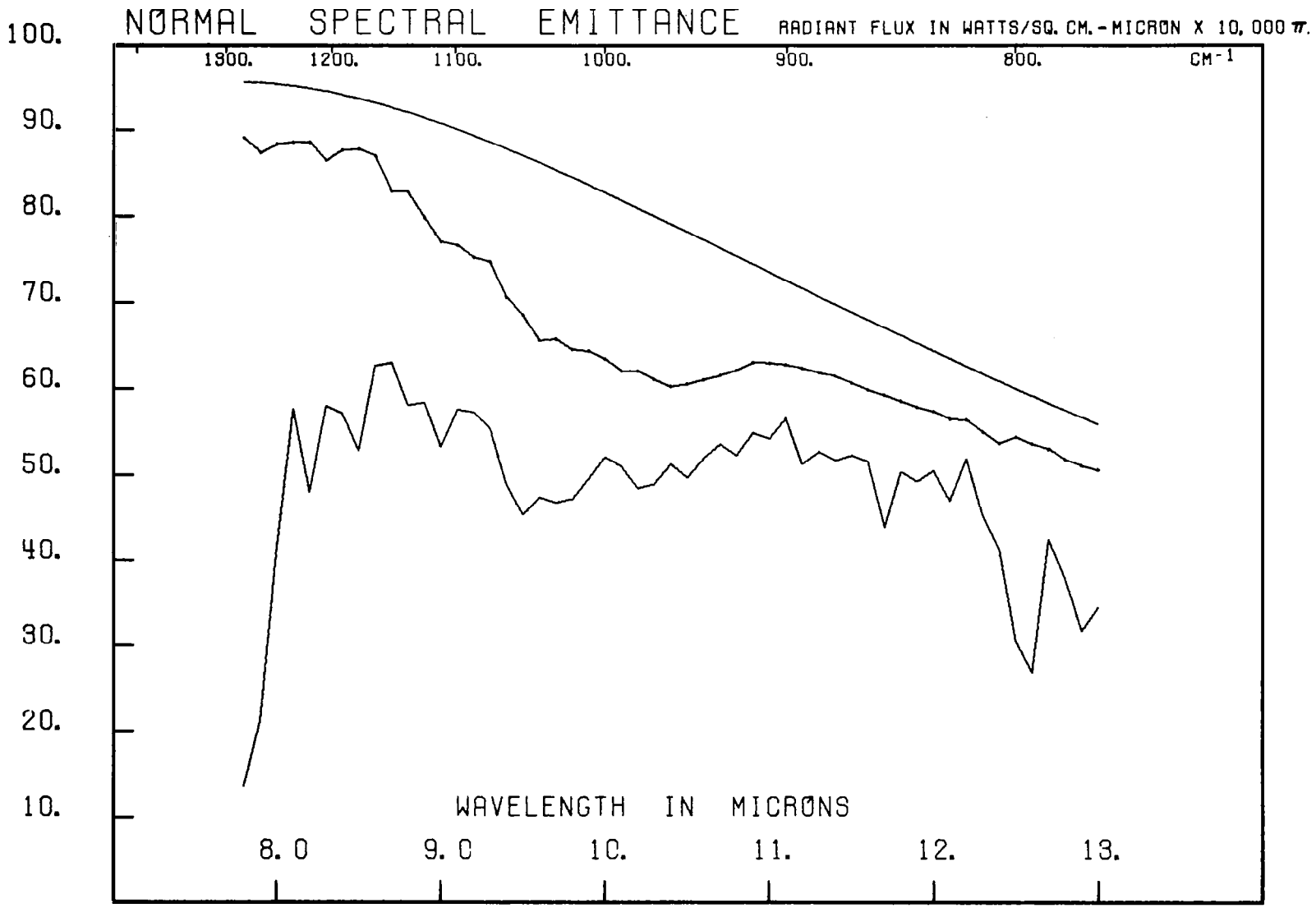

FIG. B-12 SERPENTINE (USNM 145) NORMAL SPECTRAL EMITTANCE – RADIANT FLUX IN WATTS/SQ. CM-MICRON × 10,000 π. Rough broken surface as received was used.

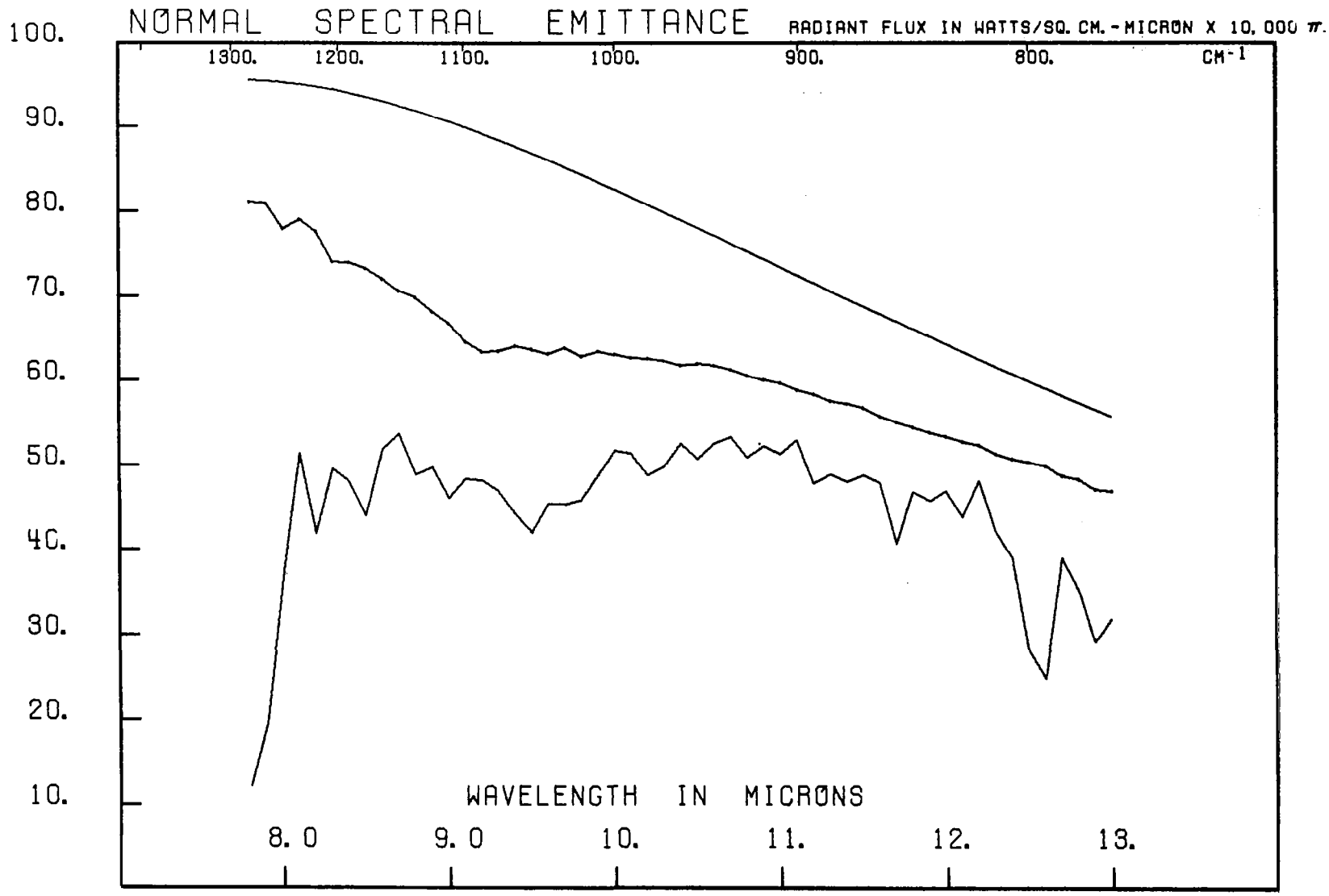

FIG. B-13 OBSIDIAN – Clear Lake, Calif. (SRI 3365) NORMAL SPECTRAL EMITTANCE – RADIANT FLUX IN WATTS/SQ. CM-MICRON × 10,000π. Uneven flinty surface was used, smooth but not flat.

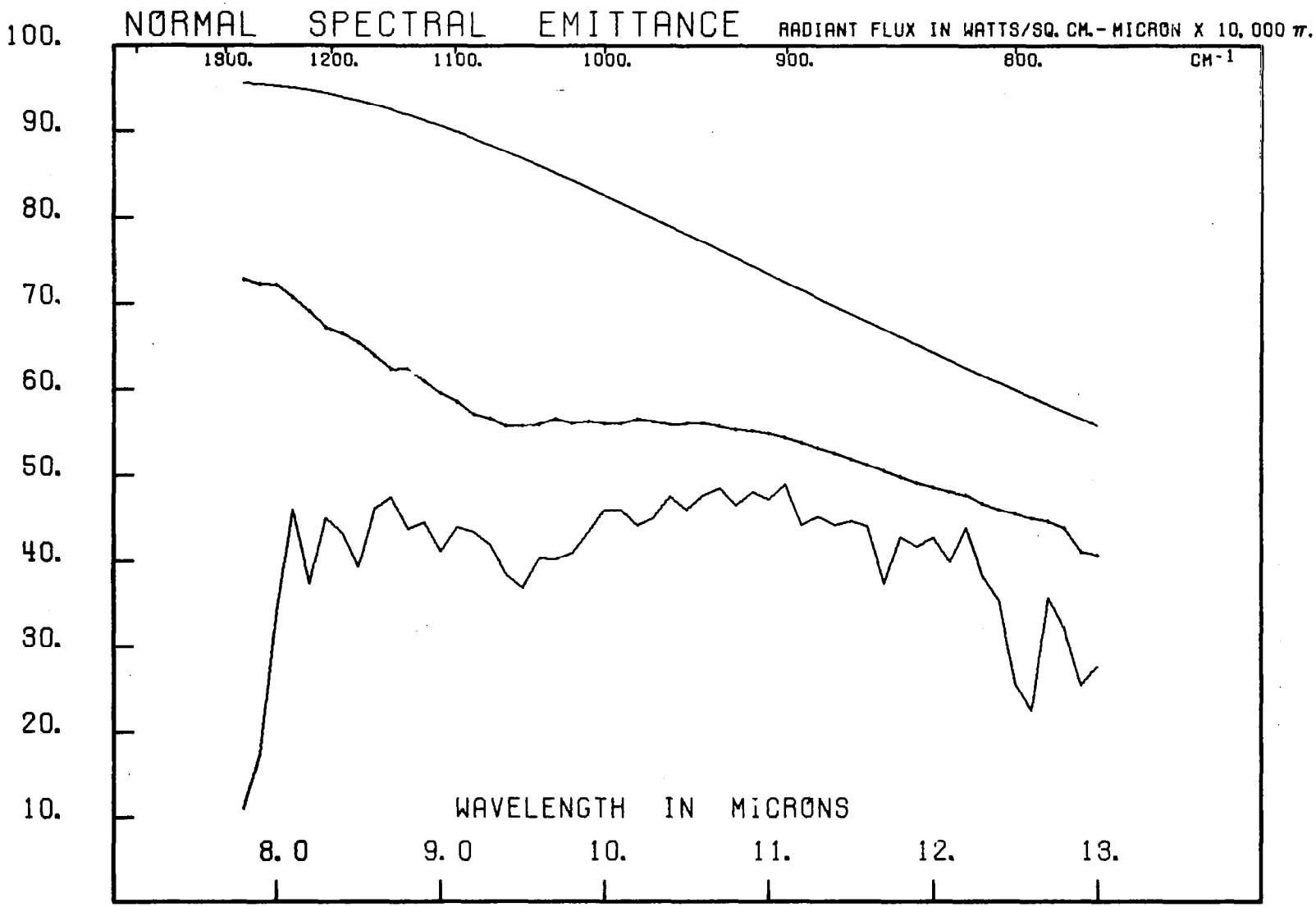

FIG. B-14 OBSIDIAN – Clear Lake, Calif. (SRI 3424) NORMAL SPECTRAL EMITTANCE – RADIANT FLUX IN WATTS/SQ. CM - MICRON × 10,000π. *Rough surface used which was uneven but smooth in places.*

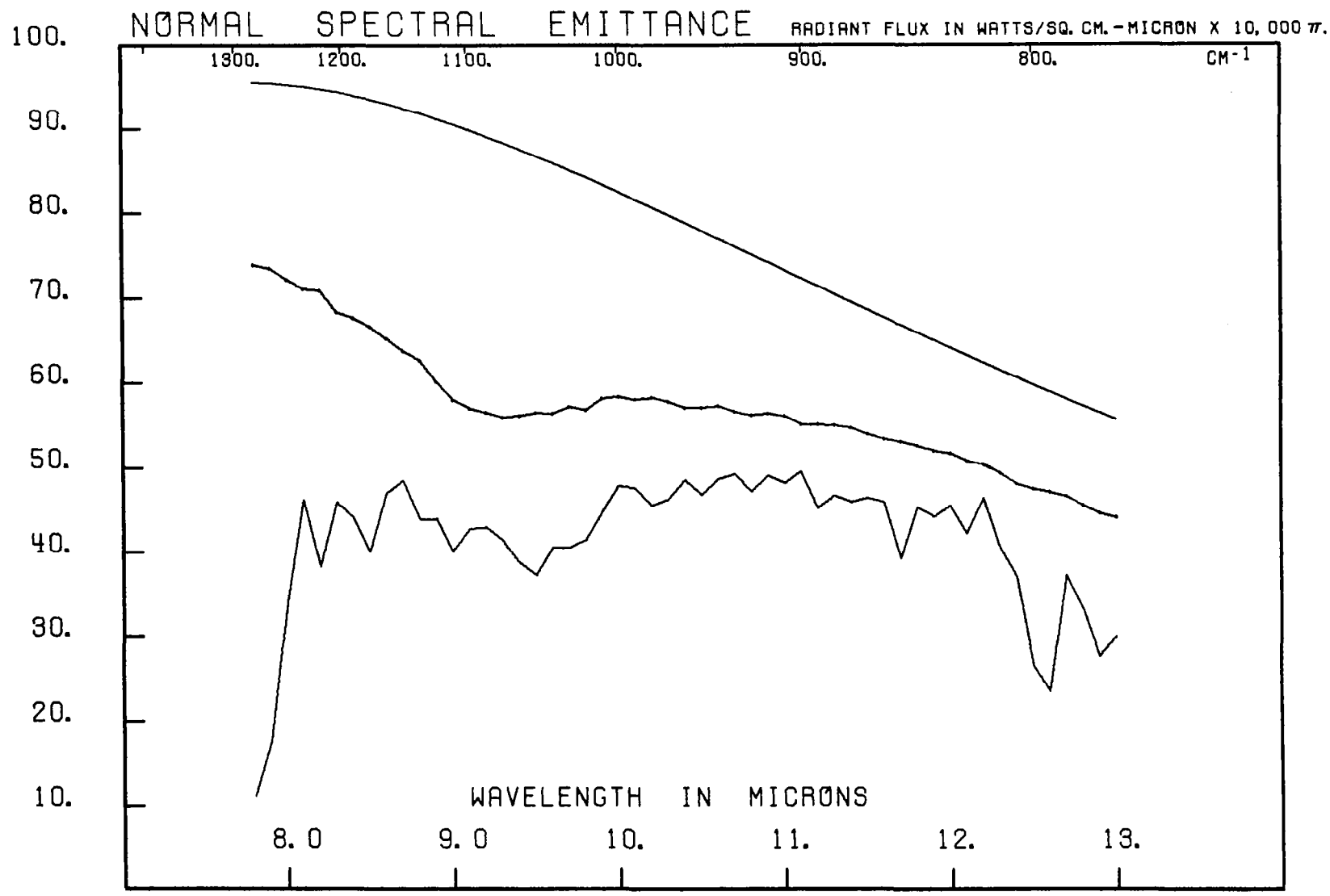

FIG. B-15 TEKTITE, W. Australia (SRI 3535) NORMAL SPECTRAL EMITTANCE – RADIANT FLUX IN WATTS/SQ. CM-MICRON × 10,000 π. Natural pitted but rounded outer surface of tektite was used. Sample was not sawn or ground but used as found.

APPENDIX C

SURFACES OF VARYING PARTICLE SIZE: RADIANT ENERGY PLOTS

In a comparable manner to that described for Appendix B, the following curves were prepared for rock and mineral surfaces of varying particle sizes.

Radiant energy levels of 375°K for the sample source and that of the radiation after 3.4 miles of sea level path length (Taylor and Yates, 1956) were again used.

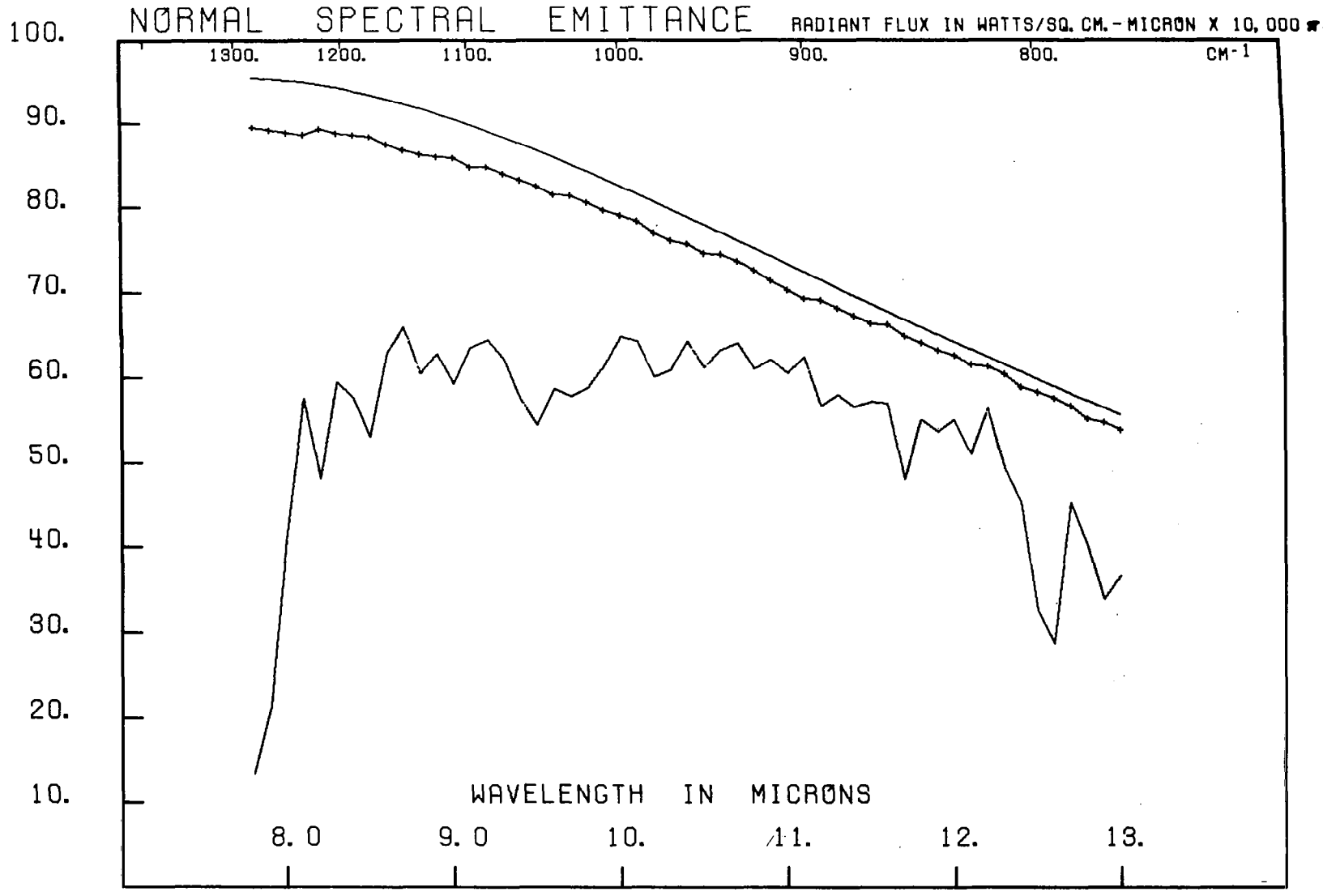

FIG. C-1 CARBON BLACK · NORMAL SPECTRAL EMITTANCE – RADIANT FLUX IN WATTS/SQ. CM-MICRON × 10,000 π.
One of the samples used as blackbody in the early stages of the work. It is quite "black" in the infrared region as may be seen from the close proximity of its spectrum to the Planck Wien energy line. This should be contrasted with Fig. C-16 of a white Al_2O_3 powder (200 A particle size) which is "black" in the infrared region.

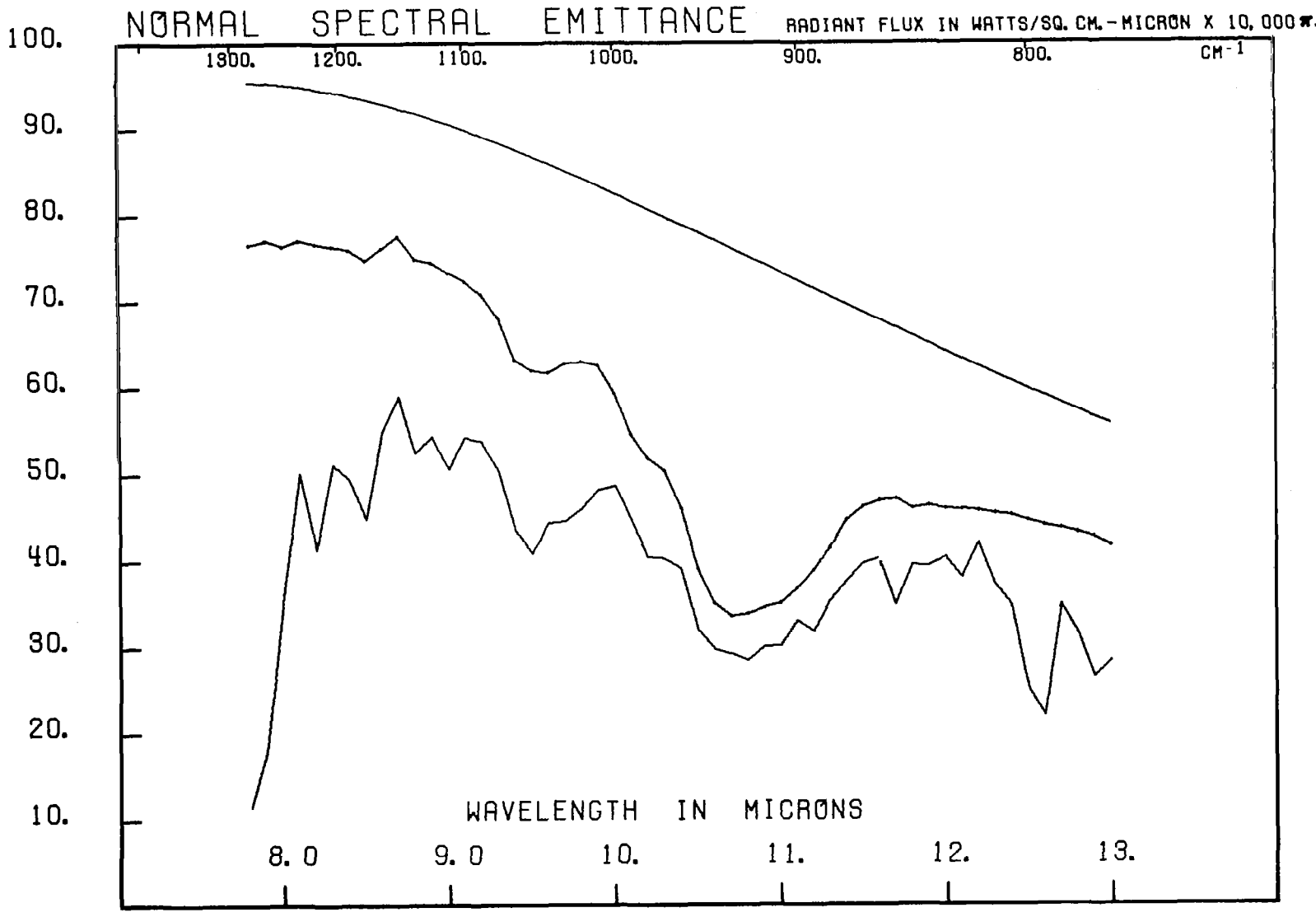

FIG. C-2 DUNITE – POLISHED. (SRI 3390) · NORMAL SPECTRAL EMITTANCE – RADIANT FLUX IN WATTS/SQ. CM – MICRON × 10,000 π.

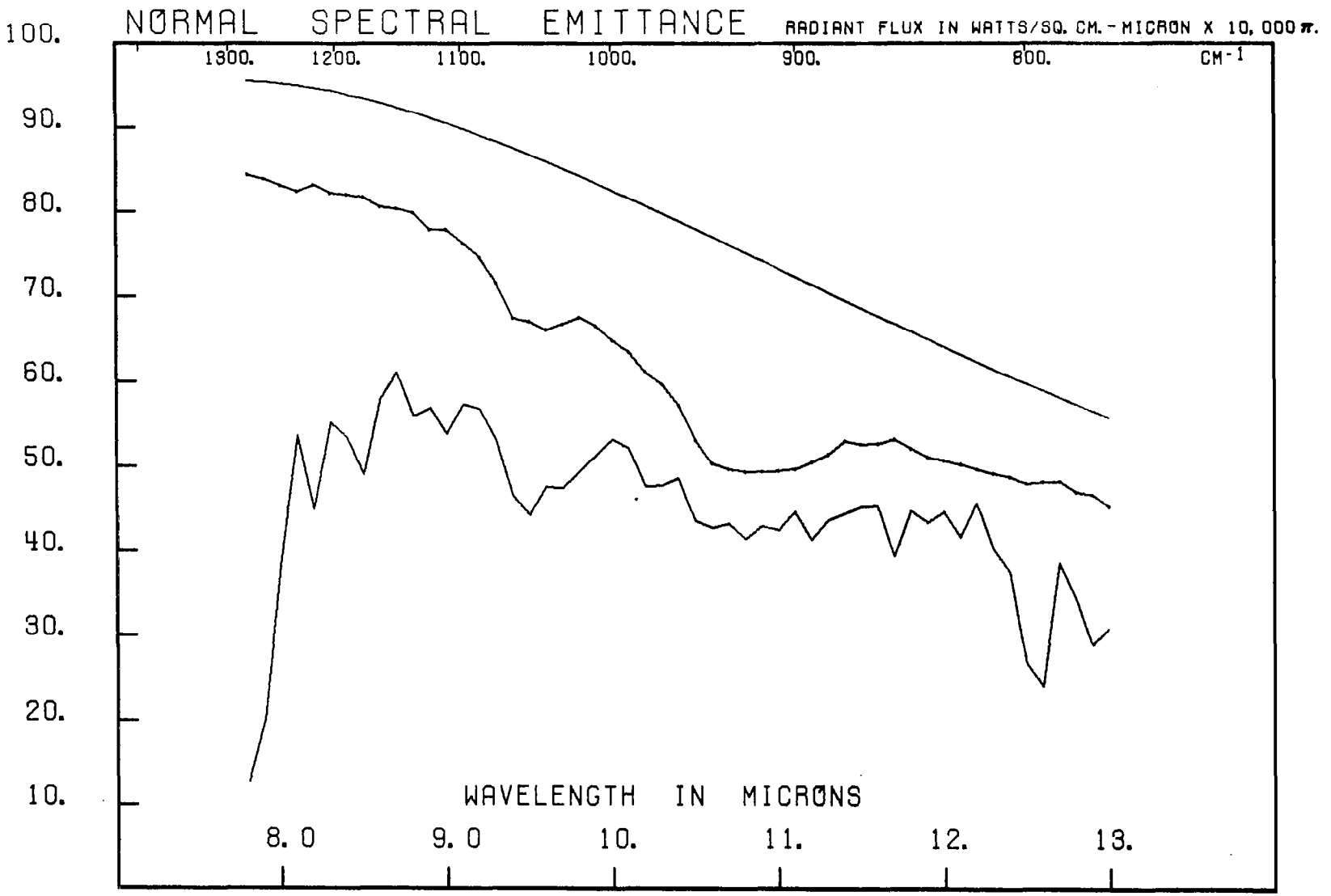

FIG. C-3 DUNITE – ROUGH · NORMAL SPECTRAL EMITTANCE – RADIANT FLUX IN WATTS/SQ. CM-MICRON × 10,000 π.
Same sample as Fig. C-2, but the unpolished sawn surface was used.

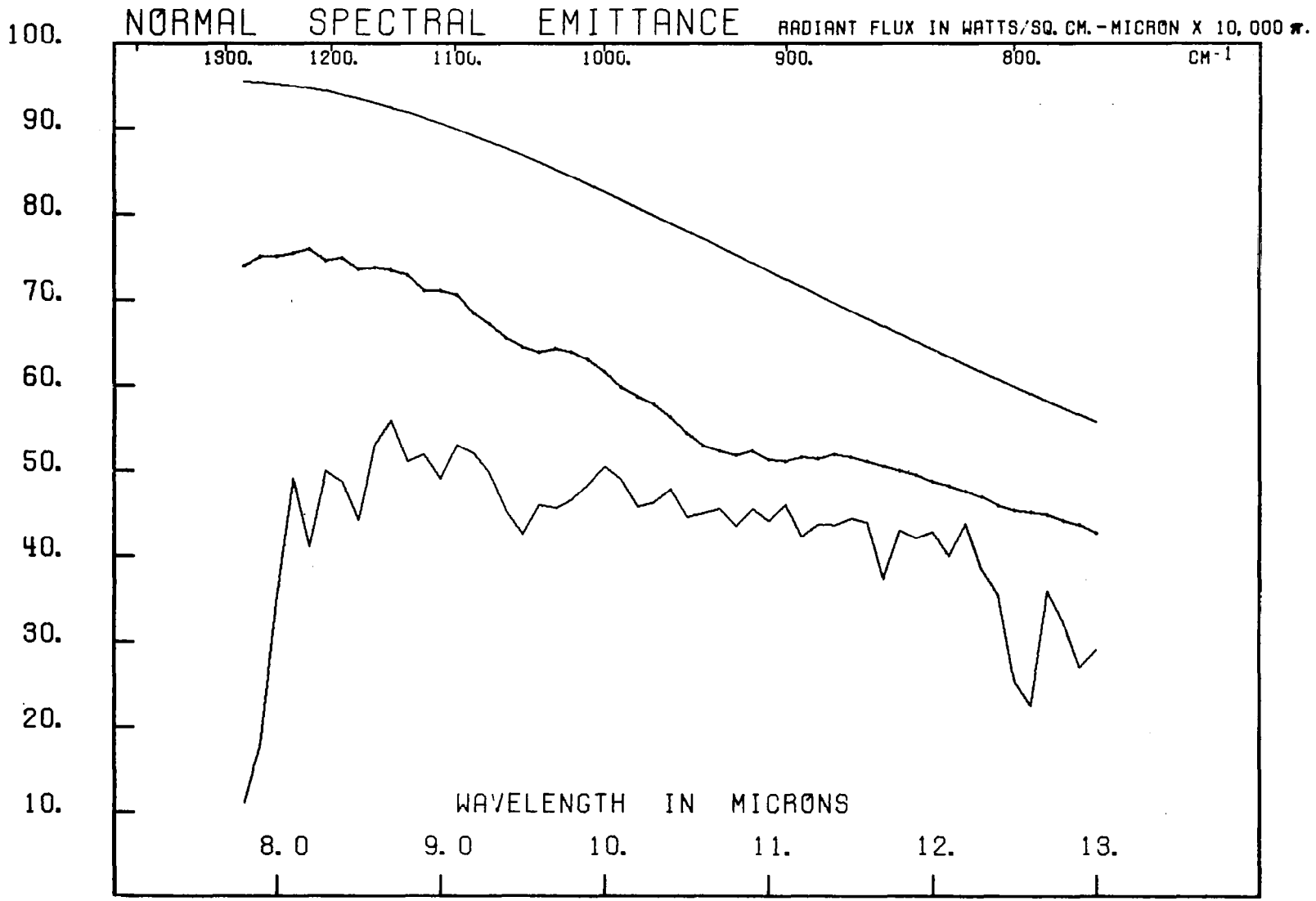

FIG. C-4 DUNITE – ROUGH + SAND · NORMAL SPECTRAL EMITTANCE – RADIANT FLUX IN WATTS/SQ. CM-MICRON × 10,000 π.
A thin layer (2 – 3 mm thick) of clear dunite sand (300μ particles) was placed on the rough dunite surface.

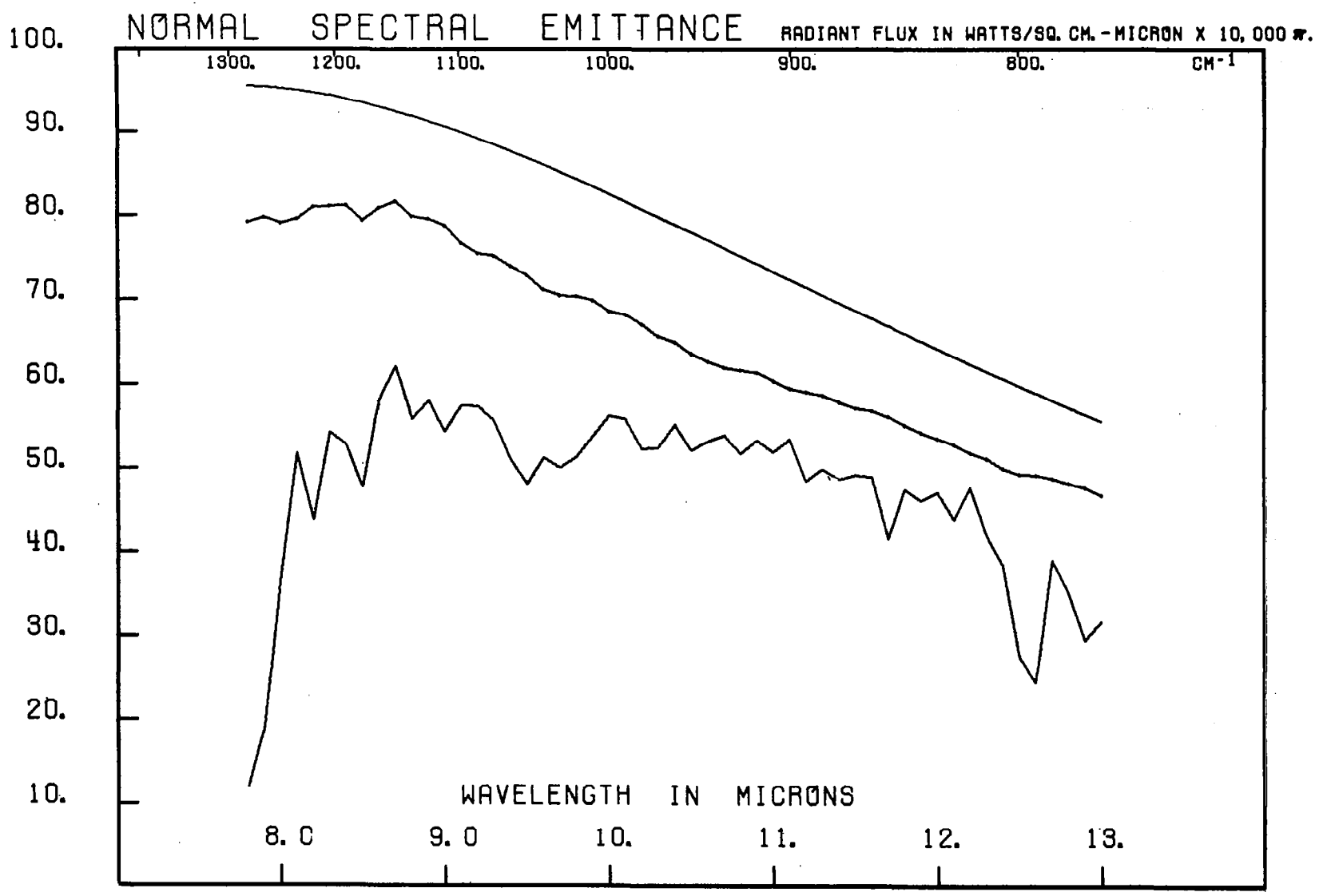

FIG. C-5 DUNITE – ROUGH + DUST · NORMAL SPECTRAL EMITTANCE – RADIANT FLUX IN WATTS/SQ. CM-MICRON × 10,000 π.
A thin layer (2 – 3 mm thick) of clean dunite dust (10 to 25μ particles) was placed on the rough dunite surface.

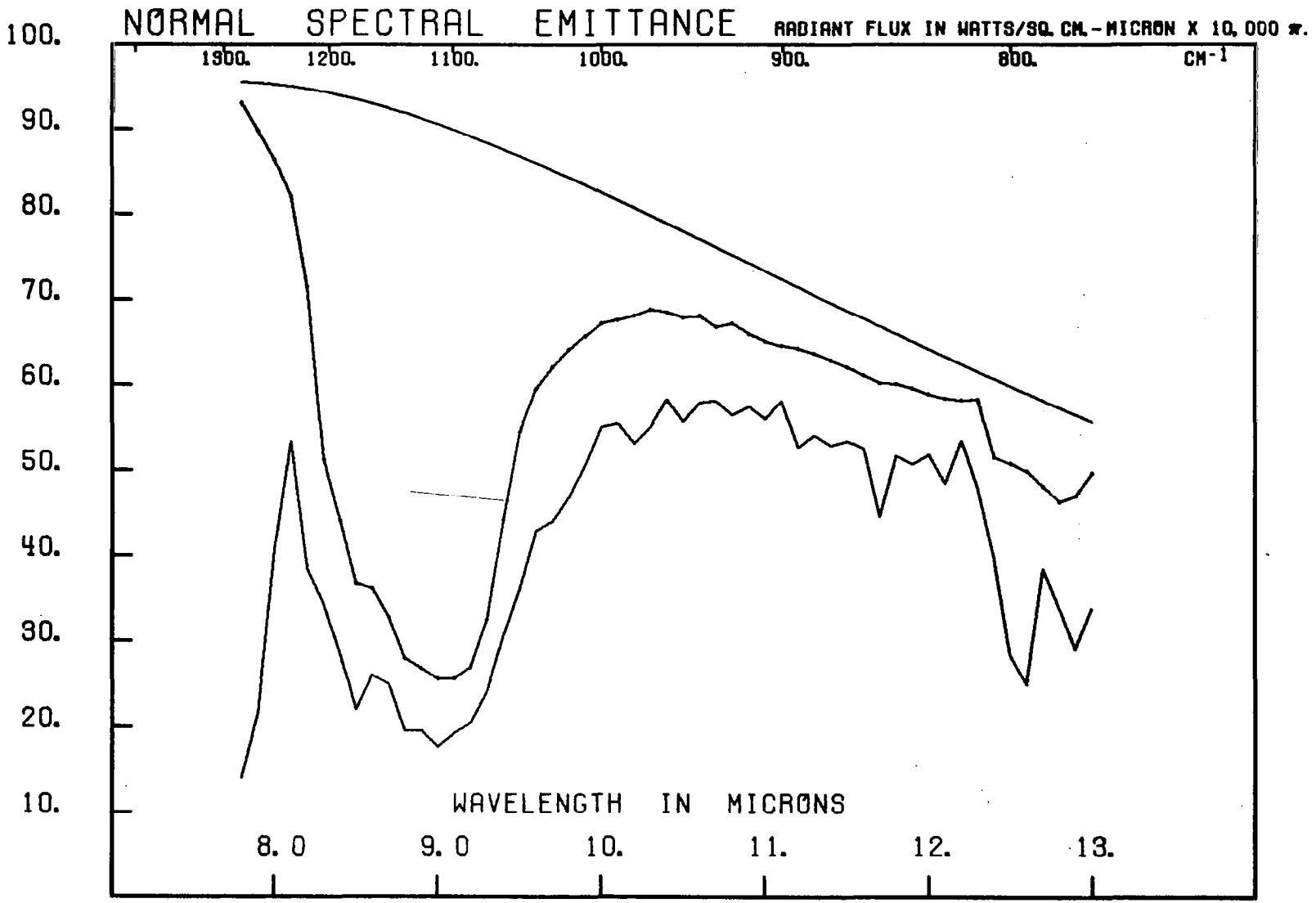

FIG. C-6 QUARTZ, X-CUT, POLISHED · NORMAL SPECTRAL EMITTANCE – RADIANT FLUX IN WATTS/SQ. CM-MICRON × 10,000 π.
An X-cut quartz radio oscillator plate was used for the sample. Plate was 6 mm thick.

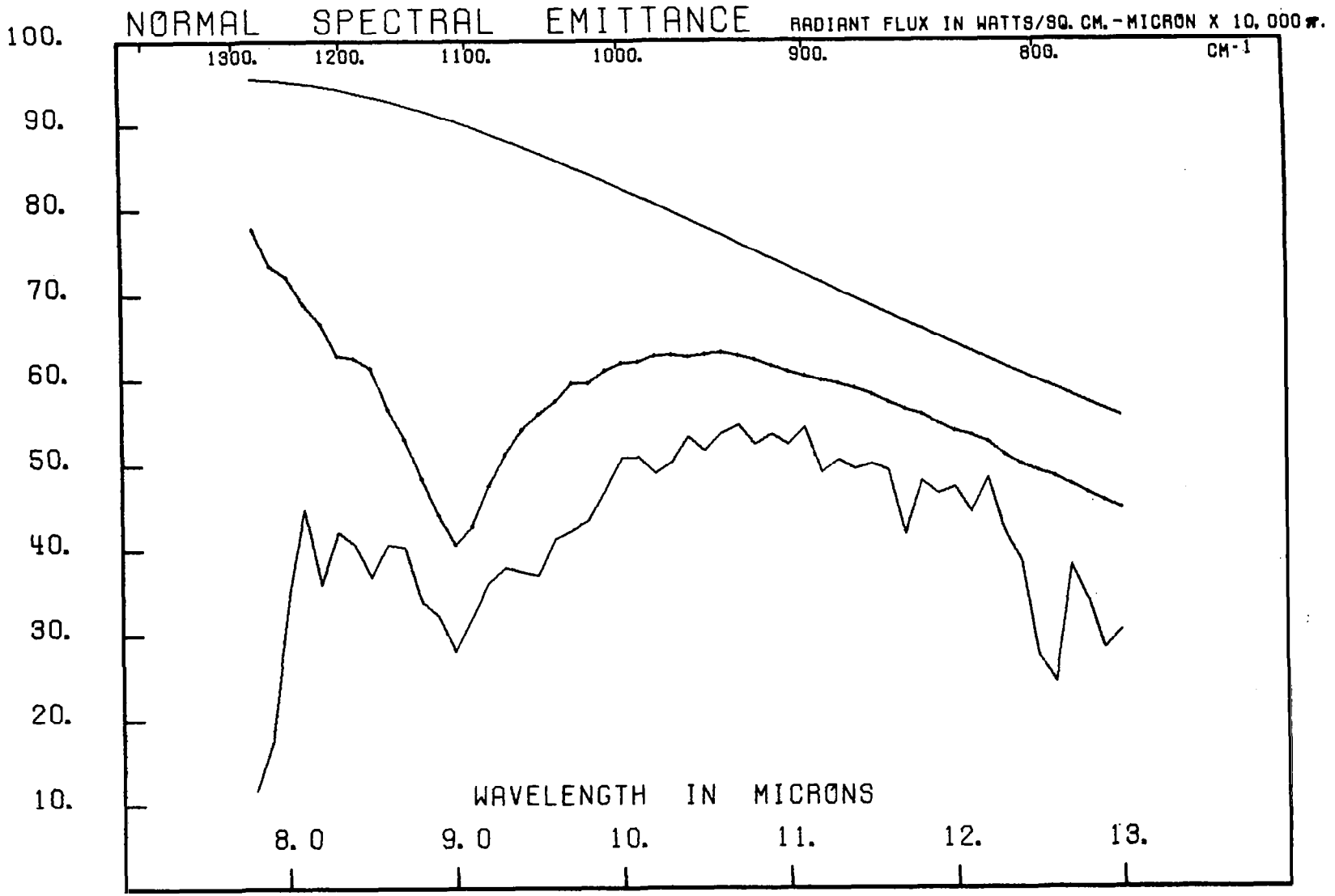

FIG. C-7 QUARTZ, FUSED · NORMAL SPECTRAL EMITTANCE – RADIANT FLUX IN WATTS/SQ. CM-MICRON × 10,000 π.
Disc of optical grade, clear transparent fused quartz used as the sample. Disc was 2 mm thick.

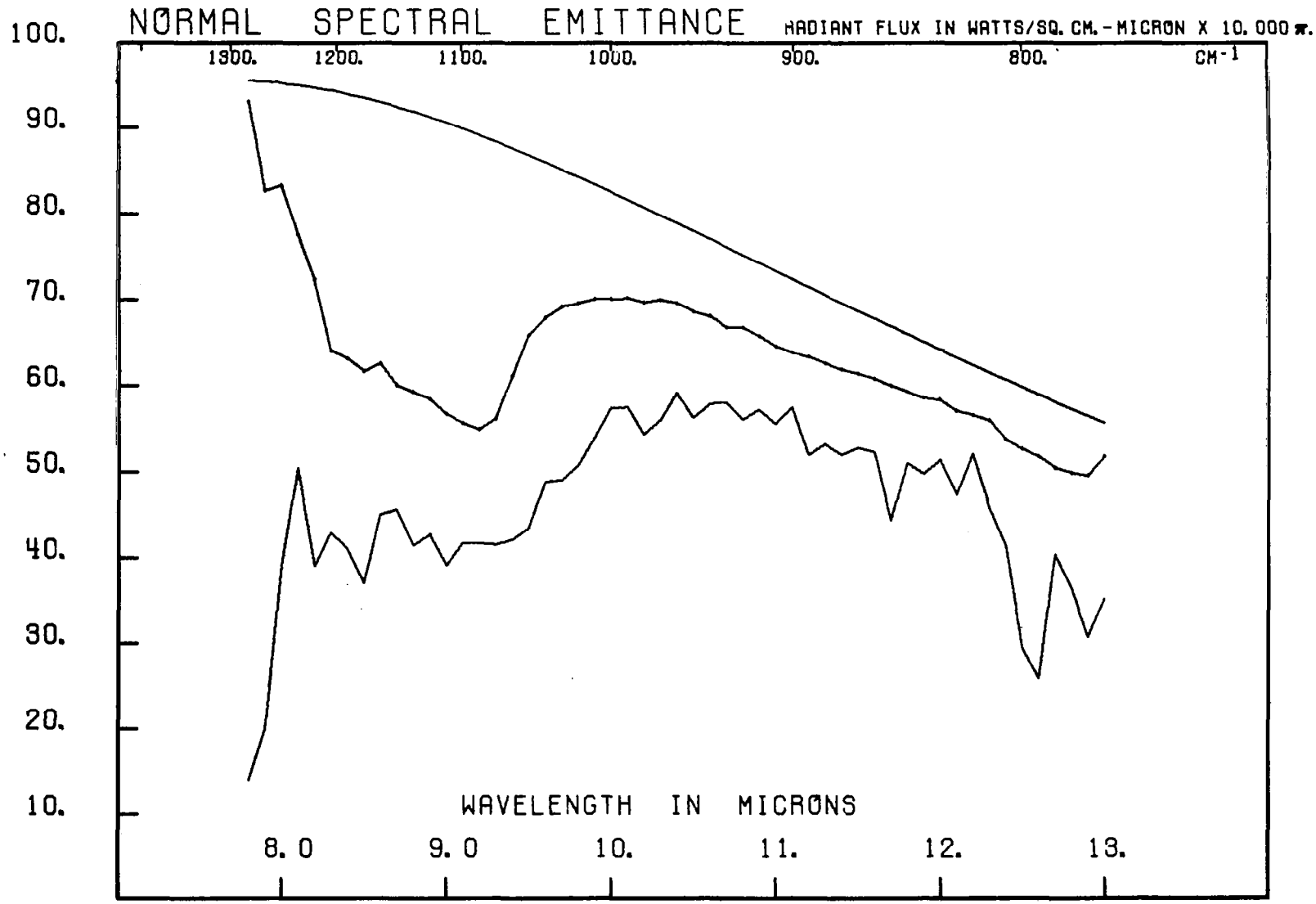

FIG. C-8 QUARTZ, X-CUT, ROUGH · NORMAL SPECTRAL EMITTANCE – RADIANT FLUX IN WATTS/SQ. CM-MICRON × 10,000 π. Identical plate as used in Fig. C-6, but roughened by sandblasting, which produced a frosted layer 0.5 to 1.0 mm thick, with some concentric fractures penetrating into the plate.

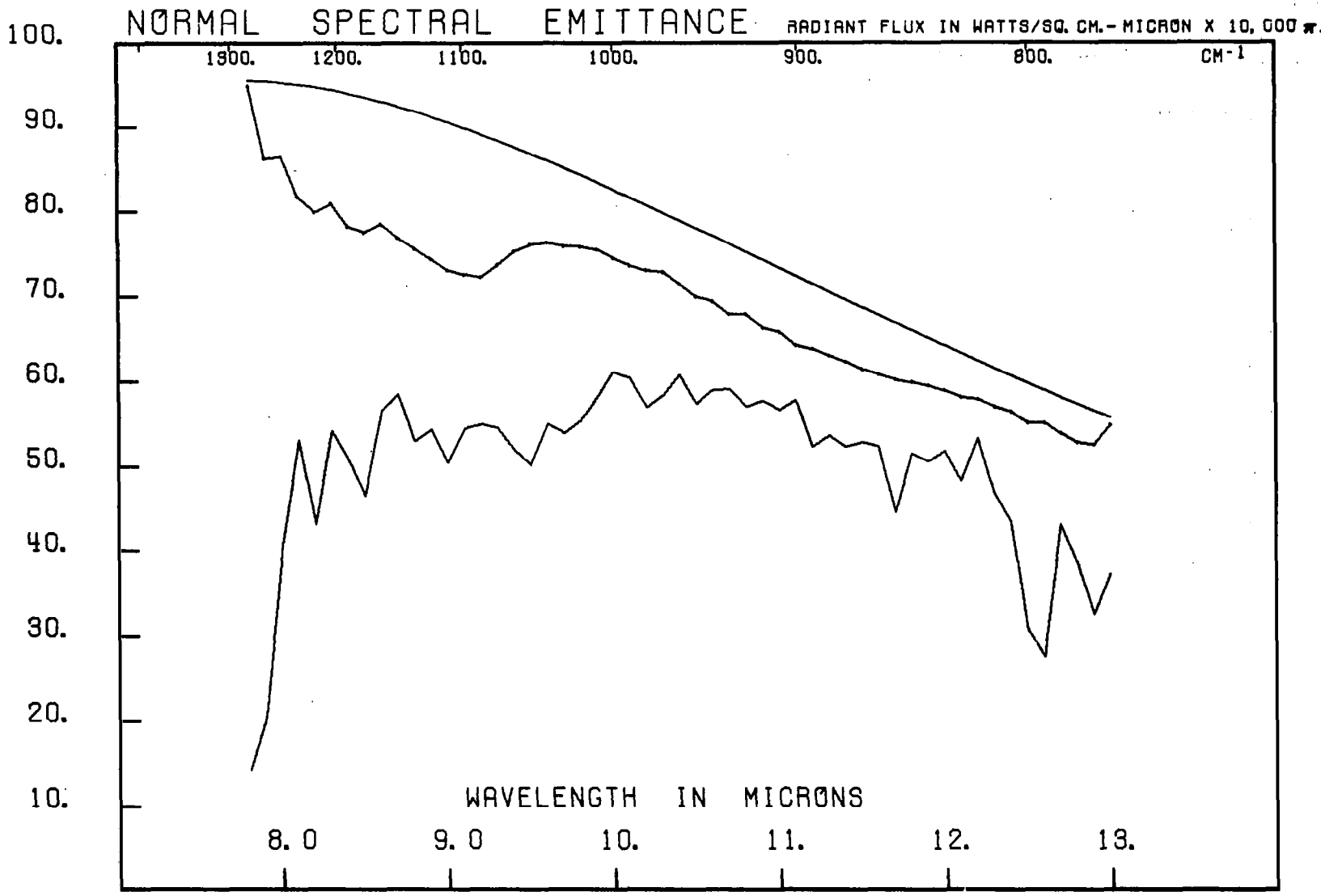

FIG. C-9 QUARTZ POWDER (25 to 45μ size) · NORMAL SPECTRAL EMITTANCE – RADIANT FLUX IN WATTS/SQ. CM-MICRON × 10,000π. Material sized by water elutriation to be within these limits. See photograph in text.

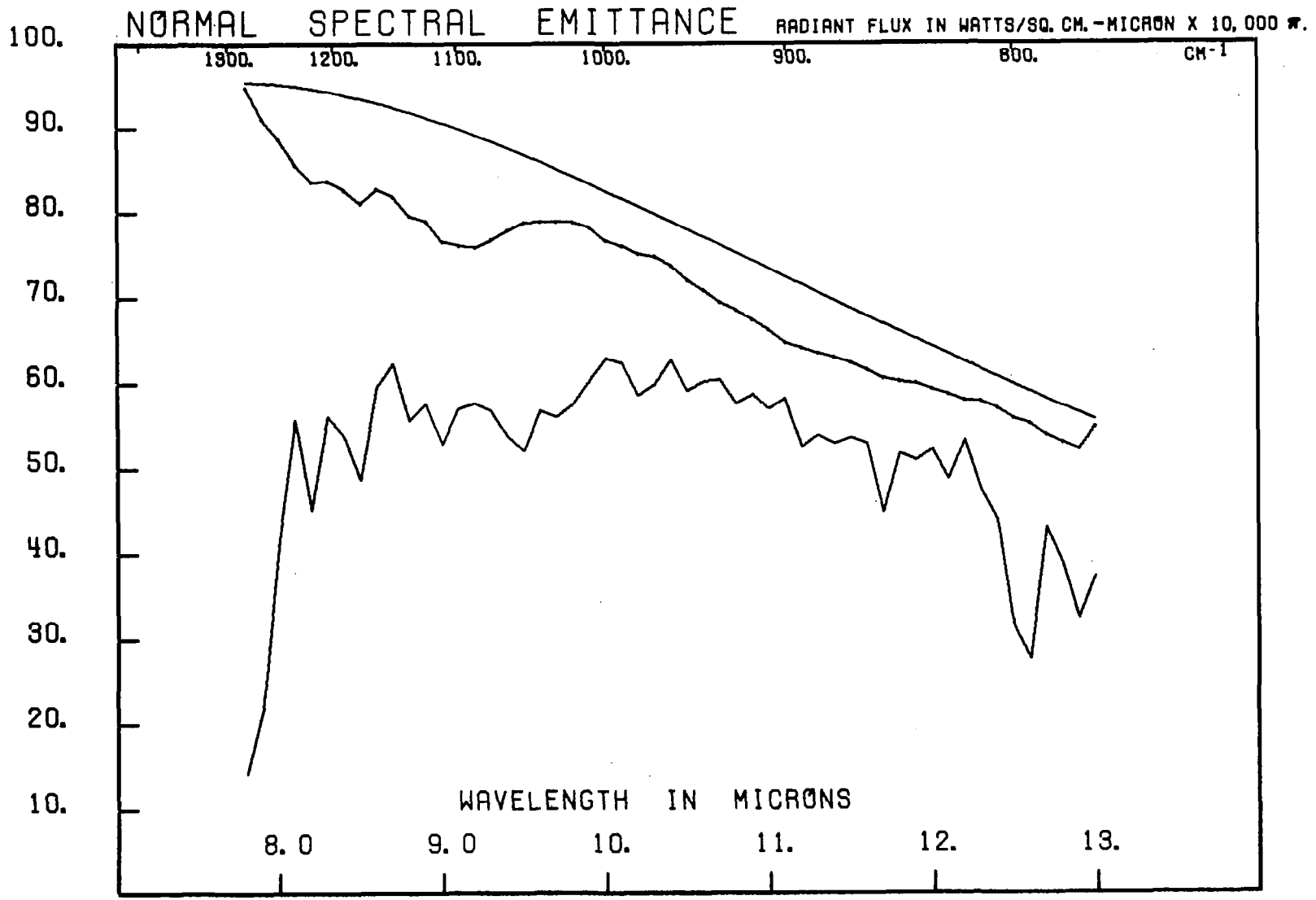

FIG. C-10 QUARTZ POWDER (10 to 25μ size) · NORMAL SPECTRAL EMITTANCE – RADIANT FLUX IN WATTS/SQ. CM-MICRON × 10,000π. Material sized by water elutriation.

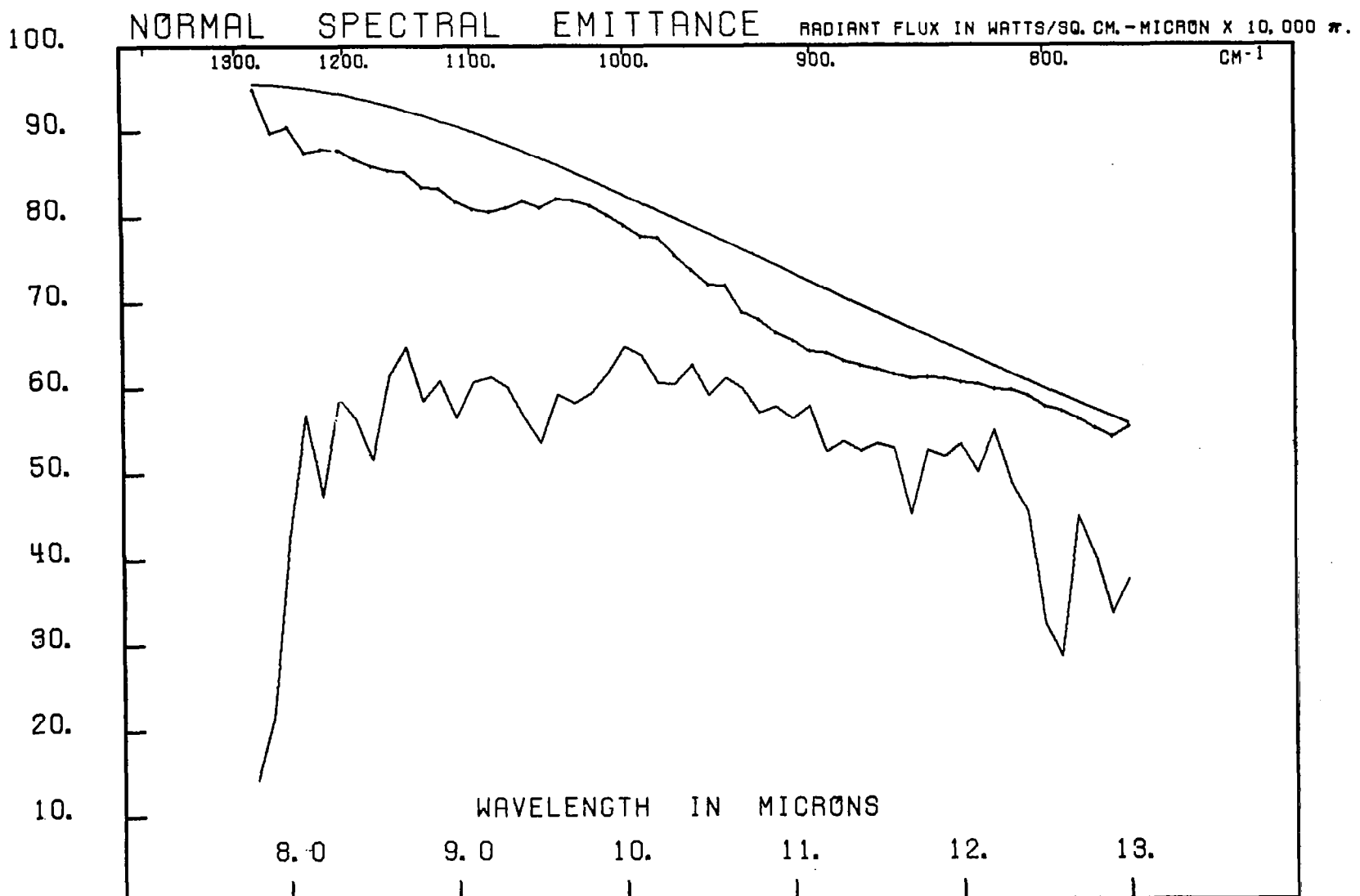

FIG. C-11 QUARTZ POWDER (1 to 10μ size) · NORMAL SPECTRAL EMITTANCE – RADIANT FLUX IN WATTS/SQ. CM – MICRON × 10,000π. Material sized by water elutriation.

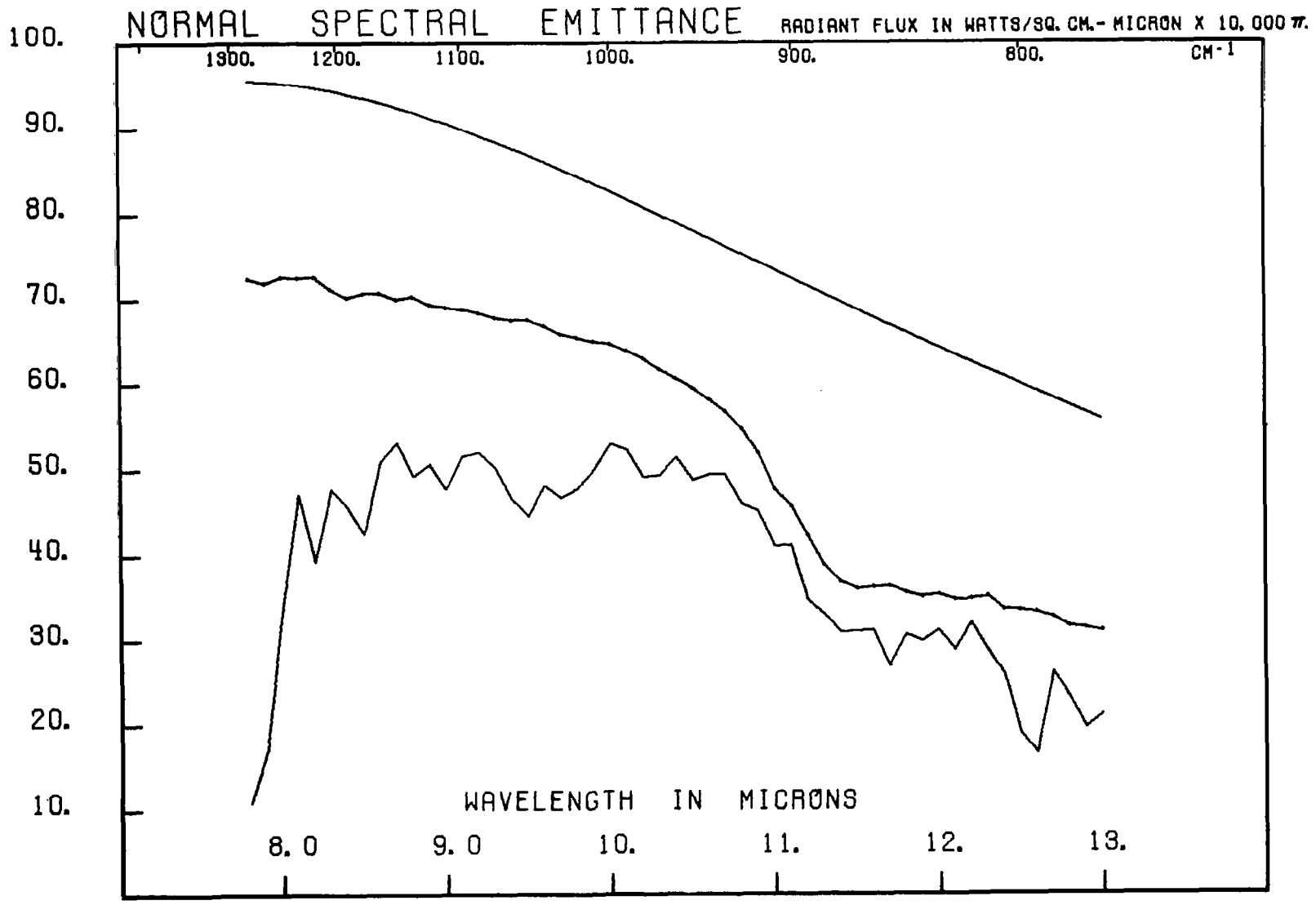

FIG. C-12 ALUMINA – SAPPHIRE SHEET · NORMAL SPECTRAL EMITTANCE – RADIANT FLUX IN WATTS/SQ. CM – MICRON × 10,000π. Synthetic sapphire sheet, 0.5 mm thick (Hypalox, RK 37 Tr, American Feldmuehle Corp.)

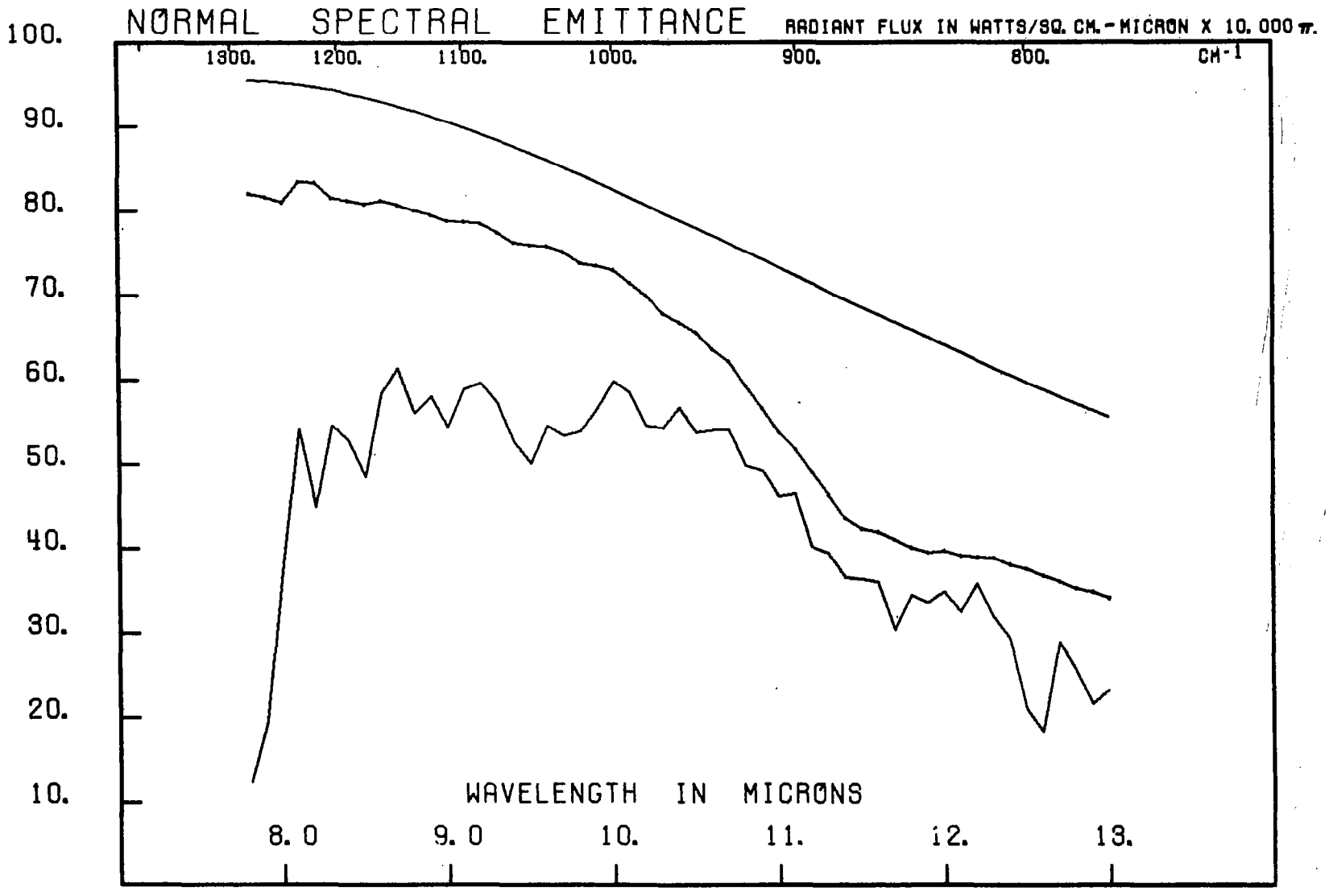

FIG. C-13 ALUMINA – SAPPHIRE ROD · NORMAL SPECTRAL EMITTANCE – RADIANT FLUX IN WATTS/SQ. CM-MICRON × 10,000 π.
Pieces of 6 mm diameter synthetic sapphire rod, clear white, slightly frosted surface.

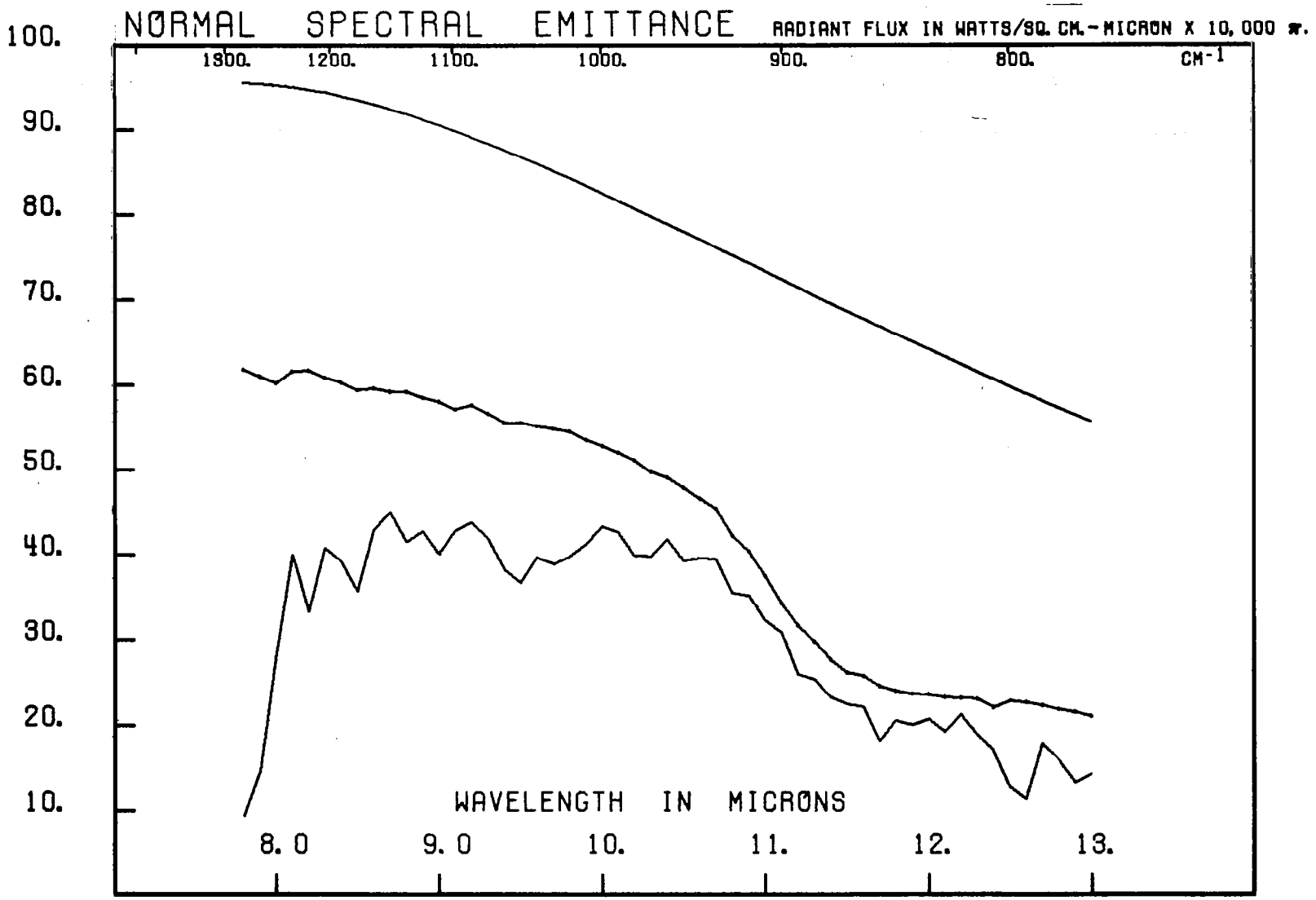

FIG. C-14 ALUMINA – ALUNDUM PLATELETS · NORMAL SPECTRAL EMITTANCE – RADIANT FLUX IN WATTS/SQ. CM-MICRON × 10,000π. Fragment of a fused alumina "alundum" combustion boat. Aggregate of 1 – 2 mm crystals with semi-smooth prepared surfaces.

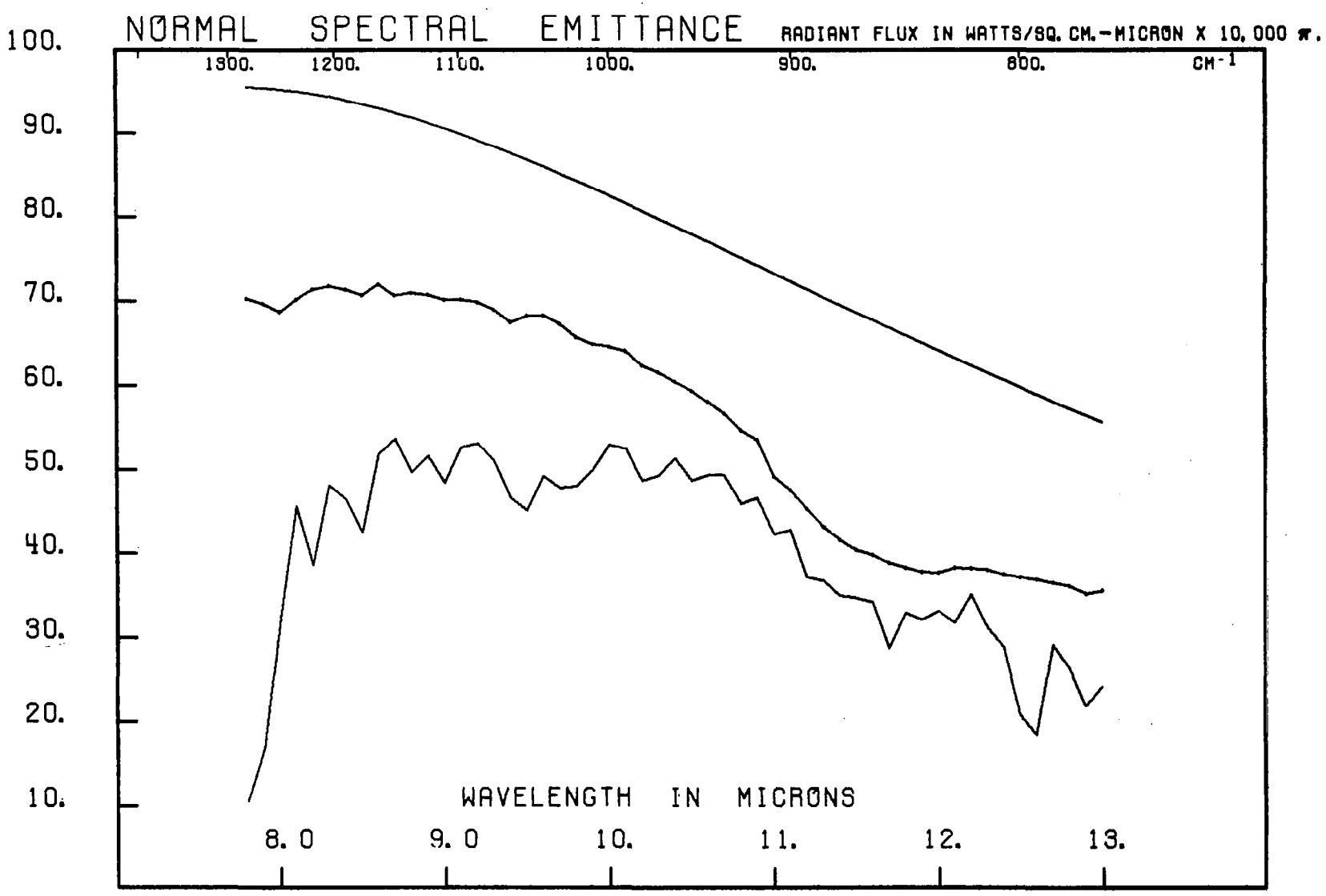

FIG. C-15 ALUMINA – ALUNDUM TUBING · NORMAL SPECTRAL EMITTANCE – RADIANT FLUX IN WATTS/SQ. CM-MICRON × 10,000π. Very fine grained, pure Al_2O_3 ceramic tubing 4 mm diameter. Opaque white, smooth (but not polished) curved surface.

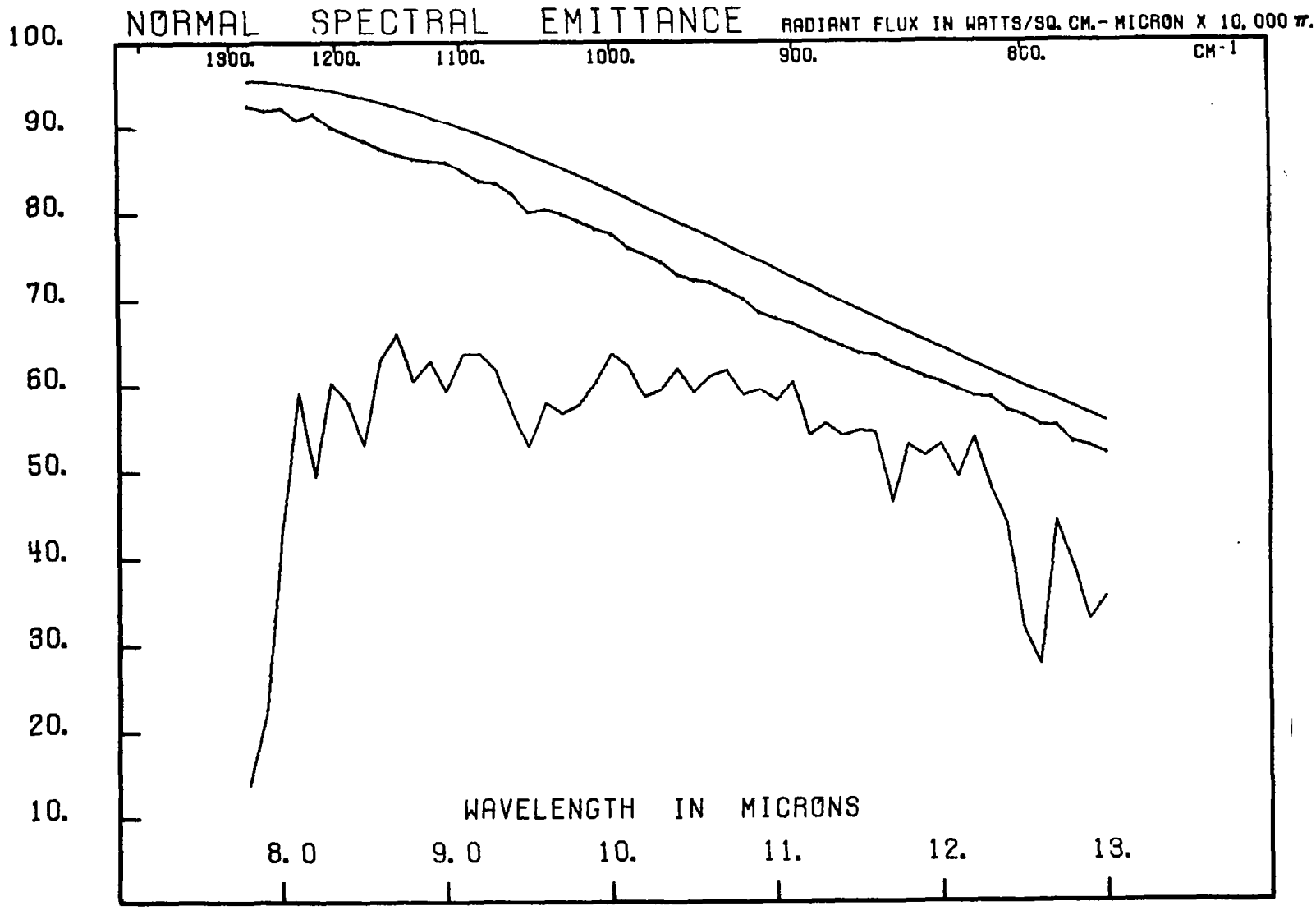

FIG. C-16 ALUMINA – POWDER ·NORMAL SPECTRAL EMITTANCE – RADIANT FLUX IN WATTS/SQ. CM-MICRON × 10,000 π.
Very fine grained (200 Angstrom particles) pure alumina powder, sifted into fairy-castle structures.

"The aeronautical and space activities of the United States shall be conducted so as to contribute . . . to the expansion of human knowledge of phenomena in the atmosphere and space. The Administration shall provide for the widest practicable and appropriate dissemination of information concerning its activities and the results thereof."

—NATIONAL AERONAUTICS AND SPACE ACT OF 1958

NASA SCIENTIFIC AND TECHNICAL PUBLICATIONS

TECHNICAL REPORTS: Scientific and technical information considered important, complete, and a lasting contribution to existing knowledge.

TECHNICAL NOTES: Information less broad in scope but nevertheless of importance as a contribution to existing knowledge.

TECHNICAL MEMORANDUMS: Information receiving limited distribution because of preliminary data, security classification, or other reasons.

CONTRACTOR REPORTS: Technical information generated in connection with a NASA contract or grant and released under NASA auspices.

TECHNICAL TRANSLATIONS: Information published in a foreign language considered to merit NASA distribution in English.

TECHNICAL REPRINTS: Information derived from NASA activities and initially published in the form of journal articles.

SPECIAL PUBLICATIONS: Information derived from or of value to NASA activities but not necessarily reporting the results of individual NASA-programmed scientific efforts. Publications include conference proceedings, monographs, data compilations, handbooks, sourcebooks, and special bibliographies.

Details on the availability of these publications may be obtained from:

SCIENTIFIC AND TECHNICAL INFORMATION DIVISION

NATIONAL AERONAUTICS AND SPACE ADMINISTRATION

Washington, D.C. 20546